



# Optimisation multi-échelle de structures composites à parois minces intégrant une stratégie de modélisation global-local

Michele Iacopo Izzi

## ► To cite this version:

Michele Iacopo Izzi. Optimisation multi-échelle de structures composites à parois minces intégrant une stratégie de modélisation global-local. Matériaux composites et construction. HESAM Université, 2021. Français. NNT : 2021HESAE017 . tel-03675259

**HAL Id: tel-03675259**

**<https://pastel.hal.science/tel-03675259>**

Submitted on 23 May 2022

**HAL** is a multi-disciplinary open access archive for the deposit and dissemination of scientific research documents, whether they are published or not. The documents may come from teaching and research institutions in France or abroad, or from public or private research centers.

L'archive ouverte pluridisciplinaire **HAL**, est destinée au dépôt et à la diffusion de documents scientifiques de niveau recherche, publiés ou non, émanant des établissements d'enseignement et de recherche français ou étrangers, des laboratoires publics ou privés.

**ÉCOLE DOCTORALE SCIENCES DES MÉTIERS DE L'INGÉNIEUR**  
**Institut de mécanique et d'Ingénierie de Bordeaux (I2M)**  
**Campus de Bordeaux-Talence**

# THÈSE

présentée par : **Michele Iacopo IZZI**

soutenue le : **07 Mai 2021**

pour obtenir le grade de : **Docteur d'HESAM Université**

préparée à : **École Nationale Supérieure d'Arts et Métiers**

Spécialité : **Conception**

**Multi-scale optimisation of  
thin-walled composite structures integrating  
a global-local modelling strategy**  
**(Optimisation multi-échelle de structures composites  
à parois minces intégrant une stratégie  
de modélisation global-local)**

**THÈSE dirigée par :**  
**M. MONTEMURRO Marco**

**et co-encadrée par :**  
**M. PAILHES Jérôme, Mme. CATAPANO Anita**

**Jury**

**M. Paolo VANNUCCI**, PU, LMV, Université de Versailles Saint-Quentin  
**M. Joseph MORLIER**, PU, ICA, ISAE-SUPAERO  
**M. Alberto PIRRERA**, AP (MCF HDR), ACCIS, University of Bristol  
**M. François-Xavier IRISARRI**, PhD, DMSC, ONERA  
**M. Marco MONTEMURRO**, PU, I2M, Arts et Métiers Bordeaux-Talence  
**M. Jérôme PAILHES**, PU, I2M, Arts et Métiers Bordeaux-Talence  
**Mme. Anita CATAPANO**, MCF, I2M, Bordeaux INP  
**M. Antonio COSCULLUELA**, PhD, CEA CESTA

Président  
Rapporteur  
Rapporteur  
Examinateur  
Examinateur  
Examinateur  
Examinatrice  
Invité









*Ai miei cari e  
all'immenso dono del loro amore.*

*To my dear ones and to  
the immense gift of their love.*

---

# Contents

|   |            |
|---|------------|
| <b>Acknowledgements</b>   | <b>v</b>   |
| Funding . . . . .   | vi         |
| <b>Acronyms</b>   | <b>vii</b> |
| <b>1 Preamble</b>   | <b>1</b>   |
| 1.1 The thesis context: the PARSIFAL project . . . . .  | 1          |
| 1.2 The thesis work objectives . . . . .  | 9          |
| 1.3 The thesis outline . . . . .  | 13         |
| <b>2 State of the art</b>   | <b>15</b>  |
| 2.1 On the preliminary design of large-scale thin-walled structures . . . . .   | 16         |
| 2.2 On global-local modelling approaches . . . . .  | 18         |
| 2.3 On the optimisation of constant-stiffness composite structures . . . . .  | 20         |
| 2.3.1 Single-level design approach for CSCLs . . . . .  | 21         |
| 2.3.2 Multi-level design approaches for CSCLs . . . . .   | 23         |
| 2.4 On the optimisation of variable-stiffness composite structures . . . . .  | 28         |
| 2.4.1 Single-level design approach for VSCLs . . . . .  | 30         |
| 2.4.2 Multi-level design approaches for VSCLs . . . . .   | 31         |
| 2.5 Conclusions . . . . .   | 34         |
| <b>3 Design of large-scale thin-walled metallic structures</b>  | <b>37</b>  |
| 3.1 Research article – Multi-scale optimisation of thin-walled structures by considering a global/local modelling approach . . . . .                  | 38         |
| <b>4 First experimental validation of the Multi-Scale Two-Level optimisation strategy</b>   | <b>57</b>  |
| 4.1 Research article – Least-weight composite plates with unconventional stacking sequences: design, analysis and experiments . . . . .               | 58         |
| <b>5 Design of large-scale thin-walled composite structures</b>   | <b>77</b>  |
| 5.1 Research article – A multi-scale two-level optimisation strategy integrating a global/local modelling approach for composite structures . . . . . | 78         |
| <b>6 Preliminary structural design of the PrandlePlane aircraft</b>   | <b>95</b>  |

|          |  |            |
|----------|--|------------|
| 6.1      | A modular modelling and optimisation approach . . . . .  | 95         |
| 6.2      | Least-weight design of the PrandlePlane aircraft structure . . . . .   | 98         |
| 6.2.1    | Geometry and materials . . . . .   | 98         |
| 6.2.2    | Loads and boundary conditions . . . . .  | 100        |
| 6.2.3    | Design criteria and variables . . . . .  | 102        |
| 6.3      | Finite element modelling of the PrandlePlane structure . . . . .   | 105        |
| 6.4      | Results . . . . .  | 107        |
| 6.5      | Conclusions . . . . .  | 110        |
| <b>7</b> | <b>Multi-level design of variable-stiffness composite structures</b>   | <b>113</b> |
| 7.1      | Research article – Strength and mass optimisation of variable-stiffness composites in the polar parameters space . . . . . | 114        |
| <b>8</b> | <b>Conclusions and prospects</b>   | <b>143</b> |
| 8.1      | General conclusions . . . . .  | 143        |
| 8.2      | Prospects . . . . .  | 148        |
|          | <b>Dissemination activity</b>  | <b>151</b> |
|          | Research articles published in international journals . . . . .  | 151        |
|          | Presentations in international conferences . . . . .   | 151        |
|          | Presentations in national conferences . . . . .  | 152        |
|          | <b>Thesis overview in French</b>   | <b>153</b> |
|          | Préambule . . . . .  | 153        |
|          | Le contexte de la thèse : le projet PARSIFAL . . . . .   | 153        |
|          | Les objectifs de la thèse . . . . .  | 155        |
|          | État de l’art . . . . .  | 156        |
|          | Le travail de thèse . . . . .  | 158        |
|          | Perspectives . . . . .   | 163        |
|          | <b>Bibliography</b>  | <b>165</b> |



---

# Acknowledgements

This manuscript marks the finish line of a big stage of a journey that has begun more than three years ago. I am proud of the achievement, but also aware that this would not have been possible without the contribution of many people I met during the trip; people I feel the need to thank here.

First of all, thank you to Marco, Anita and Jérôme for having accompanied me over these years, for your big availability, for the interesting exchanges (both scientific and not), for the constructive discussions we had and for all your useful advices.

Thank you to the promoters of the PARSIFAL project for having created this thesis opportunity and to all the partners for the beautiful collaborative experience.

Thank you to the reviewers and examiners for having kindly agreed to evaluate my work; it has been genuinely pleasant and constructive to exchange with you.

Thank you to the many professors, researchers, and technicians with whom I had the opportunity to interact; all highly experienced people from whom I have learned a lot.

Thank you to the trainees for having accepted the challenge of working with me on the subject of this thesis and bringing a different point of view.

Thank you to my friends. The *new ones*, which I was lucky enough to find along the way: the *'spatriati*, the *bande des ouilles*, the whole IMC gang and more. You all have been for me a real family away from home.

But thank you also to the *old* friends for your long-distance support.

Finally, it is impossible not to thank mum and dad, Luigi, all my family and Adele, for all your love and continuous support.

I hope I have been able to return even a small part of what I have received from all of you. Thank you,

*Michele Iacopo*

\* \* \*

Questo manoscritto segna l'arrivo di una grande tappa di un viaggio iniziato più di tre anni fa. Sono fiero del traguardo raggiunto, ma anche consapevole che ciò non sarebbe stato possibile senza l'apporto di molte persone incontrate durante il viaggio; persone che sento la necessità di ringraziare qui.

Innanzitutto grazie Marco, Anita e Jérôme per avermi accompagnato in questi anni, per la vostra grande disponibilità, per gli interessanti scambi (scientifici e non), per le discussioni costruttive avute e per i vostri utili consigli.

Grazie ai promotori del progetto PARSIFAL per avere creato questa opportunità di tesi ed a tutti i partner per la bella esperienza collaborativa.

Grazie ai revisori ed esaminatori per aver gentilmente accettato di valutare il mio lavoro; è stato sinceramente piacevole e costruttivo confrontarmi con voi.

Grazie ai molti professori, ricercatori, tecnici cui ho avuto occasione di interagire; tutte persone di grande esperienza da cui ho imparato molto.

Grazie agli stagisti per essersi prestati ad esplorare nuovi terreni con me ed aver apportato un punto di vista differente.

Grazie agli amici. I *nuovi*, che ho avuto la gran fortuna di trovare durante il percorso: gli *'spatriati*, la *bande des ouilles*, tutta la combricola dell'IMC e non solo. Siete stati per me una vera famiglia lontano da casa.

Ma grazie anche ai *vecchi* amici per il vostro sostegno a distanza.

Infine, impossibile non ringraziare mamma e papà, Luigi, tutta la mia famiglia ed Adele, per tutto il vostro amore e continuo supporto.

Spero di esser riuscito a restituire anche solo una piccola parte di quello che ho ricevuto da tutti voi. Grazie,

*Michele Iacopo*

## Funding

This thesis presents part of the activities carried out within the research project PARSIFAL (Prandtlplane ARchitecture for the Sustainable Improvement of Future AirpLanes), which has been funded by the European Union under the Horizon 2020 Research and Innovation program (grant agreement No. 723149).

---

# Acronyms

**AFP** Automated Fibre Placement

**ATL** Automated Tape Laying

**BC** boundary condition

**BIANCA** Biologically Inspired ANalysis of Composite Assemblages

**BLC** basic loading condition

**BWS** best wing system

**CLT** Classic Laminate Theory

**CNLPP** constrained non-linear programming problem

**CSC** constant-stiffness composite

**CSCL** CSC laminate

**DA** deterministic algorithm

**DC** design criterion

**DLR** German Aerospace Center (Deutsches Zentrum für Luft- und Raumfahrt)

**DOMES** Deterministic Optimisation of Macroscopic laminatEs via Splines

**ELF-PAM** ELliptical Fuselage PArametric Models

**ENSAM** Arts et Métiers Institute of Technology (Ecole Nationale Supérieure des Arts et Métiers)

**ERASMUS** EvolutionaRy Algorithm for optimiSation of ModUlar Systems

**FE** finite element

**FSDT** First-order Shear Deformation Theory

**FUO** fuselage optimisaion

**GA** genetic algorithm



**GFEM** global FE model

**GL** global-local

**HESLT** Higher-order Equivalent Single Layer Theory

**ICAO** International Civil Aviation Organization

**LC** load case

**LFEM** local FE model

**LFI** Laminate Failure Index

**LL** Limit Load

**LP** Lamination Parameter

**LSO** lifting system optimisation

**MS1** MileStone 1

**MS2LOS** Multi-Scale Two-Level optimisation strategy

**MSOS** multi-scale optimisation strategy

**NURBS** Non-Uniform Rational B-Spline

**PARSIFAL** Prandtlplane ARchitecture for the Sustainable Improvement of Future Air-  
pLane

**PP** Polar Parameter

**PrP** PrandtlPlane

**QT** Quasi-Trivial

**SE** super element

**TLAR** top-level aircraft requirement

**UL** Ultimate Load

**UNIFI** University of Pisa

**VAT** variable angle tow

**VSC** variable-stiffness composite

**VSCL** VSC laminate

**WP** work package

**ZOI** zone of interest

---

# Preamble

*Voi, speculatori, non vi fidate delli autori che hanno sol co' l'immaginazione voluto farsi interpreti fra la natura e l'omo, ma sol di quelli che, non coi cenni della natura, ma co' gli effetti delle sue esperienze hanno esercitato i loro ingegni.*

---

Leonardo da Vinci

## 1.1 The thesis context: the PARSIFAL project

In the last decades, the passengers air traffic has seen a remarkable increase. Historical data show that the number of annual revenue passenger kilometres<sup>1</sup> has experienced an almost steady logarithmic growth, with an average annual increase of 4.3%, thus a doubling every fifteen years (Airbus s.a.s., 2019). The recent COVID-19 outbreak surely had a strong impact on the air transport market (Pearce, 2020b), but this market has shown a strong resilience to external economic shocks in the past and, according to recent forecasts, the global trend is not expected to be considerably affected in the long term (Pearce, 2020a). The air transportation market has to face this constant increase in demand in a challenging context. In fact, most of the actual airport infrastructures are already congested with very limited or no expansion possible, especially in Europe. Moreover, the regulation about the aircraft environmental impact (both in terms of noise and emissions) becomes increasingly restrictive. The conventional *tube and wing* aircraft configuration has seen big improvements in the last decades but is now reaching its maximum potential with small margins left for the improvement of its performances. This scenario is pushing for the development of innovative and disruptive aircraft configurations.

PARSIFAL (Prandtlplane ARchitecture for the Sustainable Improvement of Future AirpLane) is a research project<sup>2</sup> funded by the European Union under the Horizon 2020 Research and Innovation program, started in May 2017 and concluded in July 2020. It aimed at proposing a solution for the challenges that the aeronautic industry is facing. Eight partners, from four European countries, have collaborated in the PARSIFAL project: University of Pisa (UNIPi), the project coordinator, from Italy, the French aerospace research

---

<sup>1</sup>Usually referred to as RPKs: it is the cumulative number of kilometres flown by passengers for whose transportation an air carrier receives commercial remuneration.

<sup>2</sup>[www.parsifalproject.eu](http://www.parsifalproject.eu)



Figure 1.1: Artistic representation of a PrandtlPlane aircraft.

centre ONERA in Paris and the Arts et Métiers Institute of Technology of Bordeaux-Talence (ENSAM) in France, the Delft University of Technology (TUD) in Netherlands, the German Aerospace Center (DLR), and the company SkyBox Engineering in Italy. Moreover, an advisory board made of independent consultants from aviation industry and representatives of aircraft manufacturers (Leonardo, Airbus), airport management companies (Milan and Tuscany airports) and airlines (KLM) supported the research activities by representing the market interests.

The solution proposed in PARSIFAL is the *PrandtlPlane* configuration, shown in an artistic representation in Fig. 1.1.

About one century ago, Prandtl (1924) identified in a comparative study a lifting system with a box configuration in the front view, that he called the *best wing system* (BWS). Such configuration is the *best solution* minimising the induced drag among all the possible lifting systems sharing the same span and the total amount of lift. Few decades later, Frediani and Montanari (2009) have shown that a closed-form-solution of the minimum induced drag problem exists, proving Prandtl's finding. The BWS application to aircraft of different category and size has been studied at University of Pisa since the 1990s. In honour of Prandtl, aircraft with such a box wing configuration have been called PrandtlPlane (PrP).

For a large aircraft, the induced drag constitutes 40-45% of the total drag during cruise and about 80% during take-off. By employing the PrP configuration, a reduction of such component of about 20-30% can be achieved for typical applications. The consequent increase in aerodynamic efficiency (the ratio between lift and drag) can either be used to reduce fuel consumption (for a given payload-mission scenario) or to increase the payload capability (for a given set mission-fuel consumption). In both cases, this results in a reduction of the environmental impact and the cost per passenger.

The main goal of the PARSIFAL project was to demonstrate the feasibility of the introduction of the PrP configuration into the market, and the interest in doing so. This feasibility study has been conducted by the different partners assessing different aspects: economic, aerodynamic, architectural, structural, environmental, propulsive, flight mechanics, etc. In the early phases of the project, a preliminary market analysis has been con-

ducted (PARSIFAL Project Consortium, 2017a). A forecast on the air traffic demand has been produced, setting the time horizon to 2032: the main results are reported in Fig. 1.2. According to these results, most of the future demand increase will be on connections in

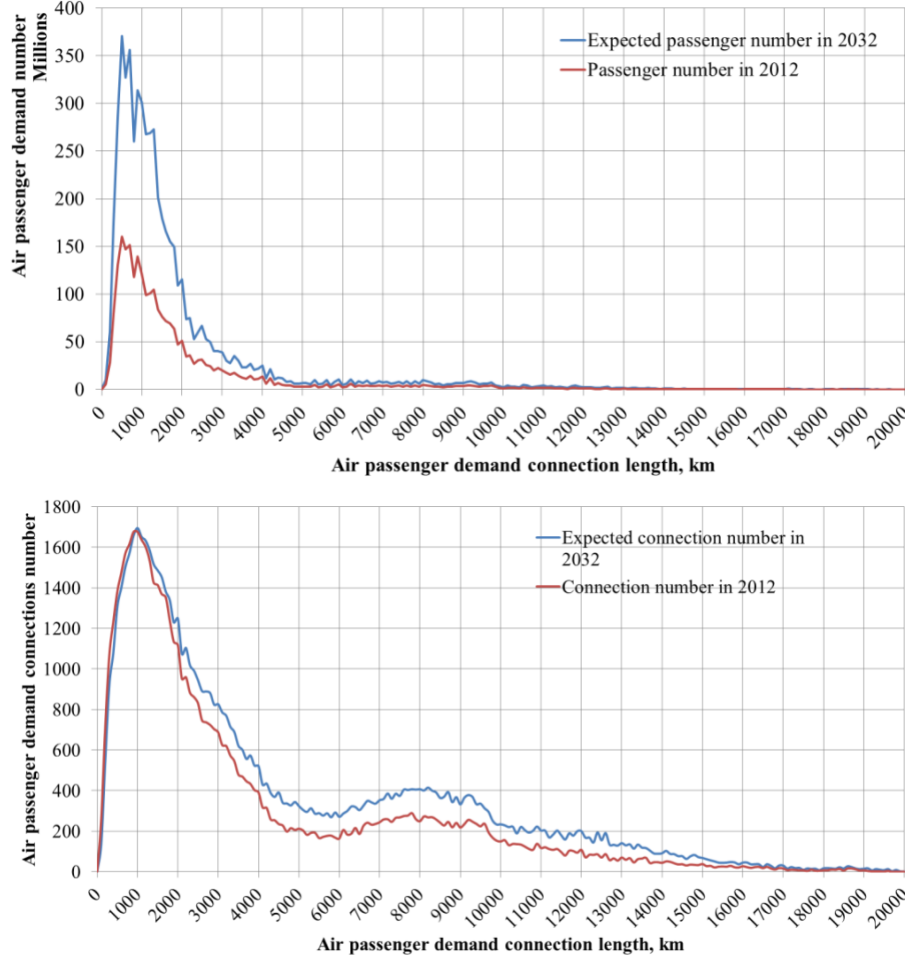


Figure 1.2: Forecast on the air passenger demand distribution in 2032, in comparison to the contemporary one (connections with more than a thousand annual passengers) (PARSIFAL Project Consortium, 2017a).

the range from 500 to 4000km. These connections are, nowadays, mainly ensured by airplanes belonging to the Airbus A320 and the Boeing 737 (B737) families and operated on airports respecting the International Civil Aviation Organization (ICAO) aerodrome reference code 4C specification (where 4 indicates a take-off field length greater than 1800m and C refers to a maximum wingspan of 36m). These results have driven the identification of the best market segment to be targeted in the project: it is described through a set of target performances called *top-level aircraft requirements* (TLARs), which are presented in Tab. 1.1 (PARSIFAL Project Consortium, 2017a, 2020a). These TLARs identify an aircraft which operates on the same short-to-medium routes (below 4000km) of the A320/B737 aircraft families, having the same overall dimensions, but able to transport about 50% more passengers (a capacity typical of larger aircraft like the A330/B767). It corresponds to a market segment previously unexplored, as it can be clearly seen by placing the PARSIFAL proposition in the pax-range diagram of the contemporary aircraft

## 1. PREAMBLE

Table 1.1: Top-Level Aircraft Requirements considered in the PARSIFAL project (PARSIFAL Project Consortium, 2017a, 2020a).

| Requirement  | Value       |
|--|-------------|
| Maximum passenger number (full density)                          | 320         |
| Minimum passenger number @MTOW <sup>1</sup>                      | 250         |
| Maximum range at max payload (harmonic range) [km]               | 4000        |
| Minimum cruise Mach  | 0.78        |
| Initial Cruise Altitude (ICA) [kft (km)]                         | 36.0 (11.0) |
| Maximum operating cruise altitude [kft (km)]                     | 38.5 (11.7) |
| Time to climb from 1500 ft to ICA [min]                          | 35          |
| Maximum take-off field length at sea level (SL) [m]              | 2200        |
| Landing distance @(MLW <sup>2</sup> , SL, ISA <sup>3</sup> ) [m] | 1850        |
| ICAO aerodrome reference code - aircraft approach category       | 4C - C      |
| Engine number  | 2           |

<sup>1</sup> Maximum Take-Off Weight

<sup>2</sup> Maximum Landing Weight

<sup>3</sup> International Standard Air

market (Fig. 1.3). The main reason for this has to be searched in the technological limitations that the PARSIFAL project aims to overcome. These requirements brought to the

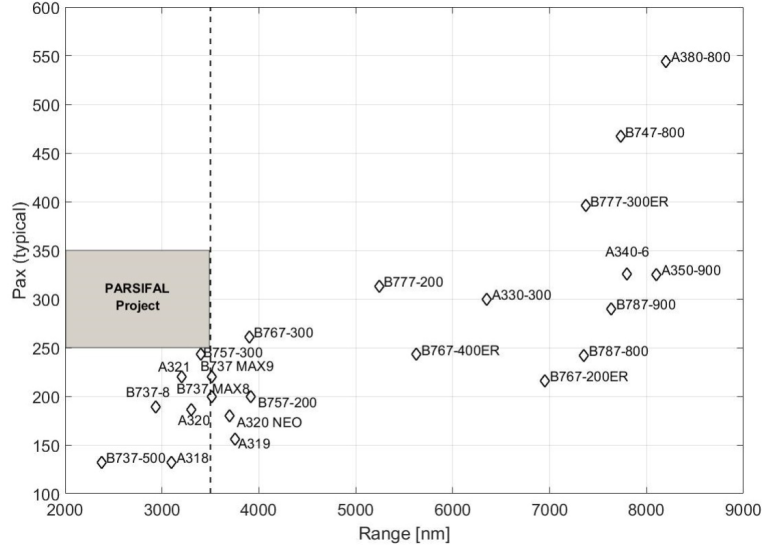


Figure 1.3: Placement of the PARSIFAL proposal in the pax-range diagram of the contemporary aircraft market (limited to the two main manufacturers) (PARSIFAL Project Consortium, 2017b).

definition of the PARSIFAL proposed configuration, whose main features are presented in Tab. 1.2, in which the PrP is also compared to a conventional competitor aircraft, while some visual representations are provided in Figs. 1.4 and 1.5.

The principal effects of the introduction of the PARSIFAL proposal into the market and its use instead of a typical single aisle aircraft, can be summarised as follows (PARSIFAL

Table 1.2: Main features of the PARSIFAL proposal in comparison to a conventional competitor aircraft (PARSIFAL Project Consortium, 2020a).

| Feature                            | PrP   | A321 NEO |
|------------------------------------|-------|----------|
| Maximum take-off weight [tons]     | 126   | 97       |
| Wingspan [m]                       | 36    | 35.6     |
| Overall length [m]                 | 44.3  | 44.51    |
| Overall height [m]                 | 9.43  | 11.76    |
| Fuselage height [m]                | 4.17  | 4.14     |
| Fuselage width [m]                 | 5.39  | 3.95     |
| Maximum passengers                 | 308   | 240      |
| Cabin layout                       | 2-4-2 | 3-3      |
| Max. capacity of LD3-45 containers | 12    | 10       |

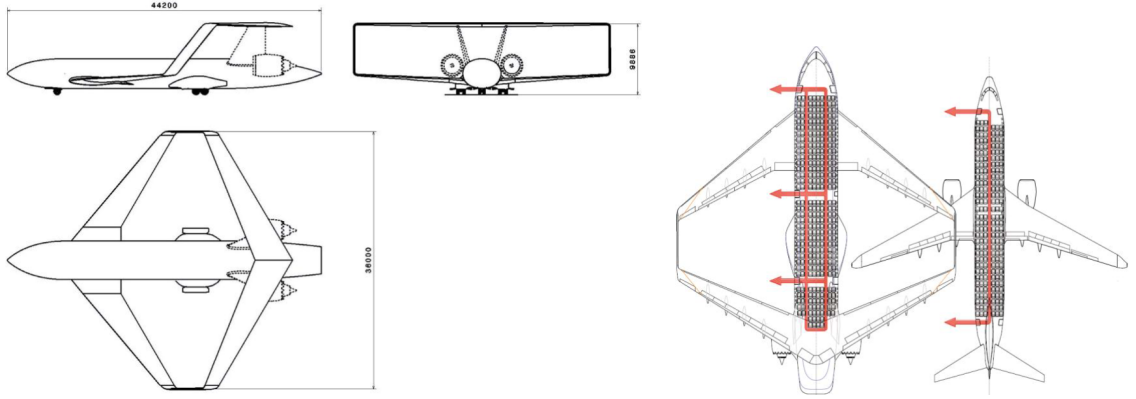


Figure 1.4: Three views of the PARSIFAL proposal (left) and comparison between its interior layout and exit paths and those of a typical single aisle configuration (right) (PARSIFAL Project Consortium, 2018).

Project Consortium, 2020a):

- Environmental impact:
  - Emission reduction per passenger up to 20% for carbon dioxide ( $CO_2$ ), water vapour and sulphur dioxide ( $SO_2$ ), greater than 15% for unburned hydrocarbons (HC), negligible for nitrogen oxides ( $NO_x$ ).
  - Up to 17% and 18% reduction of the Global Warming Potential on 20- and 100-years horizon (GWP20 and GWP100), respectively.
  - Up to 23% and 20% reduction of the Global Temperature change Potential on 20 and 100 years horizon (GTP20 and GTP100), respectively.
  - reduction of the average level of noise for a given airport and daily passenger traffic.
- Productive impact:
  - Increase from less than 200 to more than 300 available seats without changing the required airport apron space or, alternatively, an up to 15% reduction in the required apron space to transport a given number of passengers.

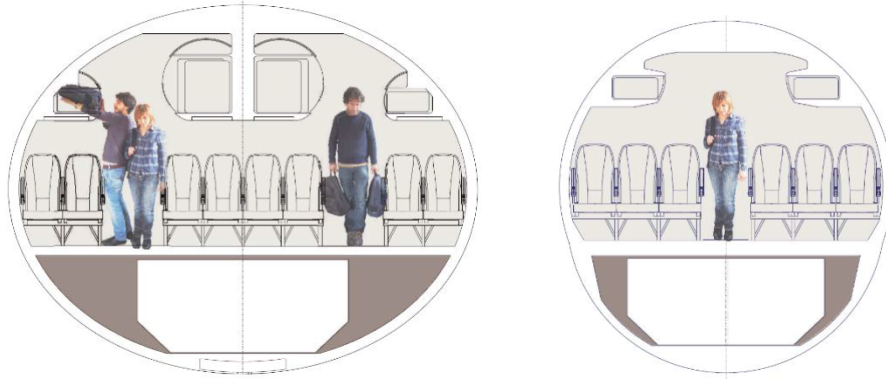


Figure 1.5: Comparison between the cabin section of the PARSIFAL proposal (left) and that of a typical single aisle configuration (right) in the high-density arrangement (PARSIFAL Project Consortium, 2018).

- Reduction of fuel consumption per RPK up to 20% with respect to aircraft belonging to the A320/B737 family.
- Economic impact:
  - Possibility to reduce the average ticket price up to 13% while keeping the same break-even point or, alternatively, to increase the produced value, thanks to the reduction of the cost per available-seat-kilometre.
- Logistic impact:
  - Small increase in turnaround time (11% outstation, 25% full service) for a higher payload capability (+63% passengers, +71% containers).
  - Compatibility with present ICAO 4C airports infrastructures.

These outcomes are the results of several underlying improvements and innovations made by the project partners, not only limited to the aerodynamic idea which motivated the project. In fact, besides the reduction of the induced drag, the PrP configuration brings other interesting advantages and opportunities: an increased safety thanks to a smooth stall behaviour and a post-stall phase characterised by only a partial reduction of manoeuvrability and controllability; a pitch damping higher than that of a conventional configuration, which results in more comfort and safety; the possibility to adopt innovative manoeuvre schemes like the *direct lift control*<sup>3</sup> and the *pure couple control*<sup>4</sup> thanks to the ability to accommodate control surfaces on both the front and rear wing; the ability to design a lighter structure taking advantage of the peculiar architecture; the possibility to evaluate the employment of different innovative propulsion solutions. On the other hand, the newness of the proposed configuration makes historical statistical data and known established solutions not *a priori* trustworthy, or not applicable at all. This has constituted a major challenge in the PARSIFAL project, but also a stimulus for the development of new knowledge and design methods. It is especially true for the structural design of the aircraft, since, unlike what happen in conventional configuration, the fuselage and the lifting system are over-constrained.

---

<sup>3</sup>The ability to alter the amount of lift without affecting the pitch moment.

<sup>4</sup>The ability to generate a pure pitch moment without altering the lift.

The project was organised into eight different work packages (WPs), organically distributed among the partners, with multiple interactions (see Fig. 1.6). ENSAM Bordeaux

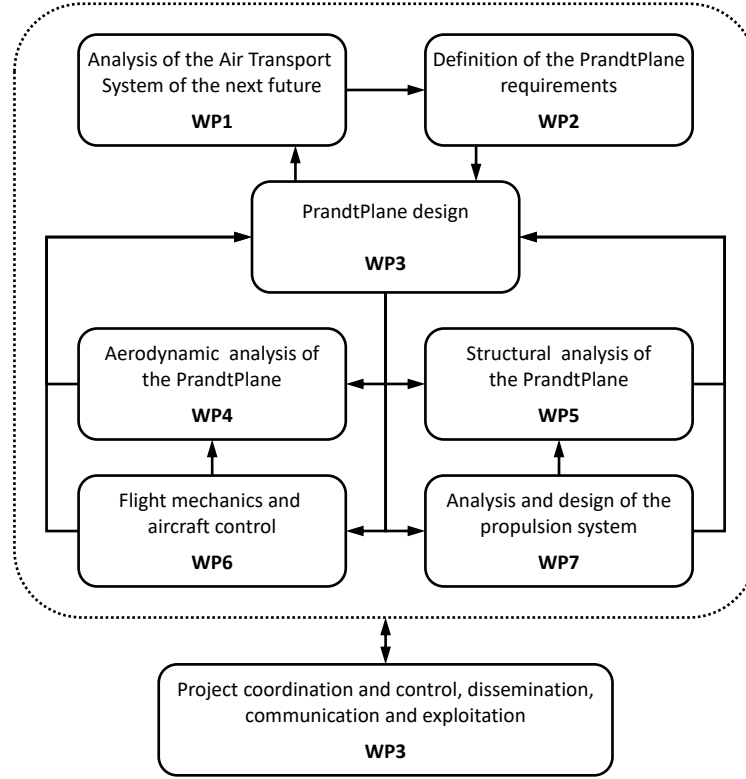


Figure 1.6: PARSIFAL working packages and their interactions.

was the leader of the WP5, entitled *Structural Analysis of the PrandtlPlane*, which has been carried out in collaboration with UNIPi and DLR. The main initial input of the activities of this WP was the definition of a reference configuration of the PrP, internally referenced by the project partners as MileStone 1 (MS1). It was the result of the conceptual design phase carried out, in accordance with the TLARs presented in Tab. 1.1, by SkyBox and UNIPi with the contribution of all the other partners in the context of the activities of WP3 (*PrandtlPlane Design*). MS1 notably included initial versions of macroscopic geometrical data (the cabin layout, the aircraft external geometry, the internal volume available for structural components), of inertial data (the location and mass of the landing gears and the engines and estimates about the mass distributions of all other on-board systems), of aerodynamic loads distributions. A first-guess sizing of the structural components, to be used for the initial activities of WPs other than the WP5, was also provided, obtained by manual adjustment exploiting information coming from both first-approximation models (e.g. beam-like models) and finite element (FE) analyses, and considering a limited set of design requirements.

The activities of WP5 had four main objectives:

1. To develop innovative optimisation procedures to be employed for the preliminary design of aeronautical structures, either metallic or composite. Such optimisation procedures should be able to:

- 1.1. Overcome the limitations of current common-use optimisation procedures for



- large-scale thin-walled (composite) structures and properly deal with the hyperstatic nature of the PrP architecture.
- 1.2. Effectively integrate all relevant design requirements in this design phase (notably, requirements related to the manufacturability of innovative composite solutions made of variable stiffness laminates and constant-stiffness blended ones), in order to maximise the compliance of the obtained solutions with the following design phases.
  2. To validate the developed optimisation procedures:
    - 2.1. Numerically, through the solution of benchmark problems taken from literature.
    - 2.2. Experimentally, through tests on simple composite structures and on composite stiffened panels.
  3. To perform a preliminary structural design of the PrP, for both a metallic variant and a composite one, employing the developed optimisation procedures and targeting, in particular:
    - 3.1. The main structural components of the fuselage.
    - 3.2. The main structural components of the lifting system.
  4. To verify the compliance of the optimal metallic PrP with respect to aeroelasticity requirements.

All the related activities have been carried out at ENSAM, except for those related to Objective 4, which have been performed by UNIPi and University Carlos III of Madrid, in the role of UNIPi's subcontractor. Concerning the activities related to Objective 3, the connection regions between the fuselage and the lifting system have only been modelled through low-fidelity FE models at ENSAM, while a *design of experiments* activity, based on a more detailed modelling, has been carried out by J.-N. Walther at DLR.

The team involved in the PARSIFAL activities carried out at ENSAM is composed of several people, all members of the Mechanical Engineering and Design (IMC) department of the Bordeaux Institute of Mechanical Engineering (I2M):

- Marco Montemurro, full professor at ENSAM Bordeaux. Co-author of the project proposal, he is the main supervisor of the PARSIFAL activities carried out at ENSAM. With Anita Catapano, associate professor at Bordeaux INP, they are at the origin of the *multi-scale two-level* optimisation strategy, a key ingredient of the optimisation procedures for composite structures proposed in the WP5.
- Jérôme Pailhès and Nicolas Perry, full professors at ENSAM Bordeaux, and Elise Gruhier, associate professor at ENSAM Bordeaux. Supervisors of the PARSIFAL activities carried out at ENSAM.
- Enrico Panettieri, associate professors at ENSAM Bordeaux. He is the ENSAM front-man and manager of the activities related to the PARSIFAL project. He contributed to the initial formulation of part of the innovative multi-scale optimisation procedures proposed in the WP5 and to their application to the PrP structure, with a focus on the modelling of the connection regions; he worked on the initial formulation of manufacturing requirements for the design of composite structures with blended laminates; he worked on the experimental activity on composite stiffened panels.

- Michele Iacopo Izzi (the writer). Ph.D. fellow at ENSAM Bordeaux. He worked on the formulation of innovative multi-scale optimisation procedures, to their numerical validation, and to their application in the design of the PrP structure, with a focus on its fuselage; he carried out the experimental validation activities; he worked on the development of numerical tools for the optimisation of variable-stiffness composite structures.
- Marco Picchi Scardaoni. Ph.D. student at UNIPi and ENSAM Bordeaux. He joined the ENSAM team halfway through in the context of a joint supervision PhD program. He worked on the application of the previously developed multi-scale optimisation procedures to the PrP lifting-system structure and to a first adaptation for their use in a deterministic optimisation context. He worked on an improved formulation of the manufacturing requirements for the design of composite structures with blended laminates.

The one presented above is the context in which the work described in this PhD thesis took place.

## 1.2 The thesis work objectives

The problem of the preliminary design of thin-walled structures, either metallic or composite, typical of the aeronautical field is addressed in this Ph.D. thesis.

Mass control is a major concern in the aeronautical field, and the structural design problem is often formulated as a constrained optimisation problem, usually in the form of the weight minimisation of the structure subject to a set of mechanical and geometrical requirements. The *semi-monocoque* architecture (of which an example is shown in Fig. 1.7) have soon become a standard choice for the structures of both the fuselage and the wing, thanks to their inherently favourable stiffness-to-weight ratio. This structure



Figure 1.7: View of a structure having a semi-monocoque architecture: a fuselage structure.

architecture is a modular one, composed of sub-structures (the *stiffened panels*), which are made, in turn, of thin plates. For their nature, structures of this type present two characteristic scales at which different phenomena take place, which corresponds to just as many requirements involved in the design process. Requirements related to the structure

mass, to its stiffness, to aeroelastic phenomena, are formulated at the *global scale* of the structure, i.e. the scale of the whole aircraft. At the *local scale*, i.e. the scale of the stiffened panels and of the plates of which the wing and fuselage architectures are composed, other phenomena take place, like those related to the buckling behaviour and to the strength of the structure. Each scale (and each phenomenon to be assessed) has distinct needs in terms of modelling, so, in order to have a good computational efficiency, different models must be employed (Venkataraman and Haftka, 2004). The various procedures available for the design of these structures differentiate in the way each scale is handled and the scale transition is managed. The main limitations observed in common-use design procedures are essentially related to these two aspects: in particular, the non-optimal definition of the design variables involved in each scale, the limited accuracy of the methods employed for the assessment of the structure responses, a poor information transfer between modelling scales (Grihon et al., 2009a). The formulation of a proper *multi-scale* optimisation procedure is needed for the correct design of this type of structures.

In the continuous pursuit for lightness of the aeronautical domain, mainly due to the high specific stiffness and strength they offer, composite materials are earning increasingly attention. In most recent aircraft, like the Airbus A350 XWB and the Boeing 787, composite materials constitute about half of the aircraft weight and the main structural components are made of high-performance composite laminates<sup>5</sup>. Despite their large use, there still is a lack of knowledge concerning composite materials (notably concerning the way to optimise them), which results in a low cost-effectiveness of their use and in a limited exploitation of their interesting properties (Petrolo, 2019). Composite laminates present *per se* a multi-scale behaviour that leads to the identification of three characteristic scales: the *microscopic scale*, governed by the properties of the constituent phases (fibres and matrix), and by their interaction; the *mesoscopic scale* of the plies, seen as equivalent homogeneous anisotropic layers; the *macroscopic scale* of the laminate, where an equivalent homogeneous anisotropic single-layer plate is considered. Designing composite laminates with the best possible structural efficiency requires elastic tailoring, i.e. the optimisation of both their geometric form and their material properties. The historical approach of directly optimising the plies orientations, hence acting at the mesoscopic scale of the laminate in order to meet requirements mostly formulated at the macroscopic one, presents a number of weaknesses. The number of design variables, being directly proportional to the number of layers, rapidly increases when a thick laminate is considered and/or multiple laminates have to be optimised at the same time, moreover, when designing for lightness, the number of layers composing the laminate and, accordingly, the number of design variables is itself a design variable; the design problem formulated with respect to such design variables usually results highly non-convex. Finally, as a consequence of the aforementioned lack of knowledge, it is common-practice to enforce restrictions on the nature of the stacking sequences, either in the form of sufficient but not-necessary conditions to avoid some undesired elastic couplings in the laminates behaviour, or as experience-based guidelines to limit crack propagation and delamination, which further complicate the design problem.

*Multi-level* design strategies try to overcome some of these problems. These strategies allow formulating and solving the optimisation problem at the macroscopic and mesoscopic scales in (at least) two sequential levels: firstly, the structural optimisation is performed in terms of macroscopic properties of the laminate, through a suited representation; then,

---

<sup>5</sup>Here, *high-performance composite laminates* refers to layered plates made of plies containing long continuous straight (non-woven) fibres.

the laminate lay-up design is carried out by retrieving suitable stacks corresponding to the optimum macroscopic properties of the laminate. Of course, feasibility conditions have to be enforced during the first level in order to ensure the existence of a solution of the second one. The Multi-Scale Two-Level optimisation strategy (MS2LOS), firstly introduced by Montemurro et al. (2012a,b), is one of such strategies, and is the one embraced in this work.

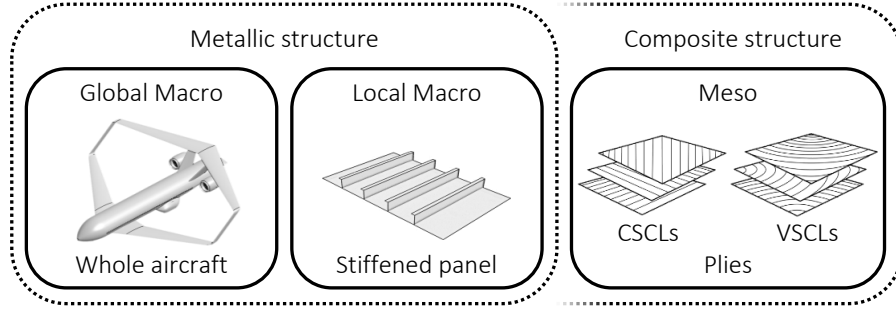


Figure 1.8: Considered characteristic scales of a typical large-scale thin-walled (composite) structure.

When a large-scale thin-walled composite structure is considered, the designer has to deal with the multi-scale nature of both the structure architecture and the employed material (Fig. 1.8). Although for the assessment of most of the phenomena described above, both at the structure global and local scales, a macroscopic description of the laminate is enough, the failure phenomenon of composite materials is usually evaluated at the mesoscopic scale and the definition of the laminates stacking sequences is a key step of the design process of these structures. Concerning the microscopic scale, even if some relevant phenomena happen at this scale too, it is not object of study in this thesis and is, thus, disregarded in the following. In the context of the typical conceptual-preliminary-detailed design phases organisation, it is of paramount importance to ensure maximum consistency between the preliminary results and the final product: the following detailed design phase should enrich the preliminary results and not *repair* them (Grihon et al., 2009a). This is especially true when dealing with composite materials within multi-level design/optimisation procedures: it must be ensured that the final solutions correspond to a structure that not only respects all considered design criteria, but is also manufacturable, hence the need to consider manufacturability requirements since the early design stages.

Moreover, when dealing with a PrP aircraft, a further complication arises. Separating the design of the fuselage from that of the wings does not ensure to obtain a correct design of the entire structure because of the peculiar nature of the PrP architecture. Designing the fuselage and the wings as isolated parts could even lead to infeasible solutions: for the correct assessment of the structural responses of the PrP, the whole structure has to be modelled. Furthermore, the number of design variables needed for the description of the lifting system is naturally higher for such an aircraft than for a conventional one, since two main wings are present. Consequently, the computational effort needed to deal with such a great number of design variables all at once, and with the whole aircraft model, can easily overcome the capabilities of the IT infrastructure typically available into a research laboratory.

The formulation of new procedures for the preliminary design of large-scale thin-walled composite structures must deal with all the aforementioned aspects. The first main ob-

jective of this work is to overcome some of the limitations identified in common-use design procedures with the final aim to obtain better-performing structures of this type.

Only constant-stiffness composite (CSC) laminates (CSCLs), i.e. laminates having uniform macroscopic mechanical properties across their surface, have been considered above. However, a complete exploitation of the composites potential cannot be achieved by limiting the study to this class. To take full advantage of the directional properties of the basic material (i.e. the fibre-matrix set), the mechanical properties must be tailored locally over the laminate surface, obtaining a new generation of high-performance composite laminates, i.e. the variable-stiffness composite (VSC) laminates (VSCLs). The bigger the stress gradients in the laminates composing the structure, the higher the performance gains obtainable by adopting such class of composite materials. Various formats of laminates have such property. In this thesis the focus is put on variable angle tow (VAT) laminates: layered plates made of constant-thickness plies containing long continuous ordered steered fibres. Manufacturing processes to obtain them are quite recent and still present some specific limitations. The development of suited design procedures for structures made of VSCLs is essential to foster their broad adoption in the industry. Such design procedures should not only consider all the aspects presented above for CSCLs, but they should also efficiently deal with design variables that assume the form of distributions across the laminate surface. This brings to an important increase in their number, and ensuring the continuity (and the smoothness) of the field becomes a task of capital importance. Finally, as in the case of CSCLs, the integration of process-related manufacturability requirements since the early stage of the design process is fundamental to reduce the gaps between the various design phases.

The second main objective of this work is the development of a design procedure, and the related numerical tools, for the concurrent optimisation of geometrical and material design variables describing VSCLs.

Three main phases can be identified in this work:

1. First, the focus is put on large-scale thin-walled metallic structures. This choice allows to only target the global and local scales and the information transfer among them. A multi-scale optimisation strategy (MSOS) that relies on FE analyses employing a global-local (GL) modelling approach has been developed in this phase. The assessment of the phenomena happening at both scales is carried out through dedicated FE models that ensure the required level of accuracy, while the adoption of a GL modelling approach guarantees coherence among the various models and contributes keeping the computational effort low. The solution search is carried out by means of a genetic algorithm that combines exploration capability and information exploitation to find the true global optimum solution.
2. Then, the possible performance gain obtainable by employing straight-fibre composite laminates in these structures is evaluated. An additional working scale, the mesoscopic scale of the composite material, is considered here, while a macroscopic description of the laminates is employed at the global and local ones. The additional layer of complexity represented by the possibility of optimising the material properties as well as the geometrical ones of the structure, is faced by integrating the aforementioned GL modelling approach into a multi-level design strategy, the MS2LOS. Here also, a genetic algorithm is employed to carry-out the solution search.
3. Finally, the possibility to better exploit the directional properties of high-performance composite materials through the concept of VSCLs is investigated. The problem

of the efficient optimisation of this type of structures is studied. Specific theoretical and numerical design tools are developed here, still in the framework of the MS2LOS. The focus is shifted on lower scale structural components. Due to the characteristics of the optimisation problem formulated for these structures, the use of meta-heuristic algorithms for the solution search can be inefficient and can lead to sub-optimal solutions. Therefore, a deterministic algorithm (DA) is here used instead. To cope with this choice, the analytic expression of the gradient of the response functions associated to all requirements considered in the optimisation process has been derived. Requirements on strength, mass, maximum tow curvature, and buckling load have been considered. Concerning the latter, an initial study (Fiordilino, Izzi, and Montemurro, 2021), not reported in this thesis, has been conducted in collaboration with Ph.D. student G. A. Fiordilino.

All the methodologies and tools developed in these phases have been validated, either numerically, by applying them to benchmark structures taken from the literature, or through experimental activities. Most of them have also been applied to the preliminary design of the structure of the PARSIFAL proposal; this has required specific actions to account for the PrP configuration having an internally over-constrained structure.

### 1.3 The thesis outline

The thesis is organised in seven chapters.

Chapter 2 presents an overall literature survey on the various topics studied in this work.

Chapters 3-7 present the core activities of the thesis, covering the different phases of the work described shortly above. In Chapters 3-5 and 7, the content is presented by directly reporting the related article, published in an international journal.

More in detail, in Chapter 3, the GL-MSOS is presented and numerically validated through the solution of the least-weight design problem of a reference metallic fuselage barrel taken from the literature.

An experimental activity is presented in Chapter 4: through the design, analysis and testing of non-conventional straight-fibre composite plates, a first experimental validation of the MS2LOS is achieved.

The combination of the GL-MSOS and of the MS2LOS results in the definition of the GL-MS2LOS for large-scale thin-walled composite structures, which is presented and numerically validated in Chapter 5. Here the optimisation of the same reference fuselage barrel introduced in Chapter 3, this time made of straight-fibres composite laminates, is performed.

In Chapter 6, the developed optimisation strategies are applied to the over-constrained structure of the PrP aircraft proposed in the PARSIFAL project.

The focus is shifted on structures made of VSCLs in Chapter 7, where specific tools for their optimal design are developed. The theoretical framework of the MS2LOS is enriched to deal with requirements on strength, mass, and maximum tow curvature. A numerical platform for the deterministic optimisation of VSCLs is developed and tested on benchmark problems taken from literature. The concept of variable-thickness VSCLs is also investigated in this chapter.

Chapter 8 ends this thesis with some general conclusions and prospects of this work.



---

## State of the art

As introduced in Chapter 1, this thesis deals with the preliminary design of large-scale thin-walled composite (and metallic) structures typical of the aeronautical field. These semi-monocoque structures present multiple working scales, of which three are considered in this work:

**The global macroscopic scale** of the whole aircraft, where a macroscopic description of the laminates behaviour is employed.

**The local macroscopic scale** of the stiffened panels and of the plates composing the fuselage and wing architectures, where the laminates behaviour is described macroscopically.

**The mesoscopic scale** of the plies, seen as equivalent homogeneous anisotropic layers.

In order to optimise this type of structures, a suited multi-scale design procedure must be developed, which is able to combine, on the one hand, a proper handling of the three characteristic scales and their interactions, and, on the other hand, computational efficiency.

The current standard format of composite materials employed when high structural performances are required is the CSCL, i.e. a layered plate made of plies containing long continuous straight (non-woven) fibres. Both the geometrical and the material properties of each laminate composing a CSC structure can be tailored (uniformly over the laminate surface) to the design needs, unlocking new margins of improvement in their optimisation with respect to metallic counterparts.

Wider tailoring possibilities are offered when adopting the VSCL format, made possible by the recent developments in manufacturing processes. In this case, a point-wise variation of the geometrical and the material properties across each laminate is possible. Both the CSCL and the VSCL formats give a new, unprecedented freedom to the designer, but also open new challenges to be faced during the design process.

In this chapter, the state of the art about the development of design strategies that allow facing these challenges is presented.

In Sec. 2.1, the focus is put on the management of the link between the global and the local scales characterising large thin-walled structures. In this context, of course, the metallic variant of these structures, which can be seen as a sub-case of the most general anisotropic material one, does not require the definition of a mesoscopic scale.

In Sec. 2.2 an overview on global-local modelling approaches, one of the key ingredients of the optimisation procedure presented in this thesis, is provided.



In Sec. 2.3, a literature survey about strategies for the optimisation of CSC structures is provided, focusing on the challenges related to the link between the macroscopic and the mesoscopic scales of these structures.

In Sec. 2.4, the specificities of VSCLs are targeted by presenting the state of the art on strategies for their optimal design.

Finally, Sec. 2.5 ends this chapter with some concluding remarks.

At the end of these sections, when relevant, some notes about the correct bibliographic placement of the various parts of the work presented in this thesis are provided.

**Remark.** *Because of the article-based format chosen for this thesis, most of the information provided in this chapter is also present in the journal articles reported in Chapters 3-5 and 7. In each article the relevant information needed for the correct bibliographic placement of the corresponding part of the work is briefly provided.*

## 2.1 On the preliminary design of large-scale thin-walled structures

The preliminary phase of aircraft structural design is mostly based on analytical or semi-empirical methods. Such methods have been developed since 40s especially in USA (Gerard, 1958; Kuhn et al., 1952; Wignot et al., 1944) and have been continuously improved during the years until becoming an established reference for aircraft designers (Bruhn, 1973; Niu, 1988; Rivello, 1969; Williams, 1960). These methods are based on several simplifying hypotheses. For example, when dealing with the fuselage design, at the global scale circular cross-sections are considered, whose geometry and boundary conditions (BCs) are symmetric with respect to the aircraft longitudinal plane. Stringers are taken into account by considering a homogeneous skin of equivalent thickness (greater than the true thickness of the skin) or by considering *lumped* models, in which multiple physical elements are represented by only one finite element<sup>1</sup>. When pressurisation is taken into account, the classical equations for axial-symmetrical infinite vessels with regularly spaced frames are used (Bruhn, 1973). At the stiffened panel scale, for the calculation of buckling loads, plane or curved plates with uniformly loaded edges and perfect BCs (usually in the form of simply supported edges) are considered; the stringers are considered as isolated elements and the Euler column buckling equations are used (Anderson and Takahashi, 2017; Niu, 1988).

Preliminary design procedures for thin-walled structures have been developed integrating the aforementioned methods into sequential (Anderson and Takahashi, 2017) or iterative procedures (Boni, 2004; Boni and Fanteria, 2004; Grihon et al., 2009b), of which an example is reported in Fig. 2.1. The solution is searched by means of DAs using an initial guess solution chosen by means of handbook methods. In order to properly exploit the effectiveness of the gradient-based algorithm, the number of design variables is reduced by *slaving* or *linking* them together, sometimes enforcing fabrication requirements, more often using experience or simplified empirical rules. For example, the shape of the cross-section of stiffening elements is set *a priori*, with only a scaling factor used to size them. Of course, this approach extremely shrinks the design domain and, in conjunction with the use of DAs for the solution search, results in the unlikelihood of finding the true global optimum solution of the design problem.

---

<sup>1</sup>For example using a single *equivalent* rod element for taking into account the presence of four consecutive stringers.

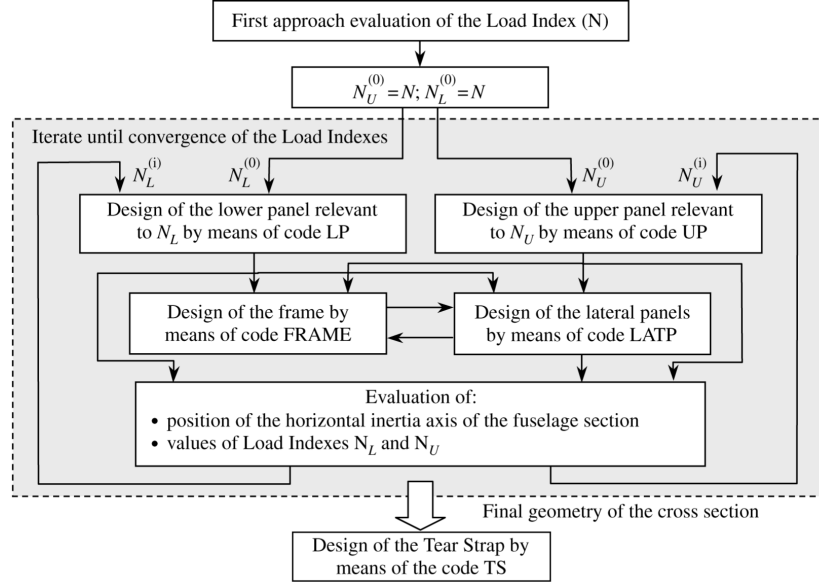


Figure 2.1: Classical integrated iterative design procedure for a fuselage section from literature (Boni and Fanteria, 2004). LP, UP, LATP, FRAME, and TS are the codes for the deterministic optimisation of the lower fuselage panel, the upper fuselage panel, the lateral fuselage panel, the frame cross section, and the tear strap, respectively.

Several works on improved analytical or numerical methods for predicting the mechanical response of stiffened panels, especially regarding the buckling and post-buckling behaviour of such components (Hughes et al., 2004; Loughlan, 1994; Stamatelos et al., 2011) can be found in literature. However, the aforementioned simplifying hypotheses are still used.

In 1972, Sobieszczanski and Loendorf (1972) proposed a mixed optimisation method in which a lumped global FE model (GFEM) was used instead of analytical formulae to evaluate the stiffness of the fuselage in order to obtain a better approximation of the loads to be used on local buckling evaluations performed using classical analytical methods. Similarly, Fischer et al. (2012) proposed a multi-level framework for optimisation of lightweight structures in which a simplified GFEM evaluates the average membrane and bending loads for the local optimisation of panels performed using VICONOPT, a program based on analytical solutions for prismatic plane panels with simple supported edges or periodic BCs. An analogous work is presented by Grihon et al. (2009b) in which the tool ASSIST for the buckling and post-buckling analyses based on engineering formulae was employed. They also considered the possibility of using a surrogate model to speed-up the process. A surrogate model is also adopted by Vankan et al. (2014a) for the multi-scale optimisation of a fuselage barrel. In this case the surrogate model is used for buckling failure evaluations and it is generated by means of buckling analyses on a parametric high-fidelity local FE model (LFEM) of an isolated stiffened panel with idealised BCs. Later, Vankan et al. (2014b) compared the results of the previous work to those obtained employing a high-fidelity GFEM, founding a lack of accuracy in the assessment of the local scale buckling in the formers, highlighting, thus, the detrimental effect of using idealised BCs.

In all the aforementioned works, the local analyses and the related optimisations follow the global scale ones and are performed by considering fixed internal loads (resulting from

the GFEM analysis), hence neglecting the load redistribution happening at the upper scale consequent to the variation of geometry at the local one. Similar problems are highlighted by Grihon et al. (2009a) in a review of the numerical optimisation methods developed/applied at AIRBUS: they identified the inaccuracy of some analytical models and the lack of load redistribution evaluation during the local scale optimisation as the main weaknesses and causes of inconsistency in the passage from the preliminary design phase to the following detailed one.

For real-world engineering problems, it is preferable to assess the response of the structure, at both the global and local scale, by means of suitable FE models. This task must be achieved in a computationally efficient manner and with a proper management of the information transfer between global scale and local scale models. To this purpose, in this thesis GL modelling approaches are integrated into MSOSs for the preliminary design of large-scale thin-walled structures.

## 2.2 On global-local modelling approaches

Global-local modelling approaches associated to FE analyses have mainly been investigated during 80s and 90s (Cormier et al., 1999; Hirai et al., 1984, 1985; Jara-Almonte and Knight, 1988; Mao and Sun, 1991; Sun and Mao, 1988; Whitcomb, 1991). Most of the first works were motivated by the need to obtain better accuracy on indirect outputs of the FE model (i.e. strain and stress) on some localised zones of interest (ZOIs) (Cormier et al., 1999; Hirai et al., 1984, 1985; Jara-Almonte and Knight, 1988; Mao and Sun, 1991; Sun and Mao, 1988) of a big structure or to retrieve information around not modelled geometrical details (Whitcomb, 1991), without solving a complete refined model, a sometimes non-viable possibility due to limited computational resources of that period. During the last two decades, as a consequence of the improved computational capabilities, GL approaches have been developed and used also to assess more complex phenomena like local plasticity (Gendre et al., 2009), crack propagation (Guidault et al., 2007), delamination in composite structures (Akterskaia et al., 2018), strong non-linear phenomena, or to implement a strong parallelisation of the computation using domain decomposition techniques (Cresta et al., 2007). GL modelling strategies can be grouped into three categories, differentiated by their basic work-flow: a) *sub-modelling* techniques (Cormier et al., 1999; Mao and Sun, 1991; Sun and Mao, 1988; Whitcomb, 1991), b) *condensation/zooming* techniques (Hirai et al., 1984, 1985), c) *multi-scale* techniques (Akterskaia et al., 2018; Cresta et al., 2007; Guidault et al., 2007).

The GL approaches belonging to the sub-modelling category are characterised by the presence of three common steps, which, referring to Fig. 2.2, are:

1. Firstly a linear analysis on a GFEM with a course mesh is run (Fig. 2.2a).
2. GFEM results are used to identify one or more ZOIs (e.g. the grey area in Fig. 2.2a). A refined LFEM, which can also take into account complex non-linear phenomena, is created for each ZOIs (Fig. 2.2b).
3. A second analysis is performed only on the LFEM imposing displacements provided by the GFEM as additional BCs. The complete solution of the problem is obtained assembling the results of the LFEM to those of the non-local region of part of the GFEM (Fig. 2.2c).

The results of the last step present a discontinuity of internal forces at the GL interface caused by the stress redistribution due to local effects. If such effects are considered non-negligible a correction iterative step must be added, in which GFEM and LFEM analyses alternate until the required convergence is achieved. An alternative formulation making

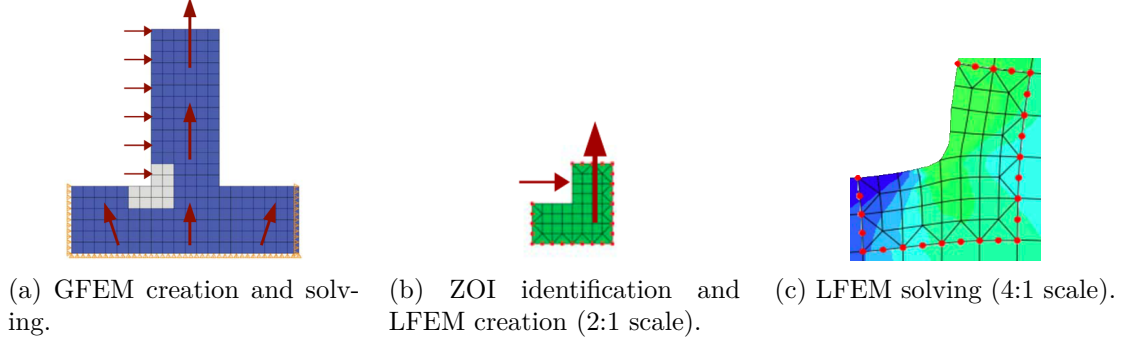


Figure 2.2: Usual work-flow of sub-modelling GL techniques (Gendre et al., 2009).

use of forces and stiffness instead of displacements in the information transfer between GFEM and LFEM has been proposed too (Jara-Almonte and Knight, 1988). The research works that belong to this category differentiate mainly in the handling of the correction step, proposing different convergence criteria and convergence enhancing techniques. Main advantages of this category of GL approaches are a low required computational effort and their simple implementation adopting common commercial FE software (a property that could be called *non-intrusiveness* of the approach). The major drawback is the possible need of the correction step that can nullify the computational advantage.

The condensation/zooming GL approach (Hirai et al., 1984, 1985) also present three main steps in its usual work-flow: the first step is identical to the one of the sub-modelling approach, while difference can be found at both the second and the third step (Fig. 2.3). At the former, besides the refined LFEM, also a condensed version of the *out of interest* region of the GFEM is created, in the form of a super element (SE) (Fig. 2.3b) through the process of *sub-structuring*. At the latter, the refined LFEM and the SE are assembled and solved together (possibly taking into account complex non-linear phenomena in the LFEM). This

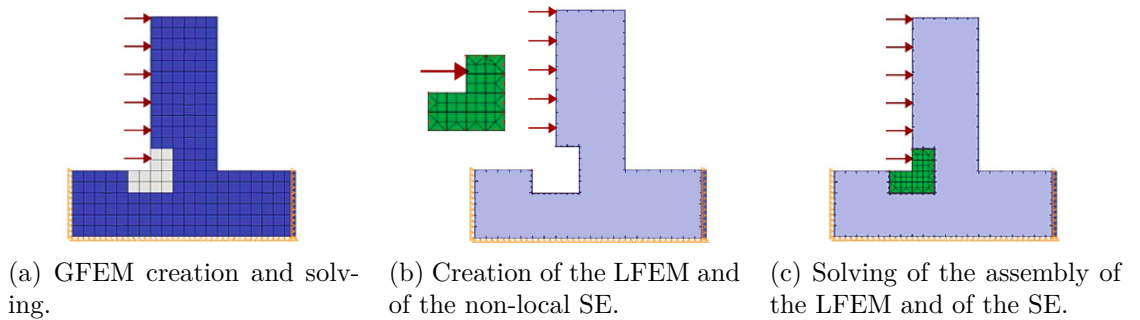


Figure 2.3: Usual work-flow of condensation/zooming GL techniques.

category of GL approaches is non-intrusive and does never require an iterative corrective step, but, from a computational point of view, it is more expensive than the sub-modelling approach.

The last category of GL approaches can be referred to as multi-scale. The works falling under this classification are chronologically the most recent ones. Most of these works are developed for specific applications, usually for the assessment of complex non-linear phenomena (e.g. crack propagation (Guidault et al., 2007), progressive delamination (Akerskaia et al., 2018), deep post-buckling (Cresta et al., 2007)). These are always two-way GL approaches, with a bi-directional and iterative information transfer between the GFEM and the LFEM: the passage from the GFEM to the LFEM is the usual displacement-based one, while the inverse passage usually happens through an update of the stiffness matrix of the elements of the global model, based on information obtained during the LFEM analyses. The main advantage of this type of approaches is an improved computational efficiency in complex analyses, with the possibility to further increase it by strongly parallelising the analysis by means of domain decomposition techniques (as in the example reported in Fig. 2.4). However, these are intrusive approaches, meaning that their implementation needs the creation of specific tools not available in commercial FE software.

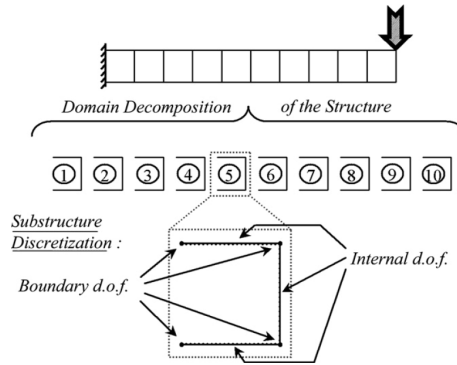


Figure 2.4: Domain decomposition of a modular structure for the assessment of its post-buckling behaviour through parallel computing (Cresta et al., 2007).

In the work presented in this thesis, the sub-modelling GL approach is employed in the design of large-scale thin-walled metallic or composite structures for the accurate and efficient assessment of the phenomena involved at the stiffened panel scale through the use of LFEMs with realistic BCs derived from the GFEM of the whole structure (Chapters 3, 5 and 6). Moreover, the sub-structuring process, a key ingredient of the condensation/zooming GL approach, is involved, in Chapter 6, in the definition of a strategy for the efficient optimisation of the over-constrained PrP structure.

## 2.3 On the optimisation of constant-stiffness composite structures

The constant demand of lightweight structural elements with enhanced mechanical performances has led to an increasing use of composite materials in the last few decades. Fibre-reinforced composites present specific stiffness and strength properties that make them really appealing when compared to metallic alloys.

The current standard format for the application of composite materials in high-performance structures are the CSCLs, layered plates made of plies containing long continuous

straight (non-woven) fibres. The behaviour of these materials gives the designer the opportunity to tailor the material properties of each laminate composing the structure to the design needs. A lot of research has been carried out in looking for the best strategy to optimise CSC structures in order to either minimise the mass (without losing performances with respect to a given *reference solution*) or improve mechanical performances (without increasing the mass with respect to a reference configuration). Nonetheless, the problem is still open. The design of a composite structure is a challenging task and can be considered as a multi-scale optimisation problem. The complexity of the design process is actually due to two intrinsic properties of composite materials, i.e. heterogeneity and anisotropy. Heterogeneity gets involved mainly at the microscopic scale, whilst anisotropy intervenes at both the mesoscopic and the macroscopic one. The main consequence of anisotropy is the introduction of some phenomena and issues that do not exist in metals (e.g. extension-bending coupling, delamination, residual stresses, free-edge stresses, different failure mechanisms, etc.). A further complication of using composite materials, instead of metallic alloys, is that the design process must deal with a significant number of design variables at different scales. In fact, though the use of laminated structures is not a recent achievement in structural mechanics, up to now no general method exists for their optimum design.

### 2.3.1 Single-level design approach for CSCLs

Traditionally, the design of CSC structures has been carried out by directly optimising the orientation of the fibres within each ply of the laminate composing the structure. This approach is usually referred to as *single-level* or *bottom-up* because the designer operates at the lowest considered scale (i.e. the mesoscopic one) in order to meet requirements mostly formulated at the macroscopic ones.

Numerous works adopting the single-level approach can be found in the literature (Ghiasi et al., 2009). Adali et al. (1994) investigated the post-buckling stiffness maximisation problem of simply supported biaxially loaded laminated plates using five pre-set symmetrical angle-ply stacking sequences consisting of eight plies. In this way the number of design variables reduces to one (for each configuration) and the optimisation was carried out by means of the Golden Section method. Later, Adali et al. (1995) focused on the problem of maximising the first buckling load of a bi-material multilayer plate. They considered three different cases, i.e. a plate composed of eight, twelve or sixteen plies, respectively. In each case, the stacking sequence is balanced and symmetric. The orientations were limited to the *canonical set*  $\{0^\circ, \pm 45^\circ, 90^\circ\}$  and a formulation based on Boolean variables was used. The approaches developed in these two works have then been used in the framework of multi-objective optimisation problems (Adali et al., 1996, 2003). Haftka and Walsh (1992) used integer programming for both the least-weight design and the maximisation of the first buckling load problems by considering symmetric balanced stacks wherein the orientations were constrained to get the values in the canonical set. These problems were solved by considering additional requirements on the percentage rule and overall in-plane stiffness value. Le Riche and Haftka (1993) made use of a genetic algorithm (GA) to solve the problem of maximising the first buckling load of a multilayer plate with a given number of plies. Also, in this work, symmetric balanced stacks with orientation angles getting values in the canonical set were considered. Furthermore, an *ad-hoc* genetic operator, i.e. the *permutation* operator, was proposed to increase the efficiency of the calculations. Still in the context of the first buckling load maximisation problem, Aymerich and Serra (2008) used the Ant Colony Optimisation method (consid-

ering balanced symmetrical stacking sequences in the usual domain of orientations) which was characterised by a better efficiency, in terms of computational effort, when compared to GA-based strategies. Irisarri et al. (2009) performed a multi-objective optimisation process of laminated plates using a Pareto-based evolutionary algorithm. In their application, the mass reduction was obtained by gradually decreasing the number of plies until the optimisation constraints are no longer satisfied. In this interesting work symmetric balanced stacks were employed and the orientation of each couple of plies belonged to a set bigger than the canonical one, i.e.  $(0_2^\circ, \pm 15^\circ, \pm 30^\circ, \dots, 90_2^\circ)$ . Furthermore, a set of design guidelines (U.S. Department of Defense, 2002) were integrated in the optimisation process, though the flexural behaviour of the laminate was only approximated.

In all the studies presented above, approximate analytical models are used for the assessment of the response of the structure. Accordingly, the main limitations in doing this are the lack of accuracy and the limited applicability of such methods that rely on simplifying hypotheses, especially in terms of applied BCs, often non-representative of the operative conditions of studied components. Some authors proposed the use of improved semi-analytical formulations based on the Rayleigh-Ritz method. For example, Bisagni and Vescovini (2015) have applied this method to better describe the interaction between the skin and the stringers in the evaluation of the buckling performances of stiffened panels. However, the compliance of frames/ribs was still neglected, and the structure was considered infinitely periodic. In other works, surrogate models built on results of LFEM analyses were employed, but the problem of the representativeness of the employed BCs still persist (Vankan et al., 2014a,b) and the phenomenon of mode switching can lead to a further inaccuracy in the evaluation of the buckling response (Irisarri et al., 2011). Another limitation of the above works, concerns the nature of the considered stacking sequences: in each study, it is set *a priori* and the orientation angles are always limited to get values in a predefined set, usually the canonical set, rarely an extended one. Moreover, further empirical design rules (U.S. Department of Defense, 2002), more or less justified, are usually enforced too. This is usually done to explicitly limit the extent of the design space and to improperly enforce some desired properties of the laminate. Two examples are the use of symmetric stacking sequences, a sufficient but not necessary condition for membrane-bending uncoupling and the use of balanced stacks to obtain orthotropic laminates. When symmetric stacks are used, the design is achieved considering half of the layers, which means also half of the design variables. Conversely, the use of balanced stacks, a sufficient condition for membrane orthotropy, leads systematically to misleading solutions: whenever such a rule is used, bending orthotropy, a rather difficult property to achieve (Montemurro, 2015a), is simply understated, assumed, but not really obtained, as in (Le Riche and Haftka, 1995; Liu et al., 2004; Nagendra et al., 1996; Todoroki and Haftka, 1998). All these aspects clearly contribute to strongly shrink the design domain.

Most of the choices of these authors, concerning both the modelling aspects and the design domain definition, are the expression of their attempt to limit the big computational effort needed to solve the problem they were dealing with. Indeed, the problem of the optimal design of laminated structures, formulated in the domain of the plies orientations, presents a huge number of design variables (in the most general case, equal to the total number of plies composing the structure), and results highly non-convex. As pointed out by Venkataraman and Haftka (2004) the increase of computational resources availability, on the one hand, and the parallel escalation in complexity of the simulation models, on the other hand, are still limiting the possibility to solve optimisation problems on large and complex structures described by many variables. In this scenario, the development of

*multi-level* design strategies finds strong motivation.

### 2.3.2 Multi-level design approaches for CSCLs

Multi-level design strategies allow formulating and solving the optimisation problem at the macroscopic and mesoscopic scales in two, or more, sequential *levels*, resulting, thus, in a *top-down* design approach. At the first level, the laminates composing the structure are modelled as equivalent single layer plates: here the true structural optimisation is performed in terms of their macroscopic properties, through a suited representation. The lay-up design constitutes the second level (or, more in general the last one) of these strategies, wherein at least one<sup>2</sup> stacking sequence corresponding to the optimum macroscopic properties found at the first level is searched for each laminate constituting the structure. Such research is usually performed through the solution of a minimum-distance problem. Clearly, it is of paramount importance to enforce feasibility conditions in the first-level problem to ensure the existence of a solution to the second-level one.

The main advantage in employing a multi-level approach is the strong reduction of the number of design variables involved at the first level of the procedure, where the true structural optimisation problem is solved. Moreover, the non-convexity typical of the design problem formulated with respect to the plies orientations is relaxed, sometimes even suppressed, in the first-level problem of a multi-level design strategy. The main disadvantage is the necessity to formulate all the design requirements involved in the problem, including those typical of the lower scales as requirements concerning failure and manufacturability, as equivalent constraints at the macroscopic scale of the laminate, which reveals, often, a rather difficult task.

Two main multi-level approaches exist in the literature, which primarily differ in terms of the mathematical representation used to describe the macroscopic behaviour of the laminate: the approach based on the use of *lamination parameters* and the one based on the use of *polar parameters*.

#### The multi-level approach based on lamination parameters

The most common approach makes use of the Lamination Parameters (LPs) coupled with the parameters of Tsai and Pagano (Jones, 1975) in the framework of the Classic Laminate Theory (CLT).

Diaconu et al. (2002a) presented a general framework for determining the feasible region in the LPs space for general composite laminate design. Their method does not give any explicit relationship between LPs, but only a *numerical definition* of the boundary of the feasible domain. Later they presented a work on the layup optimisation of thick laminates for maximising the first natural frequency (Diaconu et al., 2002b). In this context, a multi-level optimisation approach including a numerical verification on the feasibility of the optimum solutions is proposed. Liu et al. (2004) considered the problem of the maximisation of the first buckling load of a multilayer plate in the flexural LPs space. The optimum solutions are only given in terms of flexural LPs characterising the equivalent homogeneous anisotropic plate at the macroscopic scale, since the lay-up design phase is not considered. Bloomfield et al. (2008) presented a two-step optimisation strategy for symmetric laminates made of plies getting values in a predefined set of possible orientations. The strategy is applied to the problem of mass minimisation of a simply supported

---

<sup>2</sup>The problem is not bijective: a given stacking sequence corresponds to only one set of macroscopic properties, however the opposite is not true.



multilayer plate with uniformly loaded edges, subject to analytically-computed constraints on the plate failure and buckling load. Their results highlight the interest in widening the canonical set of plies orientation by adding  $\pm 30^\circ$  and  $\pm 60^\circ$  values. Liu et al. (2012) dealt with the maximisation of the laminate stiffness subject to a given set of optimisation constraints. During the first step, the optimisation problem is solved in the LPs space wherein the feasible region has been approximated by the one that can be obtained by considering only six different orientation angles. Herencia et al. (2008) employed an analogous strategy for the weight minimisation of composite panels with T-shaped stiffeners made of symmetric laminates with plies orientations in the canonical set under strength, buckling and technological design requirements. Buckling constraints are computed by employing an approximated semi-analytical method. Stacking sequences found at the second step are slightly heavier and not always match the optimum LPs found at the first step.

The integration of strength requirements in multi-level optimisation strategies has been limited for long time, because of the localised nature of the failure mechanisms, which occur at the ply-level or at the scale of the constitutive phases. An important improvement in this sense has been achieved by IJsselmuiden et al. (2008). They built a conservative failure envelope that guarantees a failure-free region in the LPs space, based on the phenomenological failure criterion proposed by Tsai and Wu (1971).

An application of the LPs-based approach on a full-scale structure can be found in the work of Bramsiepe et al. (2018) where the least-weight design problem of a lifting system structure is solved. Failure, buckling and blending requirements are considered: the structure is made of symmetric laminates with plies angles varying with a step of  $15^\circ$ . To evaluate the buckling load of the skin, the analytical formula for a simply supported plate subject to uni-axial load is used, retrieving the span-wise load component from a coarse GFEM. Moreover, the load redistribution is not directly considered, but the structural optimisation is performed under fixed loads at each iteration.

Few other works in which the multi-level approach based on the LPs is employed for the design of CSDLs can be found in the review article by Albazzan et al. (2019).

The representation based on the use on LPs successfully allows reducing the number of design variables: at most, 12 LPs are needed to describe the anisotropic behaviour of a laminate in the CLT framework, indeed. However, some limitations arise:

- The LPs are not tensor invariants, while some of the Tsai and Pagano parameters are not invariants and they are non independent (Jones, 1975).
- Both the LPs and the Tsai and Pagano parameters have not an immediate physical meaning. Consequently, the authors adopting this representation make a systematic use of the same simplifying hypotheses and design guidelines presented in Sec. 2.3.1, which operate on the nature of the laminates stacking sequences. Unfortunately, the use of these rules shrinks the design space and drives the optimisation algorithm towards suboptimal solutions.
- When using the LPs for the representation of the macroscopic properties of the laminates in combination with the well-known simplifying rules, the direction of the main orthotropy axis of the material is implicitly set with the designer's choice of the reference frame and is not optimised during the design process. This can result in a further detrimental restriction of the design space because it implies a designer's insight on the nature of the optimal solution that is not always possible.

- Finally, being formulated into the CLT framework, the LPs are not suited for the representation of the macroscopic mechanical behaviour of moderately-thick and thick laminates.

### The multi-level approach based on polar parameters

A second compact representation of the macroscopic behaviour of laminates available in the literature is the *polar method*.

Introduced by Verchery (1982), the polar method allows representing any plane tensor by means of tensor invariants, the Polar Parameters (PPs). The representation of the laminates macroscopic behaviour through PPs presents multiple advantages: a) it is a representation based on tensor invariants; b) the PPs have an immediate physical meaning and are related to the symmetries of the tensor; c) a rotation of the reference frame can be expressed in a straightforward way. Originally developed in the CLT framework, this representation has been initially enriched and deeply studied by Vannucci and his co-workers. Vannucci (2005) presented a critic review of the method in which he highlighted its theoretical bases, and the mathematical, graphical and physical interpretation of the PPs. In this work, he also provided a summary of the early researches he carried out with his co-workers on the analysis of the elastic, thermal and hygral properties of laminates and on their design. In a later work, Vannucci (2010) used the polar method to show that the *special* orthotropy of paper, previously explained only by means of a microstructured continuum model, actually corresponds to a peculiar type of orthotropy of the compliance tensor, hence it is completely justifiable using a classical continuum orthotropic model. Catapano et al. (2012) used this representation for the formulation of common phenomenological failure criteria for orthotropic sheets through invariants. Taking advantage of the clear physical meaning of the PPs, Montemurro et al. (2012c) assessed the problem of the design of laminates with the minimum number of plies able to meet given sets of elastic requirements. Vannucci (2013) provided the analytic expression of the bounds of the feasible domain of PPs describing the membrane and the bending behaviour of laminates made of identical plies. However, a recent study (Picchi Scardaoni and Montemurro, 2021) has demonstrated the non-convexity of the feasible domain in both the LPs and the PPs spaces, and concluded that all the bounds computed up to now, for both representations, only identify the convex hull of the true feasible domain. In 2015, Montemurro (2015a,b,c) extended the polar method to the case of Higher-order Equivalent Single Layer Theories (HESLTs), opening the possibility to confidently employ the polar method for the description of the elastic behaviour of thicker laminates. A unified formulation of a laminate-level failure criterion based on PPs in the framework of the CLT has been proposed by Catapano et al. (2015), and later generalised to the First-order Shear Deformation Theory (FSDT) (Catapano and Montemurro, 2019). In the latter work, thanks to the polar method, the relationship between the PPs representing the laminate stiffness properties and strength ones at the laminate level was derived in closed form.

The polar method generalised to the case of HESLTs is at the basis of the MS2LOS, a framework adopting a multi-level approach for the design of composite structures firstly introduced by Montemurro et al. (2012a,b). The MS2LOS aims at proposing a very general formulation of the design problem of composite structures by considering, as design variables, the full set of geometric and mechanical parameters defining the behaviour of the structure at hand, at each characteristic scale. Thanks to the use of the polar method, the formulation of requirements on the elastic macroscopic behaviour of the laminates can be done directly on their PPs, without introducing the aforementioned simplifying

rules. Moreover, non-physically-based design guidelines are usually disregarded, in both the first-level and the second-level problem, in order to not artificially shrink the design domain. During the last few years, the MS2LOS has been employed for the optimal design of various CSC components and structures. Montemurro et al. (2012a,b) employed it in the least-weight design of a one-bay wing-box structure with a requirement on the buckling load of the structure. Catapano and Montemurro (2014a,b) formulated into the MS2LOS framework the problem of the optimal design of sandwich plates. In this work, they optimised not only the two CSCLs constituting the plates skins, but also the geometrical parameters describing the aluminium honeycomb core. In a following work, Montemurro et al. (2016) further generalised such problem by considering a metallic cellular core whose unit cell shape is described by a Non-Uniform Rational B-Spline (NURBS) curve. Montemurro et al. (2018) applied the MS2LOS to the least-weight design of the repetitive unit of a composite stiffened panel considering requirements on its buckling load and on its manufacturability. In this work, as well as in the above ones, *on-line* FE analyses are performed for the assessment of the mechanical response of the considered structure during the optimisation process. Conversely, the use of a surrogate model is investigated by Audoux et al. (2020), still in the context of the optimisation of a composite stiffened panel in the MS2LOS framework. An innovative surrogate model based on NURBS hyper-surfaces is employed in the first-level problem to evaluate the buckling load of the structure.

In all the aforementioned works the special *in-house* GAs Biologically Inspired ANalysis of Composite Assemblages (BIANCA) (Montemurro, 2012) and Evolutionary Algorithm for optimisation of Modular Systems (ERASMUS) (Montemurro, 2018), its evolution, which can deal with constrained non-linear programming problems (CNLPPs) defined over a design space of variable dimension, are employed as solution tools.

**Quasi-trivial stacking sequences.** Strictly related to the polar method and commonly employed in the application of the MS2LOS, the concept of *quasi-trivial* stacking sequences deserves to be mentioned too. A common wish, when designing composite structures, is to obtain optimal solutions showing some degree of *predictability* in their mechanical behaviour, usually formulated in the requirements of membrane/bending uncoupling and homogeneity (i.e. the property of having the same elastic properties in membrane and bending) of the laminates. Vannucci and Verchery (2001) used the polar formalism to derive the equations defining the general conditions for these two requirements for a laminate made of identical plies. They discovered a family of exact solutions to these equations, which they called Quasi-Trivial (QT) stacking sequences.

Consider the constitutive law of the laminate in the FSDT framework:

$$\begin{Bmatrix} \mathbf{n} \\ \mathbf{m} \\ \mathbf{q} \end{Bmatrix} = \begin{bmatrix} \mathbf{A} & \mathbf{B} & \mathbf{0} \\ & \mathbf{D} & \mathbf{0} \\ \text{sym} & & \mathbf{H} \end{bmatrix} \begin{Bmatrix} \boldsymbol{\varepsilon}_0 \\ \boldsymbol{\chi}_0 \\ \boldsymbol{\gamma}_0 \end{Bmatrix}, \quad (2.1)$$

In Eq. (2.1),  $\mathbf{A}$ ,  $\mathbf{B}$  and  $\mathbf{D}$  are the membrane, membrane/bending coupling and bending stiffness tensors of the laminate, while  $\mathbf{H}$  is the out-of-plane shear stiffness tensor.  $\mathbf{n}$ ,  $\mathbf{m}$  and  $\mathbf{q}$  are the vectors of membrane forces, bending moments and shear forces per unit length, respectively, whilst  $\boldsymbol{\varepsilon}_0$ ,  $\boldsymbol{\chi}_0$  and  $\boldsymbol{\gamma}_0$  are the vectors of in-plane strains, curvatures, and out-of-plane shear strains of the laminate middle plane, respectively. For convenience, it is useful to introduce the laminate normalised stiffness tensors:

$$\mathbf{A}^* := \frac{1}{h} \mathbf{A}, \quad \mathbf{B}^* := \frac{2}{h^2} \mathbf{B}, \quad \mathbf{D}^* := \frac{12}{h^3} \mathbf{D}, \quad \mathbf{H}^* := \frac{1}{h} \mathbf{H}, \quad (2.2)$$

where  $h$  is the total thickness of the laminate. The membrane/bending uncoupling and the homogeneity conditions read, respectively:

$$\mathbf{B}^* = \mathbf{0}, \quad \mathbf{C} := \mathbf{A}^* - \mathbf{D}^* = \mathbf{0}, \quad (2.3)$$

where  $\mathbf{C}$  is called homogeneity stiffness tensor. For a laminate made of identical plies

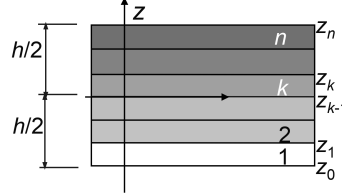


Figure 2.5: Laminate stacking scheme.

ordered as in Fig. 2.5, the expressions of these tensors in terms of the geometrical and material parameters of the stack are:

$$\mathbf{B}^* = \frac{1}{n^2} \sum_{k=1}^n b_k \mathbf{Q}^{\text{in}}(\delta_k), \quad \mathbf{C} = \frac{1}{n^3} \sum_{k=1}^n c_k \mathbf{Q}^{\text{in}}(\delta_k). \quad (2.4)$$

In Eq. 2.4,  $\mathbf{Q}^{\text{in}}$  is the in-plane reduced stiffness tensor of the ply,  $n$  is the number of plies in the laminate and coefficients  $b_k$  and  $c_k$  read, respectively:

$$b_k := 2k - n - 1, \quad c_k := 2n^2 - 12k(k - n - 1) - 4 - 6n. \quad (2.5)$$

A QT stack is a  $n$ -layers stack wherein only  $m$  (with  $m < n$ ) different orientations are present, and where the position of the plies sharing the same orientation is such that their contribution to the membrane/bending coupling tensor and/or to the homogeneity stiffness tensor is null regardless of the value of the ply orientation. The set of layers sharing the same orientation in a QT stack is called *saturated group* (SG). These conditions can be analytically formulated as:

$$\mathbf{B}^* = \frac{1}{n^2} \sum_{i=1}^m \left[ \mathbf{Q}^{\text{in}}(\delta_i) \sum_{k \in \text{SG}_i} b_k \right] = \mathbf{0} \quad \forall \delta_i \quad \rightarrow \quad \sum_{k \in \text{SG}_i} b_k = 0 \quad \forall i, \quad (2.6)$$

$$\mathbf{C} = \frac{1}{n^3} \sum_{i=1}^m \left[ \mathbf{Q}^{\text{in}}(\delta_i) \sum_{k \in \text{SG}_i} c_k \right] = \mathbf{0} \quad \forall \delta_i \quad \rightarrow \quad \sum_{k \in \text{SG}_i} c_k = 0 \quad \forall i. \quad (2.7)$$

Therefore, a QT stack can satisfy the uncoupling and/or homogeneity requirements regardless of the value of the orientation characterising each SG. Stacking sequences belonging to this family are obtained by means of a combinatorial algorithm, but their search is limited by the computational cost of the operation that rapidly increases as the number of plies composing the stack increases. Recently, Garulli et al. (2018) presented a general version of the combinatorial algorithm to find QT stacks and a set of prescribed rules to obtain QT sequences by superposing any number of QT elementary stacks (i.e. the ones formerly obtained by combinatorial calculation). In this way, QT solutions with an arbitrarily large number of plies can be readily obtained. QT stacks have often been used as design space for the solution of the second-level problem in the application of the MS2LOS. It is worth mentioning that symmetric stacks constitute a very small sub-set of QT ones, in the order of one out of tens of thousands. Therefore, the use of QT stacks represent a major improvement, in terms of size, over the classical one of symmetric stacks.

Most of the work presented in this thesis moves in the framework of the MS2LOS. In Chapter 4, the MS2LOS is applied to the least-weight design of a moderately thick plate subject to requirements on its in-plane stiffness and first buckling load. The annexed experimental activity provides a first experimental validation of the effectiveness of the MS2LOS and of the very general unconventional QT stacking sequences resulting from the process. In the following chapters the focus is put on the first-level problem of the MS2LOS. In Chapter 5, the MS2LOS is combined to the GL-MSOS presented in Chapter 3, to formulate a general design procedure for large-scale thin-walled CSC structures, called GL-MS2LOS. It is applied to the solution of the realistic engineering benchmark problem of designing a fuselage barrel taken from the literature. This provides a numerical validation of the proposed procedure, in preparation for its application to the design of the structure of the PrP aircraft presented in Chapter 6. Finally, in Chapter 7, the problem of the optimal design of VSCs structures in the MS2LOS framework is faced (more details on this topic are provided in the next section).

### 2.4 On the optimisation of variable-stiffness composite structures

The recent development of new manufacturing technologies is allowing a greater exploitation of the directional properties of composite materials through the concept of VSCLs. Unlike traditional CSCLs, a point-wise variation of the macroscopic mechanical properties can be obtained over the surface of a VSCL. This characteristic can be achieved by various formats of VSCLs. VAT laminates present a continuous variation of the stacking sequence across the laminate surface obtained by steering the fibres inside each layer. VSCLs having this format can be obtained employing manufacturing processes like the Automated Fibre Placement (AFP), the Fused Filament Fabrication and the Continuous Filament Fabrication. In *patch* laminates, a discrete variation of the laminate thickness and stacking sequence is obtained by dropping or adding straight-fibre layers, in various zones, called patches, of the surfaces. A simultaneous, continuous, and related variation of fibres direction and layer thickness is obtained through the Continuous Tow Shearing process (Kim et al., 2012, 2014). Theoretically, some *intermediate* formats could also be obtained taking advantage of some functionality of these manufacturing processes, e.g. the tow-drop capability offered by AFP machines.

The local material tailoring possibility makes VSCLs really appealing every time a non-uniformity of the stress field across the laminates surface occurs. Typical conditions are the stress concentration around some geometrical details of a structure (e.g. the windows of an aircraft fuselage or any other opening), the stress redistribution occurring during the buckling of laminates composing stiffened structures, the stress field resulting from uneven loads.

The idea of VSCLs is not new: in 1969, an early experimental investigation by Hyman et al. showed that an improvement of about 43% of the tensile strength could be achieved by locally distorting the fibres grid around an open hole instead of just drilling it afterwards. However, the adoption of VSC structures is still limited. On the one hand, this is due to the newness and immaturity of the manufacturing processes, which still present some limitations, produce under-performing results and/or introduce some undesired defects in the final product. On the other hand, for VSCLs, as well as for CSCLs, the problem of finding a general strategy for their optimum design is still open.

Concerning the manufacturing processes, each technology presented above is receiving important interest, in both the industrial and the academic words, thanks to some specific advantages it offers. Nowadays, the most mature one of them is the AFP process, and, consequently, the most studied and commonly employed VSCL format is the VAT laminate, which is the one considered in this thesis. The AFP process combines the differential tow payout capability of the Filament Winding process to the compaction and cut–restart capabilities of the Automated Tape Laying (ATL) one. When producing a component with this technology, an ensemble, called *course*, of up to 32 individually-fed fibres tows is laminated onto the surface of a mould. Each tow can be individually cut and restarted during the placement, allowing to reduce the amount of waste material during production. The AFP machine consists in the union of a placement head (illustrated in Fig 2.6) and a computer-controlled high-precision robot. The freedom and precision of movement of the robot allows the production of complex components with a higher level of repeatability and productivity with respect to manual lay-up. Moreover, this process allows to steer the tows during placement, and, consequently, to produce VAT laminates. However, the AFP

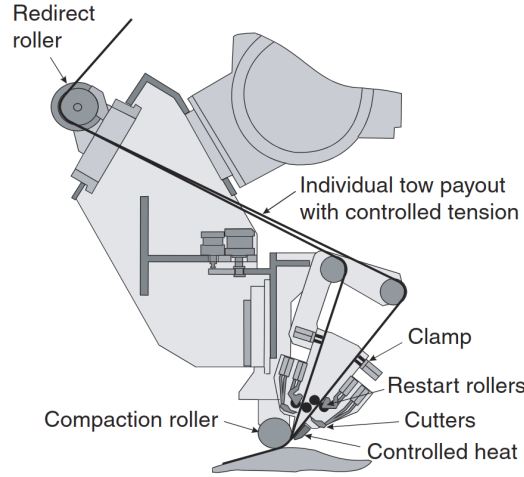


Figure 2.6: Typical tow-placement head (Evans, 2001).

process presents some limitations (Blom et al., 2010), the most constraining one being the presence of a minimum allowable value for the steering radius of fibres. Moreover, this process introduces some defects, in the form of tow gaps and/or overlaps, which can be reduced thanks to the tow cut-restart capability, but not eliminated, every time adjacent fibres paths are converging or diverging, as shown in Fig. 2.7. These defects can have an important impact on the performances of the obtained structures, as shown by multiple numerical and experimental works (Croft et al., 2011; Lan et al., 2016; Marouene et al., 2016; Nik et al., 2014; Wu et al., 2009, 2013).

From a design perspective, all the difficulties presented in in Sec. 2.3 about the design of CSCLs, arise for VSCLs too. The issues related to the high number of design variables to deal with is even amplified, because of the additional spatial variation of the fibres directions and mechanical properties across the VSCLs surface. Moreover, a complete design strategy for VSCLs should also account for the feasibility of the obtained solutions by including constraints related to the employed manufacturing process; the most basic ones for VAT laminates being the continuity and smoothness of the design variables distributions. Finally, due to the characteristics of the optimisation problems formulated for these structures, the use of DAs is usually preferred for the solution search over that of

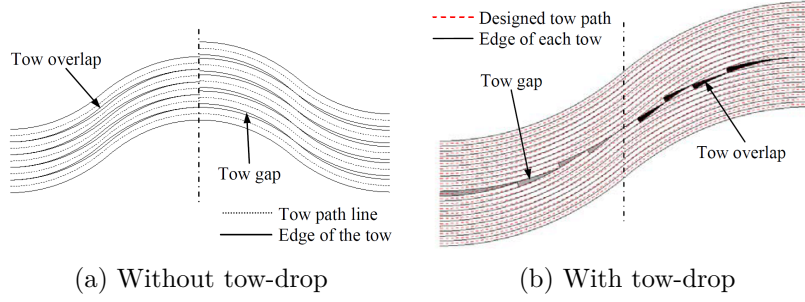


Figure 2.7: Tow gap and overlap formation (Kim et al., 2011).

meta-heuristic algorithms, which can be inefficient and can lead to sub-optimal solutions. However, to guarantee the best possible exploitation of a DA, in terms of both efficacy and computational efficiency, the analytical expression of the gradient of all the response functions involved in the optimisation process should be provided.

As discussed in Sec. 2.3 regarding the design of CSCLs, also for VSCLs two different approaches are available in the literature (Ghiasi et al., 2010): the *single-level* and the *multi-level* approaches.

#### 2.4.1 Single-level design approach for VSCLs

Various analytical/numerical strategies have been developed, over the years, to find optimised VSC solutions by adopting the single-level approach. The idea of locally aligning the main orthotropy axis of the material to the principal stress and/or strain direction, a common practice for stiffness-oriented optimisation, is exploited by Hyer and Charette (1991) to increase the failure load of open hole plates under tension.

This alignment was achieved through an iterative procedure wherein a single layer of fibres-paths is optimised point-wise. Both the Tsai-Wu and the max-strain failure criteria are computed on a layer-by-layer basis to predict the failure load and the failure mode, obtaining theoretical improvements in strength up to 89% over the quasi-isotropic  $[\pm 45/0/90]_{25}$  configuration having the same geometry. They also evaluated the effect of their curvilinear designs on the buckling load of the structure, finding that the improvements in tensile performances were obtained at the expense of buckling ones. Later, Hyer and Lee (1991) directly investigated the possibility to improve the buckling capacities of a plate with a central hole. A single layer of fibres-paths, discretised into 18 regions with constant fibres orientation, was optimised employing a DA driven by a sensitivity analysis based on finite differences. Tosh and Kelly (2000) introduced the concept of *load paths* in the context of the maximum strength design of VSCLs. They experimentally showed that better results in terms of strength are obtained when aligning the fibres with the load paths, instead of aligning them with the principal stress directions, in the case of open-hole tension and pin-loaded tests. The authors also intuitively found that adding a few layers with curvilinear paths locally orthogonal to the main ones further improves strength.

A common belief when dealing with the optimisation of VSCLs is that maximising the stiffness implicitly implies a proper maximisation of the strength. However, even if the relation between the two problems has been recently found (Catapano and Montemurro, 2019), it has been shown that the two formulations are not equivalent (Catapano and Montemurro, 2020; IJsselmuiden et al., 2008; Khani et al., 2011).

In most of the early works, the layers fibres-paths are described through a given discretisation, usually corresponding to the mesh of the FE model used for the assessment of the physical responses. Moreover, the study was limited to mono-layer or over-simplified symmetric VSCLs in order to limit the number of design variables involved in the optimisation process. For the same reason, some authors have opted for the use of an *in-layer* parametrisation of the fibres-paths, which ensures, at the same time, their continuity. Gurdal and Olmedo (1993) introduced a fibres-path parametrisation wherein the fibre orientation angle varies linearly along a given direction and is kept constant along the perpendicular one. Although the linear fibre orientation variation represents a strong limitation for design purposes, it has widely been used for the optimisation of VSCLs, achieving good results. For example, Tatting and Grdal (2001, 2002) used such parametrisation for the maximisation of the buckling load of rectangular panels employing the Rayleigh–Ritz method. Their results have later been confirmed by means of accurate non-linear FE analyses by Lopes et al. (2008), who also performed a first-ply failure check, finding that an increase of both the buckling and the failure loads up to about 35% was obtained. Alhajahmad et al. (2008) used the same parametrisation for the failure load maximisation of a fuselage panel with a cut-out, modelled as a two-dimensional plate, and loaded by a combination of pressure and in-plane loads. A 16-layer point-wise symmetric and balanced stacking sequence with only two independent fibres-paths of the type  $[\pm\theta_1/\pm\theta_2]_{2S}$  is considered for a total number of four design variables. The optimisation was performed using a simulated-annealing optimiser. Failure is verified using the Tsai-Wu failure criterion, evaluated by means of FE analyses. Improvements up to 30% in the load carrying capacity of the structure were obtained when compared to the quasi-isotropic design. A piecewise bi-linear interpolation was used by Huang and Haftka (2005) to represent the fibres orientations near a hole of one of the layers of a laminate withstanding uni-axial tensile load for maximising its failure load. The solution search was performed by alternating the conjugate gradient method and a genetic algorithm to avoid local optima, obtaining a load-carrying capacity twice than that of a CSCL with the stack  $[0/\pm 45]_S$ . Other authors used more general parametrisations of the fibres-paths: e.g. Nagendra et al. (1995) used NURBS curves, while Wu et al. (2012) proposed the use of Lagrangian polynomials, which give an advantage in the implementation of a modified version of the Rayleigh-Ritz method for the evaluation of the buckling load.

Of course, the main drawback of the *direct approach* is related to the number of design variables that could easily become prohibitive for thicker VSCLs. Moreover, the physical responses involved in the problem formulation are highly non-convex in terms of the local fibre orientation angle.

### 2.4.2 Multi-level design approaches for VSCLs

When employing a multi-level approach for the design of VSCLs, the same advantages presented in in Sec. 2.3 are obtained. However, the number of design variables needed at the first level (where the true structural design is performed) to describe the laminate macroscopic properties of a VSCL is higher than that required for a CSCL, because of the non-uniformity of such properties across the surface of the former.

The same dichotomy between LPs-based and PPs-based approaches introduced in Sec. 2.3 also holds for the optimal design of VSCLs.



### The multi-level approach based on lamination parameters

Works presenting a LPs-based multi-level approach appeared the first. Setoodeh et al. (2006) formulated the problem of minimum compliance of VSCLs in the domain of the LPs. The design variables were defined at the nodes of the FE model used for the response evaluation, establishing a strong coupling between meshing choices and optimisation problem formulation. The related optimisation problem results convex in terms of the LPs (if one approximate the LPs feasibility domain by means of its convex-hull) and was solved using a Feasible Sequential Quadratic Programming solver. Theoretical results showed big improvements with respect to optimised balanced CSC solutions, with a reduction of the compliance up to about 52%. However, the second-level solutions, i.e. the fibres-paths corresponding to the optimal LPs distributions, were not obtained. IJsselmuiden et al. (2010) faced the problem of the buckling load maximisation of VSCLs. They proposed the use of a separable conservative approximation scheme for the evaluation of the buckling load, which results, in this way, a convex function of the LPs. The design variables (i.e. the LPs) were defined at the nodes of a FE model and the corresponding VSCLs were considered to be locally balanced and symmetric. Although the adjoint method is used to efficiently compute the gradient of the objective function, the use of sufficiently refined FE models was prevented by the consequent excessive computational cost caused by the mesh-dependent definition of the design variables. Corresponding fibres-paths were not provided in this work, while successive attempts to retrieve them resulted in an incomplete fitting of the first-level results. Khani et al. (2011) employed the laminate-level failure criterion introduced by IJsselmuiden et al. (2008) to maximise the failure load of a quarter of a square VSC layered plate with a central hole under tensile load. The hypotheses of point-wise symmetric and balanced stacks were made and the design variables describing the VSCL were defined node-wise. Their results, obtained by employing a DA, showed significant improvements of the failure load (almost three times greater than that of an isotropic solution and two times greater than that characterising a VSCL optimised with respect to stiffness requirements). Optimal fibres-paths for a 16-ply balanced and symmetric VSCL, corresponding to the optimal design in the LPs space, are provided in this work, however they were obtained without taking into account their manufacturability and there is no information on the coherence between the fibres-paths and the LPs distributions. Peeters et al. (2015) proposed a method for including the manufacturing-related steering constraint into the second-level problem formulation, i.e. the design of optimal fibres-paths. Their method is surely effective, however, because no *equivalent* constraint is formulated and enforced at the first level of the design procedure, there is no guarantee to obtain an exact correspondence between optimal fibres-paths and target LPs distributions.

The multi-level approach based on LPs has been widely used in the literature (additional works adopting this approach are presented in the review article by Albazzan et al. (2019)), and has produced very interesting results, however the limitations presented in Sec. 2.3.2 still hold. Moreover, in most of the works adopting this approach, a strong and improper coupling is established between the FE model mesh and the definition of the first-level design variables, which forces the authors to make an unnecessary compromise between computational cost of the optimisation process and accuracy in the assessment of the structural response. An isolated exception is the work by Wu et al. (2015), who proposed the use of B-spline entities for the description of the LPs distributions.

### The multi-level approach based on polar parameters

Concerning the use of the PPs into the multi-level design of VSCLs, a first application can be found in the work of Jibawy et al. (2011). They presented a two-level methodology for the design of optimal orthotropic uncoupled VSCLs under membrane-only or bending-only loading. The compliance minimisation problem was faced. First-level solutions were found by employing an iterative procedure in which the design variables (defined per element) and the stress field are alternately updated using an analytical method and a FE analysis, respectively. At the second level, analytical solutions were found under the form of cross-ply and angle-ply laminates, but their feasibility was not ensured. Catapano et al. (2015) faced the problem of the simultaneous optimisation of strength and stiffness of VSCLs under membrane loading. An iterative procedure alternating the solution of local optimisation problems (per element and with a fixed stress field), achieved analytically or numerically, and the update of the stress field by means of a FE analysis, was employed at the first level. The lay-up design was performed, employing a GA, for each element of the employed FE model; the absence of any continuity constraint led to infeasible solutions. Moreover, the study was conducted under the hypothesis of mutual independence of the elastic and strength properties of the laminate, which was proven false in a later work (Catapano and Montemurro, 2019). In 2016, Montemurro and Catapano presented an enriched version of the MS2LOS framework. The use of B-spline entities was introduced for the description of all design variables distributions (the local PPs at the first level, the local fibres directions at the second level), which automatically ensures their continuity across the laminate surface. By doing so, the definition of the design variables is unrelated to the mesh of the employed FE model and a significant reduction of their number is achieved (without degrading the accuracy of the response evaluations), when compared to FE-based definitions. The buckling load maximisation problem was solved in this work by coupling the *in-house* GA ERASMUS with a classic DA. A constraint on the maximum curvature of the fibres was also considered in this work. However, because such constraint was only formulated at the second level, obtainable fibres-paths were not ensured to completely correspond to the distributions of PPs obtained at the first-level. Later, Montemurro and Catapano (2017) identified a sub-class of VSCLs for which a family of fibres-paths exactly corresponding to a given distribution of PPs could readily be obtained. A first formulation of the maximum tow curvature constraint at the first level was presented in this work for this VSCLs sub-class. The compliance minimisation problem was faced in a following work (Montemurro and Catapano, 2019). Unlike what done in previous works, in which a numerical evaluation of the gradient of the objective and constraint functions was used during the deterministic optimisation phase, a closed-form expression of the gradient of the VSCL strain energy and of the feasibility constraints was derived in this work by exploiting the properties of the B-Spline entities. A similar activity has recently been carried out by Fiordilino et al. (2021) while facing the design problem of the buckling load maximisation of VSCLs. They have analysed two benchmark problems taken from the literature, and obtained results showing a buckling load up to three times higher than that of reference quasi-homogeneous isotropic solutions. Moreover, they have also compared their results to optimised VSCL solutions taken from the literature and obtained by means of the design approach based on LPs: an improvement of the buckling load in the range 13-16% is found. In a very recent work, Catapano and Montemurro (2020) investigated the problem of the design of VSCLs against failure. At the first level the macroscopic optimisation of the VSCL is performed by directly minimising the Laminate Failure Index (LFI), a quantity introduced by the same authors for the formulation of a laminate-level

failure criterion in a previous work (Catapano and Montemurro, 2019), through the only use of the GA ERASMUS. Feasibility constraints and a requirement on the maximum allowable tow curvature complete the first-level problem formulation. At the second level, the optimal fibres-paths are searched combining the analytical method proposed by Miki and Sugiyamat (1993) coupled with the use of QT stacking sequences (Garulli et al., 2018; Vannucci and Verchery, 2001) and a first-ply failure check is also performed *a posteriori* to confirm the integrity of obtained solutions.

Although younger, the MS2LOS seems to be a valid alternative to the multi-level approach based on the LPs for the design of VSC structures, presenting some specific advantages, as highlighted above. However, further development is still needed, particularly concerning the enrichment of the MS2LOS framework in order to allow dealing with more complex design problems including other requirements, concerning both the mechanical responses of studied structures and the manufacturability of obtained solutions.

In the work associated to this thesis, the problem of the deterministic optimisation of VSCs in the theoretical framework of the MS2LOS has been studied. Requirements on strength, mass and buckling load have been formulated by deriving the analytical expression of the relative response functions and their gradients. An improved conservative formulation has been obtained for the process-related manufacturability requirement of the maximum tow curvature, and a modification in the definition of the design variables has been presented that allows to intrinsically satisfy the point-wise feasibility conditions (on the existence of suitable stacks) without explicitly including the relative optimisation constraints in the first-level problem formulation.

Most of the outcomes of these activities are presented in Chapter 7. Concerning the buckling load requirement, an initial study, not reported in this thesis, has been conducted in collaboration with Ph.D. student G. A. Fiordilino and recently published (Fiordilino, Izzi, and Montemurro, 2021).

## 2.5 Conclusions

This literature survey has allowed to picture the state of the art of design procedures for large-scale thin-walled CSC and VSC structures typical of the aeronautical field. These structures present a multi-scale nature, due, on the one hand, to their geometry (which allows to identify a global scale and a local one), and, on the other hand, to the inherent nature of composite materials (whose behaviour can be described at the macroscopic and mesoscopic scales). The correct design of the CSC variant of these structures requires the tailoring of the geometrical and the material properties of each laminate composing them. The related design problem can be formulated as a CNLPP which involves physical responses of the structure, and design variables at all working scales. The solution of such multi-scale problem in the domain of the orientations of the laminates plies composing the structure, if formulated in the most general way, appears non-viable because of the huge number of design variables involved and the consequent computational cost. Therefore, designers usually intervene on multiple aspects of the design process trying to find the best compromise between generality of the problem formulation and the computational cost needed for its solution.

Concerning the evaluation of the structural responses, nowadays, the use of FE analyses for the assessment of global-scale phenomena is quite common; conversely, approximated analytical or semi-empirical methods are still largely employed at the local scale.

These methods rely on limiting hypotheses making their applicability not always justifiable. Some authors have proposed the use of surrogate models based on FE analyses for describing local-scale responses, but some approximations on the geometry of the stiffened panels models, the considered BCs, or both are introduced.

From a procedural perspective, the information transfer between global and local scales is often poorly managed, and the stress redistribution occurring at the global scale due to changes of the local-scale design variables is neglected. This leads to a lack of accuracy in the structural responses evaluations that, on the one hand, has a detrimental effect on the solution search in the preliminary design phase, and, on the other hand, introduces inconsistencies with the following detailed design phase.

GL modelling approaches allow overcoming some of the above limitations. When adopting such approaches, the structural responses at both global and local scales are accurately and efficiently assessed by means of FE analyses, and a coherent information transfer between the scales is guaranteed.

Concerning the definition of the problem design variables, unnecessary simplification rules and design guidelines are usually applied. This is usually done to reduce the number of design variables and to improperly enforce some desired elastic properties of the laminate. However, by doing so, the design space is extremely shrunk and, consequently, the possibilities to find the true global optimum of the problem are reduced. The adoption of a multi-level design approach allows simplifying the optimisation problem through both a relaxation of its non-convexity and a strong reduction of the number of design variables, theoretically without effectively shrinking the design space. Adopting such an approach allows formulating and solving the structural optimisation problem in terms of the macroscopic properties of the laminates, postponing the lay-up design to a second phase of the design process. However, the most commonly employed multi-level approach, i.e. the one based on the use of LPs for the representation of the laminate macroscopic behaviour, shows some limitations. Notably, a systematic use of the aforementioned simplifying rules is done when adopting such representation. This effectively nullifies some of the advantages expected from a multi-level approach, but also introduces a collateral effect: the resulting constrained LPs design space does not allow for an easy optimisation of the main orthotropy direction of the laminate.

Although less employed, the representation based on PPs shows intrinsic advantages related to its formulation based on tensors invariants. Moreover, unlike the one based on LPs, this representation is well suited for the description of the macroscopic mechanical behaviour of moderately-thick and thick laminates.

Modern manufacturing processes are allowing the production of laminates wherein a point-wise tailoring of the mechanical properties is possible, the VSCLs. These laminates are best suited for their use in structural components presenting high stress gradients. The point-wise design of VSCLs is conceptually similar to that of CSCLs, therefore all the above remarks also hold for the formers. However, some specific difficulties arise, which are related to the spatial variation of the design variables across the VSCLs surface, and to the need to account for more constraining process-related manufacturability requirements. Specific design procedures for VSC structures are less mature than those for CSC ones, and their development is progressing in parallel to that of the related manufacturing processes.

This literature review has allowed to identify the principal weaknesses in state-of-the-art design processes for large-scale thin-walled CSC structures typical of the aeronautical field and structural VSC components. In the work presented in the following chapters, specific design procedures and numerical tools have been developed, trying to overcome

some of these weaknesses and aiming at making a contribution for a more effective and efficient design of such structures.

---

## Design of large-scale thin-walled metallic structures

The article *Multi-scale optimisation of thin-walled structures by considering a global/local modelling approach*, reported in this chapter, has been published in *Proceedings of the Institution of Mechanical Engineers, Part G: Journal of Aerospace Engineering* (Izzi et al., 2021b). It deals with the preliminary design of large-scale thin-walled metallic structures typical of the aeronautical field. The GL-MSOS is presented in this article: it is a strategy ensuring accuracy and efficiency of the optimisation process for this type of structures.

When adopting the GL-MSOS, the evaluation of the mechanical responses of the structure at both global and local scales is performed by means of suited fully-parametric FE models, guaranteeing in this way, more accurate results than those provided by means of well-established simplified analytical models. The computational effort is kept low by verifying the local responses on a limited set of ZOIs, identified during the global scale analysis. The use of a GL sub-modelling approach guarantees coherence among the various FE analyses and also contributes keeping the computational effort low. The full set of design variables is considered in the formulation of the optimisation problem, without introducing simplifying hypotheses, widening, in this way, the design space and, consequently, the possibility to find a true global optimum solution. The whole process is completely automated and, once set, it does not need any further user's intervention.

The effectiveness of the proposed GL-MSOS is proven on a meaningful real-world engineering problem: the least-weight design of a fuselage barrel belonging to the aft part of a wide-body aircraft that undergoes multiple loading conditions and subject to constraints of different nature. The design problem is formulated as a CNLPP and the solution search is carried out by interfacing the fully-parametric global and local FE models to the GA ERASMUS, which efficiently combines exploration capability and information exploitation. The obtained solution is compared to a reference configuration taken from the literature and obtained by using common-use simplifying rules and analytical models: the two configurations have a very similar mass (within 1.2% different), however, the reference configuration is infeasible and does not meet some of the more restrictive design criteria employed in this work.

# Multi-scale optimisation of thin-walled structures by considering a global/local modelling approach

Proc IMechE Part G:  
J Aerospace Engineering  
0(0) 1–18  
© IMechE 2020  
Article reuse guidelines:  
sagepub.com/journals-permissions  
DOI: 10.1177/095441002093938  
journals.sagepub.com/home/pig



Michele I Izzi<sup>1</sup> , Marco Montemurro<sup>1</sup> , Anita Catapano<sup>2</sup> ,  
Daniele Fanteria<sup>3</sup>  and Jérôme Pailhès<sup>1</sup>

## Abstract

In this work, a design strategy for optimising thin-walled structures based on a global-local finite element (FE) modelling approach is presented. The preliminary design of thin-walled structures can be stated in the form of a constrained non-linear programming problem (CNLPP) involving requirements of different nature intervening at the different scales of the structure. The proposed multi-scale optimisation (MSO) strategy is characterised by two main features. Firstly, the CNLPP is formulated in the most general sense by including all design variables involved at each pertinent scale of the problem. Secondly, two scales (with the related design requirements) are considered: (a) the structure macroscopic scale, where low-fidelity FE models are used and (b) the structure mesoscopic scale (or component level), where more accurate FE models are involved. In particular, the mechanical responses of the structure are evaluated at both global and local scales, avoiding the use of approximated analytical methods. The MSO is here applied to the least-weight design of an aluminium fuselage barrel of a wide-body aircraft. Fully parametric global and local FE models are interfaced with an in-house metaheuristic algorithm. Refined local FE models are created only for critical regions of the structure, automatically detected during the global analysis, and linked to the global one, thanks to the implementation of a sub-modelling approach. The whole process is completely automated, and once set, it does not need any further user intervention.

## Keywords

Optimisation, genetic algorithms, fuselage, stiffened panels, finite element method, global/local modelling approach

Date received: 31 October 2019; accepted: 3 June 2020

## Introduction

Mass control is a major concern in the design of airplanes. For this reason, the design of aircraft structures is often formulated as a constrained non-linear programming problem (CNLPP). The main objective is the mass minimisation subject to a given number of design requirements stated as optimisation constraints. *Semi-monocoque* structures have soon become a standard choice for both the fuselage and the wing, thanks to their high stiffness-to-weight ratio. Due to their nature, the design criteria (DC) for such structures involve both local phenomena (i.e. at the scale of the single component such as a stiffened panel) and global ones (i.e. at the scale of the whole structure). For this reason, a multi-scale modelling approach reveals necessary to properly describe the interdependency of the different phenomena and, consequently, a suitable multi-scale optimisation (MSO) strategy, integrating such a modelling approach, shall be defined.

The preliminary phase of aircraft structural design is mostly based on analytical or semi-empirical methods. Such methods have been developed since 40s especially in USA<sup>1–3</sup> and have been continuously improved during the years until becoming an established reference for aircraft designers.<sup>4–7</sup> These methods are based on several simplifying hypotheses. For example, when dealing with the fuselage design,

<sup>1</sup>Arts et Métiers Institute of Technology, Université de Bordeaux, CNRS, INRA, Bordeaux INP, HESAM Université, I2M UMR 5295, Talence, France

<sup>2</sup>Bordeaux INP, Université de Bordeaux, Arts et Métiers Institute of Technology, CNRS, INRA, HESAM Université, I2M UMR 5295, Talence, France

<sup>3</sup>Department of Civil and Industrial Engineering - Aerospace Division, University of Pisa, Pisa, Italy

## Corresponding author:

Marco Montemurro, Arts et Métiers Institute of Technology Centre de Bordeaux-Talence Esplanade des Arts et Métiers, Talence 33405,

at the global scale, circular cross-sections are considered, whose geometry and boundary conditions (BCs) are symmetric with respect to the aircraft longitudinal plane. Stringers are taken into account by considering a homogeneous skin of equivalent thickness (greater than the true thickness of the skin) or by considering lumped models wherein a group of stringers is merged in one rod element. When pressurisation is taken into account, the classical equations for axial-symmetrical infinite vessels with regularly spaced frames are used.<sup>7</sup> At the stiffened panel scale, for the calculation of buckling loads, plane or curved plates with uniformly loaded edges and idealised BCs (usually in the form of simply supported edges) are considered; the stringers are considered as isolated elements, and the Euler column buckling equations are used.<sup>6,8</sup>

Preliminary design procedures for thin-walled structures have been developed integrating the aforementioned methods into sequential<sup>8</sup> or iterative procedures.<sup>9–11</sup> The solution is searched by means of deterministic algorithms using an initial guess set by means of handbook methods. In order to properly exploit the effectiveness of the deterministic algorithm, the number of design variables is reduced by ‘slaving’ or ‘linking’ them together by enforcing fabrication requirements or using experience or simplified empirical rules. Of course, this approach extremely shrinks the design domain.

Several works on improved analytical or numerical methods for predicting the mechanical response of stiffened panels, especially regarding the buckling and post-buckling behaviour of such components<sup>12–14</sup> can be found in literature. However, the aforementioned simplifying hypotheses are still used.

In 1972, Sobieszczanski and Loendorf<sup>15</sup> proposed a mixed optimisation method wherein a ‘lumped’ global finite element (FE) model (GFEM) was used instead of analytical formulae to evaluate the stiffness of the fuselage in order to obtain a better approximation of the loads to be used on local buckling evaluations. Similarly, Fischer et al.<sup>16</sup> proposed a multi-level framework for optimisation of lightweight structures wherein a simplified GFEM evaluates the average membrane and bending loads for the local optimisation of panels performed using VICONOPT, a program based on analytical solutions for prismatic plane panels with simple supported edges or periodic BCs. An analogous work is presented by Grihon et al.<sup>9</sup> where the tool ASSIST for the buckling and post-buckling analyses based on engineering formulae was employed. They also considered the possibility of using a surrogate model to speed up the process. A surrogate model is also adopted in Vankan et al.<sup>17</sup> for the MSO of a fuselage barrel. In this case, the surrogate model is used for buckling failure evaluations, and it is generated by means of buckling analyses on a parametric high-fidelity local FE model (LFEM) of an isolated stiffened

panel with idealised BCs. They found a poor accuracy of the local buckling analyses and highlighted the detrimental effect of the idealised BCs.

In all the aforementioned works, the local analysis (and the related optimisation) is performed by considering fixed internal loads resulting from the GFEM, hence neglecting stress redistribution due to the change of geometry at the upper scale, i.e. that of the whole structure. Therefore, the main limitation of such design procedures is related to a poor evaluation of the mechanical response of the structure, due either to the use of simplified models or to the approximation of the BCs when passing from the GFEM to the LFEM. In order to overcome these limitations, the utilisation of a proper global/local (GL) modelling approach in the framework of the MSO of thin-walled structures is proposed in this work.

GL modelling approaches allow the assessment of phenomena involved at the component level through the use of LFEMs with realistic BCs derived from the GFEM. Both models have affordable computational costs, thus they can be integrated into an optimisation strategy.<sup>18</sup> GL modelling approaches have been investigated mainly during 80s and 90s.<sup>19–25</sup> During the last two decades, as a consequence of the improved computational capabilities, GL approaches have been developed and used also to assess more complex phenomena like local plasticity,<sup>26</sup> crack propagation,<sup>27</sup> delamination in composite structures<sup>28</sup> and strong non-linear phenomena as well. Most of these works are developed for specific applications, and their implementation needs the creation of specific tools not available in commercial FE software. Apart the GL modelling strategies that do not make use of commercial FE software, the rest of GL approaches can be divided into two categories: sub-modelling<sup>22–25</sup> and condensation/zooming techniques.<sup>19,20</sup>

In the usual work-flow of sub-modelling GL approaches, firstly, a low-fidelity linear analysis on a GFEM with a coarse mesh is run to identify one or more zones of interest (ZOIs). Then, a refined LFEM is created for each ZOI, which can also take into account complex non-linear phenomena. Then, a second analysis is performed only on the LFEM imposing displacements provided by the GFEM as BCs. Moreover, iterative stages can be added if the stress redistribution due to local effects is considered non-negligible. An alternative formulation making use of forces and stiffness instead of displacements in the information transfer between GFEM and LFEM has been proposed too.<sup>21</sup>

The condensation/zooming technique<sup>19,20</sup> differs from the sub-modelling approach at the second step where the refined LFEM is solved together with a condensed version of the ‘out-of-interest’ region of the GFEM, introduced in the form of a *super-element*. From a computational point of view, the procedure is more expensive than the sub-modelling approach, but it does not require an iterative process.



In this work, an MSO of thin-walled aircraft structures making use of the sub-modelling GL approach is presented. The MSO strategy is characterised by two main features: on one hand, the full set of design variables, at each relevant scale of the problem, is considered in the design process without additional simplifying hypotheses, widening in this way the design space and, consequently, the possibility to find a true global optimum solution. On the other hand, all the DC and requirements involved into the problem formulation are evaluated by means of both GFEM and LFEMs through a suitable GL modelling approach. Computational time is kept low by verifying local responses only on the most critical ZOIs. To this purpose, pertinent DC are introduced into the GFEM to automatically identify the ZOIs and build the related refined LFEMs.

The solution search is carried out by means of the special genetic algorithm (GA) ERASMUS (Evolutionary Algorithm for optimisation of Modular Systems)<sup>29</sup> which can deal with CNLPPs defined over a design space of variable dimension.

The effectiveness of the proposed MSO strategy is proven on a meaningful real-world engineering problem: the least-weight design of a fuselage barrel belonging to the aft part of a wide-body aircraft that undergoes multiple loading conditions and subject to constraints of different nature.

The paper is organised as follows. A general description of the design problem, the underlying hypotheses and the driving DC are given in the next section. The mathematical formulation of the multi-scale design problem and the adopted numerical strategy are discussed in the Mathematical formulation of the optimisation problem section. Then, the details on the FE models and the implementation of the GL approach are presented in the fourth section

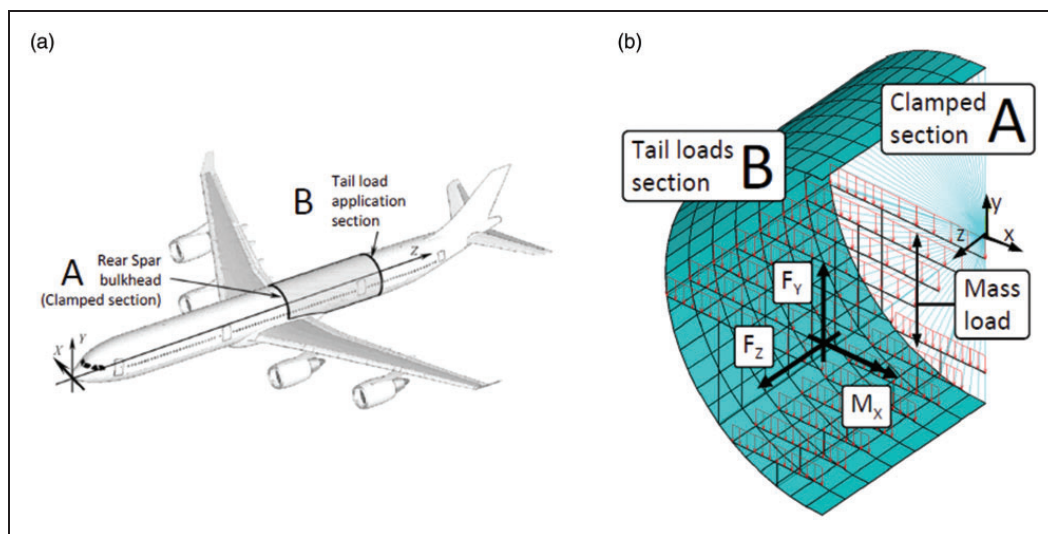
which is followed by the Numerical Results section. The final section ends the paper with some conclusions and prospects.

### Multi-scale least-weight design of a metallic fuselage section: Problem description

The MSO strategy presented in this study is applied to the least-weight design of an aluminium fuselage barrel of a wide-body aircraft. The fuselage barrel has a circular cross-section and is located between the wing rear spar and the tail, as shown in Figure 1. The fuselage barrel is clamped at the rear spar section (section A), and loads coming from the tail are applied to section B. Payload weight and pressurisation are also taken into account. More details on the BCs and the load cases (LCs) considered in the design process will be given in the sections ‘Hypotheses and Design Criteria’ and ‘Load cases’.

The main geometrical parameters of the fuselage cross-section, the structural architecture and loads are taken from Boni and coworkers<sup>11,30</sup> where an iterative design procedure integrating several analytical methods was presented. Their solution is hereafter referred as *literature solution* (LSol).

The main geometrical parameters of the fuselage barrel are reported in Table 1. The remaining data necessary to define LSol can be found in Table 2: the meaning of some of these parameters is explained in the Design variables section. The generic stiffened panel geometry considered in this study is shown in Figure 2. It is composed of hat-shaped stringers and floating frames with a Z-shaped cross-section connected to the skin by means of ‘shear-tie’ components; no ‘stringer tie’ or ‘tear strap’ components are present. Floor beams with an I-shaped cross-section



**Figure 1.** Location of the fuselage barrel<sup>30</sup> (a) and detail of the applied BCs (b).

and tubular struts complete the set of structural components.

All the components of the structure are considered made of 2024-T3 aluminium alloy whose mechanical and physical properties have been taken from Department of Defense<sup>31</sup> and are reported in Table 3.

### Hypotheses and Design Criteria

The case study here presented moves in the framework of the preliminary design phase of aircraft structures. During this phase, tents of LCs are assessed to properly design the main components of the structure in order to comply with certification specifications.<sup>32</sup> Such LCs are the result of a combination of basic

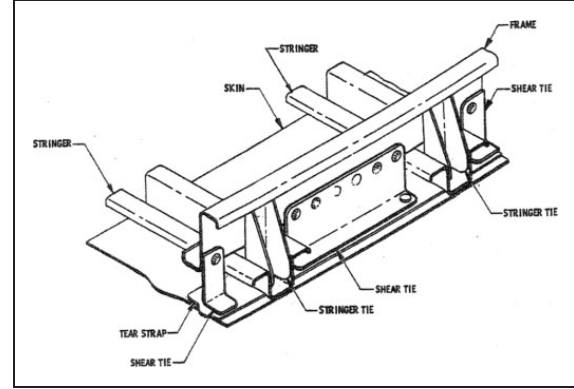
loading conditions (BLCs) of different nature, e.g. flight loads due to symmetrical manoeuvres, to asymmetrical ones or to gusts, ground loads, pressurisation, etc. In this work, only a sub-set of LCs, presented in the Load cases section, is considered.

**Table 1.** Main geometrical parameters of the fuselage barrel.<sup>11,30</sup>

| Component   | Value |
|---|-------|
| Fuselage diameter (mm)                                | 5640  |
| Number of bays  | 7     |
| Bay pitch (mm)  | 500   |
| Upper-deck floor vertical position (mm) <sup>a</sup>  | −152  |
| Lower-deck floor vertical position (mm) <sup>a</sup>  | −2130 |
| Struts position on upper-deck floor beam <sup>b</sup> | 1/3   |
| Struts position on lower-deck floor beam <sup>b</sup> | 1/4   |

<sup>a</sup>Referred to the horizontal axis through the geometrical centre of the fuselage cross-section.

<sup>b</sup>Normalised with the floor beam length and referred to the aircraft symmetry plane.



**Figure 2.** Architecture of the stiffened panel.

**Table 3.** Material properties of 2024-T3 aluminium alloy.<sup>31</sup>

| Propriety                     | Symbol     | Value  |
|-------------------------------|------------|--------|
| Young's modulus (MPa)         | E          | 72,395 |
| Poisson's ratio               | $\nu$      | 0.33   |
| Tensile yield stress (MPa)    | $\sigma_y$ | 290    |
| Tensile ultimate stress (MPa) | $\sigma_u$ | 434    |
| Density (g/cm <sup>3</sup> )  | $\rho$     | 2.78   |

**Table 2.** Geometrical parameters of the literature solution.<sup>11,30</sup>

| Component                              | Value |
|--|-------|
| Frame flange width ( $w_3^{Fr}$ ) (mm) | 35.0  |
| Frame web height ( $w_3^{Fr}$ ) (mm)   | 165.0 |
| Frame thickness ( $t^{Fr}$ ) (mm)      | 1.5   |
| Cabin floor beams web height (mm)      | 240.0 |
| Cabin floor beams flange width (mm)    | 156.0 |
| Cabin floor beams thickness (mm)       | 2.5   |
| Cargo floor beams web height (mm)      | 180.0 |
| Cargo floor beams flange width (mm)    | 60.0  |
| Cargo floor beams thickness (mm)       | 1.5   |
| Struts external diameter (mm)          | 21.5  |
| Struts internal diameter (mm)          | 15.5  |

| Component  | Top  | Lateral | Bottom |
|--|------|---------|--------|
| Stringer free flanges width ( $w_1^{St}$ ) (mm)  | 7.6  | 8.5     | 19.1   |
| Stringer bonded flange width ( $w_3^{St}$ ) (mm) | 12.6 | 10.9    | 35.4   |
| Stringer height ( $w_4^{St}$ ) (mm)              | 24.2 | 26.2    | 61.9   |
| Stringer thickness ( $t^{St}$ ) (mm)             | 1.4  | 3.2     | 1.8    |
| Skin thickness ( $t^{Sk}$ ) (mm)                 | 2.0  | 1.6     | 2.3    |
| Skin panels count ( $n$ ) (–)                    | 28   | 22      | 18     |

Moreover, for each LC, the material behaviour is supposed linear elastic, and the FE analyses are carried out by assuming small displacements and strains.

Concerning the modelling of the structural components, the following simplifications have been introduced:

1. In agreement with the preliminary design framework, only major components of the structure are modelled (i.e. skin, frames, stringers, floor beams and struts).
2. Floor beams and struts have a predefined geometry which is kept unchanged during optimisation.
3. Perfect bonding condition applies to the interface of the structural elements.
4. Connection zones (e.g. floor beams to frames or skin to skin) and opening/cut-out in the skin are not explicitly modelled.

Three main groups of criteria can be identified for the preliminary design phase, i.e. criteria related to (a) static loads, (b) fatigue loads and (c) aeroelasticity phenomena.

Regarding static loads, certification specifications<sup>32</sup> identify two types of design loads: *limit loads* (LLs) and *ultimate loads* (ULs). LLs are the maximum loads expected in service that the structure must be able to support without detrimental permanent deformations. ULs are equal to LLs multiplied by a prescribed factor of safety (usually 1.5). The structure must withstand ULs without failure for at least 3 s. For instance, for the wide-body civil aircraft class, LLs in symmetrical manoeuvres (neglecting gust loads) occur at load factors (the ratio of the aerodynamic force component normal to the longitudinal axis of the aeroplane to its weight)  $n_g = 2.5$  and  $n_g = -1$ . This work focuses on this class of DC.

As far as fatigue phenomena are concerned, the design of the structure should be performed in such a way that ‘catastrophic failure due to fatigue, manufacturing defects, environmental deterioration, or accidental damage, must be avoided throughout the operational life of the aeroplane’.<sup>32</sup> To achieve this goal, two approaches are possible. On one hand, in the framework of the *safe-life* approach, a component should be designed to last the whole operational life. On the other hand, according to the *damage tolerance* approach, a potential damage in the structure should not become critical before the next planned inspection. In this work, only one fatigue DC following the safe-life approach is employed in terms of an equivalent static check (more details are given in the following sections).

Finally, no aeroelastic criteria are used.

The following set of DC is integrated in the design process:

DC1: The global stiffness of the structure must be greater than the stiffness of LSol.

DC2: The average equivalent stress in the panels skin must not exceed the yielding stress of the material, considering a factor of safety  $F_S = 1.5$  (in agreement with CS 25.303 in European Aviation Safety Agency<sup>32</sup>), under LLs.

DC3: The average equivalent stress in the skin must not exceed the ultimate strength of the material under ULs.

DC4: No critical fatigue failure must occur caused by the hoop stress in the skin due to pressurisation.

DC5: No buckling must occur in the stiffened panels under ULs (no-buckling design approach).

DC6: Only manufacturable solutions are considered.

DC2 and DC3 are expressed in terms of average stresses in order to neglect the effect of local stress concentrations that could be strongly affected by the accuracy of the FE model and that constitute the object of the detailed design phase (performed after the preliminary design phase).

DC4 is a criterion against the nucleation of cracks in the longitudinal joints between the stiffened panels. It is translated into an equivalent static check according to the methodology reported in Boni<sup>11</sup> and Dai et al.<sup>33</sup> Such method is based on the definition of the Detail Fatigue Rating (DFR) parameter. It is defined as the maximum stress of a sinusoidal load with a ratio  $R = \sigma_{\min}/\sigma_{\max} = 0.06$  producing in  $10^5$  cycles the same damage of a given fatigue load spectrum. Starting from the knowledge that the maximum hoop stress due to pressurisation of an ATR<sup>®</sup> aircraft is  $\sigma_h^{\max} = 95$  MPa for  $N = 70,000$  flights,<sup>11</sup> it is possible to compute the equivalent DFR as follows

$$\text{DFR} = \sigma_{\text{mo}} \sigma_h^{\max} (1 - R) \left\{ 0.53 \sigma_h^{\max} (1 - R) + S^{5 - \log N \text{FRF}} [0.94 \sigma_{\text{mo}} - 0.47 \sigma_h^{\max} (1 + R)] \right\}^{-1}, \quad (1)$$

where  $\sigma_{\text{mo}}$  and  $S$  are fatigue material properties that, for a generic aluminium alloy, assume the values  $\sigma_{\text{mo}} = 310$  MPa and  $S = 2$ ;  $R = 0$  for the pressurisation cyclic load; FRF is the Fatigue Reliability Factor, i.e. a factor of safety fixed at  $\text{FRF} = 1.5$ .

Under the hypothesis that the required DFR of a structural detail is independent of the aircraft class, one can easily invert equation (1) to compute the maximum allowable hoop stress  $\sigma_h^{\text{adm}}$ . Supposing a target of  $N = 22,500$  flights, typical for a wide-body aircraft, a value of  $\sigma_h^{\text{adm}} = 126$  MPa is obtained.

### Load cases

Eight LCs are defined by linear superposition of two BLCs: a cruise loading condition (load factor  $n_g = 1$ ) without pressurisation, identified as BLC<sub>1g</sub>, and a pressurisation loading condition, identified as BLC<sub>p</sub>. In both BLCs, fuselage sections A and B are modelled as rigid and BCs are applied to their centres: section A

is always clamped, while pertinent tail forces and moments are applied at section B.

Under  $BLC_{1g}$ , payload weight is applied as a distributed load on floor beams. Structural mass is considered by applying additional loads on the upper-deck floor beams, on the basis of statistical estimated structural weight. Tail loads are computed in such a way to obtain in the check zone (i.e. the middle bay of the fuselage barrel) a maximum bending moment  $M_x = 5.0 \cdot 10^6$  Nm and a vertical shear force  $F_y = -370000$  N (in agreement with Boni and Fanteria<sup>30</sup>). A good estimation of the loading condition at a different value of the load factor is obtained by scaling  $BLC_{1g}$  by that value.

When using  $BLC_p$ , the effect of the maximum operating differential pressure (corresponding to the maximum relief valve setting) is taken into account as internal pressure on the skin plus an equivalent longitudinal force applied to section B of the fuselage barrel. By scaling  $BLC_p$ , the effect of different values of differential pressure can be assessed.

Data used for defining  $BLC_{1g}$  and  $BLC_p$  are reported in Table 4. The eight considered LCs are defined in Table 5 in which, for each LC, the assessed DC is also indicated. Aerodynamics loads on the fuselage have been neglected.

**Table 4.** Basic loading conditions data.

| Load  | $BLC_{1g}$         | $BLC_p$          |
|---|--------------------|------------------|
| Upper-deck floor beam total load (N)          | 10,000             | –                |
| Lower-deck floor beam total load (N)          | 5000               | –                |
| Bending moment $M_x$ at section 'B' (Nm)      | $4.305 \cdot 10^6$ | –                |
| Vertical shear force $F_y$ at section 'B' (N) | –310,000           | –                |
| Internal pressure (MPa)                       | –                  | 0.068            |
| Longitudinal force $F_z$ (N) <sup>a</sup>     | –                  | $1.7 \cdot 10^6$ |

<sup>a</sup>Equivalent to internal pressure times fuselage cross-section area.

**Table 5.** Load cases definition and associated design criterion.

| LC | $BLC_{1g}$ factor | $BLC_p$ factor | DC  |
|----|-------------------|----------------|-----|
| 1  | 1.00              | 1.00           | DC1 |
| 2  | 2.50              | 1.00           | DC2 |
| 3  | –1.00             | 1.00           | DC2 |
| 4  | 3.75              | 1.00           | DC3 |
| 5  | –1.50             | 1.00           | DC3 |
| 6  | 0                 | 1.00           | DC4 |
| 7  | 3.75              | 0              | DC5 |
| 8  | –1.50             | 0              | DC5 |

LC: load case; DC: design criterion.

## Mathematical formulation of the optimisation problem

### Design variables

Only geometrical design variables have been considered in this study. They can be grouped with respect to the component they are referred to.

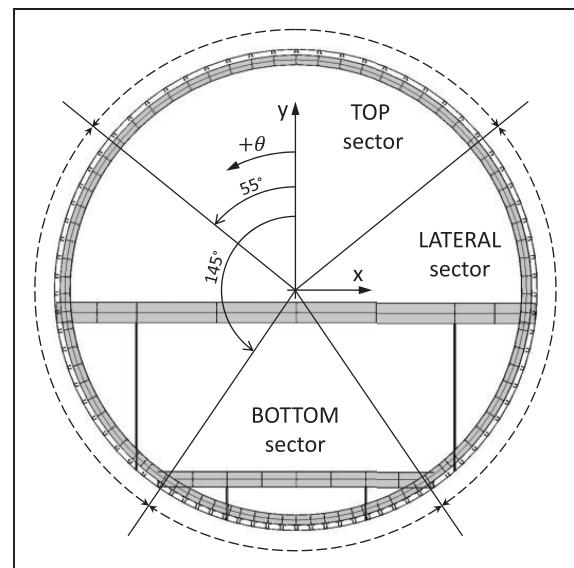
**Stringers and skin.** Three circumferential sectors are identified as in Figure 3: 'top', 'lateral' and 'bottom'. For each sector:

- the stringers section is hat-shaped, and four variables,  $w_1^{St}$ ,  $w_3^{St}$ ,  $w_4^{St}$  and  $t^{St}$ , are needed to describe its geometry (Figure 4(a));
- the skin is characterised by two variables, i.e. the thickness  $t^{Sk}$  and the number  $n$  of sub-regions between two consecutive frames and stringers (hereafter *skin panels*) within the sector.

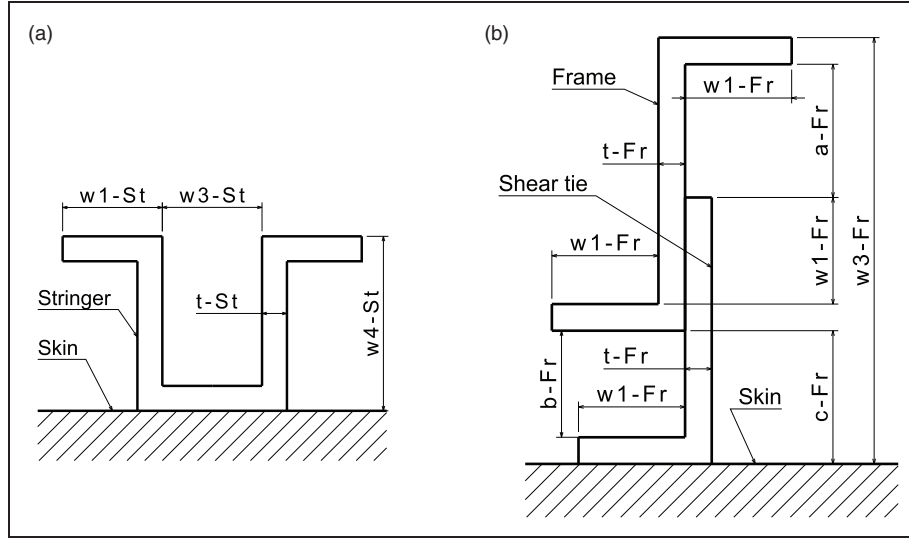
**Frame/shear-tie assembly.** Identical frames having a 'Z'-shaped cross-section with 'L' shear-tie are considered: three variables,  $w_1^{Fr}$ ,  $w_3^{Fr}$  and  $t^{Fr}$ , are needed to geometrically describe the assembly (Figure 4(b)). The distance between the floating frame and the fuselage skin depends on the maximum height of the stringers cross-sections according to the formula

$$c^{Fr} = \max_i w_4^{St-i} + 2 \text{ mm}, \quad \text{with } i = \text{Top, Lat, Bot.} \quad (2)$$

All the aforementioned design variables are collected into the vector  $\xi$ . It is noteworthy that frame pitch, floor beams and struts geometry have not been



**Figure 3.** Fuselage cross-section.



**Figure 4.** Stringers and frame/shear-tie assembly cross-section variables definition: (a) stringer cross-section and (b) frame/shear-tie cross-section.

considered among the problem design variables, rather they have been set equal to the reference values of the LSol as reported in Tables 1 and 2.

### Objective and constraint functions

The goal of the MSO strategy is the minimisation of the total mass of the fuselage barrel which can be easily expressed as

$$M(\xi) = V(\xi) \cdot \rho, \quad (3)$$

where  $V(\xi)$  is the total volume of the structure components, and  $\rho$  is the material density as defined in Table 3. As far as design requirements are concerned, one or more constraint functions are defined for each DC introduced in the Hypotheses and Design Criteria section. In particular, DC1 is formulated as a couple of constraints on the vertical displacement  $\delta_y$  and on the rotation  $\theta_x$  of the centre of section B when LC1 is considered. These constraints read

$$\begin{aligned} g_1(\xi) &= (\delta_y(\xi) - \delta_y^{\text{LSol}}) / \delta_y^{\text{LSol}} \leq 0, \\ g_2(\xi) &= (\theta_x(\xi) - \theta_x^{\text{LSol}}) / \theta_x^{\text{LSol}} \leq 0 \quad \text{at LC1.} \end{aligned} \quad (4)$$

In equation (4),  $\delta_y^{\text{LSol}} = -5.21$  mm and  $\theta_x^{\text{LSol}} = 0.065^\circ$  are the vertical displacement and rotation of the centre of section B evaluated for LSol.

DC2 is applied as a set of constraints on the maximum von Mises stress  $\langle \sigma_{eq} \rangle$  averaged on each skin panel ( $\omega_i$ ) belonging to the check zone ( $\Omega = \sum_{i=1}^N \omega_i$ , see The global/local finite element modelling approach section for more details). Such value has to be lower than the yield stress of the material under LC2 and LC3 with a factor of safety

$F_S = 1.5$ . Therefore, the related constraint inequalities are

$$\begin{aligned} g_3(\xi) &= \left( F_S \cdot \max_{\Omega} \langle \sigma_{eq}(\xi) \rangle_{\omega_i} - \sigma_y \right) / \sigma_y \leq 0 \quad \text{at LC2,} \\ g_4(\xi) &= \left( F_S \cdot \max_{\Omega} \langle \sigma_{eq}(\xi) \rangle_{\omega_i} - \sigma_y \right) / \sigma_y \leq 0 \quad \text{at LC3.} \end{aligned} \quad (5)$$

DC3 is applied in a similar way to DC2, obtaining

$$\begin{aligned} g_5(\xi) &= \left( \max_{\Omega} \langle \sigma_{eq}(\xi) \rangle_{\omega_i} - \sigma_u \right) / \sigma_u \leq 0 \quad \text{at LC4,} \\ g_6(\xi) &= \left( \max_{\Omega} \langle \sigma_{eq}(\xi) \rangle_{\omega_i} - \sigma_u \right) / \sigma_u \leq 0 \quad \text{at LC5.} \end{aligned} \quad (6)$$

As described in the Hypotheses and Design Criteria section, DC4 can be formulated as an equivalent constraint on the maximum hoop stress due to pressurisation. Such a requirement can be expressed as follows

$$g_7(\xi) = \left( \max_{\Omega} \langle \sigma_h(\xi) \rangle_{\omega_i} - \sigma_h^{\text{adm}} \right) / \sigma_h^{\text{adm}} \leq 0 \quad \text{at LC6.} \quad (7)$$

The requirement DC5 can be opportunely expressed by means of three optimisation constraints. For each circumferential sector, ULs are applied, and the most critical stiffened panel (composed of three stringers and two frames, as discussed in The global/local finite element modelling approach section) in the check zone is identified. An eigenvalue buckling



analysis is then performed on this panel in order to get a first buckling eigenvalue higher than 1 with a factor of safety  $F_S = 1.1$  (more details on this point are given in The global/local finite element modelling approach section). The related constraints read

$$\begin{aligned} g_8(\xi) &= 1.1 - \lambda^{\text{Top}}(\xi) \leq 0 \quad \text{at LC8,} \\ g_9(\xi) &= 1.1 - \lambda^{\text{Lat}}(\xi) \leq 0 \quad \text{at LC7,} \\ g_{10}(\xi) &= 1.1 - \lambda^{\text{Bot}}(\xi) \leq 0 \quad \text{at LC7.} \end{aligned} \quad (8)$$

DC6 is applied by imposing a series of inequalities involving the design variables and representing different types of manufacturability requirements.

Minimum thickness of thin-walled elements.

$$\begin{aligned} t^{\text{St}-i} &\geq 1 \text{ mm,} \quad \text{with } i = \text{Top, Lat, Bot;} \\ t^{\text{Sk}-i} &\geq 1 \text{ mm,} \quad \text{with } i = \text{Top, Lat, Bot;} \\ t^{\text{Fr}} &\geq 1 \text{ mm.} \end{aligned}$$

Minimum length of the interface flange of stiffening components for the installation of rivets.

$$\begin{aligned} w_3^{\text{St}-i} &\geq 14 \text{ mm,} \quad \text{with } i = \text{Top, Lat, Bot;} \\ w_1^{\text{Fr}} &\geq 14 \text{ mm.} \end{aligned}$$

Minimum length to thickness ratio of sheet elements.

$$\begin{aligned} w_1^{\text{St}-i} / t^{\text{St}-i} &\geq 4, \quad \text{with } i = \text{Top, Lat, Bot;} \\ w_3^{\text{St}-i} / t^{\text{St}-i} &\geq 3, \quad \text{with } i = \text{Top, Lat, Bot;} \\ w_4^{\text{St}-i} / t^{\text{St}-i} &\geq 5, \quad \text{with } i = \text{Top, Lat, Bot;} \\ w_1^{\text{Fr}} / t^{\text{Fr}} &\geq 3; \\ a^{\text{Fr}}(\xi) / t^{\text{Fr}} &\geq 3; \\ b^{\text{Fr}}(\xi) / t^{\text{Fr}} &\geq 3. \end{aligned}$$

Minimum circumferential distance between stringers.

$$\begin{aligned} \text{pitch}^{\text{St}-i}(\xi) &\geq 2 \cdot (2 \cdot w_1^{\text{St}-i} + w_3^{\text{St}-i}), \\ &\text{with } i = \text{Top, Lat, Bot.} \end{aligned}$$

These constraints behave more like logic conditions (i.e. True/False values) rather than continuous-valued functions. Inasmuch as these constraint functions are mainly related to Boolean operations, it is sufficient that each of them is satisfied regardless of its value, i.e. a value closer to the bounds would not produce any advantage.

Some of these inequalities are directly employed in the definition of the lower and upper bounds of the design variables for the problem at hand, as listed in Table 6, while the remaining inequalities are stated in the form  $l_j(\xi) \leq 0$  and then aggregated into a single constraint using the maximum operator

$$g_{11}(\xi) = \max_j l_j(\xi) \leq 0. \quad (9)$$

**Table 6.** Lower and upper bounds of the design variables.

| Design variable     | Unit | Lower bound | Upper bound | Step size |
|---------------------|------|-------------|-------------|-----------|
| $w_1^{\text{Fr}}$   | mm   | 20          | 50          | 0.5       |
| $w_3^{\text{Fr}}$   | mm   | 80          | 190         | 1.0       |
| $t^{\text{Fr}}$     | mm   | 1           | 4           | 0.1       |
| $w_1^{\text{St}-i}$ | mm   | 5           | 30          | 0.5       |
| $w_3^{\text{St}-i}$ | mm   | 14          | 40          | 0.5       |
| $w_4^{\text{St}-i}$ | mm   | 14          | 70          | 0.5       |
| $t^{\text{St}-i}$   | mm   | 1           | 4           | 0.1       |
| $t^{\text{Sk}-i}$   | mm   | 1           | 4           | 0.1       |
| $n^{\text{Top}}$    | –    | 18          | 38          | 2         |
| $n^{\text{Lat}}$    | –    | 13          | 31          | 1         |
| $n^{\text{Bot}}$    | –    | 12          | 26          | 2         |

With  $i = \text{Top, Lat, Bot.}$

When a completely unfeasible solution is detected (e.g. a solution with an overlap between stringers), the corresponding FE models are not generated, and the solution is penalised by assigning a high value to the objective function and a unit value to the constraints that cannot be evaluated.

It is noteworthy that the step size of the thickness of the different components has been fixed to  $\Delta t = 0.1 \text{ mm}$  to be coherent with the thickness of commercially available aluminium sheets.

Finally, the optimisation problem can be formulated as a classical CNLPP as follows

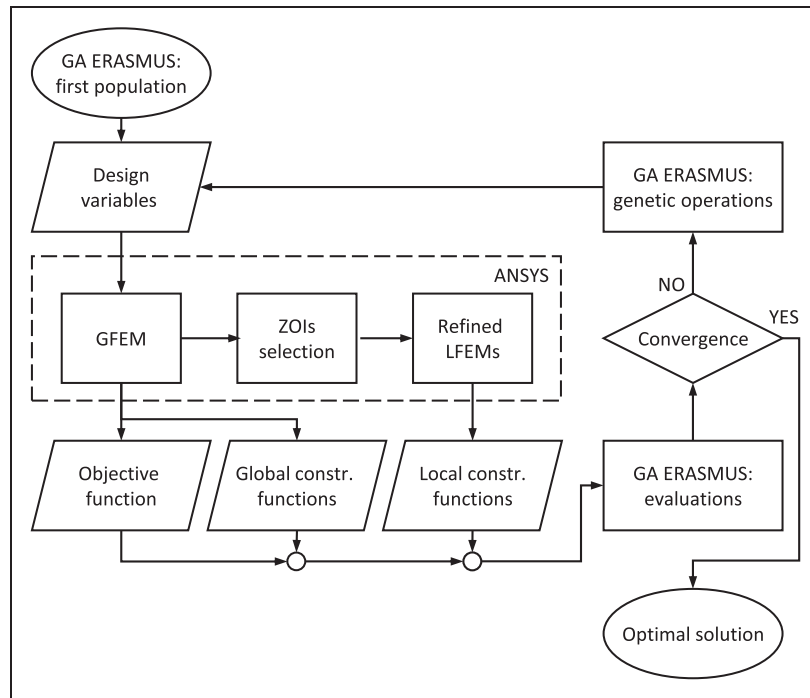
$$\begin{aligned} \min_{\xi} \quad & M(\xi), \\ \text{subject to:} \quad & \\ g_i(\xi) &\leq 0, \quad \text{with } i = 1, 2, \dots, 11. \end{aligned} \quad (10)$$

The design space of the problem is detailed in Table 6.

### Numerical strategy

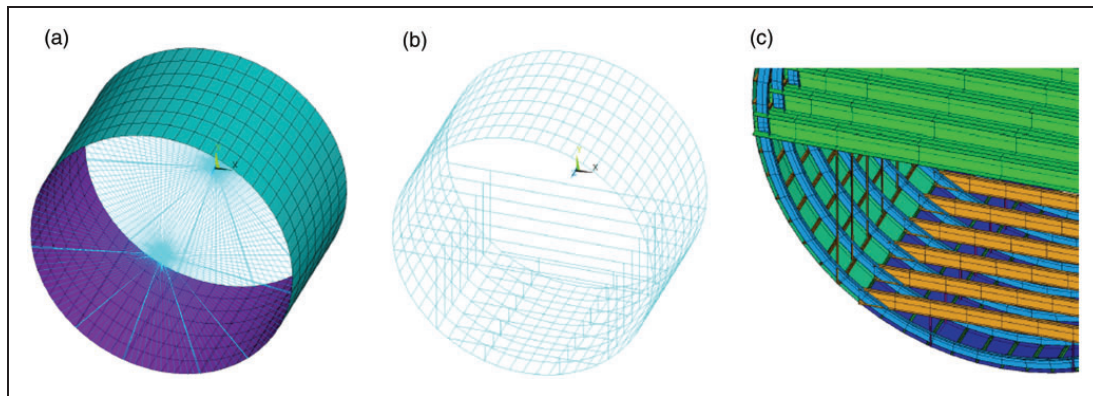
Problem (10) is a non-convex CNLPP. The total number of design variables is 21, while the number of optimisation constraints is 11. For the resolution of problem (10), the GA ERASMUS<sup>29</sup> coupled with both GFEM and LFEMs of the structure has been utilised as optimisation tool to perform the solution search, as illustrated in Figure 5. The GA ERASMUS has already been successfully applied to solve different kinds of engineering problems, see for example, Montemurro and coworkers.<sup>29,34–41</sup>

As shown in Figure 5, for each individual, at each generation, the numerical tool performs global and local FE analyses to calculate the objective function and the optimisation constraints. The FE models are implemented in the ANSYS<sup>®</sup> environment, and their input data are generated by the GA ERASMUS (more details are given in The global/local finite element modelling approach section). The GA elaborates the results provided by the GFEM and the



**Figure 5.** Flowchart of the optimisation process.

GA: genetic algorithm; ZOIs: zones of interest; GFEM: global finite element model; LFEM: local finite element model.



**Figure 6.** Global FE model: (a) shell and MPC elements, (b) beam elements and (c) detailed view with the integral shape of the elements. MPC: multi-point constraint.

LFEMs in order to execute the genetic operations and generate new individuals. These operations are repeated until the GA meets the user-defined convergence criterion. The generic individual of the GA ERASMUS represents a potential solution for the problem at hand. The genotype of the individual for problem (10) is characterised by only one chromosome composed of 21 genes, each one coding a component of the vector of design variables  $\xi$ .

### The global/local finite element modelling approach

As stated above, the FE models integrated in the optimisation process are based on a GL modelling

approach. In particular, two different models are created: the GFEM for the assessment of the behaviour of the whole fuselage barrel and refined LFEMs in order to properly evaluate local responses. LFEMs are created only at the critical ZOIs identified during the global analysis; thus, suitable criteria must be developed to accomplish this task.

Both GFEM and LFEMs are fully parametric and are built using the commercial FE code ANSYS®.

#### The GFEM

The GFEM is shown in Figure 6: it includes the seven bays constituting the fuselage barrel. The fuselage skin is modelled with eight-node SHELL281 elements,

while frames, stringer, floor beams and struts are modelled with three-node BEAM189 elements. The beam and shell elements are connected together by node merging. To take into account the actual position of the beam cross-section with respect to the skin, a section offset is applied to beam elements. Shear-tie components are not modelled, but their mechanical effect (the transfer of shear load from the frames to the skin) is ensured by the direct connection between frame and skin elements.

The element type (linear or quadratic) and mesh size have been chosen after performing a sensitivity analysis, of which the main details can be found in Appendix 1. In particular, the use of one quadratic element for each skin panel gives a good compromise between results accuracy and computational cost; thus, the mesh size has been set accordingly.

A master node is created at the centre of sections A and B and linked to the set of 'slave' nodes of the corresponding frame by means of MPC184 (multi-point constraint) elements with 'rigid beam' behaviour (Figure 6(a)). These master nodes are used to apply the BCs presented in the Load cases section. In agreement with the hypotheses and the DC discussed in the Hypotheses and Design Criteria section, only linear static analyses are performed on this model.

Of course, the first bay (from each side of the fuselage barrel) is strongly influenced by edge effects because of the proximity to zones where BCs are applied (i.e. at nodes A and B). Accordingly, only the central bay constitutes the *check zone*, where the results of the analysis are meaningful. Moreover, as explained in the Hypotheses and Design Criteria section, the elements adjacent to connection zones (e.g. floor beams to frames connections or the joints between circumferential sectors) are excluded from the check zone, as illustrated in Figure 7.

Results provided by the GFEM are used for the evaluation of the objective function and all the constraint functions except those related to buckling requirements, i.e.  $g_8$ ,  $g_9$  and  $g_{10}$ .

### The LFEMs

LFEMs are created to evaluate the first buckling load of the most critical fuselage stiffened panels. This task can be achieved only through a suitably refined FE model able to catch both global and local buckling modes.

Each LFEM includes the same number of stringers and frames, i.e. three and two, respectively, as shown in Figure 8. The local model presents a suitable extinction zone to mitigate edge effects due to the application of BCs. This extinction zone is half a skin-panel wide and surrounds the check zone, as illustrated in Figure 8. The LFEM is entirely built by using eight-node SHELL281 elements.

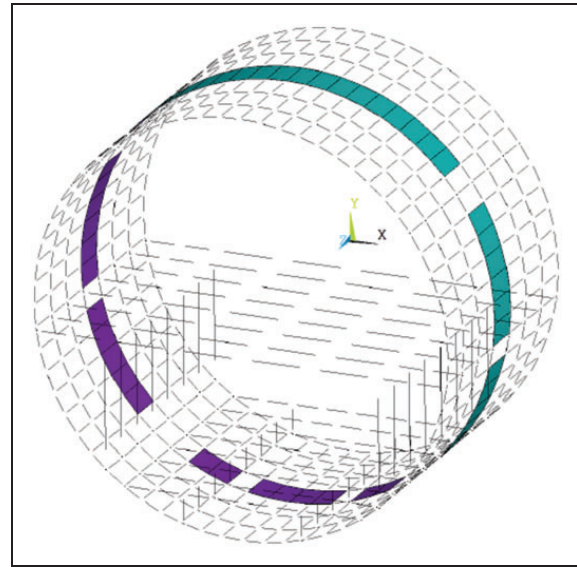


Figure 7. Check zone of the global FE model.

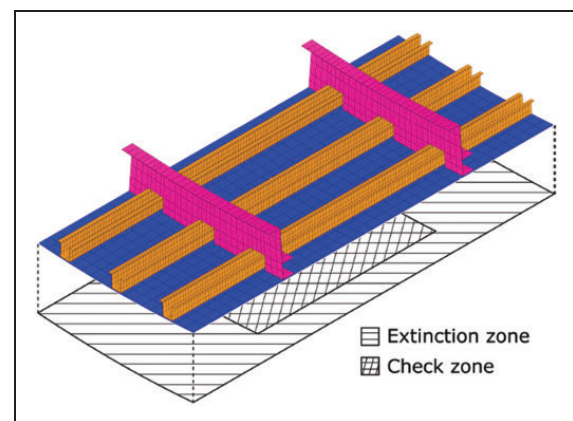


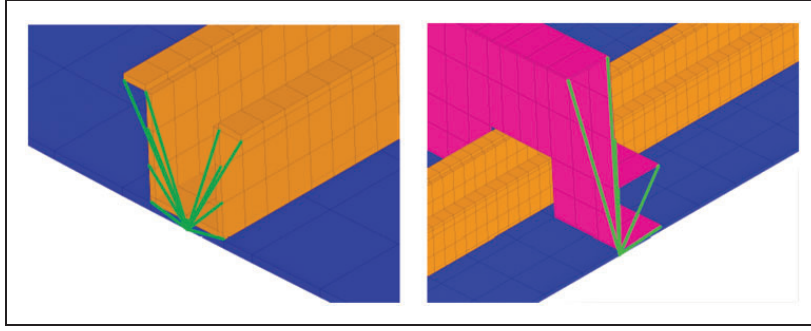
Figure 8. Typical local FE model.

Both shear-ties and stringers are tied to the skin by creating constraint equations between their interface nodes by using the ANSYS® CEINTF command.<sup>42</sup> This allows having an independent mesh size on the different components. Also for the LFEM, the mesh size is the result of a compromise between the accuracy in evaluating the first buckling load of the stiffened panel, which can occur either in the skin or in the flanges of stringers and frames, and the computational time. A sensitivity analysis has been conducted also in this case: the main results are reported in Appendix 1.

Displacement BCs extracted from the results of the global analysis are imposed to all the boundary nodes belonging to the skin of the LFEM.

To transfer the BCs to the stringers and frames, for each ending cross-section, a master node is extracted from the skin boundary nodes located at the interface between the beam reference axis and the skin in the GFEM. The coordinates of this set of master nodes





**Figure 9.** Detail of the ending cross-section of the stiffening components in the local FE model.

are recorded and passed to the LFEM (for each region of the fuselage barrel). Then, these nodes are selected and connected to those belonging to the corresponding stringer/frame ending cross-section by means of MPC184 elements with ‘rigid beam’ behaviour, ensuring in this way the kinematic compatibility between global and local models, see Figure 9.

The LFEM is built for each sector of the fuselage barrel (bottom, top and lateral). An eigenvalue buckling analysis is performed on the local models, and the lowest positive eigenvalue,  $\lambda(\xi)$ , is retrieved as output.

#### *ZOIs identification criteria and information transfer between global and local models*

In the presented MSO strategy, the fewest number of local models is checked in order to keep the computational time as low as possible. To this purpose, specific criteria have been introduced and applied to the post-processing of results coming from the GFEM in order to identify the most critical ZOIs around which LFEMs are automatically generated. For each circular sector belonging to the check zone, only one ZOI is identified and analysed.

As discussed in the sections ‘Load cases’ and ‘Objective and constraint functions’, the buckling-related constraints are evaluated for LC7 and LC8 (see Table 5). These LCs are obtained by scaling  $BLC_{1g}$  by means of a suitable load factor. Under  $BLC_{1g}$ , the stiffened panels in the top and bottom sectors are mostly subject to stress in the longitudinal direction, as shown in Figure 10. Therefore, top and bottom ZOIs are identified by looking for the *basic-panel*, i.e. the assembly composed of a stringer plus half of the adjacent skin panels, that withstands the highest compressive average longitudinal force per unit width,  $N_l^{BP}$ , computed, for the generic LC, as

$$N_l^{BP} = \frac{F^{st} + \int_{-w^{sp}/2}^{w^{sp}/2} \int_0^{r^{sk}} \sigma_l^{sk} dz dy}{w^{sp}}, \quad (11)$$

where  $F^{st}$  is the axial tensile force in the stringer,  $w^{sp}$  is the width along the hoop direction of the skin panel and  $\sigma_l^{sk}$  is the longitudinal stress in the skin.

On the other hand, the panels in the lateral sector are subject to biaxial loads corresponding to a combination of mainly shear and longitudinal stress; the latter varying from tensile to compression depending on the position of the considered stiffened panel (see Figure 10). Accordingly, a different criterion is used for the lateral sector: the ZOI is identified by looking for the most critical skin panel with respect to the buckling strength. An estimation of the buckling load is computed for each skin panel in the check zone using analytical formulae for a simply supported ‘shadow’ plate with the same dimensions of the analysed skin panel, i.e.  $a$  along the longitudinal direction and  $b$  along the hoop one, the same thickness  $t^{sk}$  and subject to the same biaxial stress field given by the average membrane forces per unit length  $N_x$ ,  $N_y$  and  $N_{xy}$ . The buckling factor due to biaxial compression forces and that due to shear forces are computed independently. An interaction equation is then used to compute the buckling factor due to the combined load. Under the hypothesis that the plate buckles with an out-of-plane displacement field described by

$$w(x, y) = \sum_{m=1}^{\infty} \sum_{n=1}^{\infty} a_{mn} \sin \frac{m\pi x}{a} \sin \frac{n\pi y}{b}, \quad (12)$$

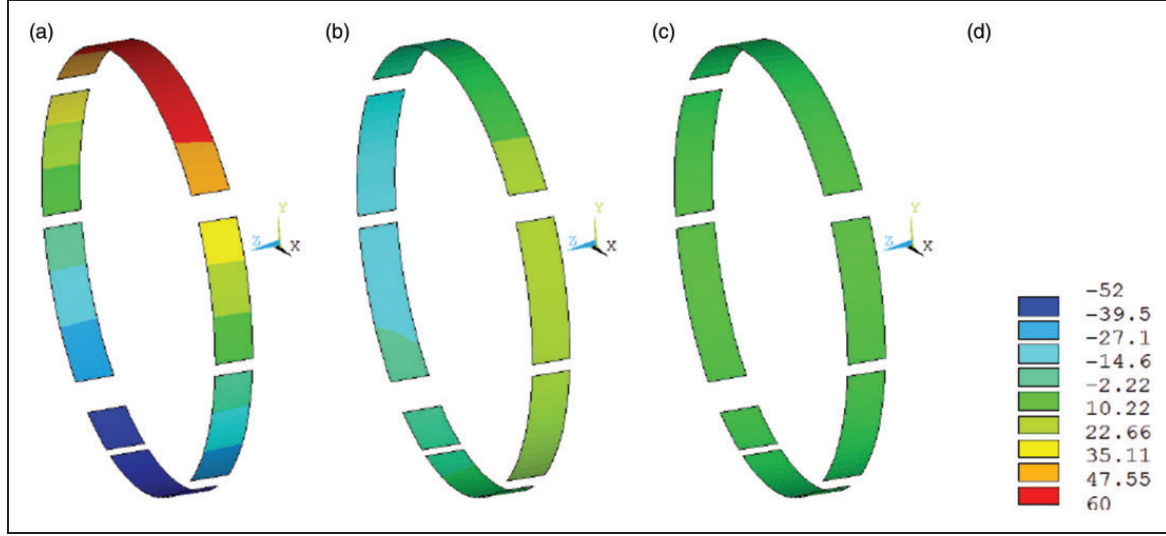
the buckling eigenvalue due to the solely compressive membrane forces per unit length  $N_x$  and  $N_y$  can be computed as<sup>43</sup>

$$\lambda^c = \min_{m,n} \pi^2 \frac{D[(m/a)^2 + (n/b)^2]^2}{N_x(m/a)^2 + N_y(n/b)^2}, \quad (13)$$

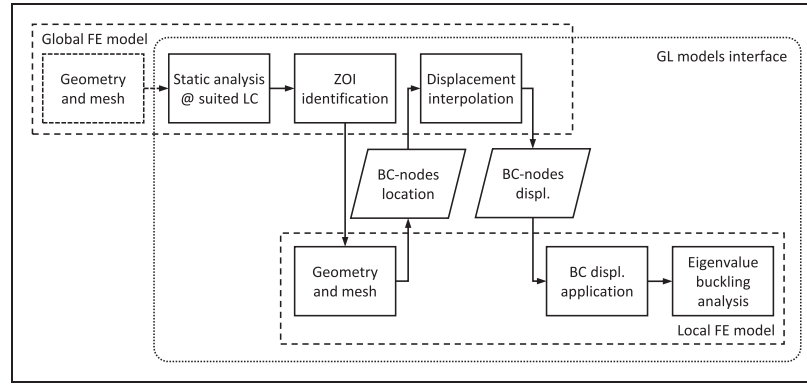
where  $x$  and  $y$  directions correspond to longitudinal and hoop ones, and  $D$  is the flexural rigidity of the plate. The buckling eigenvalue due to the shear forces per unit width  $N_{xy}$  can be approximated as<sup>43</sup>

$$\lambda^s \approx \frac{(5.35 + 4r^2)\pi^2 D}{N_{xy} c^2}, \quad (14)$$

where  $r = \min(a/b, b/a)$  and  $c = \min(a, b)$ . An interaction equation can be used to define the critical



**Figure 10.** Stress distribution in the skin panels in the check zone at BLCIg: (a) longitudinal stress, (b) shear stress, (c) hoop stress and (d) legend (MPa).



**Figure 11.** Interaction scheme between global and local finite element models.  
FE: finite element; LC: load case; BC: boundary condition; GL: global/local; ZOI: zone of interest.

condition in presence of the two loading conditions<sup>44</sup>

$$\left(\frac{1}{\lambda_{cr}^s}\right)^2 + \frac{1}{\lambda_{cr}^c} = 1. \quad (15)$$

If the critical buckling factor, for the combined loading conditions, is defined as

$$\lambda_{cr} := \frac{\lambda_{cr}^s}{\lambda_{cr}^c} = \frac{\lambda_{cr}^c}{\lambda_{cr}^s}, \quad (16)$$

one can calculate its value according to the following formula

$$\lambda_{cr} = \frac{-\frac{\lambda_{cr}^s}{\lambda_{cr}^c} + \sqrt{\left(\frac{\lambda_{cr}^s}{\lambda_{cr}^c}\right)^2 + 4\lambda_{cr}^s}}{2}. \quad (17)$$

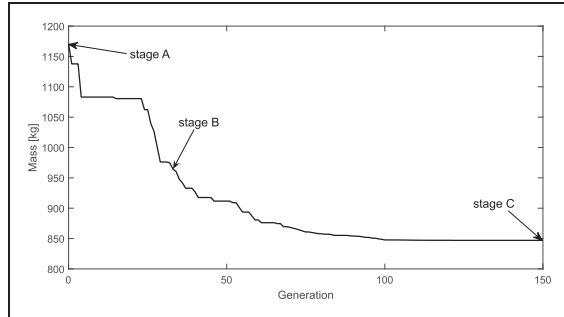
Therefore, the skin panel showing the minimum  $\lambda_{cr}$  identifies the lateral ZOI.

**Table 7.** Parameters of the GA ERASMUS used for the solution search.

| Parameter                         | Value                   |
|-----------------------------------|-------------------------|
| No. of populations                | 1                       |
| No. of individuals per population | 210                     |
| No. of chromosomes                | 1                       |
| No. of genes                      | 21                      |
| Stop criterion                    | Fixed generations (150) |
| Crossover probability             | 0.85                    |
| Mutation probability              | 0.01                    |
| Selection operator                | Roulette wheel          |
| Fitness pressure                  | 1                       |
| Elitism operator                  | Active                  |

As already stated, the displacement field resulting from the GFEM is used to define the BCs for the LFEMs. To this purpose, for each LC, the nodal displacements of the GFEM are interpolated using the

shape functions of the elements in the GFEM at the location of the boundary nodes of the LFEM. The logical flow of the process that goes from the global FE analysis to the local one is given in Figure 11.



**Figure 12.** Best individual versus iterations.

## Numerical results

The parameters of the GA ERASMUS used to perform the solution search for problem (10) are listed in Table 7. As far as the optimisation constraints are concerned, they have been handled through the Automatic Dynamic Penalisation method.<sup>45</sup> Further details on the optimisation tool and its parameters can be found in Montemurro.<sup>29</sup>

The whole optimisation process requires a computational time of approximately 14 days (i.e. around 40 s for global and local FE analyses for the generic point in the design space) when four cores of a machine with an Intel Xeon E5-2697v2 processor (2.70–3.50 GHz) are dedicated to the ANSYS<sup>®</sup> solver. However, computational time could be easily reduced by performing in parallel the FE calculations of the different individuals.

**Table 8.** Comparison of the values of the constraint and objective functions relative to different individuals.

| Function |                     | A-1    | B-1    | C-3    | C-2    | C-1 <sup>a</sup> | LSol   |
|----------|---------------------|--------|--------|--------|--------|------------------|--------|
| $g_1$    | (stiffness)         | −0.467 | −0.331 | −0.227 | −0.238 | −0.262           | −0.000 |
| $g_2$    | (stiffness)         | −0.426 | −0.115 | −0.190 | −0.179 | −0.053           | −0.000 |
| $g_3$    | (strength)          | −0.446 | −0.076 | −0.163 | −0.179 | −0.013           | +0.020 |
| $g_4$    | (strength)          | −0.683 | −0.479 | −0.573 | −0.573 | −0.426           | −0.487 |
| $g_5$    | (strength)          | −0.642 | −0.420 | −0.466 | −0.477 | −0.378           | −0.350 |
| $g_6$    | (strength)          | −0.822 | −0.718 | −0.759 | −0.760 | −0.689           | −0.726 |
| $g_7$    | (fatigue)           | −0.578 | −0.239 | −0.357 | −0.387 | −0.197           | −0.213 |
| $g_8$    | (buckling)          | −1.845 | −0.155 | −0.133 | −0.110 | −0.070           | +0.535 |
| $g_9$    | (buckling)          | −0.513 | −0.034 | −0.191 | −0.087 | −0.029           | +0.811 |
| $g_{10}$ | (buckling)          | −0.484 | −0.234 | −0.001 | −0.213 | −0.027           | +0.570 |
| $g_{11}$ | (manufacturability) | −0.024 | −0.030 | −0.560 | −0.033 | −0.545           | +1.344 |
| M        | (kg)                | 1158   | 966    | 886    | 871    | 847              | 837    |

LSol: literature solution.

<sup>a</sup>Retained optimal solution.

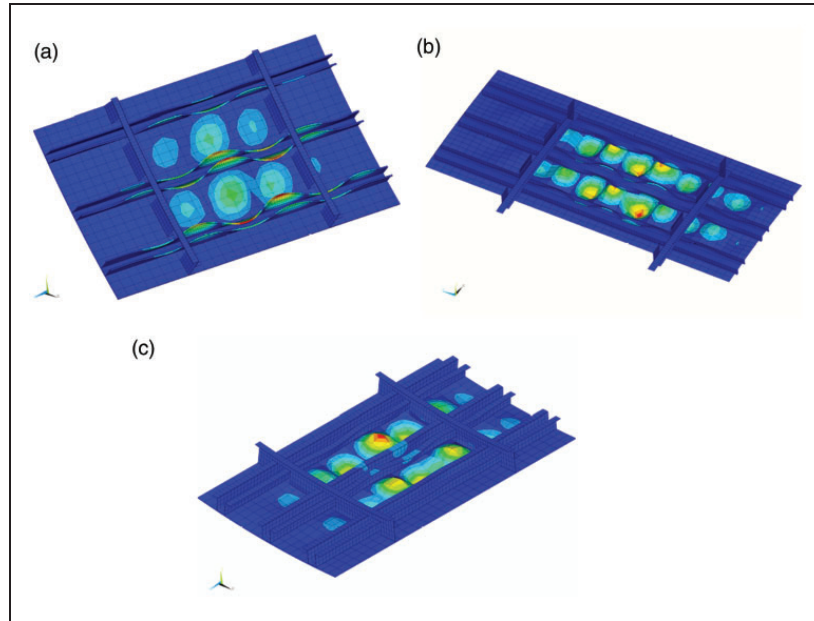
**Table 9.** Design variables values for optimal individuals at the last generation.

| Variable        | C-3  |       |      | C-2  |       |                 | C-1 <sup>a</sup>  |                   |      | LSol |       |      |
|-----------------|------|-------|------|------|-------|-----------------|-------------------|-------------------|------|------|-------|------|
|                 | Top  | Lat.  | Bot. | Top  | Lat.  | Bot.            | Top               | Lat.              | Bot. | Top  | Lat.  | Bot. |
| $w_1^{Fr}$ (mm) |      | 28.5  |      |      | 29.0  |                 |                   | 20.0 <sup>b</sup> |      |      | 35.0  |      |
| $w_3^{Fr}$ (mm) |      | 116.5 |      |      | 120.0 |                 |                   | 81.0              |      |      | 165.0 |      |
| $t^{Fr}$ (mm)   |      | 1.2   |      |      | 1.2   |                 |                   | 1.0 <sup>b</sup>  |      |      | 1.5   |      |
| $w_1^{Sc}$ (mm) | 6.0  | 8.0   | 17.5 | 6.5  | 7.5   | 18.5            | 5.0 <sup>b</sup>  | 5.0 <sup>b</sup>  | 21.0 | 7.6  | 8.5   | 19.1 |
| $w_3^{Sc}$ (mm) | 23.0 | 27.5  | 26.0 | 25.5 | 27.0  | 28.0            | 40.0 <sup>b</sup> | 24.5              | 31.0 | 12.6 | 10.9  | 35.4 |
| $w_4^{Sc}$ (mm) | 23.5 | 33.0  | 64.5 | 27.5 | 21.5  | 61.5            | 19.0              | 38.0              | 45.5 | 24.2 | 26.2  | 61.9 |
| $t^{Sc}$ (mm)   | 1.3  | 1.2   | 2.5  | 1.6  | 1.4   | 1.6             | 1.1               | 1.0 <sup>b</sup>  | 1.4  | 1.4  | 3.2   | 1.8  |
| $t^{Sk}$ (mm)   | 2.5  | 2.2   | 2.5  | 2.5  | 2.3   | 2.4             | 1.8               | 3.0               | 3.6  | 2.0  | 1.6   | 2.3  |
| $n$ (–)         | 30   | 30    | 22   | 28   | 30    | 26 <sup>b</sup> | 36                | 24                | 18   | 28   | 22    | 18   |

LSol: literature solution.

<sup>a</sup>Retained optimal solution.

<sup>b</sup>Values at the bounds of the design space (see Table 6).



**Figure 13.** Normalised displacement field (blue color = 0; red color = 1) of the first buckling mode of the local models for the optimum solution: (a) lateral sector panel, (b) top sector panel and (c) bottom sector panel.

The evolution of the objective function of the best individual for each generation of the optimisation process is shown in Figure 12. It can be noticed that the convergence is achieved after about 100 generations because no improvement in the objective function is observed in the subsequent iterations of the evolutionary process. In Figure 12, three stages can be identified corresponding to first, intermediate and last generations, i.e. stages A, B and C, respectively. The complete set of performances, in terms of constraint and objective functions, for the best individual at each stage, i.e. individuals A-1, B-1 and C-1, is reported in Table 8. Concerning stage C, two other individuals (C-2 and C-3) are reported together with the optimum solution C-1 (recall that the CNLPP is strongly non-convex). Indeed, a significant number of pseudo-optimal solutions exists at stage C that are nearly identical to solution C-1 and that are not reported here for the sake of brevity. The values of the design variables identifying the individuals C-1, C-2 and C-3 are listed in Table 9.

A quick glance to the results provided in Tables 8 and 9 suffices to infer that, due to the non-convex nature of problem (10), the GA finds almost equivalent optimal solutions, e.g. C-1, C-2 and C-3, quite different in terms of design variables, that still respect all the constraints and that have comparable values of the objective function.

Concerning the retained optimal solution, i.e. C-1, from Table 9, one can notice that some of the variables are located at the bounds of the respective intervals (see Table 6).

By observing the buckling mode of each one of the three optimised sectors for solution C-1, as illustrated in Figure 13, it can be noticed that the stringers and

the skin buckle simultaneously, in agreement with the well-established aeronautical DC that the maximum structural efficiency (in terms of best compromise between minimum weight and maximum buckling load) for stiffened structures is reached when their components buckle at the same load.<sup>46</sup>

Finally, for comparison purposes, the performances of LSol and some of its geometrical parameters, previously shown in Table 2, are also added in Tables 8 and 9, respectively. From the analysis of these results, it is clear that LSol has been obtained with different requirements than those used in this work; in particular, constraints  $g_3$ ,  $g_8$ ,  $g_9$  and  $g_{10}$  are too restrictive for LSol, which is clearly infeasible. Also the geometrical requirement  $g_{11}$  is not respected by LSol which is characterised by too close stringers in the bottom sector. Moreover, it is noteworthy that, despite of the big differences in performances, the difference in mass between C-1 and LSol is lower than 1.2%. Therefore, the proposed approach allows finding an optimal configuration of the fuselage barrel satisfying the full set of design requirements. This result constitutes a sort of ‘numerical proof’ about the limitations related to the use of simplifying hypotheses and analytical formulae/models in the framework of the preliminary design phase of aircraft structures.

## Conclusions

An MSO strategy for designing thin-walled structures integrating a dedicated GL modelling approach has been presented in this work.

As usual for this type of structures, the design problem is formulated as a CNLPP involving

constraints of different nature. The formulation of such requirements involves the structure response, at each pertinent scale, under various loading conditions. To deal with these aspects, fully parametric FE models are created at different scales for the evaluation of the most relevant phenomena. A coherent information transfer between these models is ensured by implementing a sub-modelling GL approach: BCs of the local models are directly extracted, in terms of displacements, from the results of the global analysis and properly transferred to the LFEM. LFEMs are automatically created only for critical ZOIs which are identified, by means of opportune criteria, during the global analysis. The solution search for the multi-scale CNLPP is performed by interfacing the GFEM and the LFEMs of the structure with the GA ERASMUS developed at the I2M laboratory in Bordeaux.

The proposed strategy is general and allows dealing with design variables and constraints of different nature. Every variable at each relevant scale is considered in the design process, avoiding the introduction of simplifying hypotheses in the definition of the design space, which have the main effect of shrinking it, thus preventing the possibility to find a true global optimum solution. Moreover, by employing a GL modelling approach, more accurate results are obtained than those found by means of well-established strategies that use simplified analytical models for the assessment of the mechanical response of the structure, as proven by the numerical results of this study. Finally, the whole process, once set, is fully automated and does not need the user intervention.

The effectiveness of the proposed MSO strategy is proven on a meaningful design case: the least-weight design of an aluminium fuselage barrel of a wide-body aircraft. In the considered test case, a limited, yet representative, set of loading conditions and DC are considered. Nevertheless, further criteria and LCs could be easily introduced in the general framework of the presented design strategy.

The obtained results for the presented design case seem realistic and coherent: at the component scale, the elements composing the stiffened panel (of the most critical ZOIs of the fuselage barrel) buckle simultaneously in agreement with well-established design procedures used in both academic and industrial communities.<sup>46</sup> Moreover, difference between the mass of the optimised configuration provided by the MSO and that of the reference solution (taken from the literature and obtained by using simplifying hypotheses and simple models and rules) is lower than 1.2%. However, the reference solution taken from the literature is infeasible and does not meet some of the DC employed in this work which result too restrictive. This constitutes a sort of ‘numerical proof’ about the unsuitability of some simplifying hypotheses and low-fidelity analytical/numerical models often used in the preliminary design phase of aircraft structures.

These results encourage research activity in this direction. As far as prospects of this work are concerned, the formulation of the CNLPP will be enhanced by adding requirements on the post-buckling behaviour of the most critical stiffened panel in each sector of the fuselage barrel. Moreover, research is ongoing in order to extend the MSO approach to the case of thin-walled structures made of composite materials. Of course, in this case, the design problem formulation must integrate requirements and specificities of composite solutions, e.g. suitable failure criteria at each scale (lamina-level and constitutive phases-level), delamination criteria, manufacturing requirements, etc.


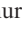


### Declaration of Conflicting Interests

The author(s) declared no potential conflicts of interest with respect to the research, authorship, and/or publication of this article.

### Funding

The author(s) disclosed receipt of the following financial support for the research, authorship, and/or publication of this article: This paper presents part of the activities carried out within the research project PARSIFAL (Prandtlplane ARchitecture for the Sustainable Improvement of Future AirpLanes), which has been funded by the European Union under the Horizon 2020 Research and Innovation Program (Grant Agreement n.723149).

### ORCID iDs

Michele I Izzi  <https://orcid.org/0000-0002-5605-2438>  
 Marco Montemurro  <https://orcid.org/0000-0001-5688-3664>  
 Anita Catapano  <https://orcid.org/0000-0002-0504-1624>  
 Daniele Fanteria  <https://orcid.org/0000-0002-2393-4450>

### References

1. Wignot JE, Combs H and Ensrud AF. *Analysis of circular shell-supported frames* (Technical Note 929). Washington, DC: National Advisory Committee for Aeronautics, 1944.
2. Kuhn P, Peterson JP and Levin LR. *Summary of diagonal tension* (Technical Note 2661). Washington, DC: National Advisory Committee for Aeronautics, 1952.
3. Gerard G. The crippling strength of compression elements. *J Aerosp Sci* 1958; 25: 37–52.
4. Williams D. *An introduction to the theory of aircraft structures*. London: Arnold, 1960.
5. Rivello RM. *Theory and analysis of flight structures*. New York, NY: McGraw-Hill College, 1969.
6. Niu MCY. *Airframe structural design: practical design information and data on aircraft structures*. Hong Kong: Connilit Press, 1988.
7. Bruhn EF. *Analysis and design of flight vehicle structures*. Cincinnati, OH: Tri-State Offset Co., 1973.
8. Anderson BK and Takahashi TT. Conceptual fuselage design with direct CAD modeling. In *17th AIAA aviation technology, integration, and operations conference*, Denver, CO, USA, 5–9 June 2017.
9. Grihon S, Samuelides M, Mervat A, et al. Fuselage structure optimisation. In: Kessler E and Guenov MD (eds) *Advances in collaborative civil aeronautical*



- multidisciplinary design optimization – progress in astronautics and aeronautics*. Reston, VA: AIAA, 2009, pp.193–245.
10. Boni L and Fanteria D. Development of analytical methods for fuselage design: validation by means of finite element analyses. *Proc IMechE, Part G: J Aerospace Engineering* 2004; 218: 315–327.
  11. Boni L. *Methodologies for the optimum design of fuselage structures of transport aircraft*. PhD Thesis, University of Pisa, Italy, 2004.
  12. Loughlan J. The buckling performance of composite stiffened panel structures subjected to combined in-plane compression and shear loading. *Compos Struct* 1994; 29: 197–212.
  13. Hughes OF, Ghosh B and Chen Y. Improved prediction of simultaneous local and overall buckling of stiffened panels. *Thin-Walled Struct* 2004; 42: 827–856.
  14. Stamatelos DG, Labeas GN and Tserpes KI. Analytical calculation of local buckling and post-buckling behavior of isotropic and orthotropic stiffened panels. *Thin-Walled Struct* 2011; 49: 422–430.
  15. Sobieszczanski J and Loendorf D. A mixed optimization method for automated design of fuselage structures. *J Aircr* 1972; 9: 805–811.
  16. Fischer M, Kennedy D and Featherston CA. Multilevel framework for optimization of lightweight structures. *Proc IMechE, Part G: J Aerospace Engineering* 2012; 226: 380–394.
  17. Vankan WJ, Noordman BAT and Kueres K. *High and low fidelity finite element modelling in aircraft composite fuselage structural analysis and optimisation*. Technical Report 2013–197, April 2014. Amsterdam, the Netherlands: National Aerospace Laboratory NLR.
  18. Venkataraman S and Haftka RT. Structural optimization complexity: what has Moore's law done for us? *Struct Multidiscip Optim* 2004; 28: 375–387.
  19. Hirai I, Wang BP and Pilkey WD. An efficient zooming method for finite element analysis. *Int J Numer Meth Eng* 1984; 20: 1671–1683.
  20. Hirai I, Uchiyama Y, Mizuta Y, et al. An exact zooming method. *Finite Elem Anal Des* 1985; 1: 61–69.
  21. Jara-Almonte CC and Knight CE. The specified boundary stiffness/force SBSF method for finite element sub-region analysis. *Int J Numer Meth Eng* 1988; 26: 1567–1578.
  22. Sun CT and Mao KM. A global-local finite element method suitable for parallel computations. *Comput Struct* 1988; 29: 309–315.
  23. Mao KM and Sun CT. A refined global-local finite element analysis method. *Int J Numer Meth Eng* 1991; 32: 29–43.
  24. Whitcomb JD. Iterative global/local finite element analysis. *Comput Struct* 1991; 40: 1027–1031.
  25. Cormier NG, Smallwood BS, Sinclair GB, et al. Aggressive submodelling of stress concentrations. *Int J Numer Meth Eng* 1999; 46: 889–909.
  26. Gendre L, Allix O, Gosselet P, et al. Non-intrusive and exact global/local techniques for structural problems with local plasticity. *Comput Mech* 2009; 44: 233–245.
  27. Guidault PA, Allix O, Champaney L, et al. A two-scale approach with homogenization for the computation of cracked structures. *Comput Struct* 2007; 85: 1360–1371.
  28. Akterskaia M, Jansen E, Hühne S, et al. Efficient progressive failure analysis of multi-stringer stiffened composite panels through a two-way loose coupling global-local approach. *Compos Struct* 2018; 183: 137–145.
  29. Montemurro M. *A contribution to the development of design strategies for the optimisation of lightweight structures*. HDR Thesis, Université de Bordeaux, Bordeaux, France, 2018.
  30. Boni L and Fanteria D. Finite-element-based assessment of analytical methods for the design of fuselage frames. *Proc IMechE, Part G: J Aerospace Engineering* 2006; 220: 387–398.
  31. Department of Defence. *Metallic materials and elements for aerospace vehicle structures MIL-HDBK-5j*. Technical Report, Department of Defence, VA, USA, January 2003.
  32. European Aviation Safety Agency. *Certification specifications and acceptable means of compliance for large aeroplanes CS-25*. Technical Report, Official Publication of the European Aviation Safety Agency, Germany, May 2018.
  33. Dai L, Chen H, Zhang Y, et al. An extended method of estimating the fatigue performance of mechanical structures with fasteners subject to shear loads. *Adv Mech Eng* 2018; 10: 1–11.
  34. Montemurro M and Catapano A. A general b-spline surfaces theoretical framework for optimisation of variable angle-tow laminates. *Compos Struct* 2019; 209: 561–578.
  35. Montemurro M, Izzi MI, El-Yagoubi J, et al. Least-weight composite plates with unconventional stacking sequences: design, analysis and experiments. *J Compos Mater* 2019; 53: 2209–2227.
  36. Panettieri E, Montemurro M and Catapano A. Blending constraints for composite laminates in polar parameters space. *Compos Part B Eng* 2019; 168: 448–457.
  37. Costa G, Montemurro M and Pailhès J. A general hybrid optimization strategy for curve fitting in the non-uniform rational basis spline framework. *J Optimiz Theory Appl* 2018; 176: 225–251.
  38. Bertolino G, Montemurro M and De Pasquale G. Multi-scale shape optimisation of lattice structures: an evolutionary-based approach. *Int J Interact Des Manuf* 2019; 13: 1565–1578.
  39. Cappelli L, Montemurro M, Dau F, et al. Characterisation of composite elastic properties by means of a multi-scale two-level inverse approach. *Compos Struct* 2018; 204: 767–777.
  40. Audoux Y, Montemurro M and Pailhès J. A surrogate model based on non-uniform rational b-splines hyper-surfaces. In: *Procedia CIRP, 28th CIRP Design Conference 2018*, Nantes, France, 23–25 May 2018, Vol. 70, pp.463–468. Elsevier.
  41. Montemurro M and Catapano A. On the effective integration of manufacturability constraints within the multi-scale methodology for designing variable angle-tow laminates. *Compos Struct* 2017; 161: 145–159.
  42. Ansys. *ANSYS mechanical APDL: contact technology guide. Release 18.1*. Canonsburg, PA: ANSYS, Inc., 2017.
  43. Timoshenko S and Gere J. *Theory of elastic stability*. 2nd ed. New York and London: McGraw-Hill Book Company Inc., 1961.
  44. Batdorf SB and Stein M. *Critical combinations of shear and direct stress for simply supported rectangular flat*

- plates (Technical Note 1223). Washington, DC: National Advisory Committee for Aeronautics, 1947.
45. Montemurro M, Vincenti A and Vannucci P. The automatic dynamic penalisation method (ADP) for handling constraints with genetic algorithms. *Comput Method Appl Mech Eng* 2013; 256: 70–87.
  46. Gerard G. *Minimum weight analysis of compression structures*. New York, NY: New York University Press, 1956.

## Appendix I. Mesh sensitivity analysis

The sensitivity analysis to the mesh parameters has been conducted by looking at the various mechanical responses of both the GFEM and the LFEM when LSol is evaluated. The mesh parameters considered are the element class, i.e. linear (L) or quadratic (Q), and the mesh size for both GFEM and LFEM. Because of the way the GL modelling approach is implemented, both global and local mesh parameters affect the local responses, while global ones only depend upon global mesh parameters. All the various combinations of the parameters have been evaluated, but, for the sake of brevity, only the most important results are reported here.

Concerning the GFEM, the mesh has been parametrised in terms of a single sizing parameter, i.e. the number of elements between two adjacent stringers (indicated with a number following the letter L/Q in the results). An automatic check has been implemented to prevent the generation of highly distorted shell elements with a threshold aspect ratio equal to two. The effect of the GFEM mesh parameters on one of the global scale responses (the rotation  $\theta_x$  of section B under LC1) and on a local scale one (the value  $\lambda^{\text{Top}}$  of the buckling factor of most critical stiffened panel of the top sector under LC8) is reported in Table 10. To obtain these results, the mesh of the LFEM is fixed to the mesh parameters set LFEM-Q1 reported in Table 11 (more details on the sensitivity analysis of the LFEM responses are given in the following paragraphs of this section). Derived

informations are reported in Figures 14 and 15. For these analyses, the total execution time has been normalised with respect to the smallest one (obtained using one linear element between stringers, i.e. mesh

**Table 11.** Mesh sensitivity of the LFEM.

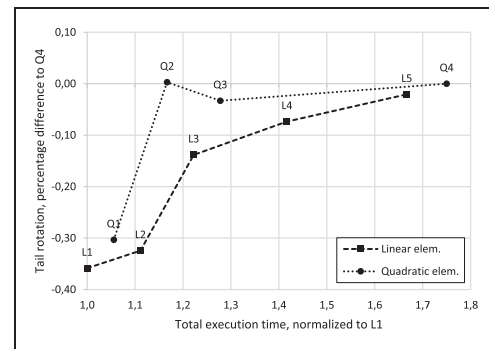
| Mesh parameters | DOFs <sup>a</sup> | Exec. time <sup>b</sup> (s) | $\lambda^{\text{Top}}$ (–) | $\lambda^{\text{Lat}}$ (–) | $\lambda^{\text{Bot}}$ (–) |
|-----------------|-------------------|-----------------------------|----------------------------|----------------------------|----------------------------|
| LFEM-L1         | 39396             | 23                          | 0.6243                     | 0.3435                     | 0.6122                     |
| LFEM-L2         | 131268            | 40                          | 0.5783                     | 0.2976                     | 0.5502                     |
| LFEM-L3         | 294048            | 75                          | 0.5691                     | 0.2864                     | 0.5327                     |
| LFEM-L4         | 498192            | 133                         | 0.5646                     | 0.2822                     | 0.5278                     |
| LFEM-L5         | 784056            | 222                         | 0.5626                     | 0.2801                     | 0.5247                     |
| LFEM-Q1         | 113880            | 38                          | 0.5651                     | 0.2886                     | 0.5297                     |
| LFEM-Q2         | 385608            | 104                         | 0.5555                     | 0.2764                     | 0.5186                     |
| LFEM-Q3         | 870000            | 261                         | 0.5556                     | 0.2760                     | 0.5188                     |

DOFs: degrees of freedom; LFEM: local finite element model.

Global mesh set at GFEM-Q1.

<sup>a</sup>Active degrees of freedom of the LFEM.

<sup>b</sup>Total execution time including GFEM analysis.



**Figure 14.** Sensitivity to the GFEM mesh parameters of the percentage difference of the rotation of section B with respect to the one obtained with mesh GFEM-Q4.

**Table 10.** Mesh sensitivity of the GFEM, main results.

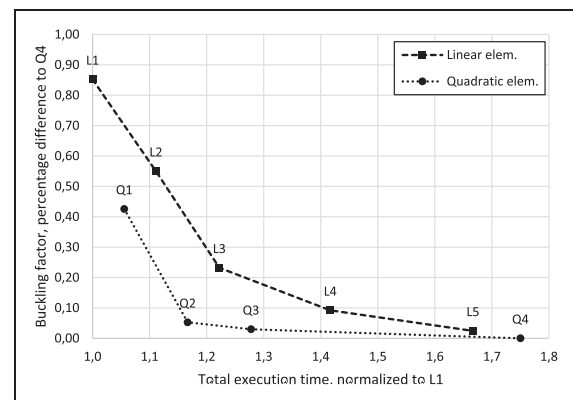
| Mesh parameters | DOFs <sup>a</sup> | Exec. time <sup>b</sup> (s) | $\theta_x$ (rad)       | $\lambda^{\text{Top}}$ (–) |
|-----------------|-------------------|-----------------------------|------------------------|----------------------------|
| GFEM-L1         | 10476             | 36                          | $1.1301 \cdot 10^{-3}$ | 0.5675                     |
| GFEM-L2         | 28428             | 40                          | $1.1305 \cdot 10^{-3}$ | 0.5658                     |
| GFEM-L3         | 53760             | 44                          | $1.1326 \cdot 10^{-3}$ | 0.5640                     |
| GFEM-L4         | 100752            | 51                          | $1.1333 \cdot 10^{-3}$ | 0.5632                     |
| GFEM-L5         | 144498            | 60                          | $1.1339 \cdot 10^{-3}$ | 0.5628                     |
| GFEM-Q1         | 28140             | 38                          | $1.1307 \cdot 10^{-3}$ | 0.5651                     |
| GFEM-Q2         | 78336             | 42                          | $1.1342 \cdot 10^{-3}$ | 0.5630                     |
| GFEM-Q3         | 150546            | 46                          | $1.1338 \cdot 10^{-3}$ | 0.5629                     |
| GFEM-Q4         | 287988            | 63                          | $1.1341 \cdot 10^{-3}$ | 0.5627                     |

DOFs: degrees of freedom; GFEM: global finite element model.

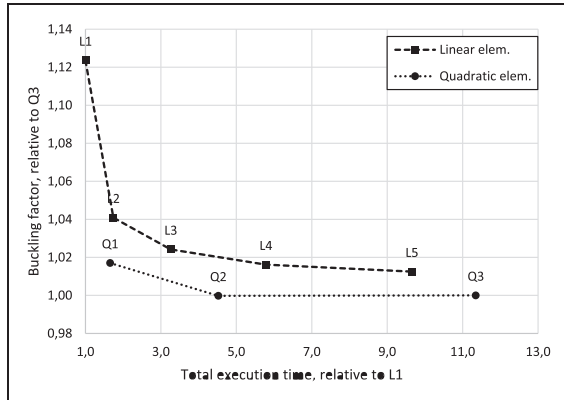
Local mesh set at LFEM-Q1.

<sup>a</sup>Active degrees of freedom of the GFEM.

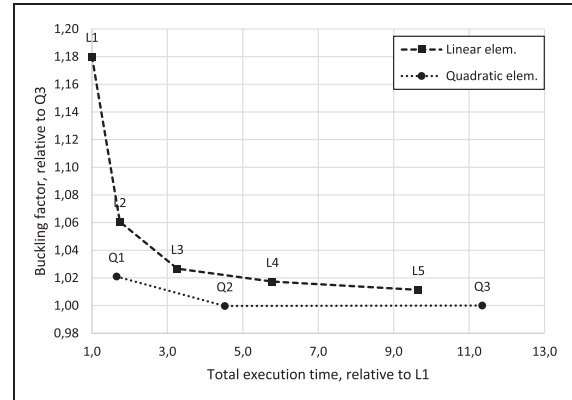
<sup>b</sup>Total execution time including LFEM analyses.



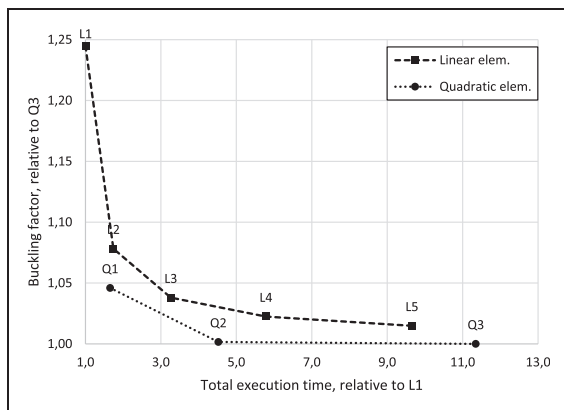
**Figure 15.** Sensitivity to the GFEM mesh parameters of the percentage difference of the buckling factor of the most critical stiffened panel in the top sector with respect to the one obtained with mesh GFEM-Q4.



**Figure 16.** Sensitivity to the LFEM mesh parameters of the buckling factor of the most critical stiffened panel of the top sector (normalised with respect to that obtained with mesh LFEM-Q4).



**Figure 18.** Sensitivity to the LFEM mesh parameters of the buckling factor of the most critical stiffened panel of the bottom sector (normalised with respect to that obtained with mesh LFEM-Q4).



**Figure 17.** Sensitivity to the LFEM mesh parameters of the buckling factor of the most critical stiffened panel of the lateral sector (normalised with respect to that obtained with mesh LFEM-Q4).

parameters set GFEM-L1), while the mechanical responses have been normalised with respect to fully converged ones (obtained with mesh parameters set GFEM-Q4). As it can be seen, the improvement obtainable by using more accurate meshes than GFEM-L1 in the evaluation of mechanical responses is rather small.

In this case, the choice of the mesh parameters set GFEM-Q1 is motivated by its ability to perfectly model the curved shape of the fuselage barrel components, with a small increase in computational time.

Also in the case of LFEM, the mesh has been parametrised in terms of a single sizing parameter. Each of the edges of the geometry describing the components has been divided in a given amount of *mesh units*. The assumption is that the buckling could occur in any one of the plate-regions composing the structure. Therefore, the numbers of mesh units must be chosen to ensure a homogeneous level of accuracy in the estimation of the buckling load in accordance with the first expected buckling mode of each plate. For example, when looking at the stringers cross-section, the free flanges have been divided in one mesh unit, the webs in three mesh units and the bonded flanges in two mesh units. Finally, automatic checks have been implemented to ensure that the final elements have nearly unitary aspect ratios. With this parametrisation set, the number of element in each mesh unit and their element class (linear, L, or quadratic, Q) constitute the mesh parameters of the sensibility analysis. The results of such analysis are reported in Table 11 and Figures 16 to 18. To obtain these results, the mesh of the GFEM is fixed to the mesh parameters set GFEM-Q1. In this case, the use of a light mesh composed of few linear shape functions elements, like LFEM-L1, shows all its limitations. For LFEM-L1, the percentage difference in the computed buckling factor reaches 25% with respect to the results obtained by a fully converged mesh like LFEM-Q3.

By considering a threshold percentage difference of 5%, the best compromise between accuracy and computational time is obtained by adopting the mesh parameters set LFEM-Q1.





# First experimental validation of the Multi-Scale Two-Level optimisation strategy

The article *Least-weight composite plates with unconventional stacking sequences: design, analysis and experiments*, reported in this chapter, has been published in *Journal of Composite Materials* (Montemurro, Izzi, El-Yagoubi, and Fanteria, 2019). It deals with the problem of the least-weight design of CSCs. The coupled numerical and experimental activities presented in this paper constitute the first experimental validation of the MS2LOS.

In this work, the MS2LOS is applied to the problem of minimising the mass of a moderately-thick CSCs layered plate subject to requirements on both its in-plane overall stiffness and its first buckling load. Such requirements are derived from their counterparts evaluated for a reference laminate (whose stacking sequence is built by using the classical rules taken from literature). In the usual work-flow of the MS2LOS the design process takes places at two consecutive levels. Firstly, the structural design problem is formulated at the macroscopic scale. Here, the laminate is seen as an equivalent homogeneous anisotropic plate whose macroscopic elastic properties are described in terms of PPs and its overall thickness, which constitute the problem design variables. The aforementioned requirements are formulated as optimisation constraints as are the feasibility conditions on the existence of a corresponding suitable stacking sequence. Secondly, the lay-up design is performed: at least one stacking sequence corresponding to the first-level results is searched. The solution is searched among QT stacking sequences, which allow obtaining exact membrane-bending uncoupling and homogeneity of the laminate, without enforcing simplifying rules on the nature of its stack (e.g. symmetry and balancing). At both the first and the second levels, the solution is searched by employing the GA ERASMUS, which, at the first level, is interfaced with a commercial FE code for the evaluation of the first buckling load of the plate (resulting from a linear eigenvalue buckling analysis).

An experimental campaign of buckling tests performed on both the reference and the optimised plates is carried out in parallel to the numerical activity. Numerical and experimental results show an excellent agreement: the optimised plate is about 10% lighter than the reference one while guaranteeing higher mechanical performances. These results constitute the first experimental validation of the effectiveness of both the MS2LOS and the very general stacking sequences resulting from its application.

# Least-weight composite plates with unconventional stacking sequences: Design, analysis and experiments

Marco Montemurro<sup>1</sup> , Michele Iacopo Izzi<sup>1</sup>, Jalal El-Yagoubi<sup>2</sup> and Daniele Fanteria<sup>3</sup>

## Abstract

This study deals with the problem of the least-weight design of a composite multilayer plate subject to constraints of different nature (mechanical, geometrical and technological requirements). To face this problem, a multi-scale two-level design methodology is proposed. This approach aims at optimising simultaneously both geometrical and mechanical parameters of the laminate at each characteristic scale (mesoscopic and macroscopic ones). In this background, at the first level (macroscopic scale), the goal is to find the optimum value of geometrical and mechanical design variables minimising the structure mass and satisfying the set of imposed constraints (on first buckling load, membrane stiffness and feasibility constraints). The second-level problem (mesoscopic scale) aims at finding at least one stacking sequence meeting the geometrical and material parameters provided by the first-level problem. The multi-scale two-level optimisation approach is based on the polar formalism to describe the macroscopic behaviour of the composites (in the framework of the equivalent single-layer theories) and on a special genetic algorithm to perform composite calculations. The optimum solutions provided by the multi-scale two-level optimisation strategy are characterised by a weight saving of about 10% with enhanced mechanical properties when compared to conventional symmetric balanced stacks. The effectiveness of the optimum solutions is also proven through an experimental campaign of buckling tests. The experimental results are in excellent agreement with those foreseen by the numerical simulations.

## Keywords

Composites, finite element method, buckling, multi-scale optimisation, lightweight structures, genetic algorithm

## Introduction

The constant demand of lightweight structures with enhanced mechanical performances has led to an increasing use of composite materials in the last few decades. Fibre-reinforced composites present specific stiffness and strength properties that make them really appealing when compared to metallic alloys. The behaviour of these materials gives the designer the opportunity to tailor the material properties according to the design needs. A lot of research has been carried out in looking for the best strategy to optimise multilayer composite plates in order to either minimise the mass (without losing performances with respect to a given *reference solution*) or improve mechanical performances (without increasing the mass with respect to a reference configuration). Nonetheless, the problem is still open. The design of a composite structure is a

quite difficult problem that can be considered as a multi-scale optimisation problem. The complexity of the design process is due to two intrinsic properties of composite materials, i.e. heterogeneity and anisotropy. Heterogeneity gets involved mainly at the microscopic scale (i.e. that of constitutive phases), whilst anisotropy intervenes at both mesoscopic scale (that of the lamina)

<sup>1</sup>Arts et Métiers ParisTech, Institut de mécanique et d'ingénierie (I2M) CNRS UMR 5295, Talence, France

<sup>2</sup>Université de Bordeaux, Institut de mécanique et d'ingénierie (I2M) CNRS UMR 5295, Talence, France

<sup>3</sup>Department of Civil and Industrial Engineering – Aerospace Division, University of Pisa, Italy

## Corresponding author:

Marco Montemurro, Arts et Métiers ParisTech – Centre de Bordeaux-Talence, Esplanade des Arts et Métiers, Talence 33405, France.  
Email: marco.montemurro@ensam.eu

and macroscopic one (that of the laminate). To deal with heterogeneity, a common strategy is to make use of homogenisation techniques.<sup>1–3</sup>

The main consequence of anisotropy is the introduction of some phenomena and issues that do not exist in metals (e.g. extension–bending coupling, delamination, residual stresses, free-edge stresses, different failure mechanisms, etc.). A further complication is that the design process must deal with a significant amount of design variables at different scales. In fact, up to now, no general methods exist for the optimum design of a composite structure.

Adali et al.<sup>4</sup> investigated the post-buckling stiffness maximisation problem of simply supported biaxially loaded laminated plates using five pre-set symmetrical angle-ply stacking sequences consisting of eight plies. In this way, the number of design variables reduces to one (for each configuration) and the optimisation was carried out by means of the Golden Section method. Later,<sup>5</sup> they focused on the problem of maximising the first buckling load of a bi-material multilayer plate. In each considered case, the stacking sequence is balanced and symmetric and the orientations are limited to the *canonical set*  $\{0^\circ, \pm 45^\circ, 90^\circ\}$ . Finally, in the literature<sup>6,7</sup> both approaches have been used in the framework of multi-objective optimisation problems.

Haftka and Walsh<sup>8</sup> used integer programming for the optimum design of symmetric balanced stacks wherein the orientations are constrained to get the values in the canonical set. These problems were solved by considering additional requirements on the percentage rule and overall in-plane stiffness value. Le Riche and Haftka<sup>9</sup> made use of a genetic algorithm (GA) to perform the solution search for the problem of maximising the first buckling load of a multilayer plate with a given number of plies. Also in this work, symmetric balanced stacks with orientation angles getting values in the canonical set were considered. Furthermore, an ad hoc genetic operator, i.e. the *permutation* operator, was proposed to increase the efficiency of the calculations.

Still in the context of the first buckling load maximisation problem, Aymerich and Serra<sup>10</sup> utilised the Ant Colony Optimisation method (considering balanced symmetric stacking sequences in the usual domain of orientations) which was characterised by a better efficiency, in terms of computational effort, when compared to GA-based strategies. Irisarri et al.<sup>11</sup> performed a multi-objective optimisation process of laminated plates using a Pareto-based evolutionary algorithm. In this interesting work, symmetric balanced stacks are employed and the orientation of each couple of plies comes from a set bigger than the canonical one, i.e.  $(0_2^\circ, \pm 15^\circ, \pm 30^\circ, \dots, 90_2^\circ)$ . Furthermore, a set of design guidelines<sup>12</sup> are integrated in the optimisation

process, though the flexural behaviour of the laminate was only approximated.

The previous works aimed at solving the design problem by directly optimising the value of the layers orientation angles without introducing a multi-scale design/optimisation approach. In each study, the nature of the stack is set a priori and the orientation angles are limited to get values in a predefined set. Moreover, further design (empirical) rules<sup>12</sup> were integrated as optimisation constraints. All these aspects contribute to strongly shrink the design domain leading the algorithm to find only suboptimal solutions. All the previous works are based on an analytical formulation of the optimisation problem. Conversely, for real-world engineering problems the mechanical response of the structure is typically evaluated by means of a suitable finite element (FE) model.

In this scenario, multi-scale optimisation strategies of composite structures which aim at formulating and solving the design/optimisation problem at each pertinent scale (without introducing simplifying hypotheses on both the nature of the stacking sequence and on the value of plies orientation) find strong motivations. When dealing with the multi-scale optimisation problem of a composite, at the macroscopic scale, the behaviour is described in terms of the laminate stiffness tensors components, regardless of the nature of the stack. When the laminate behaviour is expressed in the framework of the classic laminate theory (CLT), the Cartesian components of membrane, bending and membrane/bending coupling stiffness tensors constitute the unknowns of the problem. However, since Cartesian components are frame dependent, an alternative representation of such tensors is often used. The most common approach makes use of the well-known lamination parameters (LPs) coupled with the parameters of Tsai and Pagano.<sup>13</sup> These parameters<sup>14,15</sup> unquestionably provide a compact representation of the stiffness tensors of composite laminates in the framework of the CLT, although they are not all tensor invariants.<sup>13</sup>

Diaconu et al.<sup>16</sup> presented a general framework for determining the feasible region in LPs space for general composite laminate design. Their method does not give an explicit relationship between LPs, but only a 'numerical definition' of the boundary of the feasible domain. Later they presented a work on the layup optimisation of thick laminates for maximising the first natural frequency.<sup>17</sup> In this context, a multi-step optimisation approach including numerical verification on the feasibility of the optimum solutions is proposed. Liu et al.<sup>18</sup> considered the problem of the maximisation of the first buckling load of a multilayer plate in the flexural LPs space. The optimum solutions are only given in terms of flexural LPs characterising the equivalent homogeneous anisotropic plate.

Bloomfield et al.<sup>19</sup> presented a two-step optimisation strategy for symmetric laminates made of a predefined set of possible ply orientations. The strategy is applied to the problem of mass minimisation of a simply supported multilayer plate under different loading conditions. The results highlight the interest in widening the standard canonical set by adding  $\pm 30^\circ$  and  $\pm 60^\circ$  values. Liu et al.<sup>20</sup> presented a two-step optimisation strategy for maximising the stiffness of laminates subject to a given set of optimisation constraints. During the first step the optimisation problem is solved in the LPs space wherein the feasible region has been approximated by the one that can be obtained by considering only six different orientation angles. During the second step, a suitable stack is retrieved by solving a least-square problem in which the orientation angles of the laminae are the design variables.

As it can be inferred from the previous works, the multi-scale optimisation approach based on LPs presents two main weaknesses: LPs are not tensor invariants, while not all Tsai and Pagano parameters are invariants; both LPs and Tsai and Pagano parameters have not an immediate physical meaning related to the elastic symmetries of the stiffness tensor. Moreover, although the previous studies made use of the multi-scale optimisation strategy based on LPs, an unnecessary restriction still remains when looking for the optimum stack: in the formulation of the laminate lay-up design problem simplifying hypotheses on the nature of the stacking sequence are systematically used. These assumptions are used, on the one hand, to obtain a shortcut to a possible solution (i.e. to obtain some desired mechanical properties). On the other hand, the aim of these rules is to prevent the laminate from some undesired phenomena, though this is never clearly and rigorously stated nor proved. Unfortunately, the use of these simple rules shrinks the design space and drives the optimisation algorithm towards suboptimal solutions.

Two examples are the use of symmetric stacking sequences (a sufficient but not necessary condition for membrane-bending uncoupling) and the use of balanced stacks to obtain orthotropic laminates. However, the use of balanced stacks (a sufficient condition for membrane orthotropy) leads systematically to misleading solutions: whenever such a rule is used, bending orthotropy, a rather difficult property to achieve,<sup>21</sup> is simply understated, assumed, but not really obtained.<sup>18,22–24</sup>

To overcome the previous restrictions, in the present study the multi-scale two-level (MS2L) optimisation approach based on the Verchery's polar method<sup>25</sup> for designing anisotropic complex structures<sup>26–28</sup> is used. In this background, the design problem is formulated in the most general sense, i.e. without introducing simplifying hypotheses and by considering, as design

variables, the full set of geometric and mechanical parameters defining the behaviour of the laminate at each characteristic scale (mesoscopic and macroscopic).

In the context of the MS2L methodology, the optimisation problem is split into two distinct sub-problems. At the first level (macroscopic scale), the goal is to find the optimum value of both geometric and mechanical design variables of the laminate satisfying the design problem which is formulated in the form of a constrained non-linear programming problem (CNLPP). The second-level problem focuses on the laminate mesoscopic scale (i.e. the ply-level) and aims at finding at least one optimum stack meeting the geometrical and mechanical parameters resulting from the first-level problem.

The MS2L approach is based on the generalisation of the Verchery's polar method to the case of high-order equivalent single-layer theories<sup>21,29,30</sup> as well as on a GA previously developed by the first author.<sup>31,32</sup> The MS2L optimisation strategy has already been successfully applied in the past to many real-world engineering problems.<sup>26–28,33–38</sup>

A rigorous experimental validation of such an approach is the main purpose of this study. In this work, the MS2L optimisation strategy is applied to the problem of minimising the mass of a moderately thick multilayer plate subject to requirements on both in-plane overall stiffness and first buckling load. The numerical work is complemented by an experimental campaign that aims not only at validating the MS2L optimisation approach but also the effectiveness of the very general stacking sequences resulting from the process as well as the influence of the transverse shear stiffness on the optimum solution (that cannot be neglected for moderately thick laminate) and which can be easily integrated in the framework of the polar method.

The paper is organised as follows: an overview of both numerical and experimental activities followed by the description of the selected optimisation problem and the MS2L strategy is given in the next section. The mathematical formulation of the first-level problem is detailed in the *Mathematical formulation of the first-level problem* section, while the problem of determining suitable stacking sequences is formulated in the *Mathematical formulation of the second-level problem* section. A concise description of the FE model used in the optimisation process is given in the *FE model of the multilayer plate*, section, whilst the details about the experimental activities can be found in the *Experimental apparatus for buckling analysis* section. The comparison between numerical and experimental results is presented in the *Optimum solutions: Numerical and experimental results* section, while the *Conclusions* section ends the paper with some concluding remarks.

## Multi-scale optimisation of composite structures: Fundamental aspects

### General workflow

The workflow of the activities described in this study is shown in Figure 1.

A representative design case is considered: the least-weight design of a multilayer composite plate subject to constraints on both the first buckling load (under uni-axial compressive load) and on the overall membrane stiffness. Such requirements are derived from their counterparts evaluated for a reference laminate (whose stack is built by using the classical rules taken from literature) having the same geometry of the optimised plate and subjected to the same boundary conditions (BCs) (more details on the problem formulation at each scale are given in the next two sections).

With the aim of experimentally validating the MS2L optimisation strategy, numerical and experimental activities proceed simultaneously and interact at given moments:

- the FE model is created and its geometry and mesh properly parametrised in terms of the design variables for the problem at hand (see the *Mathematical formulation of the first-level problem* and the *FE model of the multilayer plate* sections);
- a reference plate is fabricated and tested (see the *Experimental apparatus for buckling analysis* section);
- experimental results on the reference plate are compared to those provided by the FE model to validate the latter (see the *Experimental apparatus for buckling analysis* section);
- the MS2L optimisation strategy is run by using the validated FE model to obtain the optimised plate stacking sequence (next three sections);

- the optimum plate is fabricated and tested (see the *Optimum solutions: Numerical and experimental results* section);
- experimental results on the optimum solution are compared to the numerical ones in order to give an experimental proof of the effectiveness of the stacking sequence selected by the optimisation process as well as that of the MS2L optimisation strategy itself.

All the above steps require the elastic properties of the constitutive lamina, so they have been preceded by a characterisation tests campaign.

### Problem description

The optimisation strategy presented in this study is applied to a simple composite structure, whose geometry and size are illustrated in Figure 2. The specimen illustrated in Figures 2 and 3 is a rectangular multilayer composite plate with two resin blocks at its ends that facilitate the loading in compression.

The blocks are made of epoxy resin Araldite® LY5052/Aradur® 5052, while the multilayer plate is made of the carbon/epoxy pre-preg HexPly® M21/34%/UD194/IMA-12K by Hexcel®. The elastic properties of both materials are reported in Tables 1 and 2, respectively.

The material considered in this work is a pre-preg commonly used for aeronautical applications which is composed of unidirectional intermediate-modulus carbon-fibres (IMA-12k) and epoxy-matrix (M21, 34% in weight) supplied in 300 mm wide rolls.

It is noteworthy that the elastic properties of the constitutive lamina, listed in Table 2, have been determined as a result of an experimental characterisation tests campaign, conducted at I2M laboratory

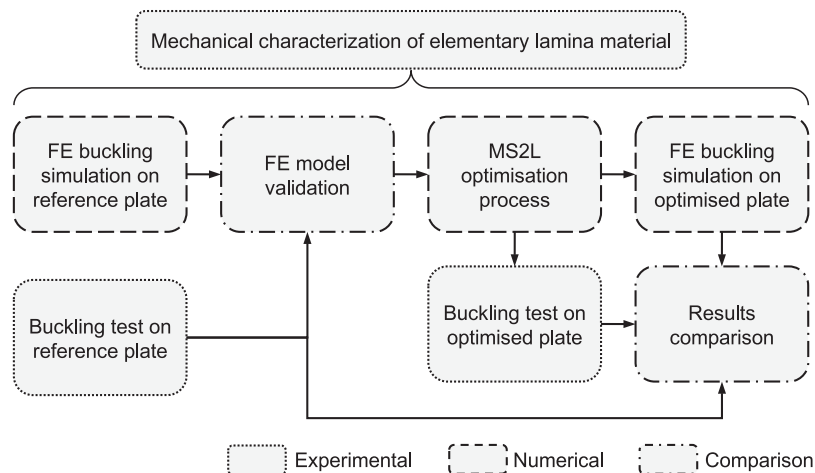
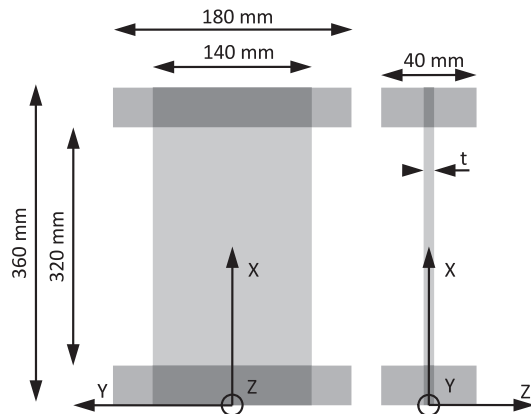
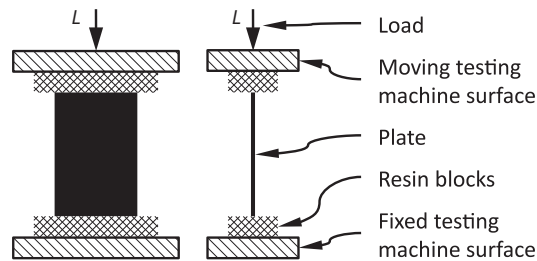


Figure 1. Numerical-experimental workflow.





**Figure 2.** Geometry and overall size of the multilayer composite plate.



**Figure 3.** Simplified loading scheme of the multilayer composite plate.

**Table 1.** Material properties of the epoxy resin Araldite® LY5052-Aradur® 5052 when considering a curing cycle of 2 h at 60°C plus 6 h at 80°C.

| Technical constants | Value  |
|---------------------|--------|
| $E$ (MPa)           | 3103.0 |
| $N$                 | 0.35   |

in Bordeaux. Tests have been performed on thin laminated strips (having a length of 250 mm and a width of 20 mm) with  $[0^\circ]_8$ ,  $[90^\circ]_8$  and  $[(\pm 45^\circ)_2]_S$  stacking sequences. The tests on  $[(\pm 45^\circ)_2]_S$  specimens respect the ASTM D3518, D3518M-94(07) standard.<sup>39</sup> Furthermore, the compressive Young's modulus along  $x_1$ -axis,  $E_1^c$ , listed in Table 2 has been taken directly from the manufacturer data-sheet: this quantity will be used to define the behaviour of the constitutive lamina into the FE model of the composite plate in order to carry out the calculation of the first buckling load as detailed in the FE model of the multilayer plate.

More details on the whole campaign of characterisation tests can be found in Izzi.<sup>40</sup>

The fundamental hypotheses about the macroscopic mechanical response of the structure focus essentially on the laminate behaviour:

- the material of the constitutive layer has a linear elastic transverse isotropic behaviour;
- the laminate is quasi-homogeneous and fully orthotropic<sup>30,28,36,37</sup>;
- at the macroscopic scale the elastic response of the laminate is described in the framework of the first-order shear deformation theory (FSDT) and the stiffness matrices of the plate are expressed in terms of the *laminate polar parameters*<sup>21,29</sup>;
- no delamination occurs neither at the interfaces between the plies nor at the interfaces between the plate and the resin blocks (perfect bonding condition).

Finally, it must be noticed that no simplifying hypotheses are made during the optimisation process on the stacking sequence of the multilayer plate, neither in terms of plies orientation angles nor in terms of the nature of the stack. Only avoiding the utilisation of a priori assumptions that extremely shrink the solution space (e.g. the utilisation of symmetric, balanced stacks to attain membrane/bending uncoupling and membrane orthotropy, respectively) one can hope to obtain the true global optimum for a given problem: this is a key-point in the proposed approach.

### Description of the multi-scale two-level optimisation strategy

The main goal of the MS2L optimisation strategy is the least-weight design of the multilayer plate subject to constraints of different nature, i.e. mechanical, geometrical as well as feasibility constraints. The optimisation procedure is articulated into the following two distinct (but related) optimisation problems.

**First-level problem.** The aim of this phase (which focuses on the laminate macroscopic scale) is the determination of the optimum value of both mechanical and geometric parameters of the laminate in order to minimise its weight and to satisfy, simultaneously, the full set of imposed requirements (formulated as optimisation constraints). At this level, the multilayer plate is modelled as an equivalent homogeneous anisotropic plate whose behaviour is described in terms of the laminate polar parameters.<sup>21,29</sup> Therefore, the design variables of this phase are both the geometric and the polar parameters of the laminate.

**Table 2.** Material properties of the carbon/epoxy pre-preg HexPly® M21/34%/ UD194/IMA-12K by Hexcel®.

| Technical constants          |                       | Polar parameters <sup>a</sup> of [Q] <sup>b</sup> |             | Polar parameters of [Q̂] <sup>c</sup> |           |
|------------------------------|-----------------------|---|-------------|---------------------------------------|-----------|
| $E_1$ (MPa)                  | 171,500.0             | $T_0$ (MPa)                                       | 21,687.9918 | $T$ (MPa)                             | 4606.1923 |
| $E_1^*$ (MPa)                | 146,000.0             | $T_1$ (MPa)                                       | 20,160.7437 | $R$ (MPa)                             | 1275.8077 |
| $E_2$ (MPa)                  | 8659.0                | $R_0$ (MPa)                                       | 15,805.9918 | $\Phi$ (deg)                          | 90.0      |
| $G_{12}$ (MPa)               | 5882.0                | $R_1$ (MPa)                                       | 17,275.5135 |                                       |           |
| $\nu_{12}$                   | 0.3245                | $\Phi_0$ (deg)                                    | 0.0         |                                       |           |
| $\nu_{23}$                   | 0.3                   | $\Phi_1$ (deg)                                    | 0.0         |                                       |           |
| Density and thickness        |                       |   |             |                                       |           |
| $\rho$ (kg/mm <sup>3</sup> ) | $1.58 \times 10^{-6}$ |   |             |                                       |           |
| $t_{ply}$ (mm)               | 0.1831                |   |             |                                       |           |

<sup>a</sup>The polar parameters of [Q] have been evaluated using  $E_1^*$  instead of  $E_1$ .

<sup>b</sup>In-plane reduced stiffness matrix of the ply.

<sup>c</sup>Out-of-plane shear stiffness matrix of the ply.

**Second-level problem.** The second level of the strategy focuses on the laminate mesoscopic scale and aims to determine a suitable lay-up meeting the optimum combination of polar and geometric parameters of the laminate provided by the first-level problem. The goal is, hence, to find at least one stacking sequence which has to be quasi-homogeneous, fully orthotropic and that has to satisfy the optimum values of the polar parameters resulting from the first step. At this level of the strategy, the design variables are the layer orientations.

### Mathematical formulation of the first-level problem

The macroscopic features of the composite have to be optimised during this phase. In particular, the mass minimisation of the laminate is here performed by satisfying, simultaneously, the set of optimisation constraints listed below:

1. a constraint on the first buckling load of the laminate (the laminate is subjected to a uni-axial compressive load);
2. a constraint on the membrane stiffness along the (in-plane) axis orthogonal to the applied load direction;
3. a feasibility constraint on the laminate polar parameters.

These aspects are detailed in the following subsections.

#### The design variables

The design variables for the problem at hand are of two types: *geometrical* and *mechanical*.

The only geometrical variable characterising the laminate at the macroscopic scale is its overall thickness

$t$ . Of course,  $t$  is considered as a discrete optimisation variable having a step equal to the thickness of the elementary layer, i.e.  $\Delta t = t_{ply}$ .

As far as the mechanical design variables are concerned, the macroscopic mechanical response of the laminate is described in the mathematical framework of the FSDT.<sup>41</sup> In this background, the constitutive law of the laminate (expressed within its global frame  $R = \{0; x, y, z\}$ ) can be stated as

$$\begin{Bmatrix} \{N\} \\ \{M\} \end{Bmatrix} = \begin{bmatrix} [A] & [B] \\ [B] & [D] \end{bmatrix} \begin{Bmatrix} \{\varepsilon_0\} \\ \{\chi_0\} \end{Bmatrix} \quad (1)$$

$$\{F\} = [H]\{\gamma_0\} \quad (2)$$

where [A], [B] and [D] are the membrane, membrane/bending coupling and bending stiffness matrices of the laminate, while [H] is the out-of-plane shear stiffness matrix. {N}, {M} and {F} are the vectors of membrane forces, bending moments and shear forces per unit length, respectively, whilst  $\{\varepsilon_0\}$ ,  $\{\chi_0\}$  and  $\{\gamma_0\}$  are the vectors of in-plane strains, curvatures and out-of-plane shear strains of the laminate middle plane, respectively.<sup>41</sup>

In order to analyse the elastic response of the multi-layer structure, the best practice consists in introducing the laminate normalised stiffness matrices

$$\begin{aligned} [A^*] &= \frac{1}{t} [A], \\ [B^*] &= \frac{2}{t^2} [B], \end{aligned}$$

$$\begin{aligned} [D^*] &= \frac{12}{t^3} [D], \\ [H^*] &= \begin{cases} \frac{1}{t} [H] & \text{(basic),} \\ \frac{12}{5t} [H] & \text{(modified)} \end{cases} \quad (3) \end{aligned}$$



As discussed in the literature,<sup>21,29</sup> in the framework of the polar formalism it is possible to express the Cartesian components of these matrices in terms of their elastic invariants. It can be proven that, in the FSDT framework, for a fully orthotropic, quasi-homogeneous laminate (i.e. a laminate having the same orthotropic behaviour in terms of normalised membrane and bending stiffness matrices and whose membrane/bending coupling stiffness matrix is null) the overall number of independent mechanical design variables describing its mechanical response reduces to only three: the anisotropic polar parameters  $R_{0K}^{A^*}$  and  $R_1^{A^*}$  and the polar angle  $\Phi_1^{A^*}$  (this last representing the orientation of the main orthotropy axis) of matrix  $[A^*]$ . For more details on the polar formalism and its application in the context of the FSDT, the reader is addressed to the literature.<sup>21,29,42</sup>

In addition, in the formulation of the optimisation problem for the first level of the strategy, the feasibility constraints on the polar parameters (which arise from the combination of the layers orientations and positions within the stack) must also be considered. These constraints ensure that the optimum values of the polar parameters resulting from the first-level problem describe a feasible laminate that will be designed during the second step of the MS2L strategy, see Vannucci.<sup>43</sup> Since the laminate is quasi-homogeneous, such constraints can be written only for matrix  $[A^*]$

$$\begin{cases} -R_0 \leq R_{0K}^{A^*} \leq R_0, \\ 0 \leq R_1^{A^*} \leq R_1, \\ 2\left(\frac{R_1^{A^*}}{R_1}\right)^2 - 1 - \frac{R_{0K}^{A^*}}{R_0} \leq 0 \end{cases} \quad (4)$$

In equation (4),  $R_0$  and  $R_1$  are the anisotropic moduli of the ply-reduced stiffness matrix.<sup>21</sup>

It is noteworthy that, for the problem at hand, the main orthotropy direction of the laminate can be set equal to zero, i.e.  $\Phi_1^{A^*} = 0$ : this means that the main orthotropy axis is aligned with the direction of the applied load. In this way  $\Phi_1^{A^*}$  is no longer a design variable.

For optimisation purposes it is useful to introduce dimensionless design variables. The dimensionless quantity related to the laminate overall thickness is, of course, the plies number  $n$ , while the dimensionless laminate polar parameters can be obtained by considering the ratio between the polar parameters of matrix  $[A^*]$  and the lamina counterparts. Therefore, the dimensionless laminate design variables can be defined as follows

$$n = \frac{t}{t_{\text{ply}}}, \quad \rho_0 = \frac{R_{0K}^{A^*}}{R_0}, \quad \rho_1 = \frac{R_1^{A^*}}{R_1} \quad (5)$$

In this background, equation (4) becomes

$$\begin{cases} -1 \leq \rho_0 \leq 1, \\ 0 \leq \rho_1 \leq 1, \\ 2(\rho_1)^2 - 1 - \rho_0 \leq 0 \end{cases} \quad (6)$$

Therefore, the dimensionless design variables defined above can be grouped into the vector of design variables

$$\xi^T = \{n, \rho_0, \rho_1\} \quad (7)$$

First and second constraints of equation (6) can be taken into account as admissible intervals for the relevant optimisation variables, i.e. on  $\rho_0$  and  $\rho_1$ . Thus, the resulting feasibility constraint on the laminate dimensionless polar parameters becomes

$$g_1(\xi) = 2(\rho_1)^2 - 1 - \rho_0 \leq 0 \quad (8)$$

For a wide discussion upon the laminate feasibility and geometrical bounds as well as on the importance of the quasi-homogeneity assumption, the reader is addressed to Vannucci.<sup>43</sup>

Finally, it must be noted that the laminate dimensionless polar parameters have to satisfy a further mechanical constraint related to the requirement on the membrane stiffness along the  $y$ -axis of the laminate global frame. This constraint can be states as

$$g_2(\xi) = 1 - \frac{A_{yy}(\xi)}{A_{yy}^{(\text{ref})}} \leq 0 \quad (9)$$

where  $A_{yy}$  is the component of the membrane stiffness matrix along  $y$ -axis, while  $A_{yy}^{(\text{ref})}$  is its reference counterpart, i.e. the same quantity evaluated on the reference configuration of the laminate which is described in the *Experimental apparatus for buckling analysis* section.

### Mathematical statement of the problem

As previously stated, the aim of the first-level optimisation is the minimisation of the laminate mass by satisfying, simultaneously, constraints of different nature.

In this context, the optimisation problem can be formulated as a classical constrained non-linear programming problem (CNLPP)

$$\min_{\xi} \frac{M(\xi)}{M^{(\text{ref})}}$$

subject to:

**Table 3.** Design space of the first-level problem.

| Design variable | Type       | Lower bound | Upper bound | Discretisation step |
|-----------------|------------|-------------|-------------|---------------------|
| $n$             | integer    | 16          | 32          | 1                   |
| $\rho_0$        | Continuous | -1.0        | 1.0         | –                   |
| $\rho_1$        | Continuous | 0           | 1.0         | –                   |

$$\begin{cases} 1 - \frac{\lambda_L(\xi)}{\lambda_L^{(\text{ref})}} \leq 0, \\ g_i(\xi) \leq 0, \quad \text{with } i=1, 2 \end{cases} \quad (10)$$

The design space of the first-level problem, together with the type of each design variable, is detailed in Table 3. In equation (10)  $M$  is the laminate mass,  $\lambda_L$  is the first buckling load of the structure (calculated by means of an eigenvalue buckling analysis, see the *FE model of the multilayer plate section*), while  $M^{(\text{ref})}$  and  $\lambda_L^{(\text{ref})}$  are the counterparts for a *reference solution* (see *Experimental apparatus for buckling analysis* section) which is subject to the same BCs as those applied to the multilayer plate that will be optimised.

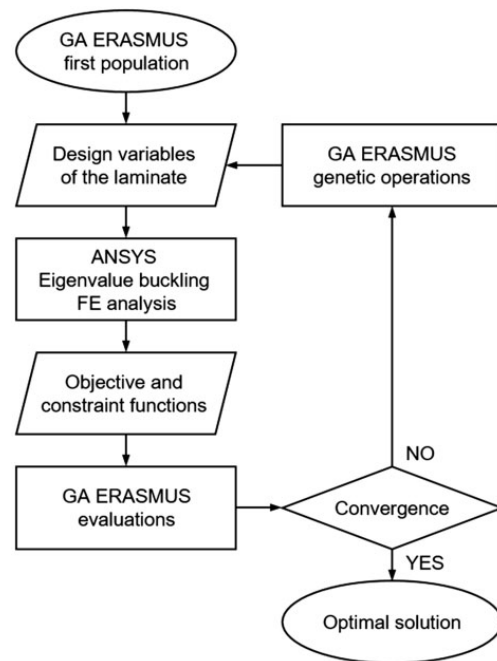
### Numerical strategy

Problem (10) is a non-convex CNLPP in terms of both geometrical and mechanical variables. Its non-linearity and non-convexity is due on the nature of the buckling load constraint that is a non-convex function. In addition, the complexity of such a problem is also due to the non-linear feasibility constraints on the laminate polar parameters.

The total number of design variables at the laminate macroscopic scale is three. The number of optimisation constraints is three too (see equation (10)). Furthermore, design variables have different nature (see Table 3): integer ( $n$ ) and continuous ( $\rho_0$  and  $\rho_1$ ) variables are involved in the definition of this CNLPP.

For the resolution of problem (10) the GA ERASMUS (Evolutionary Algorithm for optimisation of Modular Systems)<sup>32,44</sup> coupled with the FE model of the laminate (for calculating the first buckling load of the structure) has been utilised as optimisation tool for the solution search, see Figure 4. The GA ERASMUS was already successfully applied to solve different kinds of real-world engineering problems, see for example,<sup>28,34–37,45,46</sup>

As shown in Figure 4, for each individual at each generation, the numerical tool performs a FE analysis to calculate the first buckling load (eigenvalue problem) of the multilayer plate as well as its weight. The input data of the FE model of the composite structure (implemented in ANSYS® environment) are both geometrical

**Figure 4.** Logical flow of the numerical procedure for the solution search of the first-level problem.

and mechanical design variables (generated by ERASMUS). The GA elaborates the results provided by the FE model in order to execute the genetic operations. These operations are repeated until the GA meets the user-defined convergence criterion.

The generic individual of the GA ERASMUS represents a potential solution for the problem at hand. The genotype of the individual for problem (10) is characterised by only one chromosome composed of three genes, each one coding a component of the vector of design variables, see equation (7).

### Mathematical formulation of the second-level problem

The second-level problem focuses on the laminate lay-up design. The goal is to determine at least one stacking sequence satisfying the optimum values of both geometric and polar parameters resulting from the first level of the strategy and having the elastic

symmetries imposed to the laminate within the formulation of the first-level problem, i.e. quasi-homogeneity and orthotropy. In the framework of the FSDT (and when considering the polar formalism for representing the laminate stiffness matrices), this problem can be stated in the form of an unconstrained minimisation problem<sup>21,29</sup>

$$\min_{\delta} I(f_i(\delta)) \quad (11)$$

with

$$I(f_i(\delta)) = \sum_{i=1}^6 f_i(\delta) \quad (12)$$

where  $\delta \in \mathbb{R}^n$  is the vector of the layer orientations, i.e. the design variables of this phase, while  $f_i(\delta)$  are quadratic functions in the space of polar parameters, each one representing a requirement to be satisfied, such as orthotropy, uncoupling, etc. For the problem at hand the partial objective functions can be written as

$$\begin{aligned} f_1(\delta) &= \left( \frac{|\Phi_0^{A^*}(\delta) - \Phi_1^{A^*}(\delta)|}{\pi/4} - K^{A^*(opt)} \right)^2, \\ f_2(\delta) &= \left( \frac{R_0^{A^*}(\delta) - R_0^{A^*(opt)}}{R_0} \right)^2, \\ f_3(\delta) &= \left( \frac{R_1^{A^*}(\delta) - R_1^{A^*(opt)}}{R_1} \right)^2, \\ f_4(\delta) &= \left( \frac{|\Phi_1^{A^*}(\delta) - \Phi_1^{A^*(opt)}|}{\pi/4} \right)^2, \quad f_5(\delta) = \left( \frac{\|\mathbf{C}(\delta)\|}{\|\mathbf{Q}\|} \right)^2, \\ f_6(\delta) &= \left( \frac{\|\mathbf{B}^*(\delta)\|}{\|\mathbf{Q}\|} \right)^2 \end{aligned} \quad (13)$$

where  $f_1(\delta)$  represents the elastic requirement on the orthotropy of the laminate having the prescribed shape (imposed by the value of  $K^{A^*}$  provided by the first step of the procedure),  $f_2(\delta)$ ,  $f_3(\delta)$  and  $f_4(\delta)$  are the requirements related to the prescribed values of the optimal polar parameters resulting from the first-level problem, while  $f_5(\delta)$  and  $f_6(\delta)$  are linked to the quasi-homogeneity condition.

$I(f_i(\delta))$  is a positive, semi-definite, convex function in the space of the laminate polar parameters, see equations (12) and (13). Nevertheless, such a function is highly non-convex in the space of laminae orientations because the laminate polar parameters depend upon circular functions of these angles. Moreover, the absolute minima of  $I(f_i(\delta))$  are known a priori since they are the zeroes of this function. For more details

about the nature of the second-level problem, see the literature.<sup>21,29</sup>

In order to simplify the problem of retrieving an optimum stack, the search space for problem (11) has been restricted to a particular class of quasi-homogeneous laminates: the *quasi-trivial* (QT) stacking sequences which constitute exact solutions with respect to the requirements of quasi-homogeneity, i.e. functions  $f_5(\delta)$  and  $f_6(\delta)$  in equation (13) are identically null for QT stacks.

QT solutions can be found for laminates with identical plies by acting only on the position of the layers within the stack. Indeed, QT stacks are exact solutions, in terms of quasi-homogeneity condition, regardless of the value of the orientation angle assigned to each layer. In this way, orientations represent free parameters which can be optimised to fulfil further elastic requirements, i.e. functions  $f_1(\delta)$ ,  $f_2(\delta)$ ,  $f_3(\delta)$  and  $f_4(\delta)$ .

The procedure for searching QT stacks is conceptually simple. Let  $n$  be the number of layers and  $n_g \leq n$  the number of *saturated groups*.<sup>47</sup> Plies belonging to a given saturated group share the same orientation angle  $\theta_j$  ( $j = 1, \dots, n_g$ ). The idea is to look for all the permutations of the position of the plies indexes belonging to each group which meet the quasi-homogeneity condition. More details on this topic can be found in Vannucci and Verchery.<sup>47</sup>

Suppose now to fix both the number of plies and of saturated groups, namely  $n$  and  $n_g$ . As discussed in Vannucci and Verchery,<sup>47</sup> the problem of determining QT stacks for a given couple of  $n$  and  $n_g$  can give rise to a huge number of solutions: the number of QT stacks rapidly increases along with  $n$ . To this purpose a database of QT stacks has been built for different combinations of  $n$  and  $n_g$ .

For the problem at hand, the optimum number of plies  $n$  constitutes a result of the first-level problem, while the number of saturated groups  $n_g$  has been fixed a priori. Let  $n_{sol}$  be the number of QT stacks for a particular combination of  $n$  and  $n_g$ . Each solution collected within the database is uniquely defined by means of an identifier  $ID_{sol}$  (i.e. an integer) which varies in the range  $[1, n_{sol}]$ . Therefore,  $ID_{sol}$  represents a further design variable along with the  $n_g$  orientation angles of different saturated groups, i.e.  $\theta \in \mathbb{R}^{n_g}$ . The design variables can be thus collected into the following vector

$$\boldsymbol{\eta}^T = \{ID_{sol}, \theta_1, \dots, \theta_{n_g}\} \quad (14)$$

and problem (11) can be reformulated as

$$\min_{\boldsymbol{\eta}} \sum_{i=1}^4 f_i(\boldsymbol{\eta}) \quad (15)$$

$f_5(\eta)$  and  $f_6(\eta)$  being identically null.

In this background, the solution search for problem (15) is performed by means of the GA ERASMUS. In the case of QT stacks the structure of the individual genotype is simple because it is composed of a single chromosome with  $n_g + 1$  genes: the first one codes the variable  $ID_{sol}$ , whilst the remaining genes code the orientation angles of every saturated group which are discrete variables in the range  $[-89^\circ, 90^\circ]$  with a step length equal to  $1^\circ$ .

### FE model of the multilayer plate

The FE model of the multilayer plate involved in the first level of the MS2L strategy is built using the FE commercial code ANSYS®. As far as the optimisation process is concerned, a linear eigenvalue buckling analysis is conducted to determine the value of the first buckling load for each individual, i.e. for each point in the design space, at the current generation.

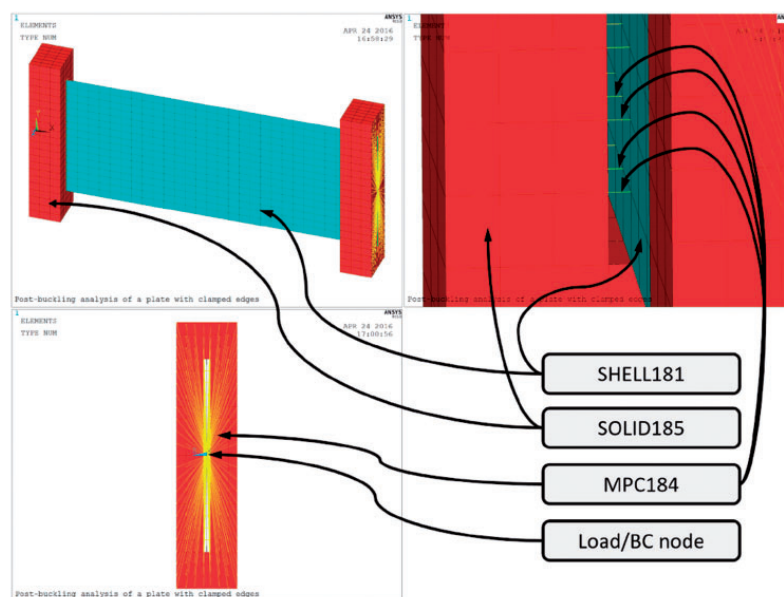
The need to analyse, within the same generation, different geometrical configurations (laminates with different geometrical and mechanical properties), each one corresponding to an individual, requires the creation of an ad hoc input file for the FE code that has to be interfaced with ERASMUS. The FE model must be conceived to account for variable geometry, material and mesh. Indeed, for each individual at the current generation, the FE code has to be able to vary such quantities; thus, a proper parametrisation of the model has to be done.

The FE model of the laminate is illustrated in Figure 5. The model has been built by using a combination of four-node shell elements with six degrees of freedom (DOFs) per node (ANSYS SHELL181 elements), eight-node solid elements with three DOFs per node (ANSYS SOLID185 elements) and non-linear multi-point constraint elements (ANSYS MPC184 elements).

SHELL181 elements have been used to model the multilayer composite plate at the macroscopic scale, regardless to the stacking sequence, i.e. their mechanical behaviour is described by defining directly the homogenised stiffness matrices  $[A^*]$ ,  $[B^*]$ ,  $[D^*]$  and  $[H^*]$  (by using a pre-integrated definition of the shell section).

SOLID185 elements have been considered to model resin blocks (full integration with incompatible modes has been set), while the compatibility of the displacement field at the interface between the plate and the resin blocks is achieved through ANSYS MPC184 elements whose formulation is based upon a classical multi-point constraint element scheme.<sup>48</sup> MPC184 elements are defined between each couple of nodes belonging to contiguous shell and solid elements, as depicted in Figure 5. In particular, MPC184 elements are defined between nodes of the middle plane of the multilayer plate (master nodes) and those belonging to the internal faces of the resin blocks (slave nodes).

Furthermore, MPC184 elements have been used to simulate the BCs imposed by the experimental apparatus (see the *Experimental apparatus for buckling analysis* section). In particular, two *pilot nodes*,



**Figure 5.** FE model of the multilayer composite plate and the details of MPC184 elements.

$A = \{0, 0, 0\}$  and  $B = \{L, 0, 0\}$ , have been defined according to the structure global frame illustrated in Figure 2 ( $L = 360$  mm is the overall length of the structure along  $x$ -axis). Then, nodes A and B have been connected (through MPC184 elements) to those located on the resin block end faces, i.e. faces located at  $x=0$  and  $x=L$ , respectively (see Figure 5). The BCs for nodes A and B are

$$\begin{aligned} \text{node A : } & u_i = 0, \beta_i = 0; \\ \text{node B : } & F_x = -1N, u_y = u_z = 0, \beta_i = 0, \quad (16) \\ & (i = x, y, z) \end{aligned}$$

In equation (16),  $u_i$  and  $\beta_i$  are nodal displacements and rotations, respectively, whilst  $F_x$  is the  $x$  component of the nodal force.

Concerning the comparison between numerical and experimental results, a non-linear buckling analysis has been performed on the FE model of the structure both on the reference structure (to validate the FE model itself) and on the optimum configurations (for verification purposes). Let  $\lambda_L$  be the value of the first buckling load resulting from the eigenvalue analysis and  $\mathbf{u}_L(x, y, z)$  the corresponding eigenvector (i.e. the normalised displacement field of the structure). In order to carry out the non-linear buckling load analysis, the initial geometry of the multilayer plate is perturbed by introducing a fictitious geometrical imperfection. As usually done in these cases,<sup>48</sup> the geometrical imperfection is simulated through a small perturbation of the nodes location by applying a scaling factor (equal to 0.1, resulting in a deformation of the same magnitude of the geometrical defects measured on the specimens) to the previous displacement field  $\mathbf{u}_L(x, y, z)$ . Only the Cartesian coordinates of the nodes are perturbed without introducing any additional stress/strain field. Subsequently, a non-linear static analysis is performed by applying to the pilot node B a compressive force

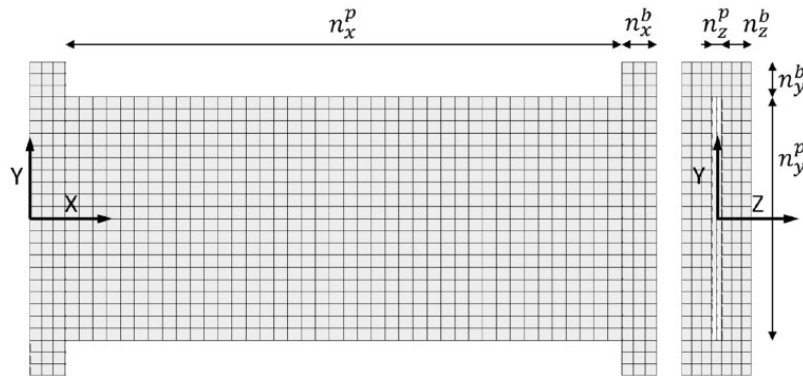
$F_x = 1.1\lambda_L$  and by stopping the analysis when that same pilot node has reached a displacement  $u_x = -0.8$  mm (i.e. approximately the same displacement measured during the experimental test on the reference specimen, see the *Experimental apparatus for buckling analysis* section). The non-linear buckling load  $\lambda_{NL}$  is then computed as the last value of the reaction force along  $x$ -axis measured at the pilot node A. The arc-length method<sup>48</sup> has been chosen as a numerical technique to find the solution for the non-linear equilibrium problem.

Finally, before starting the optimisation process, a sensitivity study (not reported here for the sake of brevity) on the proposed FE model with respect to the mesh seed parameters  $n_x^\alpha, n_y^\alpha, n_z^\alpha$  ( $\alpha = b, p$ , depending on the region), illustrated in Figure 6, has been conducted. It was observed that a mesh having  $n_x^b = n_y^b = n_z^b = 3$ ,  $n_x^p = 30$ ,  $n_y^p = 16$  and  $n_z^p = 1$  is sufficient to properly evaluate the first buckling load (both linear and non-linear) of the structure.

### Experimental apparatus for buckling analysis

A schematic representation of the specimen geometry and loading condition is given in Figures 2 and 3. The specimen reference system is shown in Figure 2: the positive  $z$ -direction points from the plate surface which is in contact to the mould (during the curing cycle) towards the other one. The edges of the plate that are in touch with the testing machine are embedded into two resin blocks. On the one hand, these resin blocks allow for an easy placement and load application during the tests. On the other hand, they avoid the introduction of high local stresses on the plate edges which can lead to a premature failure of the specimen.

Two specimens are tested: one for the reference configuration and one among the different optimum solutions provided by the MS2L optimisation method (see



**Figure 6.** Mesh seed parameters for the FE model of the multilayer composite plate.



the *Optimum solutions: Numerical and experimental results* section). Each sample is obtained from a  $420 \times 300$  mm panel fabricated by computer numerical controlled (CNC) cutting and manual lay-up of the used pre-preg composite material and then cured following the guidelines given by the manufacturer. A rectangular plate has been obtained from the central part of each panel by means of a horizontal mill equipped with a circular diamond blade, then the two long edges of the plates have been lightly ground to improve their parallelism. To embed the plates into the resin blocks, some simple custom tools have been fabricated. The blocks are formed into a semi-rigid silicon mould obtained from an aluminium CNC machined mould. The frame shown in Figure 7 has been created to keep in place the plate and the mould during the resin polymerisation process ensuring, in this way, a good and stable alignment. The so obtained specimens had some defects on their bottom and top surfaces: air bubbles coming from the polymerisation process as well as non-acceptable flatness and parallelism levels. Accordingly, by using one of the long edges of the plate as reference, the two block surfaces and the embedded ends of the plate have been milled.

Before performing the buckling tests, each specimen has undergone a series of measurements to evaluate its geometrical defects.

The frame illustrated in Figure 7 has a double function: it acts as a positioning tool for the specimen as well as a support for the measuring sensors during each test. During the test, various data have been collected (Figures 8 and 9 show the typical testing set-up):

- longitudinal displacement ( $u_x$ ) and rotations ( $\beta_y$  and  $\beta_z$ ) of the moving surface of the testing machine via three linear variable displacement transducer sensors;
- out-of-plane displacement of the middle part of the longitudinal axis of the plate via a laser sensor;
- strain data via strain gages;



Figure 7. Curing assembly.

- the applied load via a load cell.

The specimens have been tested in an MTS® Alliance RF/100 high-performance electromechanical load frame equipped with flat fixed (non-rotating) surface heads. The data have been recorded using three PC-driven data acquisition systems and then combined via time-based synchronisation.

All tests have been performed at a fixed cross-head displacement rate of 0.2 mm/min and stopped when reaching the given strain of  $\varepsilon_{max} = 0.25\%$  on one of the two back-to-back strain gages positioned at the center of the plate.

### The reference configuration: Numerical versus experimental results

Before starting the multi-scale optimisation process, a reference configuration must be defined in order to establish reference values for the mass as well as for the first buckling load and the membrane stiffness along  $y$ -axis. Of course, the reference multilayer plate has the same geometry (in plane overall size) and it is subject to the same set of BCs, as those applied on the specimen that will be optimised. As a reference solution, a symmetric quasi-isotropic laminate composed of 32 layers has been chosen. The plies are arranged according to the following stack:  $[(45^\circ, 0^\circ, -45^\circ, 90^\circ)_s]_4$ , i.e. the laminate is uncoupled and the membrane stiffness matrix is isotropic, but the bending one is totally anisotropic. This reference solution corresponds to a classical configuration utilised in the aeronautical field: its mass and its overall stiffness (both bending and membrane) still represent a 'good' compromise between lightness and stiffness requirements.

For the purposes of this work, among the different data recorded during the tests, only the applied load versus longitudinal displacement has been considered. For the reference solution, this curve is illustrated in Figure 10, where also its numerical counterpart (the buckling load resulting from both linear eigenvalue and non-linear buckling analyses) provided by the FE model is plot for comparison purposes.

A summary of the results on the reference solution is given in Table 4.

The numerical value of the buckling load ( $\lambda_{NL}$  from the non-linear simulation) shows a difference of  $-0.1\%$  compared to the experimental one, confirming in this way the excellent agreement between numerical and experimental results.

As far as the membrane stiffness along  $y$ -axis is concerned, these data have not been experimentally measured, but they are derived analytically according to the FSDT formulae.

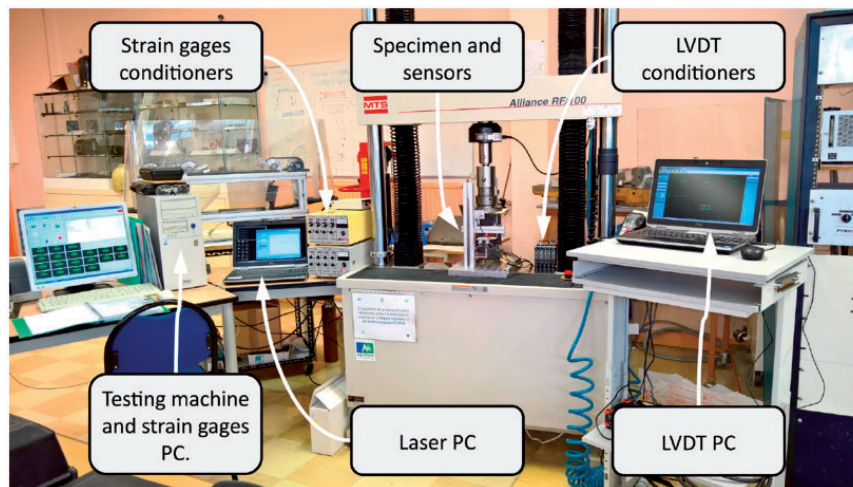


Figure 8. Testing set-up 1.

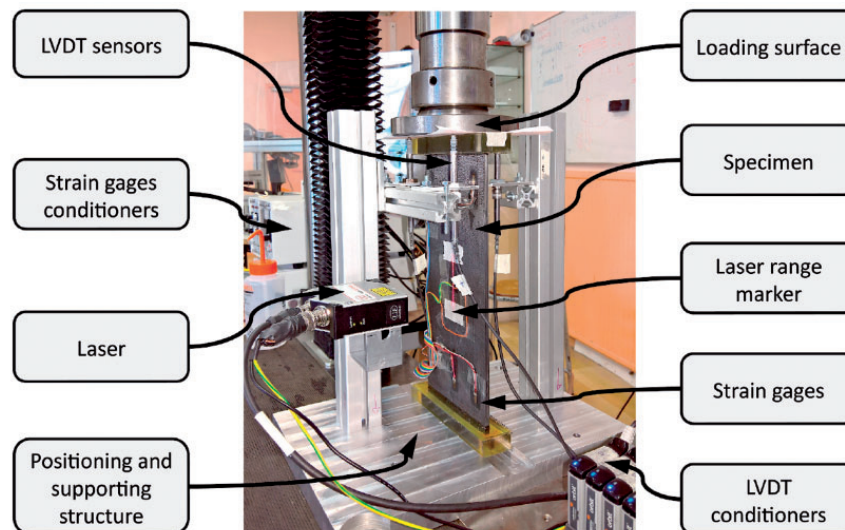


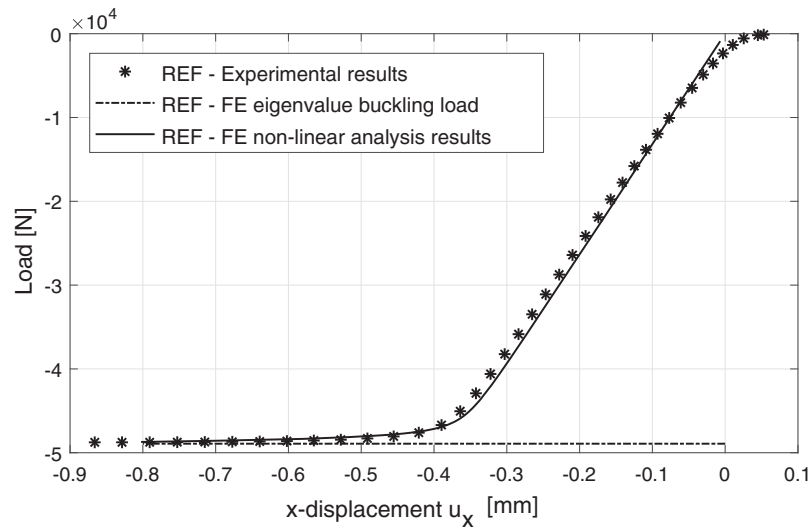
Figure 9. Testing set-up 2.

### Optimum solutions: Numerical and experimental results

The genetic parameters tuning the behaviour of the GA used to perform the solution search, for both first and second-level problems, are listed in Table 5. Moreover, concerning the constraint-handling technique for the first-level problem, the automatic dynamic penalisation (ADP) method has been considered, see Montemurro et al.<sup>44</sup> For more details on the optimisation tool and the meaning of the values of the different parameters tuning the GA, the reader is addressed to Montemurro.<sup>31</sup>

For the first-level problem, the overall optimisation process has required approximately seven days (6 s for each eigenvalue buckling analysis) using two cores of a machine with an Intel Xeon E5-2697v2 processor (2.70–3.50 GHz). The computational effort related to the second-level problem requires only few seconds on the same machine.

The optimum values of both geometric and mechanical design variables (dimensionless variables) resulting from the first level of the optimisation strategy are listed in Table 6. Since problem (10) is non-convex,



**Figure 10.** Experimental and numerical results comparison, reference solution.

**Table 4.** Numerical and experimental mechanical properties of the reference solution.

| Property              | Reference solution |
|-----------------------|--------------------|
| $n_{ply}$             | 32                 |
| $A_{yy}$ (N/mm)       | 363,326            |
| $\lambda_{(exp)}$ (N) | 48,760             |
| $\lambda_L$ (N)       | 48,924             |
| $\lambda_{NL}$ (N)    | 48,712             |

many optimal solutions exist: only the first three best configurations have been reported in Table 6. These solutions exhibit the ‘best’ compromise between lightness and the requirements on buckling and membrane stiffness. It is noteworthy that each optimum solution is composed of 29 plies, which means a weight saving of 9.4% when compared to the reference configuration of the multilayer plate. At the macroscopic scale, each one of the three laminates reported in Table 6 is quasi-homogeneous and fully orthotropic (both membrane and bending stiffness matrices) with an ordinary orthotropy shape (parameter  $K^{A^*} = 0$  because the dimensionless anisotropic polar modulus  $\rho_0$  is positive, see Montemurro<sup>21</sup>). For each solution, the dimensionless polar parameter  $\rho_1$  is about an order of magnitude lower than  $\rho_0$ : this means that the laminate tends to exhibit a *square symmetric* behaviour (for both membrane and bending stiffness matrices). For a deeper insight on these aspects, the interested reader is addressed to the literature<sup>21,29</sup>

As stated in the Mathematical formulation of the second-level problem section, the second-level problem

**Table 5.** GA parameters used for the solution search of both first-level and second-level problems.

| Property                                       | First-level pb.         | Second-level pb.        |
|--|-------------------------|-------------------------|
| N. of populations                              | 2                       | 2                       |
| N. of individuals per population ( $N_{ind}$ ) | 200                     | 500                     |
| N. of chromosomes                              | 1                       | 1                       |
| N. of genes                                    | 3                       | 3                       |
| Stop criterion                                 | Fixed generations (250) | Fixed generations (500) |
| Crossover probability                          | 0.85                    | 0.85                    |
| Mutation probability                           | 0.005(= $1/N_{ind}$ )   | 0.002(= $1/N_{ind}$ )   |
| Selection operator                             | Roulette wheel          | Roulette wheel          |
| Elitism operator                               | Active                  | Active                  |
| Isolation time                                 | 10                      | 20                      |

**Table 6.** Optimum solutions of the first-level problem.

| ID   | Design variables |          |          |
|------|------------------|----------|----------|
|      | $n$              | $\rho_0$ | $\rho_1$ |
| 1.01 | 29               | 0.9863   | 0.0978   |
| 1.02 | 29               | 0.9941   | 0.0821   |
| 1.03 | 29               | 0.9589   | 0.0929   |

is solved in the space of QT stacks. After fixing the number of plies  $n$  and the number of saturated groups  $n_g$ , the design variables are the identifier of the QT solution as well as the orientation angle of each



saturated group, see equation (14). Because problem (15) is highly non-convex in the space of the orientation angles of saturated groups, it is possible to find multiple solutions (theoretically an infinite number) meeting the optimum value of the laminate polar parameters provided by the first-level problem. A non-exhaustive list of them, in the case of  $n_g = 5$ , is presented in Table 7 and the respective mechanical properties (in terms of membrane stiffness along  $y$ -axis and buckling load resulting from the non-linear analysis) can be found in Table 8.

It is noteworthy that all these solutions are non-standard stacks. Although such sequences are neither symmetric nor balanced, they are fully orthotropic (both in membrane and bending), uncoupled and they exhibit the same elastic behaviour (in terms of normalised membrane and bending stiffness). These peculiar features are the natural result of the utilisation of very general QT stacks. Furthermore, these optimum solutions really represent equivalent configurations: they share the same number of plies and they show light differences in terms of mechanical performances. As reported in Table 8, these differences range from +1.7% to +3.9% for the buckling load and from +2.2% to +3.3% for  $A_{yy}$ . Therefore, each optimum configuration is simultaneously lighter and stiffer than the reference one and this result has been achieved only by abandoning the usual engineering rules related to the nature of the stacking sequence.

Among the solutions listed in Table 7, the stacking sequence identified by the ID 2.01 has been selected to be manufactured and tested. The load–displacement

curve for this optimum solution (both experimental and numerical results) is given in Figure 11.

The polar diagram of stack 2.01 is shown in Figure 12: only the first component of the normalised stiffness matrices of the laminate, i.e.  $\mathbf{A}^*$ ,  $\mathbf{B}^*$  and  $\mathbf{D}^*$  is represented. The solid line refers to the membrane stiffness matrix, the dashed one to the bending stiffness matrix,

**Table 8.** Mechanical properties of the optimum stacking sequences in terms of buckling load and membrane stiffness along  $y$ -axis.

| ID   | $\lambda_{NL}$ (N) | $A_{yy}$ (N/mm) |
|------|--------------------|-----------------|
| 2.01 | 50,486 (+3.5%)     | 375,219 (+3.3%) |
| 2.02 | 50,551 (+3.7%)     | 374,193 (+3.0%) |
| 2.03 | 50,662 (+3.9%)     | 375,105 (+3.2%) |
| 2.04 | 50,581 (+3.7%)     | 374,194 (+3.0%) |
| 2.05 | 50,408 (+3.4%)     | 375,303 (+3.3%) |
| 2.06 | 50,202 (+3.0%)     | 375,275 (+3.3%) |
| 2.07 | 50,494 (+3.6%)     | 375,219 (+3.3%) |
| 2.08 | 50,600 (+3.8%)     | 375,235 (+3.3%) |
| 2.09 | 50,569 (+3.7%)     | 374,482 (+3.1%) |
| 2.10 | 49,598 (+1.7%)     | 375,072 (+3.2%) |
| 2.11 | 49,638 (+1.8%)     | 374,591 (+3.1%) |
| 2.12 | 50,072 (+2.7%)     | 371,435 (+2.2%) |
| 2.13 | 49,666 (+1.9%)     | 374,627 (+3.1%) |
| 2.14 | 49,694 (+1.9%)     | 374,591 (+3.1%) |
| 2.15 | 50,488 (+3.5%)     | 374,233 (+3.0%) |

Note: For each property the percentage difference between the optimum configuration and the reference one is indicated in parentheses.

**Table 7.** Numerical results of the second-level problem (optimum stacking sequences).

| ID   | Parent | Stacking sequence  |
|------|--------|--|
| 2.01 | 1.01   | [89/0/90/90/2/90/−3/−3/2/0/−3/2/0/0/90/90/89/90/89/−3/2/90/89/90/0/0/90/2/−3]            |
| 2.02 | 1.01   | [−87/88/1/−2/−2/0/0/88/88/1/88/88/−2/1/0/88/−87/0/−87/−2/1/−2/−87/88/88/−2/1/88/0]       |
| 2.03 | 1.01   | [4/−2/0/89/89/−89/−89/−89/−2/−2/−89/0/89/−2/0/0/4/−2/4/89/−89/89/4/−2/−89/89/−89/−2/0]   |
| 2.04 | 1.01   | [−87/88/−2/1/1/88/−1/88/−2/88/−1/1/−1/1/−2/88/−87/1/−87/88/88/−2/−87/1/88/−2/88/1/−1]    |
| 2.05 | 1.01   | [−89/−2/−1/90/90/−2/6/90/−1/90/6/−2/6/90/−1/−2/−89/90/−89/−2/−2/−1/−89/90/90/−1/90/−2/6] |
| 2.06 | 1.01   | [−89/90/1/90/−4/4/−4/1/4/4/1/90/−89/−89/90/−4/90/1/−4/90/90/−89/4/1/−89/1/4/−4/90]       |
| 2.07 | 1.01   | [−89/90/3/0/0/−2/−2/90/90/3/90/90/0/3/−2/90/−89/−2/−89/0/3/0/−89/90/90/0/3/90/−2]        |
| 2.08 | 1.01   | [90/90/0/0/0/0/90/90/0/90/90/0/0/0/90/90/0/90/0/0/0/90/90/90/0/0/90/0]                   |
| 2.09 | 1.01   | [−2/0/88/−88/0/1/88/−88/1/1/88/1/−88/−88/88/88/−2/0/−2/0/0/−88/−2/0/1/88/88/1/−88]       |
| 2.10 | 1.02   | [−87/89/−9/3/89/3/6/6/−9/89/6/89/3/89/−9/89/−87/3/−87/6/3/−9/−87/89/89/−9/89/3/6]        |
| 2.11 | 1.02   | [8/−7/88/88/3/−87/−87/−7/3/−7/88/3/88/−7/−87/88/8/−87/8/−7/3/88/8/88/−7/−7/88/3/−87]     |
| 2.12 | 1.01   | [−83/87/7/−3/87/−3/−3/−3/7/87/−3/87/−3/87/7/87/−83/−3/−83/−3/−3/7/−83/87/87/7/87/−3/−3]  |
| 2.13 | 1.03   | [−87/−2/88/88/8/88/−7/−7/8/−2/−7/8/−2/−2/88/88/−87/88/−87/−7/8/88/−87/88/−2/−2/88/8/−7]  |
| 2.14 | 1.03   | [8/88/−87/−7/−7/88/3/3/−87/88/3/−7/88/−7/−87/88/8/−7/8/3/88/−87/8/−7/88/−87/88/−7/3]     |
| 2.15 | 1.01   | [−87/88/3/−2/88/−2/−2/88/−2/3/88/−2/−2/3/−2/88/−87/−2/−87/88/3/88/−87/−2/88/88/3/−2/−2]  |

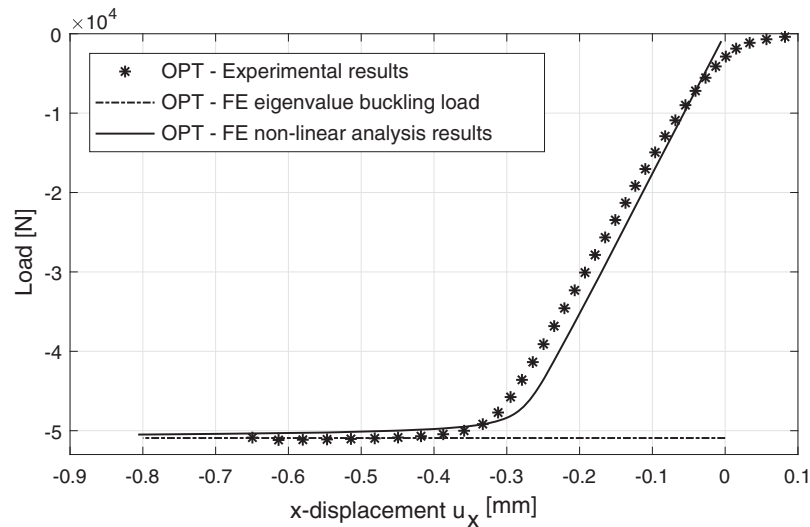


Figure 11. Experimental and numerical results comparison, optimum solution.

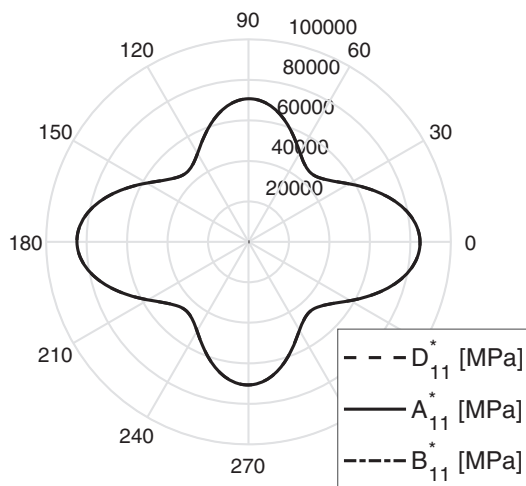


Figure 12. Polar diagram of stack 2.01.

while the dash-dotted one is linked to the membrane/bending coupling stiffness matrix. It can be noticed that the laminate is uncoupled as the dash-dotted curve disappears, homogeneous as the solid and dashed curves are coincident and orthotropic because there are two orthogonal axes of symmetry in the plane. In addition, for both laminates the main orthotropy axis is oriented at  $\Phi_1^* = 0^\circ$  according to the hypothesis of the first-level problem. Of course, the same considerations can be repeated also for the rest of the optimum solutions.

A summary of the results characterising the stack 2.01 is given in Table 9.

Also for this case, experimental and numerical results are in excellent agreement with a percentage

Table 9. Numerical and experimental mechanical properties for the optimum solution 2.01.

| Property              | Optimum solution |
|-----------------------|------------------|
| $n_{ply}$             | 29 (−9.4%)       |
| $A_{yy}$ (N/mm)       | 375,219 (+3.3%)  |
| $\lambda_{(exp)}$ (N) | 51,189 (+5.0%)   |
| $\lambda_L$ (N)       | 50,922 (+4.1%)   |
| $\lambda_{NL}$ (N)    | 50,486 (+3.6%)   |

Note: For each property the percentage difference between the optimum configuration and the reference one is indicated in parentheses.

difference of −1.4% (non-linear numerical buckling load over the experimental one), thus giving an experimental proof of the effectiveness of QT stacks and, by extension, of the MS2L optimisation process.

## Conclusions

The design strategy presented in this paper is a numerical optimisation procedure characterised by several features that make it an innovative, effective and general method for the multi-scale design of composite structures. In the present work, this strategy has been applied to the multi-scale optimisation of a composite multilayer plate.

The design process is not submitted to restrictions: any parameter characterising the structure (at each relevant scale) is an optimisation variable. This allows searching for a *true global minimum*, hard to be obtained otherwise. The multi-scale design problem has been split

into two distinct but linked non-linear minimisation problems which are solved subsequently within the same numerical procedure. The first-level problem focuses on the macroscopic scale of the panel: the laminate is considered as an equivalent homogeneous anisotropic plate and its macroscopic mechanical response is described in terms of polar parameters. Furthermore, the overall plate thickness is also determined at this level. The second level of the procedure is devoted to find at least one optimum stack meeting the elastic requirements imposed to the laminate (quasi-homogeneity and orthotropy) as well as the optimum value of the laminate polar parameters resulting from the first step.

At the macroscopic scale, the mechanical properties of the multilayer plate are represented by means of the polar formalism, a mathematical representation characterised by several advantages. The main features of the polar method are the possibility to represent in an explicit and straightforward way the elastic symmetries of the laminate stiffness matrices, the elastic and geometric bounds for the laminate polar parameters and to eliminate from the optimisation procedure redundant variables. In addition, the utilisation of the polar formalism leads the designer to easily formulate the second-level problem by taking into account in a correct and elegant way the requirements on the elastic symmetries of the structure, without making simplifying hypotheses on the nature of the stacking sequence.

As far as the optimisation calculations are concerned, they are carried out by a special GA able to integrate both continuous and discrete-valued variables during the same calculation and to effectively handle the optimisation constraints by means of the very general ADP method. For the solution of the first-level problem, the GA has been interfaced with the FE commercial code ANSYS that invokes a linear eigenvalue buckling analysis in order to compute both the objective and the constraint functions of the problem.

The utilisation of an evolutionary strategy, together with the fact that the problem is stated in the most general sense, allows finding some non-conventional configurations that are more efficient than the standard ones. In fact, the considered example proves that, when standard rules for tailoring laminate stacks are abandoned and all the parameters characterising the laminate are included within the design process, a significant weight saving can be obtained: up to 9.4% (with respect to a reference canonical stack) with enhanced mechanical properties in terms of both first buckling load and membrane stiffness along  $y$ -axis (the percentage increment range from +1.7% to +3.9% and from +2.2% to +3.3%, respectively, depending on the considered optimum solution).

In addition, experimental buckling tests have been conducted on both reference and optimum solutions. Experimental and numerical results are in excellent

agreement (maximum absolute percentage difference lower than 1.4%) confirming, in this way, the high potential of non-conventional QT solutions and, by extension, that of the MS2L optimisation approach. These encouraging results unquestionably prove the effectiveness and the robustness of the MS2L optimisation approach proposed in this work and provide confidence for further research in this direction.

As far as the perspectives of this work are concerned, research is ongoing in order to develop a suitable global/local modelling approach for composite structures to be integrated into the MS2L optimisation strategy when applied to real-world engineering problems (as the multi-scale optimisation of a wing-box structure). A proper global/local modelling is of paramount importance when both global (e.g. mass, stiffness, etc.) and local (failure criteria, local buckling, etc.) design criteria must be included into the optimisation process. These activities will be developed in the framework of the project PARSIFAL (Prandtlplane ARchitecture for the Sustainable Improvement of Future AirpLanes) funded by the European Union.


#### Declaration of Conflicting Interests

The author(s) declared no potential conflicts of interest with respect to the research, authorship, and/or publication of this article.

#### Funding

The author(s) disclosed receipt of the following financial support for the research, authorship, and/or publication of this article: This paper presents part of the activities carried out within the research project PARSIFAL (Prandtlplane ARchitecture for the Sustainable Improvement of Future AirpLanes), which has been funded by the European Union under the Horizon 2020 Research and Innovation Program (Grant Agreement no. 723149).

#### ORCID iD

Marco Montemurro  <http://orcid.org/0000-0001-5688-3664>

#### References

1. Trovalusci P. A Statistically-Based Homogenization Approach for Particle Random Composites as Micropolar Continua. In: Altenbach H and Forest S (eds) *Generalized continua as models for classical and advanced materials. Advanced Structured Materials*. 1st ed. Switzerland: Springer International Publishing, 2016, pp. 425–441.
2. Reccia E, Bellis MLD, Trovalusci P, et al. Sensitivity to material contrast in homogenization of random particle composites as micropolar continua. *Compos B Eng* 2018; 136: 39–45.
3. Leonetti L, Greco F, Trovalusci P, et al. A multiscale damage analysis of periodic composites using a couple-

- stress/cauchy multidomain model: application to masonry structures. *Compos B Eng* 2018; 141: 50–59.
4. Adali S, Verijenko V and Walker M. Optimal laminate configurations with symmetric lay-ups for maximum postbuckling stiffness. *Compos Eng* 1994; 4: 1119–1127.
  5. Adali S, Richter A., Verijenko V, et al. Optimal design of hybrid laminates with discrete ply angles for maximum buckling load and minimum cost. In: *Eighth international conference on composite structures*. *Compos Struct* 1995; 32: 409–415.
  6. Adali S, Walker M and Verijenko V. Multiobjective optimization of laminated plates for maximum prebuckling, buckling and postbuckling strength using continuous and discrete ply angles. *Compos Struct* 1996; 35: 117–130.
  7. Adali S, Lene F, Duvaut G, et al. Optimization of laminated composites subject to uncertain buckling loads. *Compos Struct* 2003; 62: 261–269.
  8. Haftka RT and Walsh JL. Stacking-sequence optimization for buckling of laminated plates by integer programming. *AIAA J* 1992; 30: 814–819.
  9. Le Riche R and Haftka RT. Optimization of laminate stacking sequence for buckling load maximization by genetic algorithm. *AIAA J* 1993; 31: 951–956.
  10. Aymerich F and Serra M. Optimization of laminate stacking sequence for maximum buckling load using the ant colony optimization (ACO) metaheuristic. *Compos Part A Appl Sci Manuf* 2008; 39: 262–272.
  11. Irisarri F-X, Bassir DH, Carrere N, et al. Multiobjective stacking sequence optimization for laminated composite structures. *Compos Sci Technol* 2009; 69: 983–990.
  12. U.S. Department of Defense. *Military handbook – MIL-HDBK-17-3F: Composite Materials Handbook – Polymer matrix composites materials usage, design and analysis*, vol. 3. USA: U.S. Department of Defense, 2002.
  13. Jones RM. *Mechanics of composite materials*. New York: McGraw-Hill, 1975.
  14. Tsai SW and Pagano NJ. Invariant properties of composite materials. Technical Report, Air Force Materials Lab, Wright-Patterson AFB, Ohio, 1968.
  15. Tsai SW and Hahn T. *Introduction to composite materials*. Chicago: Technomic, 1980.
  16. Diaconu CG, Sato M and Sekine H. Feasible region in general design space of lamination parameters for laminated composites. *AIAA J* 2002; 40: 559–565.
  17. Diaconu C, Sato M and Sekine H. Layup optimization of symmetrically laminated thick plates for fundamental frequencies using lamination parameters. *Struct Multidiscipl Optim* 2002; 24: 302–311.
  18. Liu B, Haftka RT and Trompette P. Maximization of buckling loads of composite panels using flexural lamination parameters. *Struct Multidiscipl Optim* 2004; 26: 28–36.
  19. Bloomfield M, Herencia J and Weaver P. Optimisation of anisotropic composite plates incorporating non-conventional ply orientations. In: *49th AIAA/ASME/ASCE/AHS/ASC structures, structural dynamics, and materials conference, 16th AIAA/ASME/AHS adaptive structures conference, 10th AIAA non-deterministic approaches conference, 9th AIAA Gossamer spacecraft forum, 4th AIAA multidisciplinary design optimization specialists conference*, 2008, pp. 1918, Schaumburg, IL: American Institute of Aeronautics and Astronautics.
  20. Liu S, Hou Y, Sun X, et al. A two-step optimization scheme for maximum stiffness design of laminated plates based on lamination parameters. *Compos Struct* 2012; 94: 3529–3537.
  21. Montemurro M. An extension of the polar method to the first-order shear deformation theory of laminates. *Compos Struct* 2015; 127: 328–339.
  22. Nagendra S, Jestin D, Gürdal Z, et al. Improved genetic algorithm for the design of stiffened composite panels. *Comput Struct* 1996; 58: 543–555.
  23. Le Riche R and Haftka RT. Improved genetic algorithm for minimum thickness composite laminate design. *Compos Eng* 1995; 5: 143–161.
  24. Todoroki A and Haftka RT. Stacking sequence optimization by a genetic algorithm with a new recessive gene like repair strategy. *Compos B Eng* 1998; 29: 277–285.
  25. Verchery G. Les invariants des tenseurs d'ordre 4 du type de l'élasticité. In: Boehler JP (ed) *Mechanical Behavior of Anisotropic Solids / Comportment Mécanique des Solides Anisotropes*. Netherlands: Springer, 1982, pp. 93–104. DOI: 10.1007/978-94-009-6827-1\_7.
  26. Catapano A and Montemurro M. A multi-scale approach for the optimum design of sandwich plates with honeycomb core. Part I: homogenisation of core properties. *Compos Struct* 2014; 118: 664–676.
  27. Catapano A and Montemurro M. A multi-scale approach for the optimum design of sandwich plates with honeycomb core. Part II: the optimisation strategy. *Compos Struct* 2014; 118: 677–690.
  28. Montemurro M, Catapano A and Doroszewski D. A multi-scale approach for the simultaneous shape and material optimisation of sandwich panels with cellular core. *Compos B Eng* 2016; 91: 458–472.
  29. Montemurro M. Corrigendum to “An extension of the polar method to the first-order shear deformation theory of laminates” [*Compos. Struct.* 2015; 127: 328–339]. *Compos Struct* 2015; 131: 1143–1144.
  30. Montemurro M. The polar analysis of the third-order shear deformation theory of laminates. *Compos Struct* 2015; 131: 775–789.
  31. Montemurro M. *Optimal design of advanced engineering modular systems through a new genetic approach*. PhD Thesis, UPMC, Paris VI, France, 2012.
  32. Montemurro M. *A contribution to the development of design strategies for the optimisation of lightweight structures*. HDR Thesis, Université de Bordeaux, France, 2018.
  33. Montemurro M, Vincenti A and Vannucci P. Design of elastic properties of laminates with minimum number of plies. *Mech Compos Mater* 2012; 48: 369–390.
  34. Montemurro M, Koutsawa Y, Belouettar S, et al. Design of damping properties of hybrid laminates through a global optimisation strategy. *Compos Struct* 2012; 94: 3309–3320.
  35. Montemurro M, Vincenti A, Koutsawa Y, et al. A two-level procedure for the global optimization of the damping behavior of composite laminated plates

- with elastomer patches. *J Vib Control* 2015; 21: 1778–1800.
36. Montemurro M and Catapano A. A new paradigm for the optimum design of variable angle tow laminates. In: Frediani A, Mohammadi B, Pironneau O, and Cipolla V (eds) *Variational analysis and aerospace engineering: mathematical challenges for the aerospace of the future*. Springer optimization and its applications. 1st ed., Vol. 116. Springer International Publishing, 2016, pp.375–400.
  37. Montemurro M and Catapano A. On the effective integration of manufacturability constraints within the multi-scale methodology for designing variable angle-tow laminates. *Compos Struct* 2017; 161: 145–159.
  38. Montemurro M and Catapano A. A general B-Spline surfaces theoretical framework for optimisation of variable angle-tow laminates. *Compos Struct* 2019; 209: 561–578.
  39. ASTM, D3518/D3518M-94(07). *Standard test method for in-plane shear response of polymer matrix composite materials by tensile test of a  $\pm 45^\circ$  laminate*. West Conshohocken, PA: ASTM, 2007.
  40. Izzi MI. *Multi-scale analysis, design and optimisation of multilayer plates*. Master's Thesis, Università di Pisa, 2016.
  41. Reddy JN. *Mechanics of composite laminated plates and shells: theory and analysis*. Boca Raton, FL: CRC Press, 2003.
  42. Vannucci P. Plane anisotropy by the polar method. *Meccanica* 2005; 40: 437–454.
  43. Vannucci P. A note on the elastic and geometric bounds for composite laminates. *J Elast* 2013; 112: 199–215.
  44. Montemurro M, Vincenti A and Vannucci P. The automatic dynamic penalisation method (ADP) for handling constraints with genetic algorithms. *Comput Methods Appl Mech Eng* 2013; 256: 70–87.
  45. Montemurro M, Nasser H, Koutsawa Y, et al. Identification of electromechanical properties of piezoelectric structures through evolutionary optimisation techniques. *Int J Solids Struct* 2012; 49: 1884–1892.
  46. Costa G, Montemurro M and Pailhès J. A General Hybrid Optimization Strategy for Curve Fitting in the Non-Uniform Rational Basis Spline Framework. *J Optim Theory Appl* 2018; 176: 225–251.
  47. Vannucci P and Verchery G. A special class of uncoupled and quasi-homogeneous laminates. *Compos Sci Technol* 2001; 61: 1465–1473.
  48. ANSYS, Inc. *ANSYS mechanical APDL modeling and meshing guide*. Canonsburg, PA: ANSYS, Inc., 2012.

---

## Design of large-scale thin-walled composite structures

The article *A multi-scale two-level optimisation strategy integrating a global/local modelling approach for composite structures*, reported in this chapter, has been published in *Composite Structures* (Izzi et al., 2020). It deals with the preliminary design of large-scale thin-walled CSC structures typical of the aeronautical field. The GL-MS2LOS is presented in this article.

In this work is investigated the possibility to employ the GL modelling approach presented in Chapter 3 in the context of the design of large-scale thin-walled CSC structures. The solution proposed for the efficient optimisation of this type of structures is to combine the modelling advantages of the GL-MSOS to the scales separation and design variables reduction ensured by the MS2LOS. The integration takes place at the first-level of the MS2LOS. Here, the response of the structure, described in terms of the PPs of the constitutive laminates and other geometrical design variables, is assessed by analyses performed on fully-parametric GFEM and LFEMs, whose coherency is ensured through the adoption of a sub-modelling GL approach. The second-level of the MS2LOS remains unaltered with respect to previous works and is not presented here: the lay-up design of the various laminates composing the optimised structure is performed, without introducing common-use simplifying rules, in this phase.

The effectiveness of the proposed design procedure is demonstrated by optimising the same fuselage barrel introduced in Chapter 3. The least-weight design of the structure, made of straight-fibres composite laminates, is carried out enforcing constraints on its stiffness, its failure and buckling strength under various loading conditions, its manufacturability, and the elastic behaviour of its constituting laminates. The optimal CSC configuration is compared to the optimal aluminium one presented in Chapter 3 : the composite solution shows a remarkable weight saving of about 40% while satisfying all considered design requirements.





# A multi-scale two-level optimisation strategy integrating a global/local modelling approach for composite structures

Michele Iacopo Izzi<sup>a</sup>, Marco Montemurro<sup>a,\*</sup>, Anita Catapano<sup>b</sup>, Jérôme Pailhès<sup>a</sup>

<sup>a</sup> Arts et Métiers Institute of Technology, Université de Bordeaux, CNRS, INRA, Bordeaux INP, HESAM Université, I2M UMR 5295, F-33405 Talence, France

<sup>b</sup> Bordeaux INP, Université de Bordeaux, Arts et Métiers Institute of Technology, CNRS, INRA, HESAM Université, I2M UMR 5295, F-33405 Talence, France

## ARTICLE INFO

### Keywords:

Preliminary design  
Optimisation  
Global/local modelling approach  
Composite material  
Stiffened panel  
Fuselage

## ABSTRACT

In this work, a multi-scale optimisation strategy for the preliminary design of composite structures involving design requirements at different scales, is presented. Such a strategy, denoted as GL-MS2LOS, has been formulated by integrating a dedicated global-local (GL) modelling approach into the multi-scale two-level optimisation strategy (MS2LOS).

The GL-MS2LOS aims at proposing a very general formulation of the design problem, without introducing simplifying hypotheses and by considering, as design variables, the full set of geometric and mechanical parameters defining the behaviour of the composite structure at each pertinent scale. By employing a GL modelling approach, most of the limitations of well-established design strategies based on analytical or semi-empirical models are overcome.

The effectiveness of the presented GL-MS2LOS is proven on a meaningful study case: the least-weight design of a composite fuselage barrel of a wide-body aircraft undergoing various loading conditions and subject to requirements of different nature. Fully parametric global and local FE models are interfaced with an in-house metaheuristic algorithm to perform the optimisation. Refined local FE models are created only for critical regions of the structure, automatically detected during the global analysis, and linked to the global one thanks to the implementation of a sub-modelling approach. The general nature of the GL-MS2LOS allows finding an optimised configuration characterised by a weight saving of 40% when compared to an optimised aluminium solution obtained through a similar GL optimisation strategy.

## 1. Introduction

Aircraft structural design is mainly driven by lightness-related criteria subject to a set of performance-related requirements. Thanks to their high specific stiffness and strength properties, nowadays composite materials are massively used for primary aircraft components.

Composite materials can be suitably tailored to locally enhance stiffness and strength, thus offering a significant advantage over metals. Conversely, they introduce some specific phenomena, e.g. extension-bending coupling, delamination, free-edge stresses, different failure mechanisms, etc. Moreover, the design process of a composite structure is more difficult than that characterising a metallic one because of the high number of design variables involved at different scales.

In the aeronautical industry, decades of development of metallic aircraft design has led to the well-established “semi-monocoque” configuration as the conventional architecture for both fuselage and wing structures. Then, this architecture has been extended to new composite-

based solutions.

Due to their nature, aircraft structures made of composite materials present different working scales. At higher scales, the heterogeneity of the composite material can be neglected and only the overall anisotropic behaviour of the laminates is considered. Therefore, two working scales can be identified: the “global” macroscopic scale of the whole structure and the “local” macroscopic scale of the main components (e.g. the stiffened panels) constituting the structure. At these scales each composite part is modelled as an *equivalent anisotropic homogeneous continuum*.

At the lower scale, i.e. the mesoscopic scale of the elementary lamina composing each laminate, different phenomena take place, which are related to the local stress field and to the specificity of the manufacturing process and that need different modelling strategies. Accordingly, the design of a composite structure must be formulated as a multi-scale optimisation (MSO) problem.

The design-optimisation strategies available in the literature [1,2]

\* Corresponding author.

E-mail addresses: [marco.montemurro@ensam.eu](mailto:marco.montemurro@ensam.eu), [marco.montemurro@u-bordeaux.fr](mailto:marco.montemurro@u-bordeaux.fr) (M. Montemurro).

<https://doi.org/10.1016/j.compstruct.2020.111908>

Received 30 October 2019; Received in revised form 22 December 2019; Accepted 8 January 2020

Available online 13 January 2020

0263-8223/ © 2020 Elsevier Ltd. All rights reserved.

differ (a) in the way the scale transition is handled; (b) in the models and methods used to describe the main physical phenomena involved at different scales; (c) in the algorithm employed to find an optimal solution.

Furthermore, most of the research works are applied to simple structures, like plates or simplified stiffened panels, that are the basic units of full-scale structures.

The so-called “bottom-up” approach was the first one to be used for design purposes. In this approach the plies orientation angles are directly taken as design variables, without using a dedicated multi-scale strategy. Typical examples are the works of Adali et al. [3], Haftka and Walsh [4], Le Riche and Haftka [5], Aymerich and Serra [6], Irisarri et al. [7,8], Bisagni and Vescovini [9]. Most of these works deal with the problem of the buckling load and/or post-buckling stiffness maximisation with an assigned mass [3–6,8], or the dual problem of minimising the mass under constraints on the buckling strength [4,7,9], being the buckling phenomenon a main concern when dealing with the optimisation of thin-walled structures. Due to the discrete nature of the design variables and to the non-convexity of the problem, deterministic algorithms cannot be used for the solution search, thus researchers have investigated, and compared, different meta-heuristics, including Genetic Algorithms (GAs), Integer Programming, Ant Colony Optimisation, Evolutionary Algorithms, searching for the most efficient choice.

In each one of the above studies, the nature of the stack is set *a priori* and the orientation angles are limited to get values in a predefined set, usually the *canonical set*  $\{0^\circ, \pm 45^\circ, 90^\circ\}$  and rarely an extended set like  $\{0^\circ, \pm 15^\circ, \pm 30^\circ, \dots, 90^\circ\}$ . This is usually done both to limit the extent of the design space and to (improperly) enforce some desired properties of the laminate, e.g. the use of symmetric stacking sequences, a sufficient but not necessary condition, to obtain membrane-bending uncoupling and the use of balanced stacks for orthotropic membrane stiffness matrix. Moreover, empirical rules [10] (more or less justified) are usually employed as further design requirements. All these aspects contribute to strongly shrink the design domain, hence leading the numerical tool to find only suboptimal solutions.

With the aim to reduce the number of design variables and to propose an efficient formulation of the design problem, MSO strategies for composite structures have been developed [1]. These strategies allow formulating and solving the optimisation problem at the macroscopic and mesoscopic scales in two sequential steps, resulting in a “top-down” design approach. Firstly, the structural optimisation is performed in terms of macroscopic properties of the laminate, through a suited representation. Secondly, the laminate lay-up design is carried out by retrieving suitable stacks corresponding to the optimum macroscopic properties of the laminate.

The most common MSO approach makes use of the well-known lamination parameters (LPs) coupled with the parameters of Tsai and Pagano [11]. These parameters [12,13] unquestionably provide a compact representation of the stiffness tensors of the laminate, although they are not all tensor invariants [11]. Bloomfield et al. [14] presented a two-step MSO strategy for symmetric laminates made of a predefined set of ply orientations. The strategy is applied to the problem of mass minimisation of a simply supported multilayer plate under different loading conditions. Liu et al. [15] dealt with the maximisation of the laminate stiffness subject to a given set of optimisation constraints. During the first step, the optimisation problem is solved in the LPs space wherein the feasible region has been approximated by the one that can be obtained by considering only six different orientation angles. A suitable stack is then retrieved by solving a least-square problem. In [16], Herencia et al. employed an analogous strategy for the weight minimisation of composite panels with T-shaped stiffeners made of symmetric laminates, whose ply angles belong to the canonical set and submitted to strength, buckling and technological design requirements. Buckling constraints are computed by employing an approximated semi-analytical approach. Stacking sequences found at the second step are slightly heavier and not always match the optimum LPs

found at the first step.

An application of the LPs-based MSO on a full-scale structure can be found in the work of Bramsiepe et al. [17], where the least-weight design problem of a lifting system structure is solved. Failure, buckling and blending requirements are considered: the structure is made of symmetric laminates with ply angles varying with a step of  $15^\circ$ . To evaluate the buckling load of the skin, the analytical formula for a simply supported plate under uniaxial load is used, retrieving the spanwise load component from a coarse global finite element model (GFEM). Moreover, the load redistribution is not directly considered, but the structural optimisation is performed under fixed loads at each iteration.

As it can be inferred from the previous works, the LPs-based MSO approach presents two main weaknesses: LPs are not tensor invariants and not all Tsai and Pagano parameters are invariants; both LPs and Tsai and Pagano parameters have not an immediate physical meaning related to the elastic symmetries of the stiffness tensor. The latter is the main reason at the basis of the systematic use of simplifying hypotheses and rules on the nature of the stacking sequences used in the aforementioned works.

In order to reduce the computational cost of the whole optimisation process, in all the above studies, analytical (approximate) models are used for the assessment of the response of the structure. Accordingly, the main limitations of these approaches are the lack of accuracy and the limited applicability of such methods, which rely on simplifying hypotheses, especially in terms of applied boundary conditions (BCs), often non-representative of real operative conditions.

To overcome these limitations, some authors proposed the use of improved semi-analytical formulations for composite stiffened panels based on the Rayleigh-Ritz method able to better describe the interaction between the skin and the stringers in the buckling phenomenon, but still neglecting the frames compliance and considering the structure infinitely periodic [9,16]. In other works, surrogate models built from results of FE analyses are employed, but the problem of the representativeness of the BCs still persist and the phenomenon of mode switching can lead to a further inaccuracy in the evaluation of the buckling response [8,18]. In particular, Vankan et al. [19], in a report of the Royal Netherlands Aerospace Centre (NLR) about the multi-scale optimisation of a composite fuselage barrel, compared the buckling load estimations, obtained by using a surrogate model built on the results of a parametric local FE model (LFEM) of an isolated stiffened panel subject to idealised BCs, to the results of GFEM analyses with the same refinement level. They showed the poor accuracy of the former model, highlighting the detrimental effect of the use of idealised BCs. The same problem is highlighted by Grihon et al. [20] in a review on numerical optimisation methods developed used at AIRBUS. They identified the inaccuracy of some analytical models and the lack of load redistribution evaluation during the local scale optimisation as the main weaknesses (and the main causes of inconsistency) in the passage from the preliminary design phase to the detailed one.

Therefore, the use of a proper FE modelling strategy for both global and local scales phenomena assessment is preferable in these situations, but, as pointed out by Vekataraman and Haftka [21], even considering the increase of computational resources availability, its integration in optimisation strategies could still be difficult when large and complex structures described by many variables are considered.

In order to go beyond all the aforementioned issues, a dedicated global-local (GL) FE modelling approach is here integrated in the multi-scale two-level optimisation strategy (MS2LOS) for the preliminary optimisation of composite thin-walled structures. The resulting methodology is denoted via the acronym GL-MS2LOS. The GL-MS2LOS is based on the generalisation of the Verchery's polar method [22] to the case of higher-order equivalent single layer theories [23–25] as well as on the GA ERASMUS (Evolutionary Algorithm for optimisation of Modular Systems) previously developed by Montemurro [26]. The GL-MS2LOS aims at proposing a very general formulation of the design



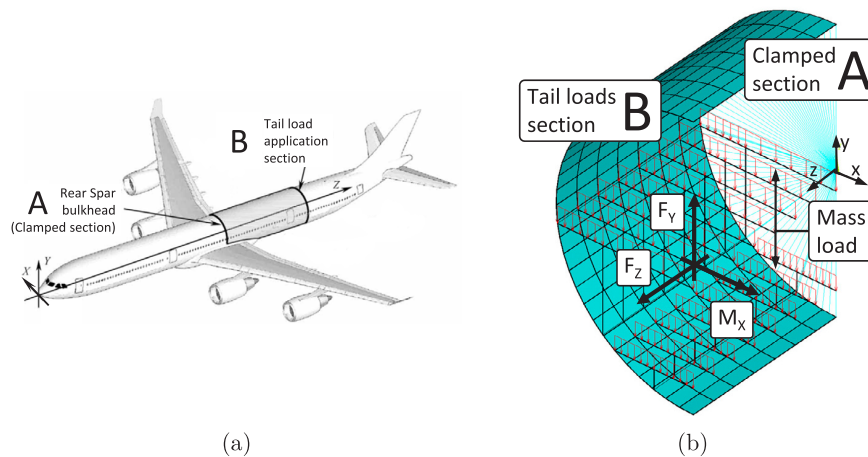


Fig. 1. Location of the fuselage barrel [37](a) and detail of the applied BCs (b).

problem, without introducing simplifying hypotheses and by considering, as design variables, the full set of geometric and mechanical parameters defining the behaviour of the composite structure at each characteristic scale (macroscopic and mesoscopic ones). Montemurro and his co-workers successfully applied the MS2LOS to the optimisation of various anisotropic structures (e.g. [26–31]) and have recently given a first experimental validation of its effectiveness [32].

GL modelling approaches allow to accurately assess phenomena involved at the local scale without the need of a refined GFEM that would require a strong computational effort to be integrated into an optimisation strategy. Instead, refined LFEMs with realistic BCs derived from a coarse GFEM analysis are used in the proposed GL-MS2LOS. Among the different GL approaches available in the literature, the sub-modelling technique [33–36] is employed in this work. In the usual work-flow of the sub-modelling GL approach, firstly a low fidelity linear analysis on a GFEM with a coarse mesh is run to identify one or more zones of interest (ZOIs). Then a refined LFEM is created for each ZOI, where a subsequent analysis is performed imposing displacements provided by the GFEM as BCs. Moreover, iterative stages can be added if the stress redistribution due to local effects is considered non-negligible.

The GL modelling approach is integrated into the first-level problem formulation of the MS2LOS. Here the MS2LOS focuses on the structural optimisation and the design variables are the polar parameters of each laminate composing the structure as well as other geometrical quantities. No assumption is made on the nature of the stacking sequences and desired elastic symmetries of the laminates are naturally got through an efficient use of the polar parameters. In this way, no restrictions are imposed on the design space and, consequently, a true global optimum can be found. All the design criteria and requirements involved into the problem formulation are evaluated by means of fully parametric GFEM and LFEMs. Computational time is kept as low as possible by verifying local responses only on the most critical ZOIs. To this purpose, pertinent design criteria are introduced into the GFEM to automatically identify the ZOIs and generate the related refined LFEMs. Moreover, inasmuch as for each set of design variables both GFEM and LFEMs are generated and no isolated optimisation is performed exclusively on LFEMs, there is no issue related to missed load redistribution evaluation.

The second level of the MS2LOS, as described in [23–32], is devoted to the stacking sequences retrieval. This paper will focus only on the first level of the MS2LOS because the procedure relative to the second level remains unchanged when compared to the aforementioned works.

The effectiveness of the GL-MS2LOS is proven on a meaningful real-world engineering problem: the least-weight design of a composite

fuselage barrel belonging to the aft part of a wide-body aircraft that undergoes multiple loading conditions and subject to constraints of different nature.

The paper is organised as follows. A general description of the design problem, the underlying hypotheses and the driving design criteria are given in Section 2. The fundamentals of the polar method extended to the case of the First-order Shear Deformation Theory (FSDT) are provided in Section 3. The mathematical formulation of the multi-scale design problem and the adopted numerical strategy are discussed in Section 4. The details on the FE models and the implementation of the GL approach are presented in Section 5. Numerical results are shown in Section 6. Finally, Section 7 ends the paper with some conclusions and prospects.

## 2. Least-weight design of a composite fuselage barrel

### 2.1. Problem description

The GL-MS2LOS presented in this study is applied to the least-weight design of a composite fuselage barrel of a wide-body aircraft. The fuselage barrel has a circular cross-section and is located between the wing rear spar and the tail, as shown in Fig. 1. The fuselage barrel is clamped at the rear spar section (section A) and loads coming from the tail are applied to section B. Payload weight and pressurisation are also taken into account. More details on the BCs and the load cases considered in the design process are given in Sections 2.2 and 2.3.

The main geometrical parameters of the fuselage barrel are reported in Table 1. The generic stiffened panel geometry considered in this study is shown in Fig. 2. It is a full composite assembly made of hat-shaped stringers and floating frames with a Z-shaped cross-section.

**Table 1**  
Main geometrical parameters of the fuselage barrel.

| Component   | Value  |
|---|--------|
| Fuselage diameter [mm]                                | 5640   |
| Number of bays  | 7      |
| Bay pitch [mm]  | 500    |
| Upper-deck floor vertical position [mm] <sup>†</sup>  | – 152  |
| Lower-deck floor vertical position [mm] <sup>†</sup>  | – 2130 |
| Struts position on upper-deck floor beam <sup>*</sup> | 1/3    |
| Struts position on lower-deck floor beam <sup>*</sup> | 1/4    |

<sup>\*</sup> Normalised with the floor beam length and referred to the aircraft symmetry plane.

<sup>†</sup> Referred to the horizontal axis through the geometrical centre of the fuselage cross-section.

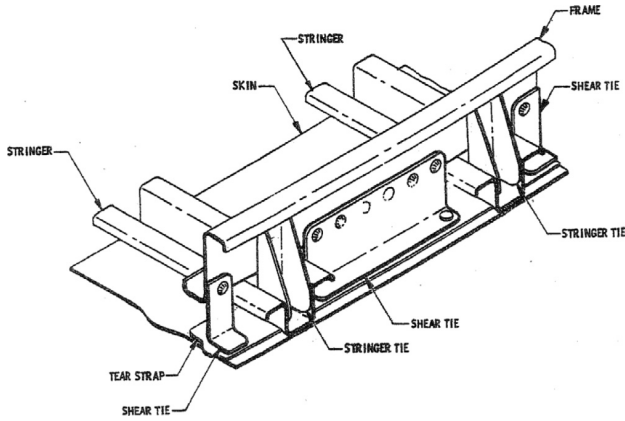


Fig. 2. Architecture of the stiffened panel [56].

Stringers are attached to the skin by means of “shear tie” components, whilst no “stringer tie” or “tear strap” components are present. Metallic floor beams with an I-shaped cross-section and metallic tubular struts complete the set of structural components.

The main structural components are made of laminates. The elementary lamina is the unidirectional T300/5208 carbon/epoxy prepreg, having a linear elastic transversely isotropic behaviour. The metallic components are made of 2024-T3 aluminium alloy, with a linear elastic isotropic behaviour. The physical properties of these materials are reported in Tables 2 and 3; the meaning of the polar parameters listed in these tables is clarified in Section 3.

A reference solution (REF) has been obtained by the authors by optimising an analogous metallic fuselage barrel, entirely made of the 2024-T3 aluminium alloy and subject to an equivalent set of design criteria, with a MSO strategy employing a GL modelling approach. The data necessary to define the reference solution can be found in Table 4; the meaning of some of these parameters is explained in Section 4.1.

**Table 2**  
Material properties of the unidirectional T300/5208 carbon/epoxy ply [38].

| Technical constants           |        | Polar parameters of $[Q^{in}]^a$ |       | Polar parameters of $[Q^{out}]^b$           |       |
|-------------------------------|--------|----------------------------------|-------|---|-------|
| $E_1$ [MPa]                   | 181000 | $T_0$ [MPa]                      | 26899 | $T$ [MPa]                                   | 5398  |
| $E_2$ [MPa]                   | 10300  | $T_1$ [MPa]                      | 24710 | $R$ [MPa]                                   | 1772  |
| $G_{12}$ [MPa]                | 7170   | $R_0$ [MPa]                      | 19729 | $\Phi$ [deg]                                | 90    |
| $\nu_{12}$                    | 0.27   | $R_1$ [MPa]                      | 21426 |   |       |
| $\nu_{23}$                    | 0.42   | $\Phi_0$ [deg]                   | 0     |   |       |
|                               |        | $\Phi_1$ [deg]                   | 0     |   |       |
| Engineering strengths         |        | Pol. par. of $[G^{in}]^c$        |       | Pol. par. of $[G^{out}]^d$ and $[g^{in}]^e$ |       |
| $X = X'$ [MPa]                | 1500   | $\Gamma_0^{in}$ [MPa]            | 7531  | $\Gamma^{out}$ [MPa]                        | 11076 |
| $Y = Z$ [MPa]                 | 40     | $\Gamma_1^{in}$ [MPa]            | 2114  | $\Lambda^{out}$ [MPa]                       | 38    |
| $Y' = Z'$ [MPa]               | 246    | $\Lambda_0^{in}$ [MPa]           | 3587  | $\Omega^{out}$ [deg]                        | 90    |
| $Q = Q'$ [MPa]                | 36     | $\Lambda_1^{in}$ [MPa]           | 1603  | $\gamma^{in}$ [MPa]                         | 137   |
| $R = R'$ [MPa]                | 68     | $\Omega_0^{in}$ [deg]            | 90    | $\lambda^{in}$ [MPa]                        | 79    |
| $S = S'$ [MPa]                | 68     | $\Omega_1^{in}$ [deg]            | 0     | $\omega^{in}$ [deg]                         | 90    |
| Density and thickness         |        |                                  |       |   |       |
| $\rho_c$ [g/cm <sup>3</sup> ] | 1.6    |                                  |       |   |       |
| $t_{ply}$ [mm]                | 0.125  |                                  |       |   |       |

<sup>a</sup> In-plane reduced stiffness matrix of the ply.

<sup>b</sup> Out-of-plane shear stiffness matrix of the ply.

<sup>c</sup> In-plane strength matrix of the ply.

<sup>d</sup> Out-of-plane strength matrix of the ply.

<sup>e</sup> In-plane strength vector of the ply.

**Table 3**  
Material properties of 2024-T3 aluminium alloy [39].

| Propriety                                 | Value |
|---|-------|
| Young's modulus, $E$ [MPa]                | 72395 |
| Poisson's ratio, $\nu$                    | 0.33  |
| Tensile yield stress, $\sigma_y$ [MPa]    | 290   |
| Tensile ultimate stress, $\sigma_u$ [MPa] | 434   |
| Density, $\rho_{Al}$ [g/cm <sup>3</sup> ] | 2.78  |

**Table 4**  
Geometrical parameters of the reference solution REF.

| Component  | Value |         |        |  |
|--|-------|---------|--------|--|
| Frame flange width ( $w_3^{Fr}$ ) [mm]           | 20.0  |         |        |  |
| Frame web height ( $w_3^{Fr}$ ) [mm]             | 81.0  |         |        |  |
| Frame thickness ( $t^{Fr}$ ) [mm]                | 1.0   |         |        |  |
| Cabin floor beams web height [mm]                | 240.0 |         |        |  |
| Cabin floor beams flange width [mm]              | 156.0 |         |        |  |
| Cabin floor beams thickness [mm]                 | 2.5   |         |        |  |
| Cargo floor beams web height [mm]                | 180.0 |         |        |  |
| Cargo floor beams flange width [mm]              | 60.0  |         |        |  |
| Cargo floor beams thickness [mm]                 | 1.5   |         |        |  |
| Struts external diameter [mm]                    | 21.5  |         |        |  |
| Struts internal diameter [mm]                    | 15.5  |         |        |  |
| Component  | Top   | Lateral | Bottom |  |
| Stringer free flanges width ( $w_1^{St}$ ) [mm]  | 5.0   | 5.0     | 21.0   |  |
| Stringer bonded flange width ( $w_3^{St}$ ) [mm] | 40.6  | 24.5    | 31.0   |  |
| Stringer height ( $w_4^{St}$ ) [mm]              | 19.0  | 38.0    | 45.5   |  |
| Stringer thickness ( $t^{St}$ ) [mm]             | 1.1   | 1.0     | 1.4    |  |
| Skin thickness ( $t^{Sk}$ ) [mm]                 | 1.8   | 3.0     | 3.6    |  |
| Skin-panels count ( $n^{Sk}$ ) [-]               | 36    | 24      | 18     |  |

## 2.2. Hypotheses and design criteria

The MS2LOS here presented is framed into the preliminary design phase of aircraft structures. During this phase, tents of load cases (LCs) are assessed to properly design the main components of the structure in order to comply with certification specifications [40]. Such LCs are the result of a combination of basic loading conditions (BLCs) of different nature, e.g. flight loads due to symmetrical manoeuvres, to asymmetrical ones or to gusts, ground loads, pressurisation, etc. In this work, only a sub-set of LCs, presented in Section 2.3, is considered. Moreover, for each LC, the material behaviour is supposed linear elastic and the FE analyses are carried out by assuming small displacements and strains.

Concerning the modelling of the structural components, the following simplifications have been introduced:

1. In agreement with the preliminary design framework, only major components of the structure are modelled (i.e. skin, frames, stringers, floor beams and struts).
2. Floor beams and struts have a predefined geometry which is kept unchanged during optimisation.
3. The elastic response of the laminates is modelled according to the FSDT.
4. Perfect bonding is assumed at the interface of the structural elements and between plies.
5. Connection zones (e.g. floor beams to frames or skin to skin) and opening/cut-out in the skin are not explicitly modelled.

Three main groups of criteria can be identified for the preliminary design phase, i.e. criteria related to: (a) static loads, (b) fatigue loads and (c) aeroelasticity phenomena.

This work focuses only on design criteria related to static loads.

Certification specifications [40] identify two types of static design

loads: *limit loads* (LLs) and *ultimate loads* (ULs). LLs are the maximum loads expected in service that the structure must withstand without detrimental permanent deformations. ULs are equal to limit loads multiplied by a prescribed factor of safety (usually 1.5). The structure must withstand ULs without failure for at least 3 s. For instance, for the wide-body civil aircraft class, LLs in symmetrical manoeuvres occur at load factors (the ratio of the aerodynamic force component normal to the longitudinal axis of the aeroplane to its weight)  $n_g = 2.5$  and  $n_g = -1$ .

The following set of design criteria (DCs) is integrated in the design process.

**DC1** The global stiffness of the structure must be greater than the stiffness of REF.

**DC2** No failure must occur under loads up to ULs.

**DC3** No buckling must occur in the stiffened panels under ULs (no-buckling design approach).

**DC4** Only manufacturable solutions are considered.

**DC5** The laminates composing the structures have a fully orthotropic (membrane and bending) quasi-homogeneous macroscopic behaviour.

DC2 is verified at the laminate-level by means of a suited failure criterion [41] (further details are given in Section 3.2).

### 2.3. Load cases

Five LCs are defined by linear superposition of two BLCs. The two BLCs are: (a) a cruise loading condition (load factor  $n_g = 1$ ) without pressurisation, identified as  $BLC_{lg}$ , and (b) a pressurisation loading condition, identified as  $BLC_p$ . In both BLCs, fuselage sections A and B are modelled as rigid sections and BCs are applied to their centres: section A is always clamped, whilst pertinent tail forces and moments are applied at section B.

Under  $BLC_{lg}$ , payload weight is applied as a distributed load on floor beams. Structural mass is considered by applying additional loads on the upper-deck floor beams, on the basis of statistical estimated structural weight (despite the exact value of the structural weight can be evaluated by applying gravity acceleration in the numerical analysis). Tail loads are computed in such a way to obtain in the check zone (i.e. the middle bay of the fuselage barrel) a maximum bending moment  $M_x = 5.0 \cdot 10^6 \text{ Nm}$  and a maximum vertical shear force  $F_y = -3.7 \cdot 10^5 \text{ N}$ . A good estimation of the loading condition at a different value of the load factor is obtained by scaling  $BLC_{lg}$  by that value.

When using  $BLC_p$ , the effect of the maximum operating differential pressure (corresponding to the maximum relief valve setting) is taken into account as internal pressure on the skin plus an equivalent longitudinal force applied to section B of the fuselage barrel. By scaling  $BLC_p$ , the effect of different values of differential pressure can be assessed.

Data used for defining  $BLC_{lg}$  and  $BLC_p$  are reported in Table 5. The five considered LCs are defined in Table 6 where, for each LC, the related design criterion is also indicated. Aerodynamics loads on the

**Table 5**  
Basic loading conditions data.

| Load  | $BLC_{lg}$         | $BLC_p$          |
|---|--------------------|------------------|
| Upper-deck floor beam total load [N]          | 10000              | –                |
| Lower-deck floor beam total load [N]          | 5000               | –                |
| Bending moment $M_x$ at section “B” [Nm]      | $4.305 \cdot 10^6$ | –                |
| Vertical shear force $F_y$ at section “B” [N] | $-3.1 \cdot 10^5$  | –                |
| Differential pressure [MPa]                   | –                  | 0.068            |
| Longitudinal force $F_z$ [N] <sup>†</sup>     | –                  | $1.7 \cdot 10^6$ |

<sup>†</sup> Equivalent to internal pressure times fuselage cross-section area.

**Table 6**

Load cases definition and associated design criterion.

| LC | $BLC_{lg}$ factor | $BLC_p$ factor | DC  |
|----|-------------------|----------------|-----|
| 1  | 1.00              | 1.00           | DC1 |
| 2  | 3.75              | 1.00           | DC2 |
| 3  | – 1.50            | 1.00           | DC2 |
| 4  | 3.75              | 0              | DC3 |
| 5  | – 1.50            | 0              | DC3 |

fuselage have been neglected.

### 3. The polar analysis of laminates

The fundamentals of the polar analysis of laminates stiffness and strength matrices are provided in this section; for a deeper insight in the matter, the reader is addressed to [23–25,41,42].

Verchery’s polar method [22] allows for expressing any  $n$ -rank plane tensor through a set of tensor invariants. In the context of this work, two types of tensors are relevant: second-rank symmetric plane tensors  $Z_{ij}$  (with  $i, j = 1, 2$ ) and fourth-rank elasticity-like (i.e. having both major and minor symmetries) plane tensors  $L_{ijkl}$  (with  $i, j, k, l = 1, 2$ ). They can be expressed in terms of their polar parameters as:

$$\begin{aligned} Z_{11} &= T + R \cos 2\Phi, \\ Z_{12} &= R \sin 2\Phi, \\ Z_{22} &= T - R \cos 2\Phi, \end{aligned} \quad (1)$$

and

$$\begin{aligned} L_{1111} &= T_0 + 2T_1 + R_0 \cos 4\Phi_0 + 4R_1 \cos 2\Phi_1, \\ L_{1122} &= -T_0 + 2T_1 - R_0 \cos 4\Phi_0, \\ L_{1112} &= R_0 \sin 4\Phi_0 + 2R_1 \sin 2\Phi_1, \\ L_{2222} &= T_0 + 2T_1 + R_0 \cos 4\Phi_0 - 4R_1 \cos 2\Phi_1, \\ L_{2212} &= -R_0 \sin 4\Phi_0 + 2R_1 \sin 2\Phi_1, \\ L_{1212} &= T_0 - R_0 \cos 4\Phi_0. \end{aligned} \quad (2)$$

In Eqs. (1) and (2),  $T$ ,  $T_0$  and  $T_1$  are the isotropic moduli,  $R$ ,  $R_0$  and  $R_1$  are the anisotropic ones, while  $\Phi$ ,  $\Phi_0$  and  $\Phi_1$  are the polar angles. Among them  $T$ ,  $R$  and  $T_0$ ,  $T_1$ ,  $R_0$ ,  $R_1$ ,  $\Phi_0 - \Phi_1$  are tensor invariants, while  $\Phi$  and one of the two polar angles,  $\Phi_0$  or  $\Phi_1$ , can be arbitrarily chosen to set the reference frame, for second and fourth order tensors, respectively.

One of the main advantages provided by the polar formalism is that requirements on elastic symmetries of the tensor can be translated into simple algebraic conditions on the related polar parameters. For example, the ordinary orthotropy of a fourth-rank elasticity-like tensor corresponds to the condition:

$$\Phi_0 - \Phi_1 = K \cdot \pi / 4 \quad \text{with } K = 0, 1. \quad (3)$$

For more details about the elastic symmetries and their expression in terms of polar parameters see [23–25].

#### 3.1. The polar formalism for the laminate stiffness matrices

In the background of the FSDT [43], the constitutive law of a laminate (expressed within its global frame) reads:

$$\begin{Bmatrix} \{N\} \\ \{M\} \\ \{F\} \end{Bmatrix} = \begin{bmatrix} [A] & [B] & 0 \\ [B] & [D] & 0 \\ 0 & 0 & [H] \end{bmatrix} \begin{Bmatrix} \{\epsilon_0\} \\ \{\chi_0\} \\ \{\gamma_0\} \end{Bmatrix}, \quad (4)$$

where  $[A]$ ,  $[B]$  and  $[D]$  are the  $3 \times 3$  membrane, membrane/bending coupling and bending stiffness matrices of the laminate, while  $[H]$  is the  $2 \times 2$  out-of-plane shear stiffness matrix.  $\{N\}$ ,  $\{M\}$  and  $\{F\}$  are the vectors of membrane forces, bending moments and shear forces per unit length, respectively, whilst  $\{\epsilon_0\}$ ,  $\{\chi_0\}$  and  $\{\gamma_0\}$  are the vectors of in-plane strains,

curvatures and out-of-plane shear strains of the laminate middle plane, respectively.

Matrices  $[A]$ ,  $[B]$ ,  $[D]$  and  $[H]$ , can be normalised to have the same units as:

$$[A^*] = \frac{1}{t}[A], \quad [B^*] = \frac{2}{t^2}[B], \quad [D^*] = \frac{12}{t^3}[D], \quad [H^*] = \frac{1}{t}[H]. \quad (5)$$

As deeply discussed in [23,24],  $[A^*]$ ,  $[B^*]$  and  $[D^*]$  behave like tensor  $\mathbf{L}$  of Eq. (2) and  $[H^*]$  behaves like tensor  $\mathbf{Z}$  of Eq. (1), therefore it is possible to express the Cartesian components of these matrices in terms of polar parameters, for an overall number of 21 parameters. It can be proven that, if the in-plane reduced stiffness matrix  $[Q^{\text{in}}]$  and the out-of-plane shear stiffness matrix  $[Q^{\text{out}}]$  of the elementary ply are known, only 12 polar parameters are independent (the relation between matrices  $[A]$ ,  $[B]$ ,  $[D]$  and  $[H]$  and matrices  $[Q^{\text{in}}]$  and  $[Q^{\text{out}}]$  can be found in Appendix A). Moreover, if, according to DC5, the hypothesis of fully orthotropic quasi-homogeneous laminate is introduced, i.e.

$$[A^*] = [D^*], \quad [B^*] = [0], \quad \Phi_0^{A^*} - \Phi_1^{A^*} = K \cdot \pi/4, \quad (6)$$

the overall number of independent polar parameters reduces to only three (because the polar parameters of matrix  $[H]$  depend upon those of matrix  $[A]$ , see [23,24]): the anisotropic polar moduli  $R_{0K}^{A^*} = (-1)^{K \cdot A^*} \cdot R_0^{A^*}$ ,  $R_1^{A^*}$  and the polar angle  $\Phi_1^{A^*}$  (this last representing the orientation of the main orthotropy axis) of matrix  $[A^*]$ . For more details on the polar formalism and its application in the context of the FSDT the reader is addressed to [23,24,42].

### 3.2. The polar formalism for the laminate strength

For the application of DC2, a general laminate-level failure criterion formulated by Catapano and Montemurro [41] is employed. This criterion represents a unified formula including various phenomenological failure criteria. The formulation used in this work is based on the Tsai-Wu (TW) failure criterion [44] that, in matrix notation, reads

$$F_{TW} = \{\sigma\}^T [F] \{\sigma\} + \{\sigma\}^T \{f\} \leq 1, \quad (7)$$

where  $\{\sigma\}$  is the stress vector in Voigt's notation, while  $[F]$  and  $\{f\}$  depend on the lamina strength properties [44].

By introducing the FSDT hypothesis of null out-of-plane stress, by separating the in-plane and out-of-plane contributions and by using the Hooke's law, Eq. (7) can be rewritten in terms of strain, obtaining:

$$F_{TW} = \{\varepsilon^{\text{in}}\}^T [G^{\text{in}}] \{\varepsilon^{\text{in}}\} + \{\varepsilon^{\text{out}}\}^T [G^{\text{out}}] \{\varepsilon^{\text{out}}\} + \{\varepsilon^{\text{in}}\}^T \{g^{\text{in}}\} \leq 1, \quad (8)$$

where  $[G^{\text{in}}]$ ,  $[G^{\text{out}}]$  and  $\{g^{\text{in}}\}$  can be considered as the in-plane, out-of-plane strength matrices and in-plane strength vector of the constitutive ply, respectively. Finally, making use of the FSDT kinematics, one can express Eq. (8) in terms of the laminate middle plane strains

$$F_{TW} = \{\varepsilon_0\}^T [G^{\text{in}}] \{\varepsilon_0\} + z^2 \{\chi_0\}^T [G^{\text{in}}] \{\chi_0\} + 2z \{\varepsilon_0\}^T [G^{\text{in}}] \{\chi_0\} + \dots + \{\gamma_0\}^T [G^{\text{out}}] \{\gamma_0\} + \{\varepsilon_0\}^T \{g^{\text{in}}\} + z \{\chi_0\}^T \{g^{\text{in}}\} \leq 1. \quad (9)$$

The *laminate failure index* is calculated by averaging Eq. (9) through the thickness of the laminate,  $t$ :

$$F_{TW}^{\text{lam}} = \frac{1}{t} \int_t F_{TW}(z) dz \leq 1. \quad (10)$$

Eq. (10) simplifies to:

$$F_{TW}^{\text{lam}} = \frac{1}{t} (\{\varepsilon_0\}^T [G_A] \{\varepsilon_0\} + \{\chi_0\}^T [G_D] \{\chi_0\} + \{\varepsilon_0\}^T [G_B] \{\chi_0\} + \dots + \{\gamma_0\}^T [G_H] \{\gamma_0\} + \{\varepsilon_0\}^T \{g_A\} + \{\chi_0\}^T \{g_D\}) \leq 1. \quad (11)$$

The details of the algebraic manipulations to get Eq. (11) can be found in [41]. Matrices  $[G_A]$ ,  $[G_B]$ ,  $[G_D]$  and  $[G_H]$  and vectors  $\{g_A\}$  and  $\{g_D\}$  represent the laminate strength matrices and vectors. In particular, the four matrices can be seen as the strength counterpart of stiffness matrices  $[A]$ ,  $[B]$ ,  $[D]$  and  $[H]$  in the FSDT framework (the definition of these matrices and vectors is reported in Appendix A). Normalised

strength matrices and vectors can be defined as follows:

$$\begin{aligned} [G_A^*] &= \frac{1}{t} [G_A], & [G_B^*] &= \frac{2}{t^2} [G_B], & [G_D^*] &= \frac{12}{t^3} [G_D], & [G_H^*] &= \frac{1}{t} [G_H], \\ \{g_A^*\} &= \frac{1}{t} \{g_A\}, & \{g_D^*\} &= \frac{2}{t^2} \{g_D\}. \end{aligned} \quad (12)$$

The polar formalism can be applied to these matrices and vectors too.

Catapano and Montemurro showed that, when the strength properties of the constitutive ply (i.e. matrices  $[G^{\text{in}}]$  and  $[G^{\text{out}}]$  and vector  $\{g^{\text{in}}\}$ , and their polar parameters) are known, the laminate strength matrices and vectors can be expressed in terms of the stiffness polar parameters described in Section 3.1. This means that polar parameters describing the laminate stiffness matrices and those describing strength matrices and vectors are not independent. Accordingly, only one of these two sets of polar parameters must be included among the design variables of the problem at hand because the remeaning set can be easily derived by using the formulae provided in [41]. When a fully orthotropic quasi-homogeneous laminate is considered, the overall number of independent polar parameters describing its behaviour (in terms of both stiffness and strength) remains three: the anisotropic polar moduli  $R_{0K}^{A^*}$  and  $R_1^{A^*}$  and the polar angle  $\Phi_1^{A^*}$  of matrix  $[A^*]$  (or matrix  $[D^*]$ ), or, alternatively, the counterpart of matrix  $[G_A^*]$  (or  $[G_D^*]$ ). More details on the polar analysis of laminates strength and on the correlation between laminate strength and stiffness polar parameters can be found in [41].

## 4. Mathematical formulation of the optimisation problem

### 4.1. Design variables

Both mechanical and geometrical design variables are considered in this study. Stringers, frames, and shear ties sections are obtained by folding fully orthotropic quasi-homogeneous laminates. The design variables can be grouped with respect to the component they are referred to.

**Stringers and skin.** Three circumferential sectors are identified as in Fig. 3: “top”, “lateral” and “bottom”. For each sector:

- the stringers cross-section is hat-shaped; four variables,  $w_1^{\text{St}}$ ,  $w_3^{\text{St}}$ ,  $w_4^{\text{St}}$  and  $t^{\text{St}}$ , are needed to describe its geometry (Fig. 4a) and two variables, i.e. the polar parameters  $R_{0K}^{A^*-\text{St}}$  and  $R_1^{A^*-\text{St}}$  are

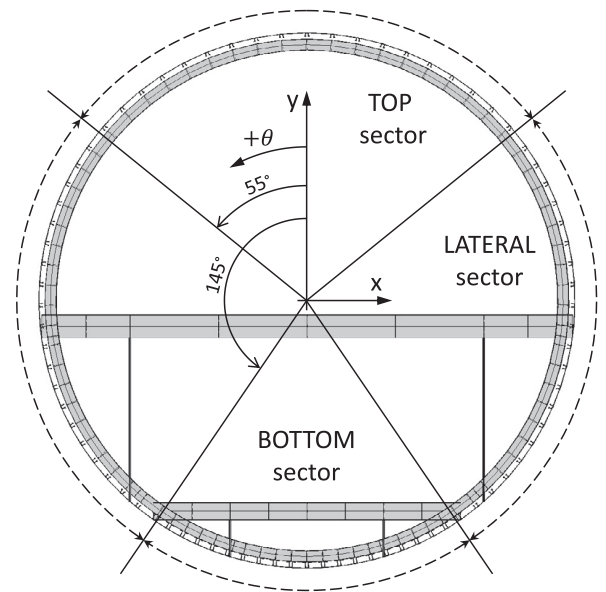


Fig. 3. Fuselage cross-section.



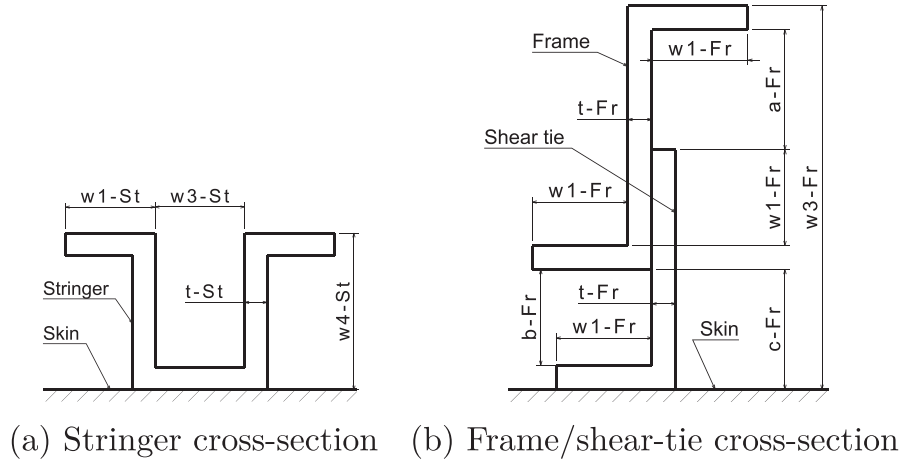


Fig. 4. (a) Stringers and (b) frame/shear-tie assembly cross-sections variables definition.

needed to describe the mechanical properties;

- the skin is characterised by two geometrical variables, i.e. the thickness  $t^{\text{Sk}}$  and the number  $n^{\text{Sk}}$  of sub-regions between two consecutive frames and stringers (hereafter indicated as *skin-panels*) within the sector and two mechanical design variables, i.e. the polar parameters  $R_{0K}^{A^{\text{Sk}}}$  and  $R_1^{A^{\text{Sk}}}$ ;

**Frame/shear-tie assembly.** Identical frames having a “Z”-shaped cross-section with “L” shear-tie are considered: three variables,  $w_1^{\text{Fr}}$ ,  $w_3^{\text{Fr}}$  and  $t^{\text{Fr}}$ , are needed to geometrically describe the assembly (Fig. 4b). The distance between the floating frame and the fuselage skin depends on the maximum height of the stringers cross-sections according to the formula

$$c^{\text{Fr}} = \max_i w_4^{\text{St}-i} + 2\text{mm}, \quad \text{with } i = \text{Top, Lat, Bot.}$$

The frames and the shear-ties are made of identical laminates whose mechanical properties are described by the two polar parameters  $R_{0K}^{A^{\text{Fr}}}$  and  $R_1^{A^{\text{Fr}}}$ , which represent the mechanical design variables.

Regarding the orientation of the main orthotropy axis of the laminates composing the different components (represented by the polar angles  $\Phi_1^{A^{\text{Sk}}-j}$  with  $j = \text{St, Sk, Fr}$ ), it has been set equal to  $0^\circ$  within the local reference system of each laminate, in such a way to align it with the fuselage longitudinal axis for stringers and skin and to follow the hoop direction for the frames.

Of course, the laminates thickness must be a multiple of the elementary ply thickness, thus the number of plies  $n_{\text{ply}}^j = t^j/t_{\text{ply}}$  ( $j = \text{St, Sk, Fr}$ ) is used as a dimensionless design variable.

Finally, the variables  $R_{0K}^{A^{\text{Sk}}-j}$  and  $R_1^{A^{\text{Sk}}-j}$  are replaced by their dimensionless counterpart (denoted as  $\rho_0^j$  and  $\rho_1^j$ ) obtained as follows:

$$\rho_0^j = R_{0K}^{A^{\text{Sk}}-j}/R_0, \quad \rho_1^j = R_1^{A^{\text{Sk}}-j}/R_1, \quad \text{with } j = \text{St, Sk, Fr}, \quad (13)$$

where  $R_0$  and  $R_1$  are the anisotropic moduli of the in-plane reduced stiffness matrix of the elementary ply given in Table 2.

All the aforementioned design variables are collected into the vector  $\xi$ . It is noteworthy that frame pitch, floor beams and struts geometry have not been considered among the problem design variables, rather they have been set equal to the reference values of solution REF, as reported in Tables 1 and 4.

#### 4.2. Objective and constraint functions

The goal of the optimisation is the minimisation of the total mass of the fuselage barrel which reads

$$M(\xi) = V_c(\xi) \cdot \rho_c + M_{\text{Al}}, \quad (14)$$

where  $V_c(\xi)$  is the total volume of the composites constituting the structure,  $\rho_c$  is density of the composite material, as defined in Table 2, and  $M_{\text{Al}}$  is the mass of the aluminium components (i.e. floor beams and struts).

As far as design requirements are concerned, one or more constraint functions are defined for DC1-4, introduced in Section 2.2. DC5 has a direct effect on the choice of the mechanical design variables as explained in Section 3.1.

DC1 is formulated as a couple of constraints on the vertical displacement  $\delta_y$  and on the rotation  $\theta_x$  of the centre of section B when LC1 is considered. These constraints read

$$\begin{aligned} g_1(\xi) &= (\delta_y(\xi) - \delta_y^{\text{REF}})/\delta_y^{\text{REF}} \leq 0, \quad \text{at LC1,} \\ g_2(\xi) &= (\theta_x(\xi) - \theta_x^{\text{REF}})/\theta_x^{\text{REF}} \leq 0, \quad \text{at LC1.} \end{aligned} \quad (15)$$

In Eq. (15),  $\delta_y^{\text{REF}} = -3.85 \text{ mm}$  and  $\theta_x^{\text{REF}} = 0.061^\circ$  are the vertical displacement and rotation of the centre of section B evaluated for solution REF.

DC2 is applied through the evaluation of the maximum laminate failure index  $\langle F_{\text{TW}}^{\text{lam}} \rangle$  of Eq. (11) averaged over the area of each skin-panel ( $\omega_j$ ) belonging to the check zone of each circumferential sector (see Sections 4.1 and 5 for more details) in order to neglect the effect of local stress/strain concentrations that could be strongly affected by the accuracy of the FE model and that constitute the object of the detailed design phase (performed after the preliminary design phase).

Such a value has to be lower than 1, by considering a factor of safety  $F_s = 2$  under both LC2 and LC3. Therefore, the related constraint inequalities are:

$$\begin{aligned} g_3(\xi) &= (F_s \cdot \max_{\Omega_{\text{Top}}} \langle F_{\text{TW}}^{\text{lam}}(\xi) \rangle_{\omega_j}) - 1 \leq 0, \quad \text{at LC2,} \\ g_4(\xi) &= (F_s \cdot \max_{\Omega_{\text{Lat}}} \langle F_{\text{TW}}^{\text{lam}}(\xi) \rangle_{\omega_j}) - 1 \leq 0, \quad \text{at LC2,} \\ g_5(\xi) &= (F_s \cdot \max_{\Omega_{\text{Bot}}} \langle F_{\text{TW}}^{\text{lam}}(\xi) \rangle_{\omega_j}) - 1 \leq 0, \quad \text{at LC2,} \\ g_6(\xi) &= (F_s \cdot \max_{\Omega_{\text{Top}}} \langle F_{\text{TW}}^{\text{lam}}(\xi) \rangle_{\omega_j}) - 1 \leq 0, \quad \text{at LC3,} \\ g_7(\xi) &= (F_s \cdot \max_{\Omega_{\text{Lat}}} \langle F_{\text{TW}}^{\text{lam}}(\xi) \rangle_{\omega_j}) - 1 \leq 0, \quad \text{at LC3,} \\ g_8(\xi) &= (F_s \cdot \max_{\Omega_{\text{Bot}}} \langle F_{\text{TW}}^{\text{lam}}(\xi) \rangle_{\omega_j}) - 1 \leq 0, \quad \text{at LC3.} \end{aligned} \quad (16)$$

In Eq. (16),  $\Omega_i = \sum_{j=1}^{N_i} \omega_j$  with  $i = \text{Top, Lat, Bot}$  represents the  $i$ -th portion of the check zone of the fuselage barrel, whilst  $\omega_j$  is the  $j$ -th skin-panel belonging to this region (more details are given in Section 5).

The requirement DC3 can be opportunely expressed by means of three optimisation constraints. For each circumferential sector, ULs are applied and the most critical stiffened panel (composed of three

stringers and two frames, as discussed in Section 5) in the check zone is identified. An eigenvalue buckling analysis is then performed on this panel. The first buckling eigenvalue has to be higher than 1, by considering a safety factor  $F_s = 1.1$  (more details on this point are given in Section 5). The related constraints read

$$\begin{aligned} g_9(\xi) &= 1.1 - \lambda^{\text{Top}}(\xi) \leq 0, \text{ at LC5,} \\ g_{10}(\xi) &= 1.1 - \lambda^{\text{Lat}}(\xi) \leq 0, \text{ at LC4,} \\ g_{11}(\xi) &= 1.1 - \lambda^{\text{Bot}}(\xi) \leq 0, \text{ at LC4.} \end{aligned} \quad (17)$$

The application of DC4 involves both mechanical and geometrical manufacturability requirements. From a mechanical perspective, the optimum laminates found as result of the first-level problem of the GL-MS2LOS, in terms of polar parameters, must correspond to feasible stacking sequences to be obtained at the end of the second-level problem. According to the formulation proposed by Vannucci in [45], such feasibility conditions, for a quasi-homogeneous orthotropic laminate, can be written only for matrix  $[A^*]$ :

$$\begin{cases} -R_0 \leq R_{0K}^* \leq R_0, \\ 0 \leq R_1^* \leq R_1, \\ 2\left(\frac{R_1^*}{R_1}\right)^2 - 1 - \frac{R_{0K}^*}{R_0} \leq 0. \end{cases} \quad (18)$$

These conditions, in terms of the dimensionless design variables introduced in Eq. (13), read:

$$\begin{cases} -1 \leq \rho_0 \leq 1, \\ 0 \leq \rho_1 \leq 1, \\ 2(\rho_1)^2 - 1 - \rho_0 \leq 0. \end{cases} \quad (19)$$

Naturally, these conditions must be satisfied by the polar parameters describing each laminate composing the structure: the first two conditions of Eq. (19) are directly used for the definition of the lower and upper bounds of the mechanical design variables (Table 7), while the third one is introduced in the problem formulation producing seven constraint inequalities ( $g_{12-18}$ ), one for each laminate.

The manufacturing requirements are applied by imposing a series of inequalities involving the geometrical design variables:

- Minimum thickness of thin-walled elements:

$$n_{\text{ply}}^{\text{St}-i}, n_{\text{ply}}^{\text{Sk}-i}, n_{\text{ply}}^{\text{Fr}} \geq 8, \quad \text{with } i = \text{Top, Lat, Bot.} \quad (20)$$

- Minimum length of the interface flange of stiffening components for the installation of rivets:

$$\begin{aligned} w_3^{\text{St}-i} &\geq 14 \text{ mm, with } i = \text{Top, Lat, Bot,} \\ w_1^{\text{Fr}} &\geq 14 \text{ mm.} \end{aligned} \quad (21)$$

- Minimum length to thickness ratio of thin-walled elements:

$$\begin{aligned} w_1^{\text{St}-i}/t^{\text{St}-i} &\geq 4, \quad \text{with } i = \text{Top, Lat, Bot,} \\ w_3^{\text{St}-i}/t^{\text{St}-i} &\geq 3, \quad \text{with } i = \text{Top, Lat, Bot,} \\ w_4^{\text{St}-i}/t^{\text{St}-i} &\geq 5, \quad \text{with } i = \text{Top, Lat, Bot,} \\ w_1^{\text{Fr}}/t^{\text{Fr}} &\geq 3, \\ a^{\text{Fr}}(\xi)/t^{\text{Fr}} &\geq 3, \\ b^{\text{Fr}}(\xi)/t^{\text{Fr}} &\geq 3. \end{aligned} \quad (22)$$

- Minimum circumferential distance between stringers.

$$\text{pitch}^{\text{St}-i}(\xi) \geq 2 \cdot (2 \cdot w_1^{\text{St}-i} + w_3^{\text{St}-i}), \quad \text{with } i = \text{Top, Lat, Bot.} \quad (23)$$

Some of these inequalities are directly employed in the definition of the lower and upper bounds of the design variables for the problem at hand, as listed in Table 7, whilst the remaining inequalities are stated in the form  $l_j(\xi) \leq 0$  and then aggregated into a single constraint using the maximum operator:

$$g_{19}(\xi) = \max_j l_j(\xi) \leq 0. \quad (24)$$

Finally, the optimisation problem can be formulated as a classical CNLPP as follows:

$$\begin{aligned} \min_{\xi} & M(\xi), \\ \text{subject to:} & \\ g_i(\xi) &\leq 0, \quad \text{with } i = 1, 2, \dots, 19. \end{aligned} \quad (25)$$

The design space of the problem is detailed in Table 7.

#### 4.3. Numerical strategy

**Problem (25)** is a non-convex CNLPP. The total number of design variables is 35, whilst the number of optimisation constraints is 19. For the resolution of problem (25) the GA ERASMUS [26] coupled with both GFEM and LFEMs of the structure has been utilised as optimisation tool to perform the solution search, as illustrated in Fig. 5. The GA ERASMUS has already been successfully applied to solve different kinds of engineering problems, see for example [26,31,32,46–53].

As shown in Fig. 5, for each individual, at each generation, the numerical tool performs global and local FE analyses to calculate the objective function and the optimisation constraints. The FE models are implemented in the ANSYS® environment and their input data are generated by the GA ERASMUS (more details are given in Section 5). The GA elaborates the results provided by the GFEM and the LFEMs in order to execute the genetic operations and generate new individuals. These operations are repeated until the GA meets the user-defined convergence criterion. The generic individual of the GA ERASMUS represents a potential solution for the problem at hand. The genotype of the individual for problem (25) is characterised by only one chromosome composed of 35 genes, each one coding a component of the vector of design variables  $\xi$ .

#### 5. The global/local finite element modelling approach

As stated above, the FE models integrated in the optimisation process are based on a GL modelling approach. In particular, two different models are created: the GFEM for the assessment of the behaviour of the whole fuselage barrel, and refined LFEMs in order to properly evaluate local responses. LFEMs are created only at the critical ZOIs identified

**Table 7**

Lower and upper bounds of the design variables.

| Design variable  | Unit | Lower bound | Upper bound | Step size |
|--|------|-------------|-------------|-----------|
| $w_1^{\text{Fr}}$  | mm   | 16          | 50          | 1         |
| $w_3^{\text{Fr}}$  | mm   | 80          | 160         | 2         |
| $n_{\text{ply}}^{\text{Fr}}$                                   | –    | 8           | 32          | 1         |
| $w_1^{\text{St}-i}$  | mm   | 5           | 30          | 1         |
| $w_3^{\text{St}-i}$  | mm   | 14          | 40          | 1         |
| $w_4^{\text{St}-i}$  | mm   | 14          | 70          | 1         |
| $n_{\text{ply}}^{\text{St}-i}$                                 | –    | 8           | 32          | 1.0       |
| $n_{\text{ply}}^{\text{Sk}-i}$                                 | –    | 8           | 32          | 1.0       |
| $n_{\text{Sk}-\text{Top}}$                                     | –    | 18          | 38          | 2         |
| $n_{\text{Sk}-\text{Lat}}$                                     | –    | 13          | 36          | 1         |
| $n_{\text{Sk}-\text{Bot}}$                                     | –    | 12          | 26          | 2         |
| $\rho_0^{\text{St}-i}/\rho_0^{\text{Sk}-i}/\rho_0^{\text{Fr}}$ | –    | –1          | 1           | *         |
| $\rho_1^{\text{St}-i}/\rho_1^{\text{Sk}-i}/\rho_1^{\text{Fr}}$ | –    | 0           | 1           | *         |

With  $i = \text{Top, Lat, Bot.}$  \* Continuous variable.

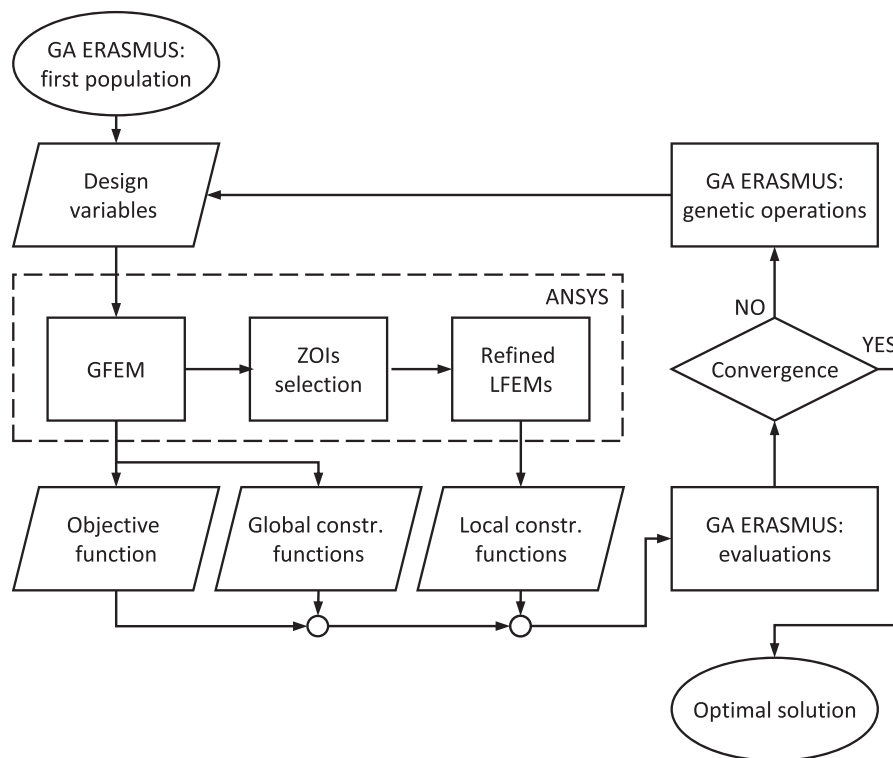


Fig. 5. Flowchart of the optimisation process.

during the global analysis, thus suitable criteria must be developed to accomplish this task.

Both GFEM and LFEMs are fully parametric and are built using the commercial FE code ANSYS®.

### 5.1. The global finite element model

The global FE model is shown in Fig. 6d: it includes seven bays constituting the fuselage barrel. The fuselage skin is modelled with 8-node SHELL281 elements, while frames, stringer, floor beams and struts are modelled with 3-node BEAM189 elements. The beam and shell elements are connected together by node merging. To take into account the actual position of the beam cross-section with respect to the skin, a section offset is applied to beam elements. Shear-tie components are not modelled, but their mechanical effect (the transfer of shear load from the frames to the skin) is ensured by the direct connection between

frame and skin elements.

The element type (linear or quadratic) and mesh size have been chosen after performing a sensitivity analysis. The mesh size is controlled by varying the number of elements along the portions of frames between two consecutive stringers (while the number of elements in the stringer directions is consequently set to the minimum value ensuring a maximum aspect ratio equal to three for the shell elements). The choice is made by looking for a good compromise between computational time and accuracy in the evaluation of the mechanical responses of the structure at both global and local scales (in fact, the mesh size at the global scale affects the BCs of the local scale analyses, as explained in Section 5.2). The details about such a sensitivity analysis are not reported here for the sake of brevity. As a result of this analysis, a total number of elements varying between 6000 and 8000 (depending on the values of the input parameters) have been used for the GFEM.

Material properties are passed to the model in two different ways.

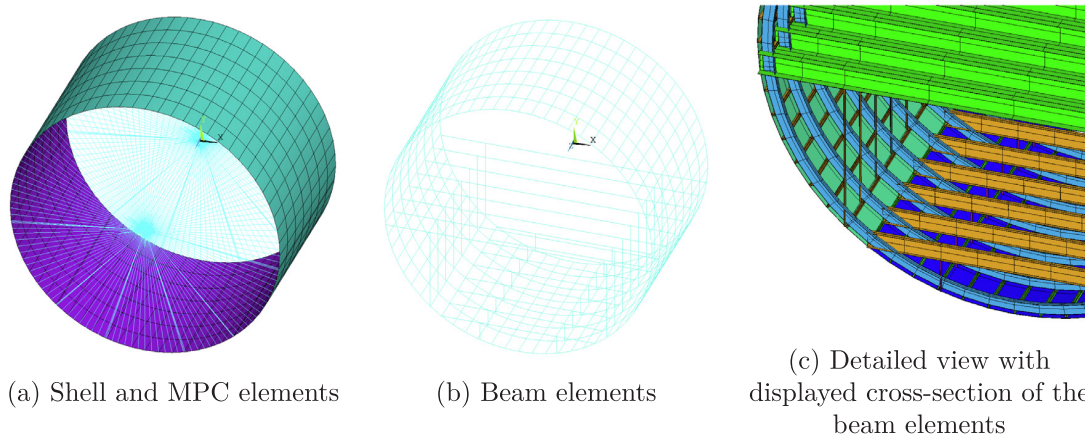


Fig. 6. Global FE model.

For the shell elements, preintegrated stiffness matrices ( $[A]$ ,  $[B]$ ,  $[D]$ ,  $[H]$ ) are obtained from the polar parameters through Eqs. (1) and (2) and passed to the model. For beam elements, custom sections are created: for each laminate, an equivalent homogeneous fictitious orthotropic material is defined (this is possible thanks to the quasi-homogeneity hypothesis) and opportunely oriented in the various sectors of the beam cross-section.

A master node is created at the centre of sections A and B and linked to the set of “slave” nodes of the corresponding frame by means of MPC184 (multi-point constraint) elements with “rigid beam” behaviour (Fig. 6a). These master nodes are used to apply the BCs presented in Section 2.3. In agreement with the hypotheses and the design criteria introduced in Section 2.2, only linear static analyses are performed on this model.

Of course, the first bays (from each side of the fuselage barrel) are strongly influenced by edge effects because of the proximity to zones where BCs are applied (i.e. at nodes A and B). Accordingly, only the central bay constitutes the *check zone*, where the results of the analysis are meaningful. Moreover, as explained in Section 2.2, the elements adjacent to connection zones (e.g. floor beams to frames connections or the joints between circumferential sectors) are excluded from the check zone, as illustrated in Fig. 7.

Results provided by the GFEM are used for the evaluation of the objective function and all the constraint functions except those related to buckling requirements, i.e.  $g_9$ ,  $g_{10}$  and  $g_{11}$ .

### 5.2. The local finite element models

LFEMs are created to evaluate the first buckling load of the most critical stiffened panels. This task can be achieved only through a suitably refined FE model able to catch both global and local buckling modes.

Each LFEM includes the same number of stringers and frames, i.e. three and two, respectively, as shown in Fig. 8. The local model presents a suitable extinction zone to mitigate edge effects due to the application of BCs. This extinction zone is half a skin-panel wide and surrounds the check zone, as illustrated in Fig. 8. The LFEM is entirely built by using 8-node SHELL281 elements with preintegrated shell sections.

Both frames and stringers are tied to the skin by creating constraint equations between their interface nodes. This allows having an independent mesh size on the different components. Also for the LFEM, the mesh size is the result of a compromise between the accuracy in evaluating the first buckling load of the stiffened panel, which can occur either in the skin or in the flanges of stringers and frames, and the computational time. A sensitivity analysis has been conducted also in this case and it is not reported here for the sake of brevity: the local

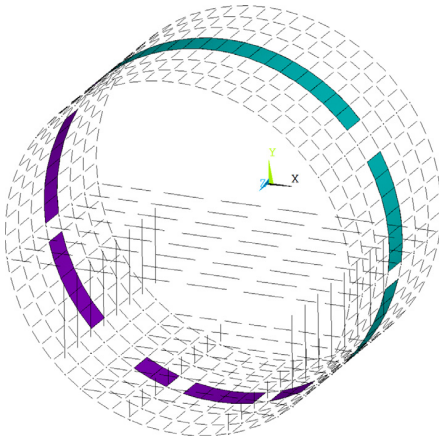


Fig. 7. Check zone of the global FE model.

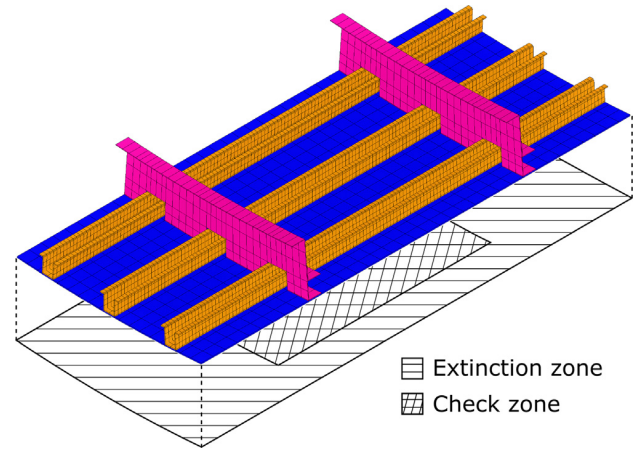


Fig. 8. Typical local FE model.

models have a total number of elements varying from 5000 to 9000 (depending on the values of the input parameters).

Displacement BCs extracted from the results of the global analysis are imposed to all the boundary nodes belonging to the skin of the local FE model.

To transfer the BCs to stringers and frames, for each ending cross-section, a master node is extracted from the skin boundary nodes located at the interface between the beam reference axis and the skin in the GFEM. The coordinates of this set of master nodes are recorded and passed to the LFEM (for each region of the fuselage barrel). Then these nodes are selected and connected to those belonging to the corresponding stringer/frame ending cross-section by means of MPC184 elements with “rigid beam” behaviour, ensuring in this way the kinematic compatibility between global and local models, see Fig. 9.

The LFEM is built for each sector of the fuselage barrel (bottom, top and lateral). An eigenvalue buckling analysis is performed on the local models, and the lowest positive eigenvalue,  $\lambda(\xi)$ , is retrieved as output.

### 5.3. ZOIs identification criteria and information transfer between global and local models

In the presented GL-MS2LOS, the fewest number of local models is checked in order to keep the computational time as low as possible. To this purpose, specific criteria have been introduced and applied to the post-processing of results coming from the GFEM in order to identify the most critical ZOIs around which LFEMs are automatically generated. For each circular sector belonging to the check zone, only one ZOI is identified and analysed.

As discussed in Sections 2.3 and 4.2, the buckling-related constraints are evaluated for LC4 and LC5 (see Table 6). These LCs are obtained by scaling  $BLC_{1g}$  by means of a suitable load factor. Under  $BLC_{1g}$ , the stiffened panels in the top and bottom sectors are mostly subject to stress in the longitudinal direction, as shown in Fig. 10. Therefore, top and bottom ZOIs are identified by looking for the *basic-panel* (BP), i.e. the assembly composed of a stringer plus half of the adjacent skin-panels, that withstands the lowest (compressive, hence negative) average longitudinal force per unit width, i.e.  $N_l^{BP}$ , computed, for the generic LC, as

$$N_l^{BP} = \frac{F^{St} + \int_{-w^{SP}/2}^{w^{SP}/2} \int_0^{f^{Sk}} \sigma_l^{Sk} dz dy}{w^{SP}}, \quad (26)$$

where  $F^{St}$  is the axial tensile force in the stringer,  $w^{SP}$  is the width, in the hoop direction, of the skin panel and  $\sigma_l^{Sk}$  is the longitudinal stress in the skin.

On the other hand, the panels in the lateral sector are subject to biaxial loads corresponding to a combination of shear and longitudinal



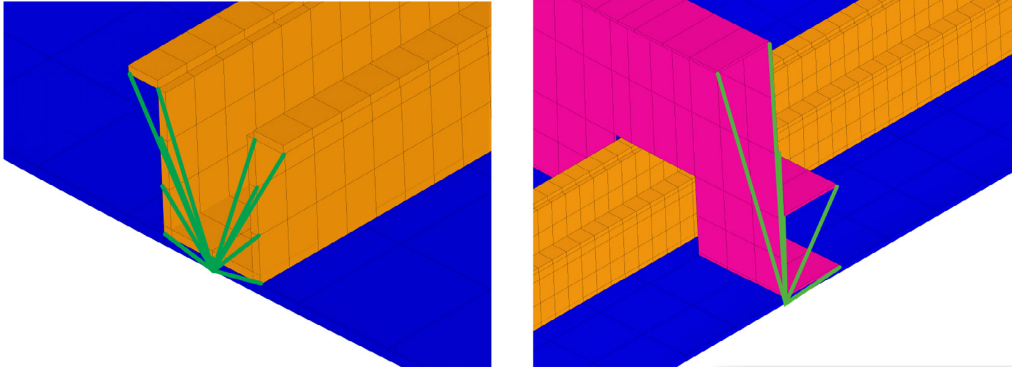


Fig. 9. Detail of the ending cross-section of the stiffening components in the local FE model.

stress; the latter varying from tensile to compression depending on the position of the considered stiffened panel (see Fig. 10). Accordingly, a different criterion is used for the lateral sector: the ZOI is identified by looking for the most critical skin-panel with respect to the buckling strength. An estimation of the buckling load is computed for each skin-panel in the check zone using the analytical formula for a simply supported plate with the same dimensions of the analysed skin-panel, i.e.  $a$  in the longitudinal direction and  $b$  in the hoop one, and subject to the same bi-axial stress field given by the membrane forces per unit width  $N_x$ ,  $N_y$  and  $N_{xy}$ . Under the hypothesis that such a plate buckles with an out-of-plane displacement field described by

$$w(x, y) = a_{mn} \sin \frac{m\pi x}{a} \sin \frac{n\pi y}{b}, \quad (27)$$

the related buckling eigenvalue can be computed as [54]

$$\lambda_b = \pi^2 \frac{D_{xx}(m/a)^4 + 2(D_{xy} + 2D_{ss})(m/a)^2(n/b)^2 + D_{yy}(n/b)^4}{N_x(m/a)^2 + N_y(n/b)^2 + N_{xy}(mn/ab)}, \quad (28)$$

where  $x$  and  $y$  axes correspond to the longitudinal and hoop directions, respectively;  $D_{xx}$ ,  $D_{xy}$ ,  $D_{yy}$  and  $D_{ss}$  are the components of the bending stiffness matrix  $[D]$  of the laminate in Voigt's notation.

The estimation of the first buckling factor for the skin-panel can be finally obtained as

$$\lambda_{cb} = \min_{m,n} (\lambda_b). \quad (29)$$

Therefore, the skin-panel showing the minimum  $\lambda_{cb}$  identifies the lateral ZOI.

As already stated, the displacement field resulting from the GFEM is used to define the BCs for the LFEMs. To this purpose, for each LC, the nodal displacements of the GFEM are interpolated using the shape functions of the elements in the GFEM at the location of the boundary nodes of the LFEM. The logical flow of the process that goes from the global FE analysis to the local one is given in Fig. 11.

## 6. Numerical results

The parameters of the GA ERASMUS used to perform the solution search for problem (25) are listed in Table 8. As far as the optimisation constraints are concerned, they have been handled through the Automatic Dynamic Penalisation (ADP) method [55]. Further details on the optimisation tool and its parameters can be found in [26].

The whole optimisation process requires a computational time of approximately 45 days (i.e. around 70 s for global and local FE analyses for the generic point in the design space) when four cores of a machine with an Intel Xeon E5-2697v2 processor (2.70–3.50 GHz) are dedicated to the ANSYS solver and the two populations are run in parallel. However, computational time could be easily reduced by performing in parallel the FE calculations of the different individuals of the same population. Indeed, since most of the computational time is spent into the FE analyses, and each analysis is independent to the others, the overall optimisation time is inversely proportional to the number of FE analyses performed in parallel.

Three individuals of the last generation of the optimisation are analysed, denoted as S1, S2 and S3 (S1 being the optimum solution).

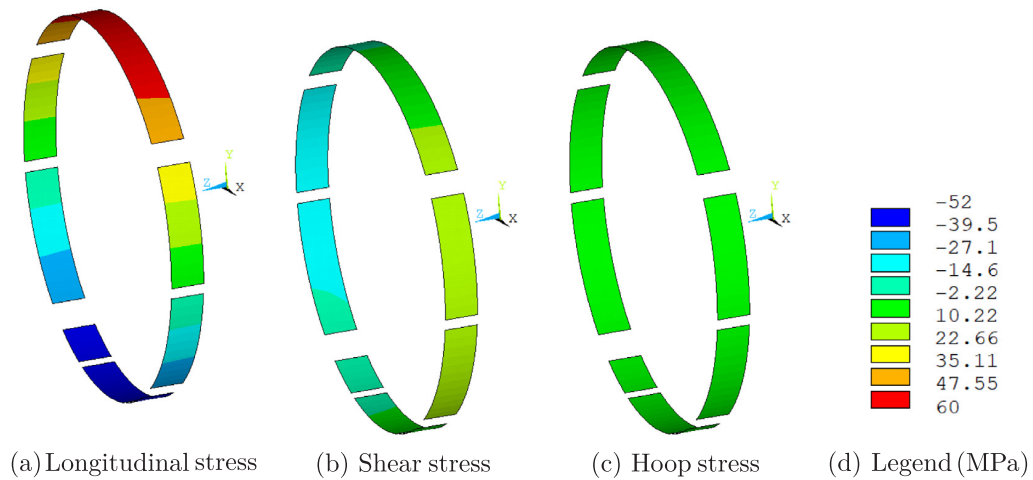


Fig. 10. Stress distribution in the skin-panels in the check zone at BLC1g.

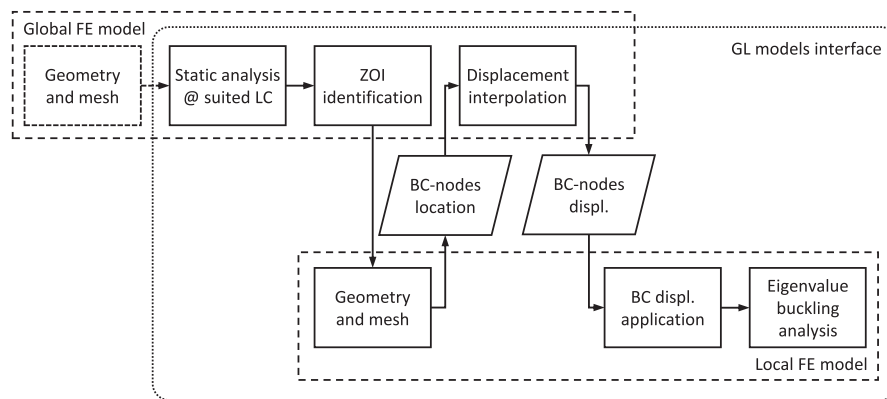


Fig. 11. Interaction scheme between global and local finite element models.

Table 8

Parameters of the GA ERASMUS used for the solution search.

| Property                         | Value                   |
|----------------------------------|-------------------------|
| N. of populations                | 2                       |
| N. of individuals per population | 400                     |
| N. of chromosomes                | 1                       |
| N. of genes                      | 35                      |
| Stop criterion                   | Fixed generations (150) |
| Crossover probability            | 0.85                    |
| Mutation probability             | 0.01                    |
| Selection operator               | Tournament              |
| Fitness pressure                 | 1                       |
| Elitism operator                 | Active                  |
| Isolation time                   | Infinite                |

Table 9

Comparison of the values of the constraint and objective functions relative to different individuals.

| Function                           | S3                     | S2                     | S1*                    |
|------------------------------------|------------------------|------------------------|------------------------|
| $g_1$ (stiffness)                  | -0.039                 | -0.062                 | -0.050                 |
| $g_2$ (stiffness)                  | -0.301                 | -0.244                 | -0.276                 |
| $g_3$ (strength)                   | -0.104                 | -0.108                 | -0.100                 |
| $g_4$ (strength)                   | -0.592                 | -0.614                 | -0.573                 |
| $g_5$ (strength)                   | -0.463                 | -0.479                 | -0.544                 |
| $g_6$ (strength)                   | -0.463                 | -0.452                 | -0.284                 |
| $g_7$ (strength)                   | -0.553                 | -0.551                 | -0.500                 |
| $g_8$ (strength)                   | -0.351                 | -0.371                 | -0.367                 |
| $g_9$ (buckling)                   | -0.303                 | -0.122                 | -0.258                 |
| $g_{10}$ (buckling)                | -0.139                 | -0.128                 | -0.126                 |
| $g_{11}$ (buckling)                | -0.189                 | -0.289                 | -0.410                 |
| $g_{12-18}$ (laminate feasibility) | <0.000                 | <0.000                 | <0.000                 |
| $g_{19}$ (manufacturability)       | <0.000                 | <0.000                 | <0.000                 |
| M[kg]                              | 529(-38%) <sup>†</sup> | 521(-38%) <sup>†</sup> | 506(-40%) <sup>†</sup> |

<sup>†</sup> With respect to  $M^{REF} = 847$  kg.

\* Retained optimal solution

The complete set of performances, in terms of constraint and objective functions, for these individuals, and the associated design variables values, are listed in Tables 9 and 10, respectively. A quick glance to these results suffices to infer that, due to the non-convex nature of problem (25), the GA finds almost equivalent optimal solutions, different in term of design variables, that still respect all the constraints and that have comparable values of the objective function. Moreover, a significant number of pseudo-optimal solutions exists that are nearly identical to solution S1 and that are not reported here for the sake of brevity.

As reported in Table 9, the constraint  $g_1$  (related to the stiffness requirement) clearly reveals the most restrictive one for the three

solutions.

Concerning the retained optimal solution, i.e. S1, from Table 10 one can notice that some of the variables are located at the bounds of the respective intervals, see Table 7. In particular, the number of skin-panels, in the three circumferential sectors are close to their upper bounds. This suggests that an even lighter solution, with closer stringers, may be found by extending the bounds of such variables.

It is noteworthy that the optimal values of the laminate polar parameters of the skin in the three sectors (small values of  $\rho_1$  and bigger negative values of  $\rho_0$ ) describe laminates characterised by an almost perfect *square symmetry* with the main orthotropic axes oriented at  $\pm 45^\circ$  with respect to the fuselage longitudinal axis. On the other hand, the optimum laminates of the frames and of the stringers, have a standard orthotropic behaviour, consequence of the bigger values of  $\rho_1$ , with the main orthotropic axis aligned with the beams longitudinal direction. This can be visualised, for example, by plotting the polar diagram of the first component of matrix  $[A]^*$  for the bottom skin laminate and for the bottom stringer one of solution S1, as shown in Fig. 12. For a deeper insight on these aspects, the reader is addressed to [23,24].

The buckling mode of the identified critical stiffened panel, for each one of the three sectors for solution S1, is illustrated in Fig. 13. It can be noticed that the stringers and the skin buckle simultaneously in the lateral and bottom sector. This is in agreement with the well-established aeronautical design criterion, stating that the maximum structural efficiency (in terms of best compromise between minimum weight and maximum buckling load) for stiffened structures is reached when their components buckle at the same load [56]. This does not occur for the top sectors stiffened panels, where the stringers appear to be oversized, with respect to buckling, and are not involved into the buckling deformation. This last point suggests that a margin of improvement for the optimisation of these components is still possible.

Finally, in Table 9, the mass of solution S1 is compared with the mass of the metallic solution RES (i.e. 847 kg): a weight saving of 40% has been obtained, which can be interpreted as a "numerical proof" of the effectiveness of the GL-MS2LOS. Therefore, the proposed approach allows finding an optimal configuration of the composite fuselage barrel satisfying the full set of design requirements, without introducing simplifying hypotheses into the design strategy at each characteristic scale.

## 7. Conclusions

A multi-scale optimisation strategy, denoted as GL-MS2LOS, for designing composite thin-walled structures has been presented in this work. Such a strategy has been formulated by integrating a dedicated global-local modelling approach into the MS2LOS, allowing in this way a proper optimisation of big composite thin-walled structures, where a

**Table 10**  
Design variables values for optimal individuals at the last generation.

| Variable          | S3     |                    |        | S2     |                    |                     | S1*    |                    |                 |
|-------------------|--------|--------------------|--------|--------|--------------------|---------------------|--------|--------------------|-----------------|
|                   | Top    | Lat.               | Bot.   | Top    | Lat.               | Bot.                | Top    | Lat.               | Bot.            |
| $w_1^{Fr}$ [mm]   |        | 20.0               |        |        | 19.0               |                     |        | 17.0               |                 |
| $w_3^{Fr}$ [mm]   |        | 97.0               |        |        | 86.0               |                     |        | 85.0               |                 |
| $t^{Fr}$ [mm]     |        | 1.125              |        |        | 1.125              |                     |        | 1.000 <sup>†</sup> |                 |
| $\rho_0^{Fr}$ [-] |        | 0.656              |        |        | 0.667              |                     |        | 0.684              |                 |
| $\rho_1^{Fr}$ [-] |        | 0.415              |        |        | 0.459              |                     |        | 0.467              |                 |
| $w_1^{St}$ [mm]   | 10.0   | 6.0                | 15.0   | 12.0   | 7.0                | 14.0                | 13.0   | 6.0                | 12.0            |
| $w_3^{St}$ [mm]   | 39.0   | 39.0               | 38.0   | 39.0   | 40.0 <sup>†</sup>  | 34.0                | 35.0   | 39.0               | 39.0            |
| $w_2^{St}$ [mm]   | 18.0   | 27.0               | 63.0   | 16.0   | 26.0               | 50.0                | 26.0   | 27.0               | 29.0            |
| $t^{St}$ [mm]     | 1.500  | 1.000 <sup>†</sup> | 3.250  | 1.625  | 1.000 <sup>†</sup> | 3.375               | 1.625  | 1.000 <sup>†</sup> | 2.750           |
| $\rho_0^{St}$ [-] | 0.627  | 0.946              | 0.864  | 0.728  | 0.922              | 0.842               | 0.758  | 0.883              | 0.940           |
| $\rho_1^{St}$ [-] | 0.275  | 0.880              | 0.738  | 0.230  | 0.796              | 0.751               | 0.285  | 0.834              | 0.884           |
| $t^{Sk}$ [mm]     | 1.375  | 1.500              | 1.375  | 1.375  | 1.625              | 1.500               | 1.250  | 1.500              | 1.500           |
| $\rho_0^{Sk}$ [-] | -0.952 | -0.757             | -0.936 | -0.957 | -0.816             | -1.000 <sup>†</sup> | -0.940 | -0.898             | -0.867          |
| $\rho_1^{Sk}$ [-] | 0.029  | 0.015              | 0.014  | 0.030  | 0.012              | 0.008               | 0.092  | 0.024              | 0.021           |
| $n^{Sk}$ [-]      | 34     | 32                 | 24     | 32     | 32                 | 22                  | 36     | 36 <sup>†</sup>    | 26 <sup>†</sup> |

<sup>†</sup> Values at the bounds of the design space (see Table 7).

\* Retained optimal solution.

global macroscopic scale and a local macroscopic one can be identified, as those commonly used in the aerospace industry.

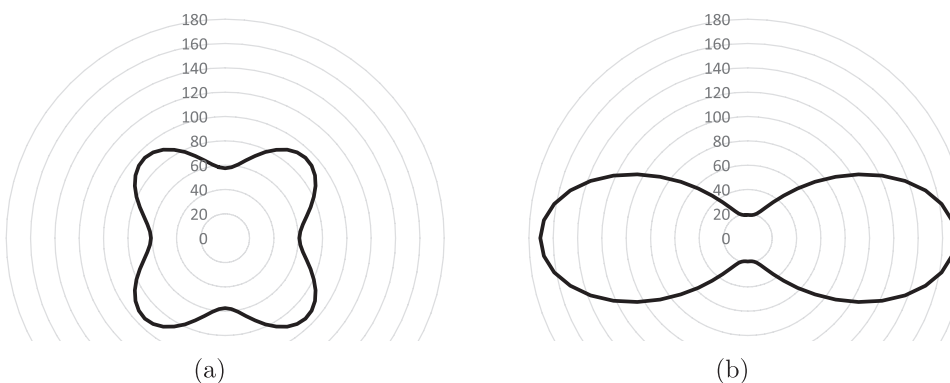
As usual for this type of structures, the design problem is formulated as a CNLPP involving requirements of different nature. In particular, some requirements involve the structure response, at different scales, under various loading conditions. To this purpose, the GL-MS2LOS aims at proposing a very general formulation of the design problem, without introducing simplifying hypotheses and by considering, as design variables, the full set of geometric and mechanical parameters defining the behaviour of the composite structure at each pertinent scale.

In the framework of the MS2LOS, the problem is split into two subsequent optimisation problems. The first-level problem represents the true structural optimisation and focuses on the macroscopic scale (both global and local models are involved). At this scale, the laminates composing the structure are considered as equivalent anisotropic single layers, whose macroscopic behaviour is described in terms of their polar parameters. The optimisation is performed by including both geometrical and macroscopic mechanical variables describing the structure into the problem formulation, without making simplifying hypotheses, neither on the nature of the stacking sequences of the laminates nor on the other design variables. The second-level

optimisation problem, not presented in this paper, is devoted to the retrieval of the laminates stacking sequences corresponding to the set of optimum polar and geometrical parameters found at the first level.

The GL modelling approach is integrated at the first level of the MS2LOS: fully parametric FE models are created at both the global and the local macroscopic scales for the evaluation of the most relevant phenomena. A coherent information transfer between these models is ensured by implementing a sub-modelling GL approach: BCs of the local models are directly extracted, in terms of displacements, from the results of the global analysis and properly transferred to the local FE model. Local FE models are automatically created only for critical ZOIs, which are identified, by means of opportune criteria, during the global analysis. The solution search for the first-level multi-scale CNLPP is performed by interfacing the GFEM and the LFEMs of the structure with the GA ERASMUS, developed at the I2M laboratory in Bordeaux.

By employing a GL modelling approach, most of the limitations of other well-established strategies are overcome; namely more accurate results than those found by means of simplified analytical models (for the assessment of the mechanical response of the structure) can be obtained. Furthermore, the load redistribution due to changes of the variables at the local scale is automatically accounted for. Finally, the



**Fig. 12.** Polar diagram of the first component of matrix  $[A]^*$  in GPa for the laminates of the bottom skin (a) and the bottom stringer (b) for solution S1. The horizontal direction represents the fuselage longitudinal axis.

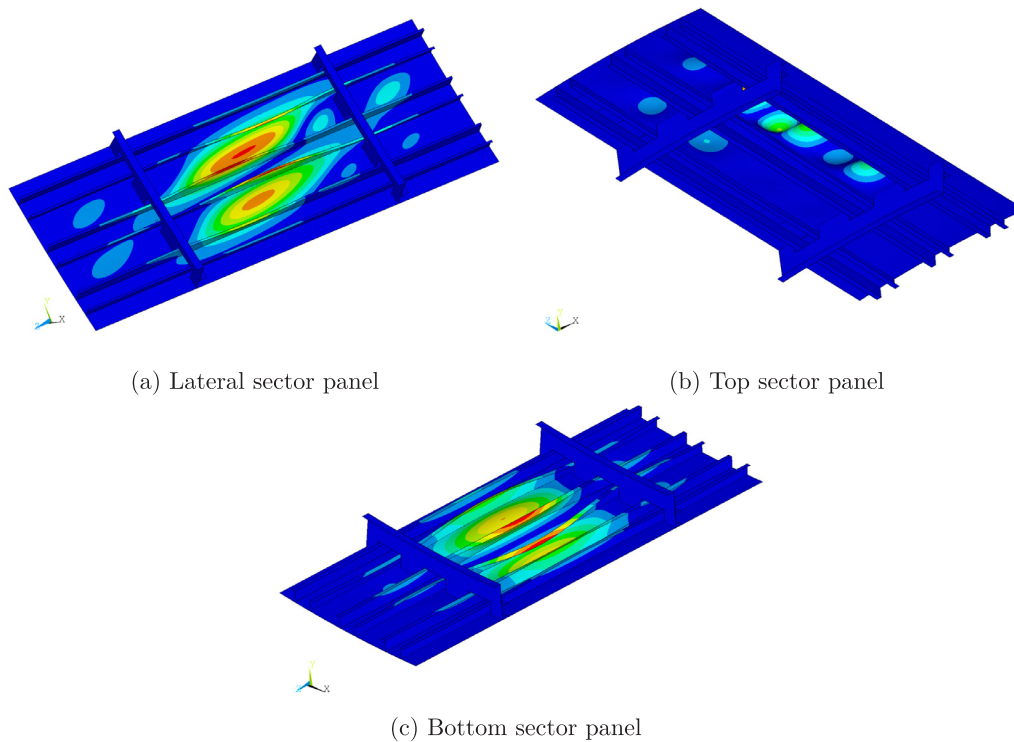


Fig. 13. Normalised displacement field for the first buckling mode of the local models for the optimum solution.

whole process, once set, is fully automated and does not need the user intervention.

The effectiveness of the presented GL-MS2LOS is proven on a meaningful design case: the least-weight design of a composite fuselage barrel of a wide-body aircraft. In the considered test case, a limited, yet representative, set of loading conditions and design criteria is considered. Nevertheless, further criteria and load cases could be easily introduced in the general framework of the presented design strategy.

The obtained optimum composite fuselage is compared to an analogous aluminium configuration (previously optimised by the authors) subject to equivalent design criteria: a weight saving of about 40% is obtained while respecting the full set of design constraints. This result is very promising, even more if considering that the floor beams and the struts have not been included in the design process.

These results encourage research activity in this direction. As far as prospects of this work are concerned, ongoing research is focused on the formulation of post-buckling requirements, on the integration of blending constraints between adjacent skin laminates and on the improvement of the strategy allowing to design composite thin-walled structures made of variable angle tow laminates.

#### Data availability

The raw/processed data required to reproduce these findings cannot

be shared at this time as the data also forms part of an ongoing study.

#### CRediT authorship contribution statement

**Michele Iacopo Izzi:** Software, Investigation, Methodology, Writing - original draft. **Marco Montemurro:** Conceptualization, Methodology, Software, Validation, Writing - original draft, Writing - review & editing, Supervision. **Anita Catapano:** Conceptualization, Methodology, Writing - review & editing, Supervision. **Jérôme Pailhès:** Writing - review & editing, Supervision.

#### Declaration of Competing Interest

The authors declare that they have no known competing financial interests or personal relationships that could have appeared to influence the work reported in this paper.

#### Acknowledgements

This paper presents part of the activities carried out within the research project PARSIFAL (Prandtlplane ARchitecture for the Sustainable Improvement of Future Airplanes), which has been funded by the European Union under the Horizon 2020 Research and Innovation Program (Grant Agreement n.723149).

#### Appendix A. Analytical expression of the laminate strength and stiffness matrices and vectors

According to the generic laminate stacking scheme of Fig. A.1, the analytical expression of the laminate stiffness matrices  $[A]$ ,  $[B]$ ,  $[D]$  and  $[H]$  is given in Eq. (A.1), while that of the laminate strength matrices  $[G_A]$ ,  $[G_B]$ ,  $[G_D]$ ,  $[G_H]$  and vectors  $\{g_A\}$  and  $\{g_B\}$  is provided in Eq. (A.2).

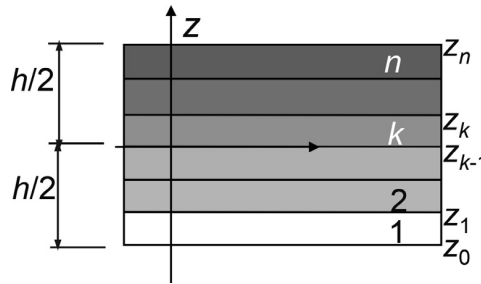


Fig. A.1. Laminate stacking scheme.

$$\begin{aligned}
 [A] &= \sum_{k=1}^n (z_k - z_{k-1})[Q^{\text{in}}(\delta_k)], \quad [B] = \frac{1}{2} \sum_{k=1}^n (z_k^2 - z_{k-1}^2)[Q^{\text{in}}(\delta_k)], \\
 [D] &= \frac{1}{3} \sum_{k=1}^n (z_k^3 - z_{k-1}^3)[Q^{\text{in}}(\delta_k)], \quad [H] = \sum_{k=1}^n (z_k - z_{k-1})[Q^{\text{out}}(\delta_k)],
 \end{aligned} \tag{A.1}$$

$$\begin{aligned}
 [G_A] &= \sum_{k=1}^n (z_k - z_{k-1})[G^{\text{in}}(\delta_k)], \quad [G_B] = \frac{1}{2} \sum_{k=1}^n (z_k^2 - z_{k-1}^2)[G^{\text{in}}(\delta_k)], \\
 [G_D] &= \frac{1}{3} \sum_{k=1}^n (z_k^3 - z_{k-1}^3)[G^{\text{in}}(\delta_k)], \quad [G_H] = \sum_{k=1}^n (z_k - z_{k-1})[G^{\text{out}}(\delta_k)], \\
 \{g_A\} &= \sum_{k=1}^n (z_k - z_{k-1})\{g^{\text{in}}(\delta_k)\}, \quad \{g_D\} = \frac{1}{2} \sum_{k=1}^n (z_k^2 - z_{k-1}^2)\{g^{\text{in}}(\delta_k)\}.
 \end{aligned} \tag{A.2}$$

The expression of the above matrices and vectors in terms of the related polar parameters can be found in [23,24,41].

## Appendix B. Supplementary data

Supplementary data associated with this article can be found, in the online version, at <https://doi.org/10.1016/j.compstruct.2020.111908>.

## References

- Ghiasi H, Pasini D, Lessard L. Optimum stacking sequence design of composite materials Part I: Constant stiffness design. *Compos Struct* 2009;90:1–11.
- Albazzan M, Harik R, Tatting B, Gürdal Z. Efficient design optimization of non-conventional laminated composites using lamination parameters: a state of the art. *Compos Struct* 2019;209:362–74.
- Adali S, Verijenko V, Walker M. Optimal laminate configurations with symmetric lay-ups for maximum postbuckling stiffness. *Compos Eng* 1994;4(11):1119–27.
- Haftka R, Walsh J. Stacking-sequence optimization for buckling of laminated plates by integer programming. *AIAA J* 1992;30(3):814–9.
- Le Riche R, Haftka R. Optimization of laminate stacking sequence for buckling load maximization by genetic algorithm. *AIAA J* 1993;31(5):951–6.
- Aymerich F, Serra M. Optimization of laminate stacking sequence for maximum buckling load using the ant colony optimization (ACO) metaheuristic. *Compos Part A: Appl Sci Manuf* 2008;39(2):262–72.
- Irisarri F, Bassir D, Carrere N, Maire J. Multiobjective stacking sequence optimization for laminated composite structures. *Compos Sci Technol* 2009;69(7–8):983–90.
- Irisarri F, Laurin F, Leroy F, Maire J. Computational strategy for multiobjective optimization of composite stiffened panels. *Compos Struct* 2011;93(3):1158–67.
- Bisagni C, Vescovini R. A fast procedure for the design of composite stiffened panels. *Aeronaut J* 2015;119(1212):185–201.
- U.S. Department of Defense, Military Handbook - MIL-HDBK-17-3F: Composite Materials Handbook, Volume 3 – Polymer Matrix Composites Materials Usage, Design and; 2002.
- Jones R. *Mechanics of composite materials*. McGraw-Hill; 1975.
- Tsai S, Pagano N. Invariant properties of composite materials. Air force materials lab Wright-Patterson AFB Ohio; 1968. Tech. rep.
- Tsai S, Hahn T. *Introduction to composite materials*. Technomic 1980.
- Bloomfield M, Herencia J, Weaver P. Optimisation of anisotropic composite plates incorporating non-conventional ply orientations. In: 49th AIAA/ASME/ASCE/AHS/ASC Structures, Structural Dynamics, and Materials Conference, 16th AIAA/ASME/AHS Adaptive Structures Conference, 10th AIAA Non-Deterministic Approaches Conference, 9th AIAA Gossamer Spacecraft Forum, 4th AIAA Multidisciplinary Design Optimization Specialists Conference; 2008. p. 1918.
- Liu S, Hou Y, Sun X, Zhang Y. A two-step optimization scheme for maximum stiffness design of laminated plates based on lamination parameters. *Compos Struct* 2012;94(12):3529–37.
- Herencia J, Weaver P, Friswell M. Initial sizing optimisation of anisotropic composite panels with T-shaped stiffeners. *Thin-Walled Struct* 2008;46(4):399–412.
- Bramsiepe K, Handojo V, Meddaikar M, Schulze M, Klimmek T. Loads and structural optimisation process for composite long range transport aircraft configuration. Atlanta, Georgia: AIAA Aviation Forum; 2018.
- Vankan WJ, Maas R, Grihon S. Efficient optimisation of large aircraft fuselage structures. *Aeronaut J* 2014;118(1199):31–52.
- Vankan W, Noordman B, Kuere K. High and low fidelity finite element modelling in aircraft composite fuselage structural analysis and optimisation. National Aerospace Laboratory NLR; 2014. Technical report 2013–197.
- Grihon S, Krog L, Bassir D. Numerical Optimization applied to structure sizing at AIRBUS: a multi-step process. *Int J Simul Multi Design Optim* 2009;3(4):432–42.
- Venkataraman S, Haftka R. Structural optimization complexity: what has moore's law done for us? *Struct Multidiscip Optim* 2004;28(6):375–87.
- Verchery G. Les invariants des tenseurs d'ordre 4 du type de l'élasticité, *Proc. of colloque Euromech 115, Villard-de-Lans, (France)*; 1979.
- Montemurro M. An extension of the polar method to the first-order shear deformation theory of laminates. *Compos Struct* 2015;127:328–39.
- Montemurro M. Corrigendum to "an extension of the polar method to the first-order shear deformation theory of laminates" [*Compos. Struct.* 127 328–339]. *Compos Struct* 2015;131(2015):1143–4.
- Montemurro M. The polar analysis of the third-order shear deformation theory of laminates. *Compos Struct* 2015;131:775–89.
- Montemurro M. A contribution to the development of design strategies for the optimisation of lightweight structures. Bordeaux, France: Université de Bordeaux; 2018. (HDR thesis), <http://hdl.handle.net/10985/15155>.
- Montemurro M, Catapano A, Doroszewski D. A multi-scale approach for the simultaneous shape and material optimisation of sandwich panels with cellular core. *Compos Part B* 2016;91:458–72.
- Montemurro M, Catapano A. On the effective integration of manufacturability constraints within the multi-scale methodology for designing variable angle-tow laminates. *Compos Struct* 2017;161:145–59.
- Montemurro M, Pagani A, Fiordilino G, Pailhès J, Carrera E. A general multi-scale two-level optimisation strategy for designing composite stiffened panels. *Compos Struct* 2018;201:968–79.
- Montemurro M, Catapano A. A general B-Spline surfaces theoretical framework for optimisation of variable angle-tow laminates. *Compos Struct* 2019;209:561–78.
- Panettieri E, Montemurro M, Catapano A. Blending constraints for composite laminates in polar parameters space. *Compos Part B: Eng* 2019;168:448–57.
- Montemurro M, Izzi M, El-Yagoubi J, Fanteria D. Least-weight composite plates with unconventional stacking sequences: design, analysis and experiments. *J Compos Mater* 2019;53(16):2209–27.
- Sun C, Mao K. A global-local finite element method suitable for parallel computations. *Comput Struct* 1988;29(2):309–15.

- [34] Mao K, Sun C. A refined global-local finite element analysis method. *Int J Numer Meth Eng* 1991;32(1):29–43.
- [35] Whitcomb J. Iterative global/local finite element analysis. *Comput Struct* 1991;40(4):1027–31.
- [36] Cormier N, Smallwood B, Sinclair G, Meda G. Aggressive submodelling of stress concentrations. *Int J Numer Meth Eng* 1999;46(6):889–909.
- [37] Boni L, Fanteria D. Finite-element-based assessment of analytical methods for the design of fuselage frames. *Proc Inst Mech Eng, Part G: J Aerospace Eng* 2006;220(5):387–98.
- [38] Zhang B, Dai R, Ma W, Wu H, Jiang L, Yan C, Zhang Y. Analysis and design of carbon fibre clamping apparatus for replacement of insulator strings in ultra-high voltage transmission line. *J Eng* 2019;2019(16):2212–5.
- [39] Metallic materials and elements for aerospace vehicle structures MIL-HDBK-5j, Tech. rep., Departement of defence – United States of America; 2003.
- [40] Certification specifications and acceptable means of compliance for large aeroplanes CS-25, Tech. rep., Official Publication of the European Aviation Safety Agency; 2018.
- [41] Catapano A, Montemurro M. On the correlation between stiffness and strength properties of anisotropic laminates. *Mech Adv Mater Struct* 2019;26(8):651–60.
- [42] Vannucci P. Plane anisotropy by the polar method. *Meccanica* 2005;40:437–54.
- [43] Reddy JN. *Mechanics of composite laminated plates and shells: theory and analysis*. Boca Raton, FL: CRC Press; 2003.
- [44] Tsai S, Wu E. A general theory of strength for anisotropic materials. *J Compos Mater* 1971;5(1):58–80.
- [45] Vannucci P. A note on the elastic and geometric bounds for composite laminates. *J Elast* 2013;112:199–215.
- [46] Costa G, Montemurro M, Pailhès J. A general hybrid optimization strategy for curve fitting in the non-uniform rational basis spline framework. *J Optim Theory Appl* 2018;176(1):225–51.
- [47] Bertolino G, Montemurro M, Pasquale GD. Multi-scale shape optimisation of lattice structures: an evolutionary-based approach. *Int J Interactive Des Manuf* 2019;13(4):1565–78.
- [48] Audoux Y, Montemurro M, Pailhes J. A surrogate model based on Non-Uniform Rational B-Splines hypersurfaces, *Procedia CIRP* 70 (2018) 463 – 468, 28th CIRP Design Conference 2018, 23–25 May 2018, Nantes, France.
- [49] Montemurro M, Catapano A. On the effective integration of manufacturability constraints within the multi-scale methodology for designing variable angle-tow laminates. *Compos Struct* 2017;161:145–59.
- [50] Cappelli L, Balokas G, Montemurro M, Dau F, Guillaumat L. Multi-scale identification of the elastic properties variability for composite materials through a hybrid optimisation strategy. *Compos Part B: Eng.* 176. <https://doi.org/10.1016/j.compositesb.2019.107193>.
- [51] Catapano A, Montemurro M, Balcou J-A, Panettieri E. Rapid prototyping of variable angle-tow composites. *Aerotecnica Missili & Spazio* 2019;98(4):257–71.
- [52] Cappelli L, Montemurro M, Dau F, Guillaumat L. Multi-scale identification of the viscoelastic behaviour of composite materials through a non-destructive test. *Mech Mater* 2019;137:103137. <https://doi.org/10.1016/j.mechmat.2019.103137>.
- [53] Montemurro M, Vincenti A, Vannucci P. Design of elastic properties of laminates with minimum number of plies. *Mech Compos Mater* 2012;48:369–90.
- [54] Rao ARM, Arvind N. A scatter search algorithm for stacking sequence optimisation of laminate composites. *Compos Struct* 2005;70(4):383–402.
- [55] Montemurro M, Vincenti A, Vannucci P. The automatic dynamic penalisation method (ADP) for handling constraints with genetic algorithms. *Comput Methods Appl Mech Eng* 2013;256:70–87.
- [56] Gerard G. *Minimum weight analysis of compression structures*. New York University Press; 1956.





# Preliminary structural design of the PrandlePlane aircraft

As explained in Chapter 1, the work presented in this thesis has been carried out in the framework of the WP5 activities of the PARSIFAL project. For the achievement of Objective 3 of such activities, the GL-MSOS and the GL-MS2LOS, respectively presented in Chapters 3 and 5, have been employed for the preliminary structural design of the PrP aircraft proposed in the project. The work presented in those chapters, not only provided a numerical validation of the effectiveness of the proposed design procedure, but also constituted a true preparatory phase, mainly in terms of design problem formulation and FE models development, for the activities presented in this chapter.

The structural design activity in PARSIFAL targets the main structural components of the fuselage and the lifting system of the aircraft, by considering both metallic and composite solutions. This activity is, essentially, the result of synergy between the activities of three of the members of the PARSIFAL team at ENSAM: Michele Iacopo Izzi, Enrico Panettieri and Marco Picchi Scardaoni.

The details of such activity and the complete outcomes of the design process have been reported in two project deliverables (PARSIFAL Project Consortium, 2020b,c), classified as confidential. This chapter only provides the highlights of part of the work, with a focus on the procedural and modelling aspects linked to the peculiarity of the PrP configuration. Moreover, this chapter is conceived to be a complement to Chapters 3 and 5, and, for the sake of brevity, the repetition of concepts already discussed in the aforementioned chapters is limited.

## 6.1 A modular modelling and optimisation approach

Two main challenges had to be faced to perform the structural optimisation of the PrP aircraft. Firstly, the preliminary design of a complex structure like that of an aircraft involves a big number of design variables. For a PrP aircraft such amount is bigger than for a conventional one, because the lifting system of the former is composed of two main wings, plus the lateral vertical surfaces.

Secondly, the PrP architecture characterising the aircraft proposed in PARSIFAL presents an interesting feature: it is *macroscopically* internally hyperstatic, which means that, if equivalent beams are used to represent the fuselage and the lifting system, they are over-constrained to each other. Moreover, the lifting system, which has an annular shape,



constitutes *per se* an over-constrained sub-structure. This characteristic has the main consequence that designing the fuselage and the lifting system as isolated parts does not ensure to obtain a correct design of the entire structure and that, for the correct assessment of the structural responses of the PrP, the whole structure has to be modelled at once.

The computational effort needed for the application of the GL design procedures previously defined, involving a GFEM of the whole aircraft structure and by considering, at once, the complete set of design variables, resulted too big for the IT infrastructure and facilities available at the ENSAM. Consequently, specific adjustments, illustrated in this chapter, had to be introduced in the design procedures.

Following the procedures presented in Chapters 3 and 5, the optimisation has been performed by interfacing the GA ERASMUS with fully-parametric GL FE models. However, the optimisation is performed alternately on two design sub-domains, represented by the two sets of design variables describing the fuselage and the lifting system structures. As illustrated in Fig. 6.1, the PrP aircraft has been divided in six regions: the two main targeted design regions, i.e. the central fuselage barrel and the lifting system (depicted in blue and green, respectively), the front<sup>1</sup> wing-fuselage connection region and the rear<sup>2</sup> one, which also includes the two fins (in red), the nose region and the tail one (in grey). The work-flow of the iterative design procedure is presented in Fig. 6.2. At each iteration,

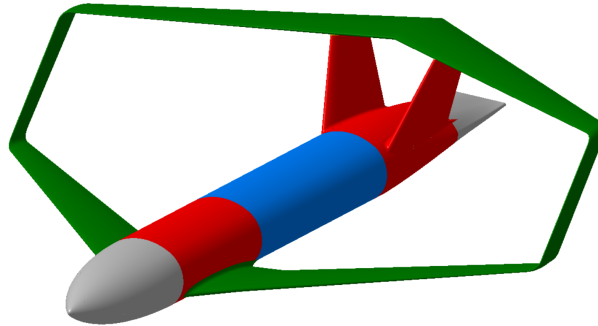


Figure 6.1: Qualitative division of the PrP aircraft structure in modelling regions (PARSIFAL Project Consortium, 2020b).

two optimisation sub-problems are solved in consecutive steps:

1. The fuselage optimisation (FUO) problem.
2. The lifting system optimisation (LSO) problem.

At each step, the suited GL design procedure (the GL-MSOS for the metallic structure, the first-level of the GL-MS2LOS for the CSC one) is employed for the solution of the relative sub-problem. To account for the hyperstatic nature of the PrP architecture, the whole aircraft structure is modelled in the GFEMs generated during the optimisation process. However, in order to limit the computational effort, only the design region interested by the optimisation process (e.g. the central fuselage barrel when solving the FUO problem) is modelled explicitly, whilst the remaining regions of the aircraft are modelled by means of condensed SEs, generated through the sub-structuring technique presented in Chapter 2. The SEs are generated prior to starting a new step of the procedure with the most recent optimal configuration available and kept constant during the step. The iterative procedure

---

<sup>1</sup>Towards the nose of the aircraft.

<sup>2</sup>Towards the aircraft aft.

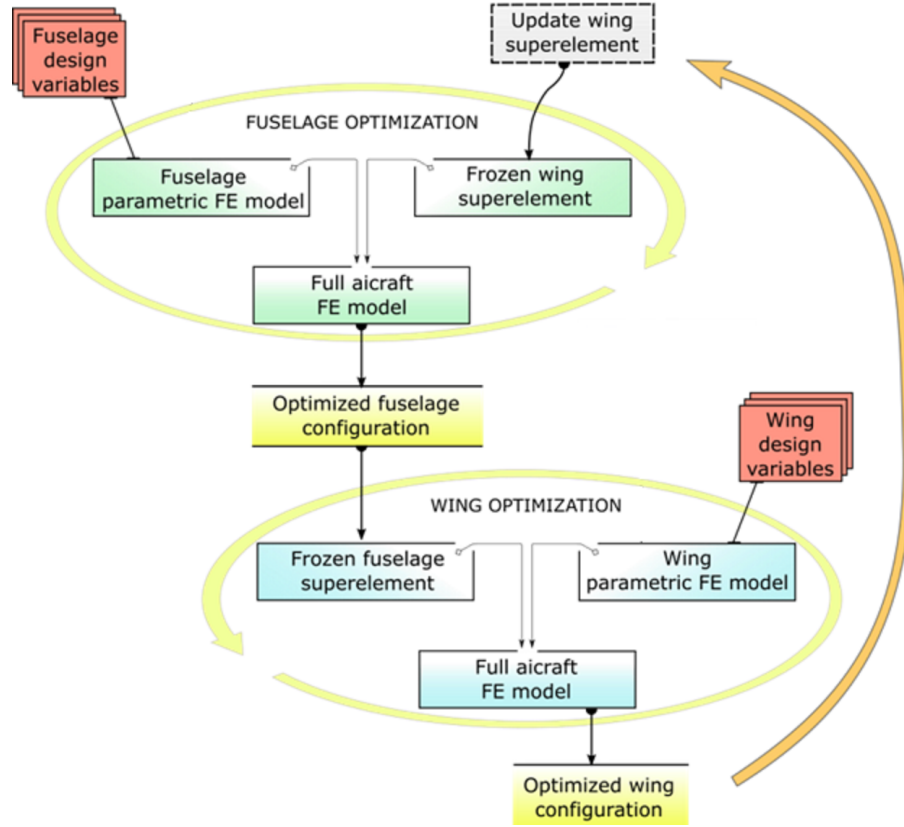


Figure 6.2: Alternated-domain iterative design procedure (PARSIFAL Project Consortium, 2020b).

is stopped when convergence is found between two analogous steps (e.g. the solutions of two consecutive FWO problems show differences that are lower than or equal to a predefined tolerance.)

The development of the FE models of the various regions of the PrP and the main responsibility for the relative optimisation (when relevant) was distributed among the three aforementioned collaborators as follows: M.I. Izzi carried out the multi-scale modelling of the fuselage and the management of the FWO problem; M. Picchi Scardaoni took care of the modelling and optimisation of the lifting system; E. Panettieri was in charge of the modelling of the remaining regions. The two target design regions, i.e. the central fuselage barrel and the lifting system, alternately appear as explicit FE models and as SEs in the GFEM of the aircraft during the optimisation process. The two fuselage-wing connection regions always appear as SEs. They are not directly involved in the optimisation process and their properties are obtained from the adjacent fuselage and lifting system regions. The two terminal regions of the fuselage (i.e. the nose and the tail) are not involved in the optimisation process and are modelled as equivalent concentrated masses. The coordination of the progress of the whole design process was ensured by the supervision role of E. Panettieri.

## 6.2 Least-weight design of the PrandlePlane aircraft structure

Two optimal structural configurations have been obtained performing the least-weight design of the PrandlePlane aircraft: a metallic optimal configuration and a CSC one. Both optimal configurations provide the geometrical properties of the main structural components of the fuselage and the lifting system of the aircraft, as well as the inertial properties of the structure of these regions. The CSC optimal configuration also includes macroscopic elastic properties of the laminates composing the structural components and the corresponding stacking sequences.

The macroscopic geometrical properties of the aircraft and the loading information are the main inputs of the structural design process. They were provided by the project partners working on WP3, firstly, as part of the set of data constituting the initial reference configuration MS1 (resulting from the conceptual design phase carried out by SkyBox and UNIP), and, later, in a refined form obtained through the contributions of all the project partners. The structural design problems (one for each material variant of the structure) have then been formulated through the selection of the design criteria (DCs) and the identification of the design variables.

### 6.2.1 Geometry and materials

Concerning the geometrical information of the aircraft and of the internal volume available for the structural components, they are provided with respect to the reference coordinate system illustrated in Fig. 6.3, whose z-axis is aligned to the fuselage longitudinal axis and passes through the fuselage cross-section geometrical centre.

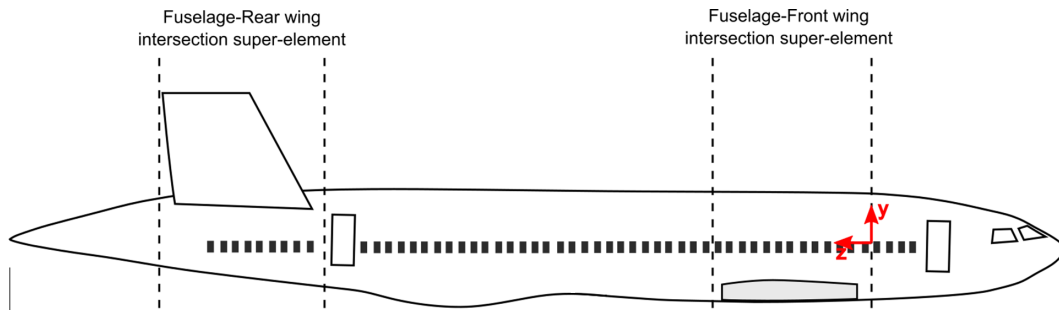


Figure 6.3: Fuselage regions division and positioning of the reference coordinate system (qualitative representation, not in scale) (PARSIFAL Project Consortium, 2020b).

The fuselage has a quasi-elliptical cross-section modelled as a perfect ellipse. The main geometrical parameters describing the cylindrical part of the fuselage are reported in Tab. 6.1. The geometry of the generic stiffened panel composing the fuselage is the one described in Chapters 3 and 5. Referring to Fig. 2 of Chapter 5, it is composed of hat-shaped stringers and floating frames with a Z-shaped cross-section, attached to the skin by means of *shear tie* components; no *stringer tie* or *tear strap* components are present. These components are made of 2024-T3 aluminium alloy in the metallic PrP, whilst they are made of laminates whose elementary lamina is the unidirectional T300/5208 carbon/epoxy prepreg in the CSC PrP. Floor beams with an I-shaped cross-section and tubular struts complete the set of structural components of the fuselage. These last components are made of 2024-T3 aluminium alloy in both the metallic and the CSC

Table 6.1: Main geometrical parameters of the cylindrical fuselage region.

| Component                         | Value |
|-----------------------------------|-------|
| Fuselage external major axis [mm] | 5391  |
| Fuselage external minor axis [mm] | 4166  |
| Upper-deck floor y-position [mm]  | −448  |
| Lower-deck floor y-position [mm]  | −1850 |
| Upper-deck struts x-position [mm] | ±1318 |
| Lower-deck struts x-position [mm] | ±288  |

aircraft variants. Moreover, they have a predefined geometry (reported in Tab. 6.2) which is kept unaltered during the optimisation process. The physical properties of the two

Table 6.2: Geometry of the floor beams and struts.

| Component                                | Value |
|--|-------|
| Upper-deck floor beams web height [mm]   | 240.0 |
| Upper-deck floor beams flange width [mm] | 156.0 |
| Upper-deck floor beams thickness [mm]    | 2.5   |
| Lower-deck floor beams web height [mm]   | 65.0  |
| Lower-deck floor beams flange width [mm] | 60.0  |
| Lower-deck floor beams thickness [mm]    | 1.5   |
| Struts external diameter [mm]            | 21.5  |
| Struts internal diameter [mm]            | 15.5  |

mentioned materials are reported in Tab. 2 and Tab. 3 of Chapter 5.

The external geometry of the lifting system is defined through the complete determination (in terms of shape and positioning) of a set of known cross-sections of the wings composing it (called *front*, *vertical* and *rear* wing) and assuming a linear shape transition between these sections. The geometrical parameters defining such sections, i.e. the coordinates of the leading edge (LE) position, the chord length and the twist angle, are provided in Tab. 6.3, while the position of the wing-box (i.e. the set of structural components) inside the wings is reported in Tab. 6.4. The supercritical aerofoil F15-11 is used (CeRAS; Risse et al., 2016).

Concerning the architecture of the wing-box, the stringers have a square T-shaped cross-section, the spars are composed of a flat web and L-shaped spar caps, and a simplified constant-thickness geometry is considered for the ribs. Shear tie, stringer-tie and tear-strap components are not modelled. For both the front and the rear wing, the ribs are parallel to the free stream direction in the region between the root and kink sections, whilst they are perpendicular to the rear and front spar, respectively, in the region between kink and tip sections (as illustrated in Fig. 6.4). For the vertical wing, the ribs are perpendicular to the spars (which are parallel to each other). In all three wings the stringers are arranged parallel to the rear spar. Further information about the geometry of the lifting system is presented in the article by Picchi Scardaoni et al. (2020a), in which the GL-MSOS is applied to the design of the isolated metallic lifting system. In the metallic variant of the PrP, shell-like components of the lifting system (i.e. the skin, the ribs, and the spar webs) are made of 2024-T3 aluminium alloy (Tab. 3 of Chapter 5), while beam-like ones (i.e. the

Table 6.3: Main geometrical parameters of the lifting system.

| Wing section          | LE coordinates [mm]          | Chord [mm] | Twist [deg] |
|-----------------------|------------------------------|------------|-------------|
| Front root            | ( $\pm 2350, -884, 1082$ )   | 7287       | 3.05        |
| Front kink            | ( $\pm 4661, -684, 3014$ )   | 5350       | 3.90        |
| Front tip             | ( $\pm 17500, -74, 13902$ )  | 1949       | 1.50        |
| Vertical root (front) | ( $\pm 18000, 426, 14705$ )  | 1852       | 1.50        |
| Vertical tip (rear)   | ( $\pm 18000, 6542, 19343$ ) | 1922       | 1.40        |
| Rear root             | ( $0, 7042, 27220$ )         | 5295       | 3.70        |
| Rear kink             | ( $\pm 5400, 7042, 25037$ )  | 4276       | 2.99        |
| Rear root             | ( $\pm 17500, 7042, 20164$ ) | 1991       | 1.40        |

Table 6.4: Position of the wing-box in percentage of the chord length from the LE.

| Wing     | Root sec. | Kink sec. | Tip sec. |
|----------|-----------|-----------|----------|
| Front    | 11 – 57%  | 15 – 70%  | 25 – 75% |
| Vertical | 20 – 80%  | -         | 20 – 77% |
| Rear     | 15 – 70%  | 15 – 70%  | 15 – 70% |

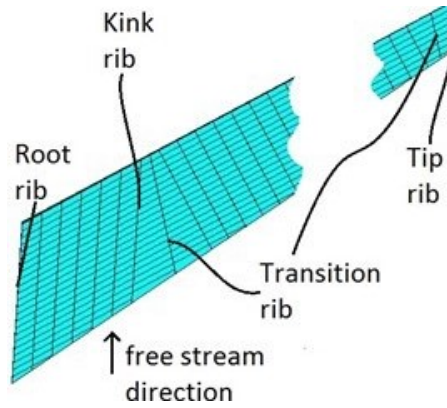


Figure 6.4: Arrangement of stringers and ribs in the front wing (Picchi Scardaoni et al., 2020a).

stringers and the spar caps) are made of 7075 aluminium alloy (whose physical properties are reported in Tab. 6.5). In the composite PrP, all components of the lifting system are made of CSDLs, whose elementary lamina is the aforementioned unidirectional T300/5208 carbon/epoxy prepreg (Tab. 2 of Chapter 5). In both variants of the PrP, the ribs are not optimised and are kept constant in a predefined configuration: either a 4 mm aluminium plate or a  $[(\pm 45^\circ)_{11}]_S$  laminate.

For all considered materials a linear elastic behaviour is assumed.

### 6.2.2 Loads and boundary conditions

During the design process, the mechanical response of the PrP aircraft has been evaluated for a selected<sup>3</sup> set of load cases (LCs). These LCs correspond to various combinations

<sup>3</sup>A sub-set of the usual set considered in the preliminary design phase of a commercial aircraft.

Table 6.5: Material properties of 7075 aluminium alloy (U.S. Departement of Defense, 2003).

| Propriety                     | Value |
|-------------------------------|-------|
| Young's modulus [MPa]         | 71000 |
| Poisson's ratio               | 0.33  |
| Tensile yield stress [MPa]    | 450   |
| Tensile ultimate stress [MPa] | 500   |
| Density [g/cm <sup>3</sup> ]  | 2.81  |

of flight loads due to symmetrical manoeuvres or gusts with different values of the load factor  $n_g$ , and of loads related to cabin pressurisation. All considered LCs are obtained as a linear superposition of two basic loading conditions (BLCs): a cruise loading condition (load factor  $n_g = 1$ ) without pressurisation, identified as BLC<sub>1g</sub>, and a nominal pressurisation loading condition, identified as BLC<sub>p</sub>.

Under BLC<sub>1g</sub>, the aircraft withstands a set of inertial and aerodynamic loads, which are nominally auto-equilibrated. Inertial loads include the payload and both structural and non-structural weight. The upper-deck floor payload has been computed considering the presence of 308 passengers and 11 flight attendants (95 kg per person), and applied as a distributed load on interested floor beams, while lower-deck floor payload has been evaluated by considering the presence of twelve full *LD3-45* containers in the cargo space. The weight of the engines, of the landing gears, and of the whole nose and tail regions is taken into account through concentrated masses (whose values have been provided by the project partners) adequately positioned and linked to the structure. In particular the main landing gear is connected to the central fuselage barrel, while the other masses are connected to the fuselage-wings connection regions. The weight of other cabin non-structural systems is estimated through statistical data (Niu, 1988) and applied as an additional distributed load on the fuselage upper-deck floor beams. The weight of the non-structural masses acting on the front and rear wings (excluding fuel) has been provided by SkyBox and computed according to statistical data (Torenbeek, 1992). It has been applied as a set of point forces and moments at the centroid of the wings ribs. The structural weight is evaluated *on-line* for each considered configuration by means of the employed GFEMs. Aerodynamic loads are derived from the lift distribution, provided by UNIPi, corresponding to the cruise of the MS1 aircraft configuration at a Mach number of 0.79 and an altitude of 11 km under maximum zero-fuel weight (MZFW) condition. Such distribution is converted into a statically equivalent system of forces and moments applied on the wings ribs. Finally, such system is conveniently scaled, during the GFEMs analysis, in order to equilibrate the changing inertial loads. Aerodynamics loads on the fuselage have been neglected. Flight loads corresponding to symmetrical manoeuvres with values of the load factor other than one are approximated by scaling BLC<sub>1g</sub> by that value.

In BLC<sub>p</sub>, the effect of the maximum operating differential pressure (corresponding to the maximum relief valve setting) is taken into account as internal pressure on the fuselage.

Symmetric BCs are applied on the aircraft longitudinal plane (plane y-z in Fig. 6.3), and two points belonging to the longitudinal fuselage axis and located inside the two fuselage-wing connection regions are constrained in order to avoid rigid motion of the aircraft, as illustrated in Fig. 6.5.

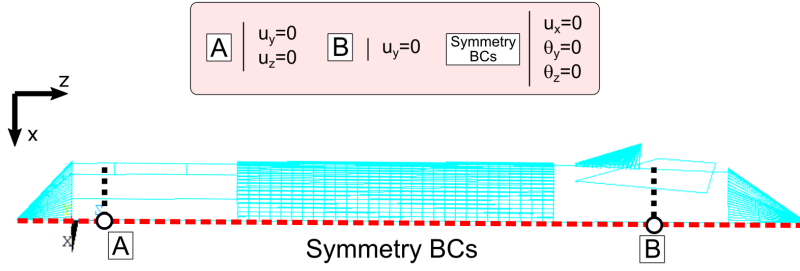


Figure 6.5: Boundary conditions applied on the aircraft. Fuselage nose on left-hand side. (PARSIFAL Project Consortium, 2020b).

### 6.2.3 Design criteria and variables

The optimisation problems of the metallic and the composite versions of the PrP aircraft are characterised by two analogous, yet different sets of DCs and variables.

#### Metallic PrandlePlane aircraft

The following set of DCs is considered in the design process of the metallic PrP aircraft:

**M-DC1** The structure must have a minimum stiffness.

**M-DC2** The average equivalent stress in the fuselage skin and lifting system skin, stringers and spars must not exceed the yielding strength of the material, considering a factor of safety  $F_S = 1.5$ , under LLs.

**M-DC3** The average equivalent stress in the fuselage skin and lifting system skin, stringers and spars must not exceed the ultimate strength of the material under ULs.

**M-DC4** No buckling must occur in the stiffened panels under ULs (no buckling design approach) with a factor of safety  $F_S = 1.1$ .

**M-DC5** No critical fatigue failure must occur:

- in the fuselage skin, caused by the cycling hoop stress due to pressurisation;
- in the wing skin, when a suitable ground-air-ground load spectrum is applied.

**M-DC6** Only manufacturable solutions are considered.

M-DC1 is expressed in terms of maximum tip displacement of the lifting system in the flight envelope, which should not exceed 15% of the wingspan. M-DC2 and M-DC3 are expressed in terms of average equivalent stress in order to neglect the effect of local stress concentrations that is strongly affected by the accuracy of the FE model and that constitute the object of the detailed design phase (performed after the preliminary design phase). M-DC4 is expressed in terms of no-buckling condition for the most critical stiffened panels identified into the central fuselage barrel and the lifting system by means of suitable criteria. Such an evaluation is done through refined LFEMs. M-DC5 is a criterion against the nucleation of cracks in the longitudinal joints between the fuselage stiffened panels and at rivets locations in the lifting systems. It is translated into an equivalent static check according to the method explained in Sec. 2.1 of Chapter 3. The load spectrum provided by Rustenburg et al. (2002) is employed for the assessment of such check on the lifting

system. M-DC6 is expressed as various requirements on the minimum thickness of thin-walled elements, on the minimum length of the interface flanges of stiffening components for rivets installation, on the minimum length to thickness ratios of sheet elements, and on the minimum distance between consecutive stringers.

The design variables involved in the design process of the metallic PrP aircraft are all geometrical and correspond to the parameters needed to completely describe the geometry of structural components of the fuselage and of the lifting system.

Concerning the fuselage, the skin thickness, the frames geometry, and the stringers geometry and spacing are optimised. Only one frame geometry is used for the whole fuselage barrel, and the frames spacing is not a design variable. Three circumferential sectors are identified on the fuselage barrel: i.e. *top*, *lateral* and *bottom* sectors (Fig. 6.6). Each sector is characterised by a different set of skin and stringers properties.

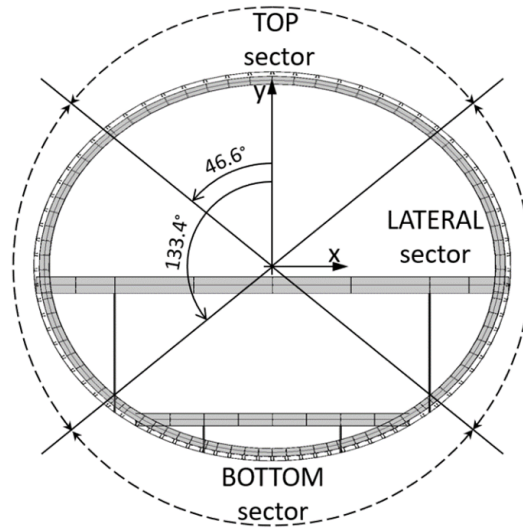


Figure 6.6: Fuselage division in circumferential sectors.

Concerning the lifting system, the skin thickness, the stringers geometry and spacing, the spars geometry, and the ribs spacing are optimised. All components are different in the front and rear wing, while the skin and the stringers are also different in upper and lower side of each wing. The geometrical parameters of the spars are not independent, rather they are linked to those of the adjacent skin and stringers. The geometry of the structural components of the vertical wings are linked to those of the two main wings. All parameters linearly vary along the wingspan: consequently, four *scaling parameters* are also included among the design variables.

### Composite PrandlePlane aircraft

The following set of DCs is integrated in the design process of the composite PrP aircraft:

**C-DC1** The structure must have a minimum stiffness.

**C-DC2** No failure must occur under loads up to ULs.

**C-DC3** No buckling must occur in the stiffened panels under ULs (no buckling design approach) with a factor of safety  $F_S = 1.1$ .



**C-DC4** Only manufacturable solutions are considered.

**C-DC5** The laminates composing the structures have a fully-orthotropic (membrane and bending), uncoupled and homogeneous macroscopic elastic behaviour.

C-DC1, is expressed as the analogous DC for the metallic PrP aircraft. C-DC2 is verified at the laminate-level by means of the laminate failure index of Eq. (11) of Chapter 5. As explained in Chapters 5 and 7, such quantity can be specialised for various phenomenological failure criteria. The formulation based on the Tsai-Wu failure criterion is used in the formulation of the FUO problem, whereas the Tsai-Hill formulation is used in that of the LSO problem. Moreover, the evaluation of the laminate failure index is not performed point-wise on the laminates, rather it is averaged over portions of the skin in order to neglect the effects of local stress concentrations that could arise because of the limited accuracy of the FE models employed in the preliminary design phase. C-DC3 is expressed as M-DC4. C-DC4 is expressed through the formulation of a set of geometrical constraints (as seen for M-DC6) and the enforcement, at the first-level of the GL-MS2LOS, of the feasibility conditions on the existence of suitable stacks (Eq. (18) of Chapter 5). Moreover, only for the lifting system, blended skins are considered. For two adjacent panels, the continuity of ply orientations, when passing from the thinner to the thicker laminate, must be ensured, as shown qualitatively in Fig. 6.7. Consequently, the blending constraints formulated by Picchi Scardaoni et al. (2020b) in the PPs space are also included in the LSO problem formulation.

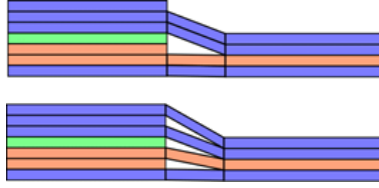


Figure 6.7: Two possible blended arrangements for two adjacent panels.

The set of structural components optimised in the design process of the metallic PrP is considered made of CSC laminates in the composite version of the aircraft. Therefore, in agreement with the adoption of the GL-MS2LOS, also mechanical design variables are considered, in addition to the geometrical ones, in the first-level phase (i.e. at the macroscopic scale, where the structural design is performed) of the design process of the CSC version of the PrP aircraft. Under the requirements corresponding to C-DC4, three PPs are needed for the description of the macroscopic mechanical behaviour of each laminate constituting the structural components (see Sec. 3.1 of Chapter 5):  $R_{0K}^{A*}$ ,  $R_1^{A*}$  and  $\Phi_1^{A*}$ . The first two of them have been considered as additional design variables (an independent set for each laminate) in the optimisation process, whilst the last one has been manually defined, for each laminate, in order to set the direction main orthotropy axis of the laminates. For the laminates composing beam-like components, this direction has been set aligned with the longitudinal axis of the component itself, while it has been aligned to the fuselage longitudinal direction for the fuselage skin, and to the stringers direction for the skin and the spars of the wings. The same three-sector division presented above is employed for the identification of fuselage design variables. Concerning the lifting system, the usual front-rear wing division is maintained, while the linear span-wise variation of the parameters has been replaced by the identification of three sectors for the front wing and two sectors for the rear one, as illustrated in Fig. 6.8.

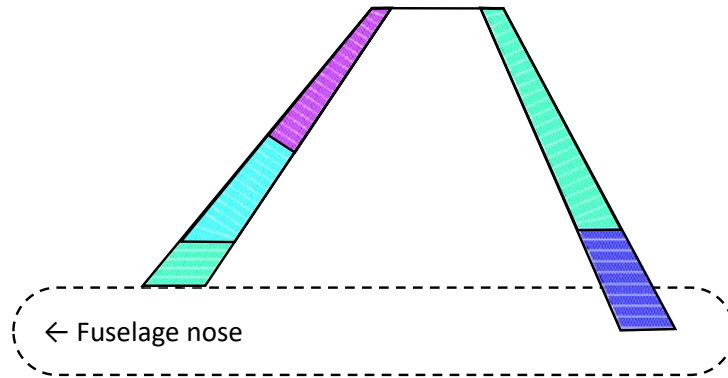


Figure 6.8: Wing division in span-wise sectors.

### 6.3 Finite element modelling of the PrandlePlane structure

As anticipated in Sec. 6.1, various approaches have been used for the modelling of the different regions of the PrP aircraft.

Concerning the two target regions of the optimisation process, i.e. the central fuselage barrel and the lifting system, the GL FE modelling approach described in Sec. 3 of Chapter 5 has been employed. The GFEM and LFEMs employed for the assessment of the mechanical response of the PrP fuselage have the same characteristics of those presented in Chapter 5. Indeed, the same set of fully-parametric ANSYS APDL codes, called ELliptical Fuselage PArametric Models (ELF-PAM) and able to generate the FE models of an any-length single-deck fuselage barrel with an elliptical cross-section and of any of the stiffened panels constituting it, has been employed in the two cases. It must be recalled that, in the fuselage GFEM, the skin is modelled using 8-node quadratic shell elements (ANSYS Shell281), while 3-node quadratic beam elements (ANSYS Beam189) are used for all other components (see Fig. 6 of Chapter 5). For the modelling of the composite structure, preintegrated shell sections are used for the skin, while for the beam elements, custom beam cross-sections are created: for each laminate, an equivalent homogeneous fictitious orthotropic material is defined (this is possible thanks to the quasi-homogeneity hypothesis) and opportunely oriented in the various sectors of the beam cross-section. The presence of the special outboard main landing gear (Nuti et al., 2018) has been taken into account as point masses rigidly linked to a portion of the frames, as shown in Fig. 6.9. The LFEM is entirely built by using 8-node quadratic shell elements with preintegrated shell sections. Each refined LFEM, employed for the assessment of the buckling requirement, includes the same number of stringers and frames, i.e. three and two, respectively, as shown in Fig. 8 of Chapter 5.

Similar modelling choices have been taken for the lifting system. However, in the lifting system GFEM, the stringers and the spar caps are modelled as rod elements (ANSYS Link180) and 4-nodes linear elements (ANSYS Shell181) have been used for the skin and the spars web. The refined LFEMs of the stiffened panels of the lifting system are 1-bay long and 5-stringer wide (Fig. 6.10) and only contain skin and stringers components, both modelled through 4-node shell elements (ANSYS Shell181). More details about the FE modelling of the lifting system can be found in the aforementioned article by Picchi Scardaoni et al. (2020a).

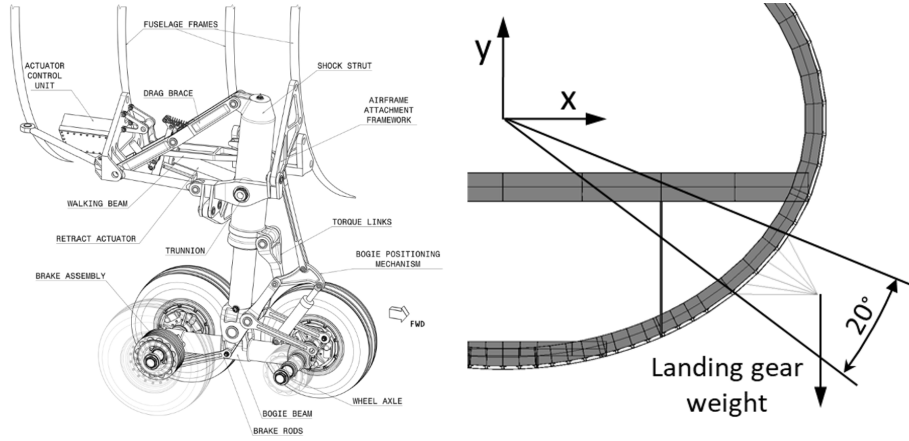


Figure 6.9: Main landing gear design (Nuti et al., 2018) and relative modelling in the fuselage GFEM.

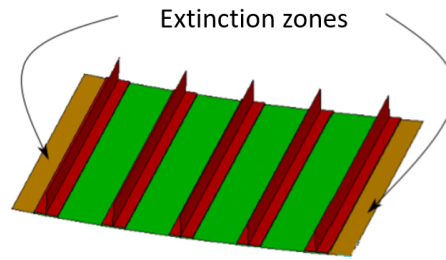


Figure 6.10: Representative LFEM of the lifting system region. (Picchi Scardaoni et al., 2020a).

Concerning the two fuselage-wing connection regions, simplified explicit FE models have been employed for the generation of the SEs. These models, shown in Figs. 6.11 and 6.12, are only composed of shell elements. The thickness of such elements accounts for the presence, in the real structure, of stringers, frames, floor beams and struts (*smeared* on the shells surface) and is updated at the end of each optimisation step using the optimised properties of the adjacent fuselage and lifting system regions. The SEs of the two fuselage-wing connection regions have been created only in the metallic version: for the design of the composite PrP aircraft, the last (*optimised*) metallic versions of these SEs have been employed for all the steps of the process.

The GFEMs of the whole aircraft used during the steps of the optimisation process are obtained by assembling the explicit GFEM of the interested region, either the central fuselage region or the lifting system one, and the SEs of the remaining regions, as shown in Fig. 6.13. A rigid connection is established between the models of the various regions by means of multi-point constraint (MPC) elements. Such elements are also used to fix the aforementioned point masses (representing the landing gears, the engines, and the tail and nose regions) and the two nodes used for the application of BCs to suited regions of the adjacent FE models.

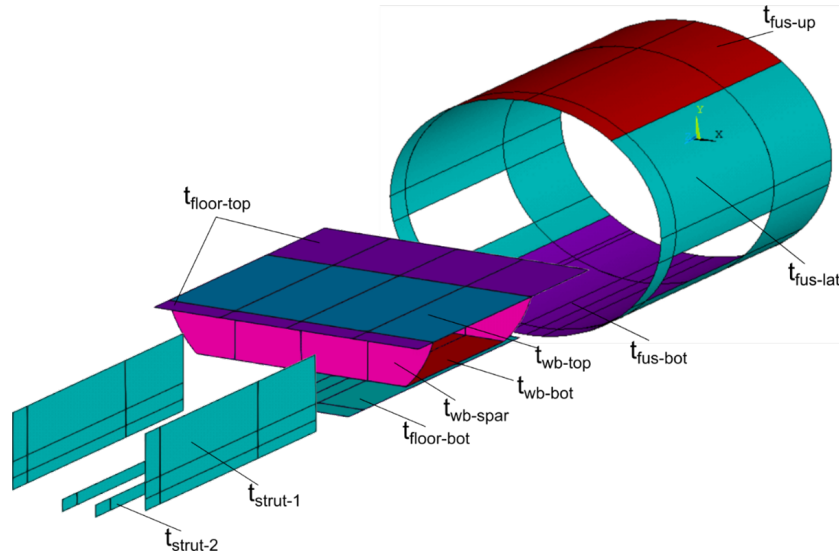


Figure 6.11: Exploded view of the FE model used for the generation of the SE of the front fuselage-wing connection region (PARSIFAL Project Consortium, 2020b).

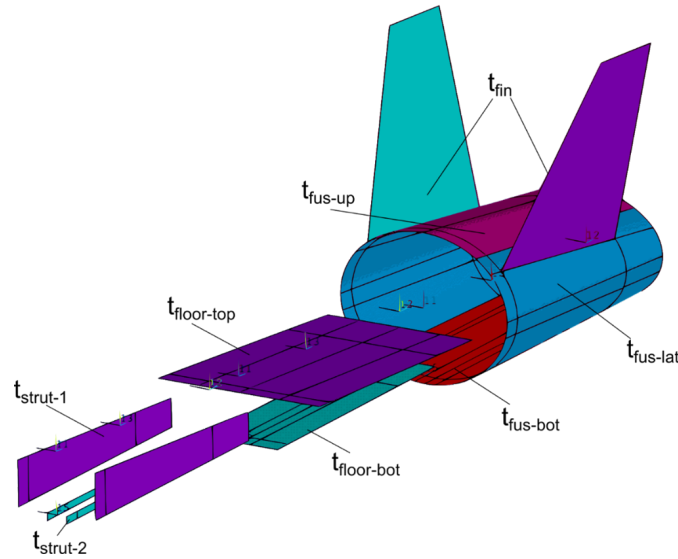


Figure 6.12: Exploded view of the FE model used for the generation of the SE of the rear fuselage-wing connection region (PARSIFAL Project Consortium, 2020b).

## 6.4 Results

A total amount of 41 and 85 design variables has been optimised for the metallic and the composite (recall that only the first-level problem of the GL-MS2LOS has been solved for the composite solution) versions of the PrP aircraft, respectively. The GA ERASMUS, interfaced with the commercial FE software ANSYS, as illustrated in Fig. 5 of Chapter 5, has been employed as optimisation tool for the solution of both the FUO and LSO problem. Two iterations of the alternated-domain design procedure of Fig. 6.2 revealed sufficient to achieve a good convergence.

The results consist of the whole set of geometrical and mechanical parameters needed

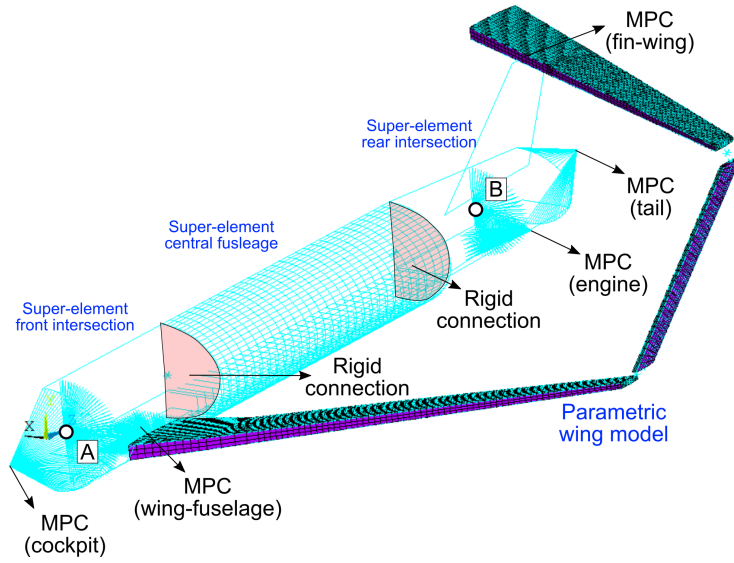


Figure 6.13: GFEM of the whole aircraft used during the LSO step (PARSIFAL Project Consortium, 2020b).

for the description of the optimised structural components. However, only a small part of these results is provided in this thesis and only in a qualitative form, due to confidentiality issues.

In Tab. 6.6, the composite solution and the metallic one are compared in terms of relative difference of the weight of their two design regions. The composite solution is characterised by a weight reduction of about 36% and 14% with respect to the optimal metallic configuration, for the main structural components of the central fuselage region and of the lifting system, respectively. The weight reduction obtained for the PrP fuselage region is coherent with that obtained in Chapter 3, where a reference fuselage barrel is considered. The breakdown of the relative weight difference for the various design sub-regions of the central fuselage region (i.e. the groups of structural components sharing the same properties) is also provided in Tab. 6.6. As it can be inferred from this data, most of the weight saving is obtained on the fuselage skin and frames, whose weakening is compensated by a strengthening of the stringers.

Table 6.6: Relative weight difference between the composite solution and the metallic one.

| Design region/sub-region | Relative weight difference |
|--------------------------|----------------------------|
| Central fuselage         | −36%                       |
| Top skin                 | −70%                       |
| Top stringers            | +25%                       |
| Lat. skin                | −52%                       |
| Lat. stringers           | −1%                        |
| Bot. skin                | −34%                       |
| Bot. stringers           | +52%                       |
| Frames                   | −60%                       |
| Lifting system           | −14%                       |

Fig. 6.14 shows the deformation of the lifting system during a pull-up manoeuvre, while the deformation of the central fuselage region under the two considered BLCs is reported in Fig. 6.15. In the latter, the effect of the presence of a double connection between fuselage and lifting system is visible in the unusual deformation of the fuselage barrel under  $BLC_{1g}$ . Finally, as an example, the first buckling modes of the critical top-sector panels of the optimal metallic fuselage and of the optimal composite one are shown in Fig. 6.16, which also highlights the different stringers spacing in the two solutions (recall that the frame spacing is the same between the two solutions).

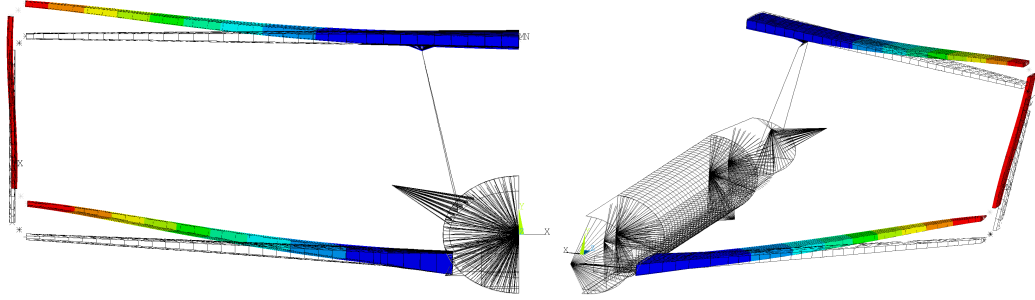
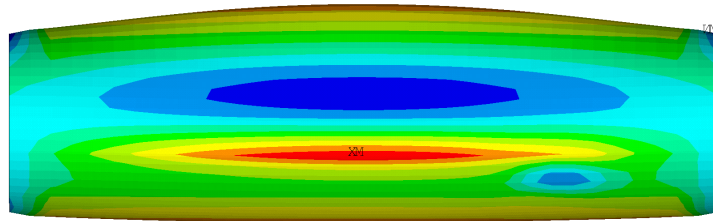
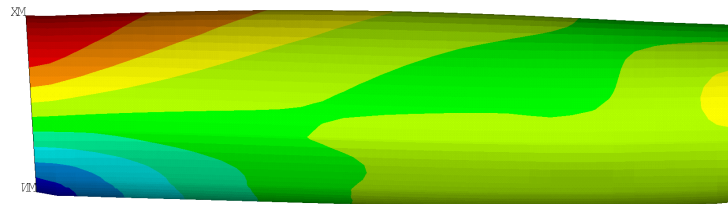


Figure 6.14: Contour plot of the vertical displacement of the lifting system during a pull-up manoeuvre.



(a) Contour plot of the hoop stress in skin under  $BLC_p$



(b) Contour plot of the longitudinal stress in skin under  $BLC_{1g}$

Figure 6.15: Deformed shape of the metallic central fuselage barrel. Fuselage nose on the left-hand side.

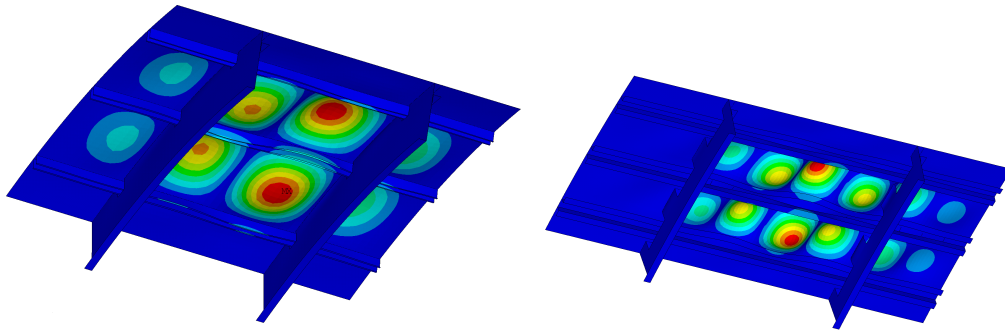


Figure 6.16: First buckling mode of the top sector ZOI of the metallic optimal fuselage (left) and of the composite one (right).

## 6.5 Conclusions

All the research activities carried out in the thesis work move in the framework of the WP5 of the European research project PARSIFAL.

The activities presented in Chapters 3, 5 and 7 target both Objectives 1 and 2 of WP5 (see Chapter 1). New or improved multi-scale design procedures for thin-walled composite structures have been developed and numerically validated through the solution of benchmark design problem taken from the literature.

In Chapter 4, one of the two planned activities of experimental validation of the proposed procedures is presented (Objective 2 of WP5). The second one of those activities, whose details are not reported in this thesis, has been carried out in collaboration with E. Panettieri and M. Montemurro and deals with the optimisation, manufacturing and testing of full-scale stiffened panels made of unconventional CSC.

In this chapter, the highlights of part of the activities carried out in pursuit of Objective 3 of WP5 are presented.

The GL-MSOS and the GL-MS2LOS, respectively presented in Chapters 3 and 5, have been employed for the preliminary structural design of the aircraft proposed in PARSIFAL. Two versions of the aircraft have been optimised: a first one with a completely metallic structure, and a second one with most of the structural components made of CSCLs. Only the main structural components of the central fuselage barrel and of the lifting system have been targeted in the design process. Similar optimisation problems have been formulated for the design of the two versions of the aircraft. In both cases, a limited, yet representative set of loading conditions and design criteria has been considered.

Because of the peculiar PrP architecture a modular approach to the modelling of the aircraft structure revealed necessary. The aircraft has been divided into six regions whose modelling activities have been shared between the members of the PARSIFAL team at ENSAM. In order to limit the computational effort needed for the optimisation of such a complex and over-constrained structure, two adaptations to the aforementioned GL multi-scale design procedures have been devised. From a procedural perspective, a multi-step alternated-domain approach is adopted: the solution search is carried out iteratively alternating the optimisation of the design variables belonging to the central fuselage barrel (FUO step) to those of the lifting system (LSO step). From a modelling point of view, in the GFEM of the whole aircraft structure, the regions not directly involved in the optimisation (e.g. all but the central fuselage region in the FUO step) are modelled in a



*condensed* way through SEs obtained by means of the sub-structuring technique.

Results have been obtained both in terms of macroscopic inertial properties distributions and in terms of detailed structural information for both variants of the aircraft structure. Clearly, there is no reference solution with which to compare the results obtained. However, the weight reduction observed when comparing the composite solution to the metallic one appear in agreement with expectations.



## Multi-level design of variable-stiffness composite structures

The article *Strength and mass optimisation of variable-stiffness composites in the polar parameters space*, reported in this chapter, has been accepted for publication in *Structural and Multidisciplinary Optimization* (Izzi et al., 2021a). It deals with the deterministic optimisation of VSCLs at the macroscopic scale. In particular, in this work, the first level of the MS2LOS for VSCs is enhanced and enriched through the formulation of requirements related to strength, mass and maximum tow curvature, and the design problem is generalised to the case of VAT laminates with non-uniform thickness.

The framework presented in this work allows for either the uniform (across the surface) or the point-wise tailoring of various properties of VSCLs: the orthotropy type and shape, the direction of the main orthotropy axis, the thickness of the laminate. Exploiting this freedom, various sub-classes of VSCLs, including both manufacturable solutions and theoretical ones, are identified and investigated in this work. The polar method is used to represent the point-wise elastic behaviour of the VSCLs. The PPs distributions and that of the thickness across the VSCL surface are described through B-spline entities: taking full advantage of their properties, the analytical expression of the response functions related to the aforementioned requirements, as well as their gradients, are derived. The structure failure load is assessed using a laminate-level failure criterion based on tensor invariants. An improved conservative formulation is proposed for the process-related manufacturability requirement on the maximum tow curvature. Moreover, a new formulation of the point-wise feasibility requirement (on the existence of suitable stacks in the second level) is proposed: a shrewd change of variable is introduced to intrinsically satisfy this requirement without introducing explicit constraint functions into the problem formulation.

Both the failure load maximisation problem (with a constraint on the structure mass) and the mass minimisation one (with a constraint on the structure strength) are solved for two benchmark structures, withstanding both in-plane and out-of-plane loads. For both structures, the effect of a constraint on the maximum tow curvature is also evaluated. Solutions belonging to various VSCLs sub-classes are obtained and discussed. Their performances are compared with those of both quasi-homogeneous isotropic solutions and an optimised VSC solution taken from the literature obtained by means of the LPs-based representation. In both cases, considerable improvements are registered, confirming the great potential of VSCLs and the effectiveness of the MS2LOS based on the polar method.

# Strength and mass optimisation of variable-stiffness composites in the polar parameters space

Michele Iacopo Izzi · Anita Catapano · Marco Montemurro

Received: 21 November 2020 / Accepted: 19 May 2021

**Abstract** A general theoretical and numerical framework for the strength and mass optimisation of variable-stiffness composite laminates (VSCLs) is presented in this work. The optimisation is performed in the context of the first-level problem of the multi-scale two-level optimisation strategy (MS2LOS) for VSCLs. Both the failure load maximisation problem (subject to a constraint on the mass) and the mass minimisation one (with a constraint on the VSCL strength) are solved for two benchmark structures. The effect of the presence of a constraint on the maximum tow curvature is also investigated. The solutions are searched by means of a deterministic algorithm by considering different scenarios in terms of the VSCL macroscopic behaviour: the orthotropy type and shape, the direction of the main orthotropy axis and the thickness of the laminate are tailored either globally (uniform over the structure) or locally. The polar method is used to represent the point-wise elastic response of the VSCL at the macroscopic scale. The distributions of the polar parameters and of the thickness are described through B-spline entities: their properties are exploited in computing physical and geometrical response functions of the VSCL as well as their gradient.

This paper presents part of the activities carried out within the research project PARSIFAL (Prandtlplane ARchitecture for the Sustainable Improvement of Future AirpLanes), which has been funded by the European Union under the Horizon 2020 Research and Innovation program (grant agreement No. 723149).

M.I. Izzi · M. Montemurro  
Arts et Métiers Institute of Technology, Université de Bordeaux,  
CNRS, INRA, Bordeaux INP, HESAM Université, I2M UMR 5295,  
F-33405 Talence, France  
E-mail: [micheleiacopo.izzi@ensam.eu](mailto:micheleiacopo.izzi@ensam.eu),  
[marco.montemurro@ensam.eu](mailto:marco.montemurro@ensam.eu)

A. Catapano  
Bordeaux INP, Université de Bordeaux, Arts et Métiers Institute of  
Technology, CNRS, INRA, HESAM Université, I2M UMR 5295, F-  
33405 Talence, France  
E-mail: [anita.catapano@bordeaux-inp.fr](mailto:anita.catapano@bordeaux-inp.fr)

The VSCL strength at the macroscopic scale is assessed using a laminate-level failure criterion in the space of polar parameters. Numerical results show considerable improvements with respect to both quasi-homogeneous isotropic structures and an optimised VSCL solution taken from the literature obtained by using the design approach based on lamination parameters. These results confirm the effectiveness of the proposed strategy and the great potential of VSCLs.

**Keywords** Variable-stiffness composite · Multi-level design · Polar method · B-spline · Strength · Optimisation · Variable-angle tow

## 1 Introduction

Nowadays, the development of new manufacturing technologies is allowing a proper exploitation of the directional properties of composite materials through the concept of variable-stiffness composite laminates (VSCLs). Unlike traditional constant-stiffness composite laminates (CSCLs), in VSCLs, a point-wise variation of the macroscopic mechanical properties can be obtained across the laminate surface. This can be achieved by means of various techniques: through a continuous in-plane steering of the fibres in variable-angle tow (VAT) laminates; by dropping or adding straight-fibre layers in laminates with variable thickness and stacking sequence; by a simultaneous and continuous variation of fibre direction and layer thickness in the case of the Continuous Tow Shearing process (Kim et al., 2014).

The local material tailoring makes VSCLs really appealing, especially for the strength optimisation of structures wherein stress concentrations, either due to geometry or loading, may occur. As an example, in an early experimental investigation, Hyman et al. (1969) showed that an improvement of about 43% of tensile strength could

be achieved by locally distorting the fibres grid around an open hole instead of just drilling it afterwards.

Traditionally, the design of VSCLs has been carried out by optimising the fibres-paths within each ply, by using the so-called *direct approach* (Ghiassi et al., 2010). Various analytical/numerical strategies have been developed, over the years, to find optimised solutions. The idea of locally aligning the main orthotropy axis of the material to the principal stress and/or strain direction, a common practice for stiffness-oriented optimisation, is exploited by Hyer and Charette (1991) to increase the failure load of open hole plates under tension. This alignment was achieved through an iterative procedure wherein a single layer of fibres-paths is optimised point-wise. Both the Tsai and Wu (1971) (TW) failure criterion (FC) and the max-strain one are computed on a layer-by-layer basis to predict the failure load and the related failure mode, obtaining theoretical improvements of the plate strength up to 89% over the quasi-isotropic  $[\pm 45/0/90]_{2s}$  configuration having the same geometry. An analogous procedure was followed by Tosh and Kelly (2000), who introduced the concept of *load paths*. They experimentally showed that better results in terms of strength are obtained when aligning the fibres with the load paths, instead of aligning them with the principal stress directions, in the case of open-hole tension and pin-loaded tests. In both works the authors also intuitively found that adding a few layers with curvilinear paths locally orthogonal to the main ones further improves strength.

A common belief when dealing with the optimisation of VSCLs is that maximising the stiffness implicitly implies a proper maximisation of the VSCL strength. However, even if the relation between the two problems has been recently found (Catapano and Montemurro, 2019), it has been shown that the two formulations are not equivalent (Ijsselmuiden et al., 2008; Khani et al., 2011; Catapano and Montemurro, 2020).

In most of the early works, the layers fibres-paths are described through a given discretisation, usually corresponding to the mesh of a finite element (FE) model used for the assessment of the physical responses. Moreover, mono-layers or over-simplified symmetric stacks were considered.

In order to limit the amount of design variables and, at the same time, ensure fibres-path continuity, some authors have opted for the use of an *in-layer* parametrisation of the fibres-paths. Gurdal and Olmedo (1993) introduced a fibres-path parametrisation wherein the fibre orientation angle varies linearly along a given direction and is kept constant along the perpendicular one. Although the linear fibre orientation variation represents a strong limitation for design purposes, it has widely been used for the optimisation of VSCLs, achieving good results. For example, Alhajmahmad et al. (2008) used this parametrisation for the failure load maximisation of a fuselage panel with a cut-out

modelled as a two-dimensional plate and loaded by a combination of pressure and in-plane loads. A 16-layer point-wise symmetric and balanced stacking sequence with only two independent fibres-paths of the type  $[\pm\theta_1/\pm\theta_2]_{2s}$  is considered for a total number of four design variables. The optimisation was performed using a simulated-annealing optimiser. Failure is verified using the TW FC, evaluated by means of FE analyses. Improvements up to 30% in the load carrying capacity of the structure were obtained when compared to the quasi-isotropic design. Huang and Haftka (2005) used a piecewise bi-linear interpolation to represent the fibres orientations near a hole of one of the layers of a laminate withstanding uni-axial tensile load for maximising its failure load. The solution search was performed by alternating the conjugate gradient method and a genetic algorithm to avoid local optima, obtaining a load-carrying capacity twice than that of a CSCL with the stack  $[0/\pm 45]_s$ . Other authors used more general parametrisations giving greater flexibility in describing the fibres-paths. Nagendra et al. (1995) used Non-Uniform Rational Basis Spline curves for the fibres paths. While Tian et al. (2021) proposed the use of a parametric divergence-free vector field point-wise tangent to the fibres. Owing to the nature of the vector field employed, resulting fibres-paths were ensured to not cross each other.

Of course, the main drawback of the *direct approach* is related to the number of design variables that could easily become prohibitive for thicker VSCL. Moreover, the physical responses involved in the problem formulation are highly non-convex in terms of the local fibres' orientation angle.

To go beyond these limitations, the so-called *multi-level approach* represents a sound alternative (Ghiassi et al., 2010). In this background, the composite design problem is split in two (or more) sub-problems. At the macroscopic scale, the VSCL is typically represented as an equivalent single layer plate whose anisotropic behaviour (which varies point-wise over the laminate) is described through a suitable representation.

To this purpose, two representations are commonly employed to describe the macroscopic response of the VSCL. The first one makes use of the lamination parameters (LPs) coupled with the parameters of Tsai and Pagano (Jones, 1975) in the framework of the classic laminate theory (CLT). This representation allows reducing the number of design variables (at most, 12 LPs are needed to describe the local anisotropic behaviour of a VSCL in the CLT framework). However, the Tsai and Pagano parameters are not all independent and they do not have a simple and immediate physical meaning. Moreover, some of them are frame dependent (Jones, 1975). The second representation available in the literature is the so-called *polar method*, which is based on the polar parameters (PPs) introduced by Verchery (1982) in the CLT framework and later ex-

tended to the case of higher-order equivalent single layer theories (HESLTs) by Montemurro (2015b,a,c). The polar formalism allows representing any plane tensor by means of tensor invariants, which are related to the symmetries of the tensor. The polar formalism generalised to the case of HESLTs is at the basis of the multi-scale two-level optimisation strategy (MS2LOS), widely used for the multi-scale design of both CSCLs (Montemurro et al., 2016, 2019; Izzi et al., 2020; Picchi Scardaoni and Montemurro, 2020; Audoux et al., 2020) and VSCLs (Montemurro and Catapano, 2016, 2017, 2019; Catapano et al., 2019; Catapano and Montemurro, 2020; Fiordilino et al., 2020).

In the framework of multi-level approaches, the determination of the optimal stacking sequences is postponed to a second phase wherein the lay-up design is typically formulated as an unconstrained least-squares problem. A further advantage of the anisotropy representation based on PPs is that both sub-problems can be formulated in the most general sense, i.e. without introducing unnecessary hypotheses on the nature of the stack to enforce desired elastic properties of the laminate (e.g. the use of symmetric stacks to get membrane-bending uncoupling or balanced stack to get membrane orthotropy, as systematically done in LPs-based approaches).

Both representations have been employed to deal with VSCLs optimisation problems involving stiffness and buckling requirements, see the works by Montemurro and Catapano (2016, 2017, 2019), Catapano et al. (2019) and Fiordilino et al. (2020) for some examples where polar formalism is used and the review article by Albazzan et al. (2019) for some works where the approach based on LPs is adopted. On the other hand, the integration of strength requirements in multi-level optimisation strategies has been limited for long time. This is due to the localised nature of the failure mechanisms, which occur at the ply-level or at the scale of the constitutive phases. Moreover, there is still a lack of a pertinent and efficient formulation of FC at the laminate level, which further contributes to the limited introduction of strength requirements in the first phase of multi-level optimisation approaches. An important improvement in this sense has been achieved by IJsselmuiden et al. (2008). Starting from the TW FC expressed in terms of strains, they built a conservative failure envelope that guarantees a failure-free region in the LPs space, independent of the stacking sequence. This laminate-level FC was used to maximise the failure load of a CSCL withstanding membrane load, and the obtained results were compared to those coming from a classical stiffness maximisation problem. In particular, depending on the material properties, strength-driven solutions can be characterised by failure loads up to 48% higher than those of stiffness-driven solutions. Later, Khani et al. (2011) employed the same laminate-level FC to maximise the failure load of a quarter of a square VSC layered plate with a central

hole withstanding tensile load. The hypotheses of point-wise symmetric and balanced stacks were made and the design variables describing the VSCL were defined element-wise. In their work the main orthotropy direction was set aligned to the main direction of the external load. Their results, obtained by employing a deterministic algorithm, showed significant improvements of the failure load (almost three times greater than that of an isotropic solution and two times greater than that characterising a VSCL optimised with respect to stiffness requirements). However, the laminate-level FC proposed by IJsselmuiden et al. is characterised by some limitations: **a)** limited accuracy when dealing with moderately thick or thick laminates and out-of-plane loads (because of the CLT framework); **b)** the coupling between the FE model mesh and design variables definition; **c)** an excessive conservativeness of the failure envelope for bending-dominated problems.

A unified formulation of a laminate-level FC based on PPs has been initially introduced in the framework of the CLT by Catapano et al. (2015) and later generalised to the first-order shear deformation theory (FSDT) by Catapano and Montemurro (2019). In particular, thanks to the polar formalism, the relationship between the PPs defining the laminate stiffness and strength matrices at the laminate level was derived in closed form. Recently, Catapano and Montemurro (2020) performed a two-level meta-heuristic optimisation of VSCLs against failure in which the aforementioned laminate-level FC is employed at the first level. At the second level, the optimal fibres-paths are searched combining the analytical method proposed by Miki and Sugiyamat (1993) coupled with the use of *Quasi-Trivial* stacking sequences (Vannucci and Verchery, 2001; Garulli et al., 2018) and a first-ply failure check is also performed *a posteriori* confirming, thus, the integrity of obtained solutions.

The present work focuses on the first-level problem (FLP) formulation and related numerical strategy of the MS2LOS for VSCLs. In particular, here the polar formalism (in the FSDT framework) and the laminate-level FC proposed by Catapano and Montemurro (2019) are used to formulate and solve two different optimisation problems. The first one deals with the failure load maximisation of a VSCL subject to a constraint on its mass, whilst the second one focuses on the VSCL mass minimisation subject to a constraint on its failure load. Moreover, the effect of the constraint on the minimum tow curvature radius, related to the manufacturability of the VSCLs is also investigated: thanks to the polar formalism this constraint can be formulated as an equivalent constraint on the PPs fields. The distribution of the design variables at the laminate level is described by means of B-spline entities in order to ensure their continuity over the structure. Moreover, due to the use of B-spline entities, the definition of the design variables is unrelated to the mesh of the FE model and a

significant reduction of their amount is achieved (without degrading the accuracy of the response evaluations) when compared to FE-based approaches (Montemurro and Catapano, 2017, 2019). The main contributions of this work are:

- a) The analytical expressions of the failure load of VSCLs and of its gradient are derived in the PPs space by taking advantage of the B-spline entities properties.
- b) The maximum admissible tow curvature requirement is formulated as an equivalent conservative constraint in the PPs space and its gradient is derived in a closed-form.
- c) The VSC design problem is generalised to the case of VAT laminates with variable thickness.
- d) A comparison of the results obtained by considering different problem formulations is presented and commented.

The effectiveness of the MS2LOS for VSCLs is shown on two meaningful benchmark problems taken from the literature.

The paper is organised as follows. An overview of the work (the considered design cases and underlying hypotheses) is given in Sec. 2. The fundamentals of the polar method in the FSDT framework are provided in Sec. 3. The mathematical formulation of the optimisation problems is discussed in Sec. 4. The details of the FE models are presented in Sec. 5. Numerical results are shown in Sec. 6, while Sec. 7 ends the paper with some conclusions and prospects.

*Notation.* Upper-case bold letters are used to indicate matrices, while lower-case bold letters indicate vectors, which are to be intended as column ones.

## 2 Work overview

### 2.1 Design cases

To show the effectiveness of the MS2LOS for the optimum design of VSCLs, two benchmark structures are considered:

- S1** A quarter of a square plate with a central hole withstanding tensile load (Fig. 1a).
- S2** A square plate with a central hole subject to pressure and bi-axial tensile load (Fig. 1b).

S1 is the typical structure used to emphasize stress concentration effects in presence of membrane loads. Its geometry and boundary conditions (BCs) are chosen in agreement with those employed by Khani et al. (2011), whose results are referred to as *literature solution* (LSol) in the following. Structure S2 is a simplified flat model of one of the panels composing a stiffened pressurised vessel of

radius  $R$  having a plugged opening and is meant to highlight bending and transverse shear effects. Details of the applied BCs for both benchmarks are given in Fig. 1. For both benchmark structures, loaded edges are constrained in such a way to remain straight while withstanding a distributed load corresponding to a given resultant force. In benchmark structure S2, the pressure acts directly on the surface of the plate and also on the hole edge, as an uniform force per unit length, representing the pressure load coming from the non-structural cup of the opening hole, which is not modelled.

The VSCLs used in these structures are made of unidirectional AS4/3501-6 carbon/epoxy pre-preg tows, whose material properties are reported in Tab. 1 (the meaning of the polar parameters reported in such table is clarified in Sec. 3). A *reference solution* (RSol) is defined as the homogeneous isotropic version of both structures with an overall thickness of  $t_{\text{RSol}} = 4.6 \text{ mm}$ .

The values of geometrical parameters and loads appearing in Fig. 1 are reported in Tab. 2: the values of the force  $\bar{F}_x$  acting on benchmark structure S1 and of pressure  $p$  acting on S2 have been set such to be critical, with respect to the employed laminate-level FC (detailed in Sec. 3.2), for the corresponding RSols.

Two different optimisation problems are solved for both benchmark structures:

- P1** The maximisation of the failure load of the VSC layered structure subject to a constraint on its mass (which must be lower than or equal to that of the corresponding RSol).
- P2** The minimisation of the mass of the VSC layered structure subject to a constraint on the failure load (which must be greater than or equal to that of the corresponding RSol).

**Remark 2.1** A slightly different formulation of both optimisation problems is obtained by also imposing a constraint on the maximum curvature of the tow. These two variants are identified as P1c and P2c.

For the solution of the aforementioned problems, point-wise fully orthotropic (both in membrane and bending), quasi-homogeneous (i.e. with a null membrane/bending coupling stiffness tensor and identical normalised membrane and bending stiffness tensors) VSCLs are considered. In particular, the focus is put on three subclasses of these VSCLs:

- C1** Constant-thickness VSCLs with *variable orthotropy direction* (CT-DVO), but uniform anisotropic moduli, i.e. with a macroscopic behaviour characterised by the same point-wise *orthotropy shape*, but with variable direction of the main orthotropy axis.
- C2** Constant-thickness VSCLs with a *fully variable orthotropy* (CT-FVO), i.e. with a macroscopic behaviour



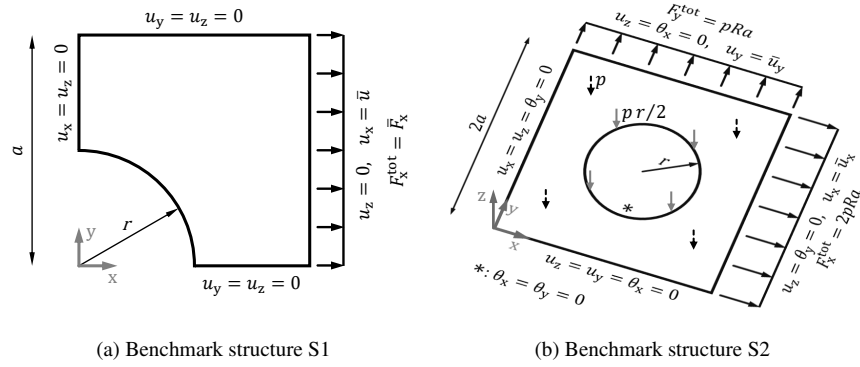


Fig. 1: Geometry and boundary conditions of benchmark structures S1 and S2.

Table 1: Material properties of the unidirectional AS4/3501-6 carbon/epoxy tow (Khani et al., 2011; Daniel and Ishai, 1994).

| Technical constants   |                             | Polar parameters of $\mathbf{Q}^{\text{in}}$ <sup>a</sup> |         | Polar parameters of $\mathbf{Q}^{\text{out}}$ <sup>b</sup>                                    |         |
|-----------------------|-----------------------------|---|---------|---|---------|
| $E_1$ [MPa]           | 142000                      | $T_0^{\text{Qin}}$ [MPa]                                  | 22040   | $T^{\text{Qout}}$ [MPa]   | 5272    |
| $E_2$ [MPa]           | 10300                       | $T_1^{\text{Qin}}$ [MPa]                                  | 19838   | $R^{\text{Qout}}$ [MPa]   | 1928    |
| $G_{12}$ [MPa]        | 7200                        | $R_0^{\text{Qin}}$ [MPa]                                  | 14840   | $\Phi^{\text{Qout}}$ [rad]  | $\pi/2$ |
| $\nu_{12}$            | 0.27                        | $R_1^{\text{Qin}}$ [MPa]                                  | 16550   |   |         |
| $\nu_{23}$            | 0.54                        | $\Phi_0^{\text{Qin}}$ [rad]                               | 0       |   |         |
|                       |                             | $\Phi_1^{\text{Qin}}$ [rad]                               | 0       |   |         |
| Engineering strengths |                             | Pol. par. of $\mathbf{G}^{\text{in}}$ <sup>c</sup>        |         | Pol. par. of $\mathbf{G}^{\text{out}}$ <sup>d</sup> and $\mathbf{g}^{\text{in}}$ <sup>e</sup> |         |
| $X$ [MPa]             | 2280                        | $T_0^{\text{Gin}}$ [MPa]                                  | 7077    | $T^{\text{Gout}}$ [MPa]   | 8637    |
| $X'$ [MPa]            | 1440                        | $T_1^{\text{Gin}}$ [MPa]                                  | 1312    | $R^{\text{Gout}}$ [MPa]   | 1647    |
| $Y = Z$ [MPa]         | 57                          | $R_0^{\text{Gin}}$ [MPa]                                  | 3206    | $\Phi^{\text{Gout}}$ [rad]  | $\pi/2$ |
| $Y' = Z'$ [MPa]       | 228                         | $R_1^{\text{Gin}}$ [MPa]                                  | 405     | $T^{\text{Ein}}$ [MPa]  | 68      |
| $Q$ [MPa]             | 40                          | $\Phi_0^{\text{Gin}}$ [rad]                               | $\pi/4$ | $R^{\text{Ein}}$ [MPa]  | 68      |
| $R = S$ [MPa]         | 71                          | $\Phi_1^{\text{Gin}}$ [rad]                               | $\pi/2$ | $\Phi^{\text{Ein}}$ [rad]   | $\pi/2$ |
| Density               | $\rho$ [g/cm <sup>3</sup> ] |   | 1.58    |   |         |

<sup>a</sup> In-plane reduced stiffness matrix of the ply.<sup>b</sup> Out-of-plane shear stiffness matrix of the ply.<sup>c</sup> In-plane strength matrix of the ply.<sup>d</sup> Out-of-plane strength matrix of the ply.<sup>e</sup> In-plane strength vector of the ply.

Table 2: Geometrical and loading parameters.

| Parameter                 | Symbol            | Value |
|---------------------------|-------------------|-------|
| Edge length [mm]          | $a$               | 200   |
| Hole radius [mm]          | $r$               | 100   |
| Reference thickness [mm]  | $t_{\text{RSol}}$ | 4.6   |
| Vessel radius [mm]        | $R$               | 2000  |
| Resultant axial force [N] | $\bar{F}_x$       | 79000 |
| Pressure [MPa]            | $p$               | 0.187 |

characterised by a variation of both the local orthotropy shape and the direction of the main orthotropy axis.

**C3** Variable-thickness VSCLs with a fully variable orthotropy (VT-FVO).

In this context, the adjectives constant and variable refer to the spatial variation over the laminate.

**Remark 2.2** A further sub-class of VSCLs, named **CL**, is introduced for the sole purpose of finding solutions that is more fairly comparable to LSol. VSCLs-CL corresponds to the type of laminates used by Khani et al. (2011): CT laminates having the direction of the main orthotropy axis parallel to the global x-axis, with an orthotropy shape that varies over the laminate (SVO).

The solution of problems P1c and P2c is currently limited to VSCLs belonging to sub-class C1. All the combinations of problem formulation and VSCLs sub-class investigated in this work are summarised in Tab. 3.

Table 3: Combinations of problem formulations PX and VSCLs sub-classes CX.

|    | P1 | P1c | P2 | P2c |
|----|----|-----|----|-----|
| C1 | •  | •   | •  | •   |
| C2 | •  | -   | •  | -   |
| C3 | •  | -   | •  | -   |
| CL | •  | -   | -  | -   |

Both benchmark structures share the following hypotheses:

- H1** The material behaviour is supposed linear elastic and the FE analyses are carried out by assuming small displacements.
- H2** The elastic response of the VSCLs is expressed in the FSDT framework.
- H3** Concerning VSCLs-C3, the spatial variation of thickness is considered continuous and symmetric with respect to the laminate middle plane.
- H4** All structures are considered free of defects due to the manufacturing process of VSCL, e.g. tows gaps and overlaps.

Clearly, these last two hypotheses correspond to solutions that are not manufacturable with current automated fibre placement (AFP) machines. These solutions can be interpreted as the theoretical limit achievable by using increasingly thinner and narrower tows.

## 2.2 The Multi-Scale Two-Level Optimisation Strategy

In the context of the MS2LOS, the optimum design of the VSCL is articulated in two sub-problems formally stated at different scales:

**First-level problem (FLP)** The goal of the FLP is the determination of the optimum distribution of the mechanical design variables, describing the behaviour of the VSCL at the macroscopic scale, satisfying the requirements of the design problem. At this scale, the VSCL is modelled as an equivalent homogeneous anisotropic continuum and its behaviour is described in the FSDT framework. The design variables are the laminate PPs and thickness, which vary locally over the structure.

**Second-level problem (SLP)** The SLP, which is formulated at the laminate mesoscopic scale (i.e. the ply-level), is devoted to the determination of a suitable lay-up matching the optimum distribution of PPs resulting from the FLP. The design variables are the parameters describing the fibres-paths within each lamina.

In this work only the FLP of the MS2LOS is faced and the related mathematical framework is extended to problems involving strength, mass, and maximum tow curvature requirements. Inasmuch as the SLP formulation is not

affected by the modifications introduced in the FLP (and the main steps of the related resolution strategy remain unchanged), this part will not be detailed in the following sections. For more details on the SLP formulation and on the related mathematical background, the reader is addressed to the work by Montemurro and Catapano (2016) and Catapano and Montemurro (2020).

## 3 Fundamentals of the polar method

In this section, the fundamentals of the polar analysis of laminates stiffness and strength matrices are provided; for a deeper insight in the matter, the reader is addressed to previous works (Vannucci, 2005; Montemurro, 2015b,a; Catapano and Montemurro, 2019).

Verchery's polar method (Verchery, 1982) allows to express any  $n$ -rank plane tensor through a set of tensor invariants (i.e. the PPs). In the context of this work, two types of tensors are relevant: second-rank symmetric plane tensors  $Z_{ij}$  (with  $i, j = 1, 2$ ) and fourth-rank elasticity-like (i.e. having both major and minor symmetries) plane tensors  $L_{ijkl}$  (with  $i, j, k, l = 1, 2$ ). They can be expressed in terms of their PPs as:

$$\begin{aligned} Z_{11} &= +T + R \cos 2\Phi, \\ Z_{12} &= +R \sin 2\Phi, \\ Z_{22} &= +T - R \cos 2\Phi, \end{aligned} \quad (1)$$

and

$$\begin{aligned} L_{1111} &= +T_0 + 2T_1 + R_0 \cos 4\Phi_0 + 4R_1 \cos 2\Phi_1, \\ L_{1122} &= -T_0 + 2T_1 - R_0 \cos 4\Phi_0, \\ L_{1112} &= +R_0 \sin 4\Phi_0 + 2R_1 \sin 2\Phi_1, \\ L_{2222} &= +T_0 + 2T_1 + R_0 \cos 4\Phi_0 - 4R_1 \cos 2\Phi_1, \\ L_{2212} &= -R_0 \sin 4\Phi_0 + 2R_1 \sin 2\Phi_1, \\ L_{1212} &= +T_0 - R_0 \cos 4\Phi_0. \end{aligned} \quad (2)$$

In Eqs. (1) and (2),  $T$ ,  $T_0$  and  $T_1$  are the isotropic moduli,  $R$ ,  $R_0$  and  $R_1$  are the anisotropic ones, while  $\Phi$ ,  $\Phi_0$  and  $\Phi_1$  are the polar angles. Among them  $T$ ,  $R$  and  $T_0$ ,  $T_1$ ,  $R_0$ ,  $R_1$ ,  $\Phi_0 - \Phi_1$  are tensor invariants, while  $\Phi$  and one of the two polar angles,  $\Phi_0$  or  $\Phi_1$ , can be arbitrarily chosen to set the reference frame, for second and fourth rank tensors, respectively.

One of the main advantages of the polar formalism is that requirement on elastic symmetries of the tensor can be translated into simple algebraic conditions on the related PPs. For example, the ordinary orthotropy of a fourth-rank elasticity-like tensor corresponds to the condition:

$$\Phi_0 - \Phi_1 = K \pi/4 \quad \text{with } K = 0, 1, \quad (3)$$

with  $K = 0$  and  $K = 1$ , corresponding to the so-called low shear modulus and high shear modulus orthotropy, respectively. More details about the elastic symmetries and their expression in terms of PPs can be found in the work of Vannucci (2005).

### 3.1 The polar analysis of the laminate stiffness matrices

In the framework of the FSDT (Reddy, 2003) the constitutive law of the laminate (expressed within the local frame  $\Gamma_e = \{O; x_e, y_e, z_e\}$ ) can be stated as:

$$\mathbf{r} = \mathbf{K}_{\text{lam}} \boldsymbol{\varepsilon}, \quad (4)$$

where  $\mathbf{r}$  and  $\boldsymbol{\varepsilon}$  are the vectors of the generalised forces per unit length and the strains of the laminate middle plane, respectively, whilst  $\mathbf{K}_{\text{lam}}$  is the laminate stiffness matrix (in Voigt's notation). In this framework, the analytical form of these arrays is:

$$\mathbf{r} := \begin{Bmatrix} \mathbf{n} \\ \mathbf{m} \\ \mathbf{q} \end{Bmatrix}, \quad \mathbf{K}_{\text{lam}} := \begin{bmatrix} \mathbf{A} & \mathbf{B} & \mathbf{0} \\ & \mathbf{D} & \mathbf{0} \\ \text{sym} & & \mathbf{H} \end{bmatrix}, \quad \boldsymbol{\varepsilon} := \begin{Bmatrix} \boldsymbol{\varepsilon}_0 \\ \boldsymbol{\chi}_0 \\ \boldsymbol{\gamma}_0 \end{Bmatrix}. \quad (5)$$

In Eq. (5),  $\mathbf{A}$ ,  $\mathbf{B}$  and  $\mathbf{D}$  are the membrane, membrane/bending coupling and bending stiffness matrices of the laminate, while  $\mathbf{H}$  is the out-of-plane shear stiffness matrix.  $\mathbf{n}$ ,  $\mathbf{m}$  and  $\mathbf{q}$  are the vectors of membrane forces, bending moments and shear forces per unit length, respectively, whilst  $\boldsymbol{\varepsilon}_0$ ,  $\boldsymbol{\chi}_0$  and  $\boldsymbol{\gamma}_0$  are the vectors of in-plane strains, curvatures and out-of-plane shear strains of the laminate middle plane, respectively. In order to analyse the elastic response of the multilayer plate, it is useful to introduce the laminate normalised stiffness matrices:

$$\mathbf{A}^* := \frac{1}{t} \mathbf{A}, \quad \mathbf{B}^* := \frac{2}{t^2} \mathbf{B}, \quad \mathbf{D}^* := \frac{12}{t^3} \mathbf{D}, \quad \mathbf{H}^* := \frac{1}{t} \mathbf{H}, \quad (6)$$

where  $t$  is the total thickness of the laminate.

As deeply discussed by Montemurro (2015b,a),  $\mathbf{A}^*$ ,  $\mathbf{B}^*$ ,  $\mathbf{D}^*$  behave like tensor  $\mathbf{L}$  of Eq. (2) and  $\mathbf{H}^*$  behaves like tensor  $\mathbf{Z}$  of Eq. (1), therefore it is possible to express the Cartesian components of these matrices in terms of PPs, for an overall number of 21 parameters. It can be proven that, if the elastic properties of the constitutive tow (i.e. matrices  $\mathbf{Q}^{\text{in}}$  and  $\mathbf{Q}^{\text{out}}$  and their PPs, listed in Tab. 1) are known and the hypothesis of fully orthotropic quasi-homogeneous laminate is introduced, i.e.

$$\mathbf{A}^* = \mathbf{D}^*, \quad \mathbf{B}^* = \mathbf{0}, \quad \Phi_0^{A^*} - \Phi_1^{A^*} = K^{A^*} \pi/4, \quad (7)$$

the overall number of independent PPs reduces to only three: the anisotropic polar moduli  $R_{0K}^{A^*} := (-1)^{K^{A^*}} R_0^{A^*}$  and  $R_1^{A^*}$ , which describe the *shape* of the orthotropy of matrix  $\mathbf{A}^*$ , and the polar angle  $\Phi_1^{A^*}$ , which represents the orientation of the main orthotropy axis of matrix  $\mathbf{A}^*$ . More details on the polar formalism and its application in the context of the FSDT are available in previous works (Montemurro, 2015b,a).

### 3.2 The polar analysis of the laminate strength matrices

For the assessment of failure, the general laminate-level FC formulated by Catapano and Montemurro (2019) is here employed. This criterion represents a general unified formula including various phenomenological failure criteria. The formulation used in this work is based on the TW FC. This ply-level FC can be written in the unified matrix notation as

$$F_{\text{TW}} := \boldsymbol{\sigma}^T \mathbf{F} \boldsymbol{\sigma} + \boldsymbol{\sigma}^T \mathbf{f} \leq 1, \quad (8)$$

where  $\boldsymbol{\sigma}$  is the stress vector in Voigt's notation, while  $\mathbf{F}$  and  $\mathbf{f}$  depend on the lamina strength properties (Tsai and Wu, 1971). In agreement with Khani et al. (2011), the stress dependent term  $F_{12}$  is assumed equal to

$$F_{12} = \frac{-1}{2\sqrt{X'Y'Y'}}. \quad (9)$$

By introducing the FSDT hypothesis of null out-of-plane normal stress, by separating the in-plane and out-of-plane contributions, by using the Hooke's law and exploiting the FSDT kinematics, Eq. (8) can be rewritten for each layer  $k$  in terms of the laminate middle plane strains

$$F_{\text{TW}}^k(z) = \boldsymbol{\varepsilon}_0^T \mathbf{G}_k^{\text{in}} \boldsymbol{\varepsilon}_0 + z^2 \boldsymbol{\chi}_0^T \mathbf{G}_k^{\text{in}} \boldsymbol{\chi}_0 + 2z \boldsymbol{\varepsilon}_0^T \mathbf{G}_k^{\text{in}} \boldsymbol{\chi}_0 + \boldsymbol{\gamma}_0^T \mathbf{G}_k^{\text{out}} \boldsymbol{\gamma}_0 + \boldsymbol{\varepsilon}_0^T \mathbf{g}_k^{\text{in}} + z \boldsymbol{\chi}_0^T \mathbf{g}_k^{\text{in}} \leq 1, \quad (10)$$

where the matrices  $\mathbf{G}_k^{\text{in}}$ ,  $\mathbf{G}_k^{\text{out}}$  and the vector  $\mathbf{g}_k^{\text{in}}$  depend on the strength properties of the ply (listed in Tab. 1) and on the orientation of the  $k$ -th layer. The *laminate failure index* (LFI) is calculated by averaging Eq. (10) through the thickness  $t$  of the laminate as:

$$F_{\text{TW}}^{\text{lam}} = \frac{1}{t} \int_{-t/2}^{t/2} F_{\text{TW}}^k(z) dz. \quad (11)$$

Eq. (11) simplifies to:

$$F_{\text{TW}}^{\text{lam}} = \frac{1}{t} (\boldsymbol{\varepsilon}_0^T \mathbf{G}_A \boldsymbol{\varepsilon}_0 + \boldsymbol{\chi}_0^T \mathbf{G}_D \boldsymbol{\chi}_0 + \boldsymbol{\varepsilon}_0^T \mathbf{G}_B \boldsymbol{\chi}_0 + \boldsymbol{\gamma}_0^T \mathbf{G}_H \boldsymbol{\gamma}_0 + \boldsymbol{\varepsilon}_0^T \mathbf{g}_A + \boldsymbol{\chi}_0^T \mathbf{g}_D). \quad (12)$$

Matrices  $\mathbf{G}_A$ ,  $\mathbf{G}_B$ ,  $\mathbf{G}_D$  and  $\mathbf{G}_H$  and vectors  $\mathbf{g}_A$  and  $\mathbf{g}_D$  represent the laminate strength matrices and vectors. In particular, the four matrices can be seen as the strength counterpart of stiffness matrices  $\mathbf{A}$ ,  $\mathbf{B}$ ,  $\mathbf{D}$ , and  $\mathbf{H}$ . The laminate normalised strength matrices and vectors can be defined as follows:

$$\mathbf{G}_A^* = \frac{1}{t} \mathbf{G}_A, \quad \mathbf{G}_B^* = \frac{2}{t^2} \mathbf{G}_B, \quad \mathbf{G}_D^* = \frac{12}{t^3} \mathbf{G}_D, \quad \mathbf{G}_H^* = \frac{1}{t} \mathbf{G}_H, \\ \mathbf{g}_A^* = \frac{1}{t} \mathbf{g}_A, \quad \mathbf{g}_D^* = \frac{2}{t^2} \mathbf{g}_D. \quad (13)$$

Finally, by defining

$$\mathbf{G}_{\text{lam}} := \begin{bmatrix} \mathbf{G}_A & \mathbf{G}_B & \mathbf{0} \\ & \mathbf{G}_D & \mathbf{0} \\ \text{sym} & & \mathbf{G}_H \end{bmatrix}, \quad \mathbf{g}_{\text{lam}} := \begin{Bmatrix} \mathbf{g}_A \\ \mathbf{g}_D \\ \mathbf{0} \end{Bmatrix}, \quad (14)$$

a compact version of Eq. (12) can be obtained:

$$F_{\text{TW}}^{\text{lam}} = \boldsymbol{\varepsilon}^T \frac{\mathbf{G}_{\text{lam}}}{t} \boldsymbol{\varepsilon} + \boldsymbol{\varepsilon}^T \frac{\mathbf{g}_{\text{lam}}}{t}. \quad (15)$$

**Remark 3.1** For the sake of simplicity,  $F_{\text{TW}}^{\text{lam}}$  is simply indicated as  $F$  hereafter.

To use the LFI, a suitable threshold value  $F_{\text{Th}}$  must be introduced, such that, when failure occurs

$$F \geq F_{\text{Th}}. \quad (16)$$

Employing a threshold value  $F_{\text{Th}} = 1$  does not result in a conservative choice. A thorough discussion about the choice of  $F_{\text{Th}}$  is not the main scope of this work, but the effect of this choice on the results of the optimisation problem is briefly discussed in Appendix A. In agreement with previous works making use of the LFI within the multi-scale optimisation process of real-world CSC layered structures (Izzi et al., 2020), the value  $F_{\text{Th}} = 0.5$  has been used in this work.

Of course, the arrays of Eq. (14) can be expressed in terms of PPs. Catapano and Montemurro showed that, when the strength properties of the constitutive ply (i.e. matrices  $\mathbf{G}^{\text{in}}$  and  $\mathbf{G}^{\text{out}}$  and vector  $\mathbf{g}^{\text{in}}$ , and their PPs, listed in Tab. 1) are known, the laminate strength matrices and vectors can be expressed in terms of the PPs of the laminate stiffness matrices introduced in Sec. 3.1. This means that the PPs describing the laminate stiffness and strength matrices and vectors are not independent. Accordingly, it suffices to include among the problem design variables only one of these two sets of PPs. When a fully orthotropic quasi-homogeneous laminate is considered, the overall number of independent PPs describing its behaviour (in terms of both stiffness and strength) is still equal to three: the anisotropic polar moduli  $R_{0K}^{\text{A}*}$  and  $R_1^{\text{A}*}$  and the polar angle  $\Phi_1^{\text{A}*}$  of matrix  $\mathbf{A}^*$  or, alternatively, their counterpart of matrix  $\mathbf{G}_A^*$ . More details on the polar analysis of laminates strength matrices and on the correlation between laminate strength and stiffness matrices PPs can be found in the work by Catapano and Montemurro (2019).

## 4 Mathematical formulation of the first-level problem

### 4.1 Design variables

The design variables describing the behaviour of the VSCL at the macroscopic scale are the thickness of the laminate,

$t$ , and three mechanical variables, i.e. the PPs  $R_{0K}^{\text{A}*}$ ,  $R_1^{\text{A}*}$  and  $\Phi_1^{\text{A}*}$ . For optimisation purposes, it is useful to consider the dimensionless quantities defined as follows:

$$\tau := \frac{t}{t_{\text{RSol}}}, \quad \rho_{0K} := \frac{R_{0K}^{\text{A}*}}{R_0^{\text{Qin}}}, \quad \rho_1 := \frac{R_1^{\text{A}*}}{R_1^{\text{Qin}}}, \quad \phi_1 := \frac{\Phi_1^{\text{A}*}}{\pi/2}, \quad (17)$$

In order to ensure that a feasible stacking sequence, matching the optimal distribution of PPs resulting from the FLP, could be found as a result of the SLP, the point-wise geometrical feasibility conditions proposed by Vannucci (2013) must be considered in the FLP. For a quasi-homogeneous orthotropic laminate, these constraints read<sup>1</sup>:

$$\begin{cases} -1 \leq \rho_{0K} \leq 1, \\ 0 \leq \rho_1 \leq 1, \\ 2(\rho_1)^2 - 1 - \rho_{0K} \leq 0. \end{cases} \quad (18)$$

In previous works dealing with PPs, the above conditions were introduced as explicit constraints into the FLP formulation (Montemurro et al., 2016; Montemurro and Catapano, 2017, 2019; Catapano et al., 2019; Montemurro et al., 2019; Izzi et al., 2020; Picchi Scardaoni and Montemurro, 2020; Audoux et al., 2020). Conversely, in this work, a different approach is proposed: the feasible domain of PPs identified by Eq. (18) is remapped in a unit square domain  $[0, 1] \times [0, 1]$  through the following variables change:

$$(\alpha_0, \alpha_1) := \left( \frac{\rho_{0K} - 1}{2(\rho_1^2 - 1)}, \rho_1 \right), \quad (19)$$

whose converse relation is

$$(\rho_{0K}, \rho_1) = (1 + 2\alpha_0(\alpha_1^2 - 1), \alpha_1). \quad (20)$$

All combinations of  $\alpha_0$  and  $\alpha_1$  automatically satisfy the feasibility conditions of Eq. (18), without the need of introducing explicit constraints into the FLP formulation.

In agreement with Eqs. (17) and (19), four different variables distributions, i.e.  $\tau$ ,  $\alpha_0$ ,  $\alpha_1$ ,  $\phi_1$ , uniquely describe the macroscopic mechanical behaviour of the VSCL. Each field can be either uniform or variable over the laminate, depending on the considered VSCL sub-class (see Sec. 2.1):

- When a VSCL-C1 is considered, only the dimensionless polar angle  $\phi_1$  varies point-wise over the laminate.
- When a VSCL-C2 is considered,  $\alpha_0$ ,  $\alpha_1$  and  $\phi_1$  vary locally over the structure, whilst  $t$  is uniform.
- When a VSCL-C3 is considered, all design variables vary over the structure.

<sup>1</sup> These conditions describe the convex-hull of the true feasibility domain, as recently discussed by Picchi Scardaoni and Montemurro (2021), and are valid under the hypothesis that the laminate is composed of a sufficient number of plies, whose direction can get value in a sufficiently big and scattered set.

- When a VSCL-CL is considered,  $\tau$  is uniform,  $\alpha_0, \alpha_1$  vary over the laminate, while  $\phi_1$  is identically null.

The spatial variation of the generic design variable  $\xi$  is described by means of a B-spline scalar function:

$$\xi(u_1, u_2) = \sum_{i_1=0}^{n_1} \sum_{i_2=0}^{n_2} N_{i_1, p_1}(u_1) N_{i_2, p_2}(u_2) \xi^{(i_1, i_2)},$$

with  $\xi = \tau, \alpha_0, \alpha_1, \phi_1$ , (21)

where  $\xi^{(i_1, i_2)}$  is the value of the design variable at the generic control point (CP)  $(i_1, i_2)$ , whereas  $N_{i_1, p_1}(u_1)$  and  $N_{i_2, p_2}(u_2)$  are the B-spline blending functions of degree  $p_1$  and  $p_2$ , computed at parametric coordinates  $u_1$  and  $u_2$ . These latter take values in the interval  $[0, 1]$  and are defined as:

$$\begin{aligned} (u_1, u_2) &:= (x/a, y/a) && \text{for S1,} \\ (u_1, u_2) &:= (x/2a, y/2a) && \text{for S2.} \end{aligned} \quad (22)$$

In agreement with the classical B-spline entities definitions (Piegl and Tiller, 1997),  $n_d + 1$  CPs are needed along the  $d$ -th parametric direction, for a total number of CPs equal to  $N_{\text{CP}} = (n_1 + 1) \times (n_2 + 1)$  for each B-spline entity. The blending functions are defined recursively by means of the Bernstein's polynomials, which can be defined after introducing the related *knot vectors*:

$$\mathbf{v}^{(d)T} := \left\{ \underbrace{0, \dots, 0}_{p_d}, v_{p_d}^d, \dots, v_{n_d+1}^d, \underbrace{1, \dots, 1}_{p_d} \right\}, \text{ with } d = 1, 2. \quad (23)$$

In this study, in agreement with the theoretical framework presented by Montemurro and Catapano (2019), the inner components of the knot vectors are evenly distributed in the interval  $[0, 1]$  and kept constant during the optimisation process. Moreover, the integer parameters appearing in Eq. (21), i.e.  $n_k$  and  $p_k$  are set *a priori* and are not involved into the optimisation process as design variables. As discussed by Montemurro and Catapano (2019), the generic design variable field  $\xi(u_1, u_2)$  of Eq. (21) can be the third coordinate of a B-spline surface whose first two coordinates of the surface are evaluated through the Greiville's abscissae. For more details on B-spline entities (i.e. curves and surfaces) the reader is addressed to the book of Piegl and Tiller (1997).

In this framework, the only design variables are the CPs values  $\xi^{(i_1, i_2)}$  for each variable field. The number of design variables depend on the considered VSCLs subclass as reported in Tab. 4. In the most general case, i.e. when  $\tau, \alpha_0, \alpha_1$  and  $\phi_1$  are spatially variable, the total number of variables is  $4 \times N_{\text{CP}}$  and they are grouped into the following vector of design variables:

$$\mathbf{x}^T = \left\{ \tau^{(0,0)}, \dots, \tau^{(n_1, n_2)}, \alpha_0^{(0,0)}, \dots, \alpha_0^{(n_1, n_2)}, \alpha_1^{(0,0)}, \dots, \alpha_1^{(n_1, n_2)}, \phi_1^{(0,0)}, \dots, \phi_1^{(n_1, n_2)} \right\}. \quad (24)$$

Table 4: Number of design variables for each VSCL subclass.

|    | $\tau$          | $\alpha_0$      | $\alpha_1$      | $\phi_1$        | Total                        |
|----|-----------------|-----------------|-----------------|-----------------|------------------------------|
| C1 | 1               | 1               | 1               | $N_{\text{CP}}$ | $3 + N_{\text{CP}}$          |
| C2 | 1               | $N_{\text{CP}}$ | $N_{\text{CP}}$ | $N_{\text{CP}}$ | $1 + 3 \times N_{\text{CP}}$ |
| C3 | $N_{\text{CP}}$ | $N_{\text{CP}}$ | $N_{\text{CP}}$ | $N_{\text{CP}}$ | $4 \times N_{\text{CP}}$     |
| CL | 1               | $N_{\text{CP}}$ | $N_{\text{CP}}$ | 0               | $1 + 2 \times N_{\text{CP}}$ |

## 4.2 Response functions and their gradients

As discussed in Sec. 2.1, three types of requirements are involved in the formulation of the two optimisation problems considered in this work: **a)** a requirement on the failure load of the structure; **b)** a requirement on the mass of the structure; **c)** a requirement on the curvature of the tows. In order to solve the optimisation problems by means of a suitable deterministic algorithm, analytic expressions of a response function and its gradient are required for each requirement. These functions are computed by exploiting the information coming from linear static FE analyses, whose equilibrium equations system is (expressed within the global frame of the structure  $\Gamma = \{O; x, y, z\}$ ):

$$\mathbf{K}\mathbf{u} = \mathbf{f} = \lambda \mathbf{f}_{\text{Ref}}, \quad (25)$$

where  $\mathbf{K}$  is the stiffness matrix of the structure,  $\mathbf{u}$  is the vector of the degrees of freedom (DOFs),  $\mathbf{f}$  is the vector of generalised external nodal forces defined as the product of the load factor  $\lambda$  and the reference load vector  $\mathbf{f}_{\text{Ref}}$  (the details of the FE models are given in Sec. 5). Eqs. (25) can always be reordered in such a way to group the terms related to unknown DOFs, whose corresponding generalised external forces are known, identified by the index F, and those related to known DOFs, identified by the index D:

$$\underbrace{\begin{bmatrix} \mathbf{K}_{\text{FF}}^* & \mathbf{K}_{\text{FD}}^* \\ \mathbf{K}_{\text{DF}}^* & \mathbf{K}_{\text{DD}}^* \end{bmatrix}}_{\mathbf{K}^*} \underbrace{\begin{Bmatrix} \mathbf{u}_{\text{F}}^* \\ \mathbf{u}_{\text{D}}^* \end{Bmatrix}}_{\mathbf{u}^*} = \lambda \underbrace{\begin{Bmatrix} \mathbf{f}_{\text{Ref}, \text{F}}^* \\ \mathbf{f}_{\text{Ref}, \text{D}}^* \end{Bmatrix}}_{\mathbf{f}_{\text{Ref}}^*}, \quad (26)$$

where the superscript  $*$  means *reordered* and, of course,  $\mathbf{K}_{\text{DF}}^* = \mathbf{K}_{\text{FD}}^{*T}$ .

**Remark 4.1** In the following, the superscript  $*$  and the subscripts F and D are used to indicate the same reordering and selection operations performed to obtain the terms of Eq. (26) from those of Eq. (25).

The definition of the response functions related to the failure and the maximum tow curvature requirements makes use of the maximum function, which operates on an indexed set of positive values computed per-element ( $q_e \geq 0$  with  $e \in \{1, 2, \dots, N_e\}$ ). Of course, the maximum function is not differentiable. Therefore, in order to compute the gradient of such response functions, the smooth

approximation of the maximum function given by the  $p$ -Norm operator is used:

$$pn(q_e) := \left( \sum_e q_e^p \right)^{1/p} \approx \max_e q_e, \quad (27)$$

where  $p$  is the power of the norm, which strongly affects the accuracy of the approximation.

**Proposition 4.1** *Given a desired value of maximum relative difference  $d_{\max}$ , such that*

$$\max_e(q_e) < pn(q_e) \leq (1 + d_{\max}) \max_e(q_e) \quad \forall q_e, \quad (28)$$

*the above condition can be satisfied if*

$$p = \left\lceil \frac{\log N_e}{\log(1 + d_{\max})} \right\rceil, \quad (29)$$

The proof of Proposition. 4.1 is provided in Appendix B. The derivative of the  $p$ -Norm operator with respect to the generic variable  $\xi$  reads

$$\frac{\partial(pn(q_e))}{\partial \xi} = (pn(q_e))^{1-p} \sum_e \left( q_e^{p-1} \frac{\partial q_e}{\partial \xi} \right). \quad (30)$$

#### 4.2.1 Failure load requirement

Concerning the failure load requirement, the factor of safety  $\lambda_F$  is introduced. It is defined as the minimum positive load factor leading to the failure of the structure:

$$\lambda_F := \min_e \lambda_{F,e}, \quad (31)$$

where

$$\lambda_{F,e} := \{ \lambda > 0 : F_e(\lambda) = F_{Th} \}, \quad (32)$$

$F_e$  being the LFI of Eq. (15) computed at the  $e$ -th element centroid. The value  $\lambda_{F,e}$  is the positive root of the following equation (obtained by rewriting Eq. (15) in terms of the load factor  $\lambda$  and equating it to  $F_{Th}$ ):

$$Q_e \lambda^2 + L_e \lambda = F_{Th}, \quad (33)$$

where the quantities  $Q_e$  and  $L_e$  are defined as

$$Q_e := \mathbf{e}_{Ref,e}^T \frac{\mathbf{G}_{lam,e}}{t} \mathbf{e}_{Ref,e}, \quad L_e := \mathbf{e}_{Ref,e}^T \frac{\mathbf{g}_{lam,e}}{t}, \quad (34)$$

with

$$\mathbf{e}_{Ref,e} = \mathfrak{B}_e \mathfrak{L}_e \mathbf{u}_{Ref}. \quad (35)$$

In Eq. (35),  $\mathbf{u}_{Ref}$  is the solution of Eq. (25) when  $\lambda = 1$ .  $\mathfrak{L}_e$  is the so-called generalised connectivity matrix (involving also the affine transformation aligning the element local frame  $\Gamma_e$  to the global one  $\Gamma$ ), which is defined as follows

$$\mathfrak{L}_e : \mathbf{u} \mapsto \mathbf{u}_e, \quad \mathbf{u}_e = \mathfrak{L}_e \mathbf{u}. \quad (36)$$

$\mathfrak{B}_e$  is the matrix relating the element middle plane strains to the element DOFs defined as

$$\mathfrak{B}_e : \mathbf{u}_e \mapsto \boldsymbol{\varepsilon}_e, \quad \boldsymbol{\varepsilon}_e = \mathfrak{B}_e \mathbf{u}_e. \quad (37)$$

The definition of the response function related to the failure load requirement is based on the inverse of the factor of safety:

$$f_F := pn(\lambda_{F,e}^{-1}) - 1 \approx \max_e (\lambda_{F,e}^{-1}) - 1. \quad (38)$$

By considering Eq. (33) and the expression of the  $p$ -norm operator, Eq. (38) reads:

$$f_F := \left[ \sum_e \left( \frac{-L_e + \sqrt{L_e^2 + 4Q_e F_{Th}}}{2Q_e} \right)^{-p} \right]^{1/p} - 1. \quad (39)$$

Of course, a negative value of  $f_F$  means that failure does not occur.

**Proposition 4.2** *Consider a VSC layered structure subject to given BCs. The gradient of the response function  $f_F$  can be obtained by solving:*

$$\begin{cases} \frac{\partial f_F}{\partial \xi^{(i_1, i_2)}} = -(f_F + 1)^{1-p} (l_{i_1 i_2} + \boldsymbol{\mu}^T \tilde{\boldsymbol{\psi}}_{i_1 i_2}), \\ \mathbf{K}_{FF}^* \boldsymbol{\mu}_F^* = -\boldsymbol{\psi}_F^*, \end{cases} \quad (40)$$

where:

- $\boldsymbol{\mu}$  is the auxiliary vector. If it is reordered such that  $\boldsymbol{\mu}^{*T} := \{ \boldsymbol{\mu}_F^{*T}, \boldsymbol{\mu}_D^{*T} \}$ ,  $\boldsymbol{\mu}_F^*$  is the solution of the auxiliary system, i.e. the second formula in Eq. (40), and  $\boldsymbol{\mu}_D^* = \mathbf{0}$ .
- $\boldsymbol{\psi}^{*T} := \{ \boldsymbol{\psi}_F^{*T}, \boldsymbol{\psi}_D^{*T} \}$ . Its non-reordered counterpart  $\boldsymbol{\psi}$  is defined as:

$$\begin{aligned} \boldsymbol{\psi} := \sum_e \left\{ \frac{\mathfrak{L}_e^T \mathfrak{B}_e^T}{\lambda_{F,e}^{p+1} Q_e \sqrt{\Delta_e}} \right. \\ \cdot \left[ 2 \left( F_{Th} - \lambda_{F,e} \sqrt{\Delta_e} \right) \frac{\mathbf{G}_{lam,e}}{t_e} \mathbf{e}_{Ref,e} \right. \\ \left. \left. - \lambda_{F,e} Q_e \frac{\mathbf{g}_{lam,e}}{t_e} \right] \right\}, \end{aligned} \quad (41)$$

with  $\Delta_e := L_e^2 + 4Q_e F_{Th}$ .

- $\tilde{\boldsymbol{\psi}}_{i_1 i_2}$  is a fictitious force vector defined as:

$$\begin{aligned} \tilde{\boldsymbol{\psi}}_{i_1 i_2} := \sum_{e \in S_{i_1 i_2}} \left( \frac{\partial \xi_e}{\partial \xi^{(i_1, i_2)}} \right. \\ \cdot \left. \int_{A_e} \mathfrak{L}_e^T \mathfrak{B}_e^T \frac{\partial \mathbf{K}_{lam,e}}{\partial \xi_e} \mathfrak{B}_e \mathfrak{L}_e dS \right) \mathbf{u}_{Ref}, \end{aligned} \quad (42)$$

where,  $A_e$  is the area of the  $e$ -th element.

–  $l_{i_1 i_2}$  is defined as:

$$l_{i_1 i_2} := \sum_{e \in S_{i_1 i_2}} \left\{ \frac{\partial \xi_e}{\partial \xi^{(i_1, i_2)}} \frac{\boldsymbol{\epsilon}_{\text{Ref}, e}^T}{\lambda_{F, e}^{p+1} Q_e \sqrt{\Delta_e}} \cdot \left[ \left( F_{\text{Th}} - \lambda_{F, e} \sqrt{\Delta_e} \right) \frac{\partial}{\partial \xi_e} \left( \frac{\mathbf{G}_{\text{lam}, e}}{t_e} \right) \boldsymbol{\epsilon}_{\text{Ref}, e} - \lambda_{F, e} Q_e \frac{\partial}{\partial \xi_e} \left( \frac{\mathbf{g}_{\text{lam}, e}}{t_e} \right) \right] \right\}. \quad (43)$$

The proof of Proposition 4.2 is provided in Appendix C.

**Remark 4.2** In Eq. (40), the quantity  $\boldsymbol{\mu}^T \boldsymbol{\psi}_{i_1 i_2}$  is the non-local contribution to the gradient of  $f_F$ , i.e. due to the stress redistribution consequent to a variation of  $\xi^{(i_1, i_2)}$ , while  $l_{i_1 i_2}$  is the local one.

**Remark 4.3** The quantity  $\xi_e$  appearing in Eqs. (42) and (43) indicates the value of the generic design variable  $\xi$  computed at the centroid of the  $e$ -th element, i.e.:

$$\xi_e := \xi(u_{1e}, u_{2e}). \quad (44)$$

According to Eq. (21), its derivatives read:

$$\frac{\partial \xi_e}{\partial \xi^{(i_1, i_2)}} = N_{i_1, p_1}(u_{1e}) N_{i_2, p_2}(u_{2e}). \quad (45)$$

**Remark 4.4** In Eqs. (42) and (43),  $S_{i_1 i_2}$  indicates the discretised local support of CP  $(i_1, i_2)$ , defined as:

$$S_{i_1 i_2} := \left\{ e : (u_{1e}, u_{2e}) \in \left[ v_{i_1}^{(1)}, v_{i_1+p_1+1}^{(1)} \right] \times \left[ v_{i_2}^{(2)}, v_{i_2+p_2+1}^{(2)} \right] \right\}. \quad (46)$$

As a consequence of the local support property of B-spline blending functions, the variation of the generic design variable at CP  $(i_1, i_2)$ , only influences the elements belonging to the local support of such CP. The size of the local support zone depends on the B-spline integer parameters.

#### 4.2.2 Laminate mass requirement

The evaluation function related to the laminate mass is defined as a relative difference between the laminate mass and the mass of the corresponding RSol:

$$f_M := \frac{M - M_{\text{RSol}}}{M_{\text{RSol}}}, \quad (47)$$

The mass of the laminate is approximated by discretising the thickness variation per-element:

$$M \approx \rho \sum_e (A_e t_e), \quad (48)$$

where  $A_e$  is the area of the  $e$ -th element and  $t_e$  is the thickness evaluated at its centroid (obtained as  $t_e = \tau_e t_{\text{RSol}}$ ). A negative value of function  $f_M$  means that the mass of the considered structure is lower than that of the corresponding RSol.

**Remark 4.5** The evaluation function  $f_M$  is linear with respect to the design variables  $\xi^{(i_1, i_2)}$ .

The sensitivity of  $f_M$  with respect to the generic design variable  $\xi^{(i_1, i_2)}$  reads:

$$\frac{\partial f_M}{\partial \xi^{(i_1, i_2)}} = \begin{cases} \frac{t_{\text{RSol}} \rho}{M_{\text{RSol}}} \sum_{e \in S_{i_1 i_2}} \left( A_e \frac{\partial \tau_e}{\partial \tau^{(i_1, i_2)}} \right) & \text{if } \xi = \tau, \\ 0 & \text{if } \xi \neq \tau. \end{cases} \quad (49)$$

#### 4.2.3 Maximum tow curvature requirement

The requirement on the maximum tow curvature is formulated only for the VSCLs belonging to sub-class C1 introduced in Sec. 2.1. In the PPs framework, these VSCLs are described by uniform values of  $R_{0K}^{\text{A}^*}$  and  $R_1^{\text{A}^*}$  (and, consequently, of  $\alpha_0$  and  $\alpha_1$ ), and a spatial distribution of  $\Phi_1^{\text{A}^*}$  (hence, of  $\phi_1$ ). The stacking sequences family corresponding to this class of VSCLs is the one having the form (re-elaborated from Montemurro and Catapano (2017)):

$$\delta_k(x, y) = \delta_k^0 + \Phi_1^{\text{A}^*}(x, y), \quad (50)$$

where  $\delta_k$  is the local orientation of the  $k$ -th layer of the VSCL and  $\delta_k^0$  is the orientation of the same layer of a stacking sequence corresponding to the set of PPs ( $R_{0K}^{\text{A}^*}, R_1^{\text{A}^*}, \Phi_1^{\text{A}^*} = 0$ ). The local fibre curvature  $\chi$  of the  $k$ -th layer can be computed as:

$$\chi_k(x, y) = \nabla \delta_k^T(x, y) \mathbf{t}_k(x, y), \quad (51)$$

where  $\mathbf{t}_k$  is the unit vector of direction  $\delta_k$ , i.e.  $\mathbf{t}_k^T := \{\cos \delta_k, \sin \delta_k\}$ .

In the context of the FLP of the MS2LOS for VSCLs, the distributions of  $\delta_k$  and, consequently, the local value  $\chi_k$  are unknown. However, all possible  $\chi_k$  have their absolute values upwards bounded by the supremum  $\chi$  defined as follows:

$$|\chi_k(x, y)| \leq \chi(x, y) := \|\nabla \Phi_1(x, y)\| = \sqrt{\left( \frac{\partial \Phi_1}{\partial x} \right)_{x, y}^2 + \left( \frac{\partial \Phi_1}{\partial y} \right)_{x, y}^2} \quad \forall \delta_k. \quad (52)$$

If a maximum admissible value of tow curvature modulus  $\chi_{\text{Th}}$  is known, at the macroscopic scale the manufacturability condition can be conservatively imposed on the supremum:

$$\max_{x, y} \chi(x, y) \leq \chi_{\text{Th}}. \quad (53)$$

The square of  $\chi$  is used in this work and the maximum operator is approximated through the  $p$ -Norm operator defined in Eq. (27). Therefore, the response function  $f_C$ , related to the maximum allowable curvature of the tow, is



defined as:

$$f_C := \frac{\left(\sum_e (\chi_e^2)^p\right)^{1/p} - \chi_{Th}^2}{\chi_{Th}^2} \approx \frac{\max_e \chi_e^2 - \chi_{Th}^2}{\chi_{Th}^2}, \quad (54)$$

where  $\chi_e$  is the tow curvature computed at the centroid of each element.  $\chi_e$  can be expressed in terms of the dimensionless polar angle  $\phi_1$  as

$$\begin{aligned} \chi_e^2 &= \left(\frac{\pi}{2}\right)^2 \nabla \phi_1|_e^T \nabla \phi_1|_e \\ &= \left(\frac{\pi}{2}\right)^2 \left[ \left( \frac{\partial \phi_1}{\partial u_1} \Big|_e \frac{\partial u_1}{\partial x} \Big|_e + \frac{\partial \phi_1}{\partial u_2} \Big|_e \frac{\partial u_2}{\partial x} \Big|_e \right)^2 \right. \\ &\quad \left. + \left( \frac{\partial \phi_1}{\partial u_1} \Big|_e \frac{\partial u_1}{\partial y} \Big|_e + \frac{\partial \phi_1}{\partial u_2} \Big|_e \frac{\partial u_2}{\partial y} \Big|_e \right)^2 \right]. \end{aligned} \quad (55)$$

**Remark 4.6** In agreement with Eq. (21) the terms  $(\partial \phi_1 / \partial u_j)_e$  of Eq. (55) are of the type:

$$\frac{\partial \xi}{\partial u_j} \Big|_e = \sum_{i_1=0}^{n_1} \sum_{i_2=0}^{n_2} \left[ \left( \frac{d(N_{i_j, p_j}(u_j))}{du_j} \Big|_e N_{i_k, p_k}(u_{k_e}) \right) \xi^{(i_1, i_2)} \right],$$

with  $j, k = 1, 2 \ j \neq k$ . (56)

According to Eq. (22), the derivatives of the parametric coordinates  $(u_1, u_2)$  with respect to the global ones  $(x, y)$  read

$$\begin{aligned} \partial u_1 / \partial x &\equiv \partial u_2 / \partial y = 1/a & \text{for S1,} \\ \partial u_1 / \partial x &\equiv \partial u_2 / \partial y = 1/2a & \text{for S2,} \\ \partial u_1 / \partial y &\equiv \partial u_2 / \partial x = 0. \end{aligned} \quad (57)$$

**Remark 4.7**  $f_C$  is a quadratic function of the design variables.

The sensitivity of  $f_C$  with respect to the generic design variable  $\xi^{(i_1, i_2)}$  reads:

$$\frac{\partial f_C}{\partial \xi^{(i_1, i_2)}} = \frac{(f_C + 1)^{1-p}}{(\chi_{Th}^2)^p} \sum_{e \in S_{i_1, i_2}} \left[ (\chi_e^2)^{p-1} \frac{\partial \chi_e^2}{\partial \xi^{(i_1, i_2)}} \right], \quad (58)$$

where

$$\frac{\partial \chi_e^2}{\partial \xi^{(i_1, i_2)}} = \begin{cases} \frac{\pi^2}{2} \nabla \phi_1|_e^T \frac{\partial (\nabla \phi_1|_e)}{\partial \phi_1^{(i_1, i_2)}} & \text{if } \xi = \phi_1, \\ 0 & \text{if } \xi \neq \phi_1. \end{cases} \quad (59)$$

#### 4.3 Mathematical statement of the optimisation problems

With the definition of the response functions introduced in the above section, the four optimisation problems introduced in Sec. 2.1 can be finally formulated.

Optimisation problems P1 and P1c can be stated as follows:

$$\min_{\mathbf{x}} f_F(\mathbf{x}), \quad \text{s.t.} \begin{cases} f_M(\mathbf{x}) \leq 0, \\ f_C(\mathbf{x}) \leq 0, \end{cases} \quad \text{only for P1c,} \quad (60)$$

while, optimisation problem P2 and P2c read:

$$\min_{\mathbf{x}} f_M(\mathbf{x}), \quad \text{s.t.} \begin{cases} f_F(\mathbf{x}) \leq 0, \\ f_C(\mathbf{x}) \leq 0, \end{cases} \quad \text{only for P2c.} \quad (61)$$

Problems (60) and (61) are solved by considering the four sub-classes of VSCLs identified in Sec. 2.1 and following the scheme reported in Tab. 3. For each sub-class, a corresponding vector of design variables is defined (Sec. 4.1). The lower and upper bounds for each design variable appearing in these vectors are reported in Tab. 5.

Table 5: Lower and upper bounds of the design variables.

| Design variable         | Lower bound | Upper bound |
|-------------------------|-------------|-------------|
| $\tau^{(i_1, i_2)}$     | 0           | 2           |
| $\alpha_0^{(i_1, i_2)}$ | 0           | 1           |
| $\alpha_1^{(i_1, i_2)}$ | 0           | 1           |
| $\phi_1^{(i_1, i_2)}$   | -1          | +1          |

#### 5 Finite element models

The data needed to compute the functions presented in Sec. 4.2 are retrieved from the results of FE analyses. To this purpose, a simple FE model has been created in the ANSYS APDL environment for each benchmark structure. Taking advantage of the geometrical similarities between the two structures, the FE model of benchmark structure S2 corresponds to four repetitions of the S1 one. On these FE models, linear static analyses are performed.

The VSCLs are modelled using 4-node quadrilateral shell elements (ANSYS SHELL181) organised in the structured mesh shown in Fig. 2. The mechanical properties are considered constant into each element: the design variables are evaluated at the centroid of each element and the corresponding matrices  $\mathbf{A}$ ,  $\mathbf{B}(\equiv \mathbf{0})$ ,  $\mathbf{D}$  and  $\mathbf{H}$ , obtained through Eqs. (1) and (2), are assigned to such element. The level of mesh refinement has been set after an unreported sensibility analysis looking for the best compromise between computational cost of the FE analyses and accuracy

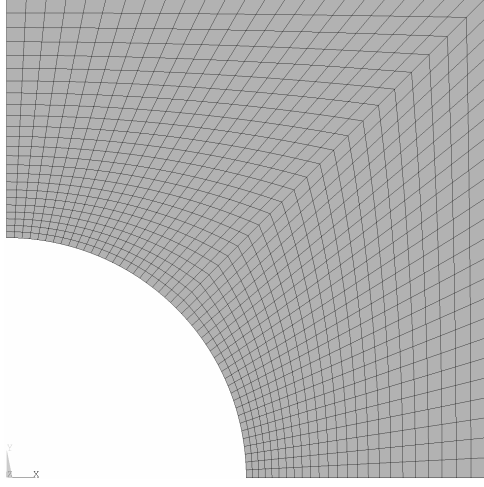


Fig. 2: FE model of benchmark structure S1.

in the approximation of the spatial distributions of both the design variables and the local response of the VSCL. The mesh of benchmark structure S1 has 1152 elements and 1225 nodes.

**Remark 5.1** *The mesh described above presents some differences with respect to the one characterising LSol (i.e. the FE model employed by Khani et al. (2011)). In the former, linear quadrilateral elements with a higher uniformity of the elements size across the laminate have been preferred over the constant-strain 3-node triangular elements used in the latter. The size of the elements at the apex of the hole edge (i.e. the critical ones in RSols) is comparable in the two models, although slightly bigger in the model used by Khani et al. (2011). The size of the elements in this region of the plate affects more the assessment of the failure load of RSols than that of the optimal solutions (which are characterised by a more uniform stress distribution). However, the difference in the factors of safety resulting from the adoption of the mesh described above and the one characterising LSol has been estimated to be of about 1%.*

The application of most of the BCs described in Fig. 1 is quite straightforward. Only the application of external in-plane distributed load under the condition of straight edge displacement needs further explanations: it is achieved by applying a single force to one of the nodes of the edge while coupling together (via constraint equations) all the DOFs (of the edge) along the force direction.

## 6 Numerical results

The Sequential Least-Squares Quadratic Programming (SLSQP) algorithm (Kraft, 1988), included in the Python library SciPy v.1.4.1 (Virtanen et al., 2020) is used to carry

Table 6: Sensibility of  $\lambda_F$  for benchmark structure S1 to the CPs grid size.

| CPs            | $\lambda_F$ | Iter. |
|----------------|-------------|-------|
| $3 \times 3$   | 4.33        | 116   |
| $5 \times 5$   | 4.61        | 150   |
| $7 \times 7$   | 5.10        | 163   |
| $9 \times 9$   | 5.24        | 165   |
| $11 \times 11$ | 5.31        | 215   |

out the solution search for problems (60) and (61). All parameters tuning the behaviour of the SLSQP algorithm are set to their default values, except parameter `ftol`, which is set to  $10^{-5}$ . For the implementation of all evaluation functions presented in Sec. 4.2, as well as their gradients, the numerical platform DOMEs (Deterministic Optimisation of Macroscopic laminatEs via Splines) has been created: developed in the Python environment, it constitutes an interface between the optimisation algorithm and the FE software, and it establishes a data structure for the definition of the design variables and a modular implementation of the various requirements.

The value of the parameter  $p$ , involved in the definition of the  $p$ -Norm operator of Eq. (27), assumes a constant value during the optimisation which has been computed through Eq. (29). A value of  $d_{\max} = 0.01$  has been used, and the number of elements  $N_e$  on which the  $p$ -Norm is evaluated is equal to the number of elements composing the FE model. A value of  $p = 709$  is obtained for benchmark structure S1 and a value  $p = 848$  for S2.

Concerning the integer parameters of the B-spline entities, the degrees of the blending function have been set to  $p_1 = p_2 = 2$  for both structures, while the number of CPs has been chosen after performing two sensitivity analyses, one for each benchmark structure. In these sensitivity analyses, problem P1 for VSCLs-C2 is solved for both benchmark structures considering square CPs grids of various size. Tabs. 6 and 7 resume the results of these studies: the choice is to use a  $9 \times 9$  CPs grid for S1 and a  $13 \times 13$  one for S2.

All the results presented in this section are obtained using the appropriate RSol as starting point: i.e. a uniform laminate having  $\tau = 1$ ,  $\alpha_0 = 0.5$ ,  $\alpha_1 = 0$  (corresponding to  $\rho_{0K} = \rho_1 = 0$ ), and  $\phi_1 = 0$ . It should be noticed that laminates having  $\rho_{0K} = \rho_1 = 0$  and different values of  $\phi_1$  are mechanically identical, but effectively constitute different starting points, hence the choice of the initial value of  $\phi_1$  affects the optimised solution. In this work, the value  $\phi_1 = 0$  has been set in order to align the initial main orthotropy axis direction to the one of the main in-plane external load acting on the structures.

In the following, the results obtained for all considered design cases are presented and commented. Results of

Table 7: Sensibility of  $\lambda_F$  for benchmark structure S2 to the CPs grid size.

| CPs            | $\lambda_F$ | Iter. |
|----------------|-------------|-------|
| $5 \times 5$   | 1.80        | 111   |
| $7 \times 7$   | 1.99        | 290   |
| $9 \times 9$   | 1.99        | 115   |
| $11 \times 11$ | 2.14        | 190   |
| $13 \times 13$ | 2.22        | 250   |
| $15 \times 15$ | 2.28        | 263   |
| $17 \times 17$ | 2.29        | 274   |
| $19 \times 19$ | 2.32        | 311   |
| $21 \times 21$ | 2.31        | 300   |

problems P1c and P2c have been obtained for two different values of maximum tow curvature, i.e.  $\chi_{Th} = 1/250 \text{ mm}^{-1}$  and  $\chi_{Th} = 1/150 \text{ mm}^{-1}$  (suggested by Nagelsmith and Guerrits (2013) as threshold values for  $1/4''$  and  $1/8''$  tows, respectively). These results are presented together with those of problem P1 for VSCLs-C1 in which there is no constraint on tow curvature. The optimised solutions are presented both in terms of their performances and of the corresponding design variables. Concerning the latter, for improved readability, instead of  $\alpha_0$  and  $\alpha_1$ , the corresponding dimensionless PPs  $\rho_{0K}$  and  $\rho_1$  are presented. For each benchmark structure and optimisation problem, results are summarised in a dedicated table wherein they are compared to the corresponding RSol. The optimised value of uniform design variables is reported directly in such tables, while a figure (whose reference is reported in the tables) is provided to show the optimised distribution of each non-uniform design variable. Moreover, the optimal fields related to the main orthotropic direction  $\Phi_1^{A*}$  are represented through streamlines plots.

Results of problems P1 and P1c for benchmark structure S1 are also compared to LSol. Concerning the comparability of these solutions, some comments are needed. Firstly, inasmuch as for benchmark structure S1 only membrane loads and uncoupled laminates are considered, there is no influence of the bending and shear behaviour of the laminate on the structural responses. Under these circumstances, the different plate theories employed by Khani et al. (2011) and in this work, (i.e. CLT and FSDT, respectively) provide the same results. Secondly, the comparison is done in terms of factors of safety and not in terms of absolute failure loads in order to attenuate the effect of using different laminate-level FC. In each work, the factors of safety are obtained as a ratio between coherent data (i.e. the failure load of the optimised configuration and that of a common reference one, both obtained through the same formulation of the laminate-level FC); then only normalised dimensionless values are compared. Finally, as explained in Remark 5.1, the factors of safety obtained by means of the FE model presented in Sec. 5 are estimated

to be about 1% higher than those obtained through a FE model having a coarser mesh equivalent to the one employed by Khani et al. (2011).

**Remark 6.1** *As explained in the above sections, this work focuses on the first-level problem. Since a deterministic algorithm is employed to perform the solution search the laminate thickness is considered as a continuous variable in the first-level problem. Of course, the optimal value of the thickness resulting from the FLP needs to be rounded up to the next integer multiple of the basic ply thickness for the definition of the SLP formulation. This leads to a systematic underestimation of the real laminate thickness at the end of the FLP which results favourable for the fulfilment of the strength requirement and has no effect on the maximum tow curvature requirement during the solution search of the SLP.*

**Remark 6.2** *All optimised solutions are feasible and are characterised by small negative values (between  $-10^{-5}$  and 0). These values are not reported in the following for the sake of brevity.*

## 6.1 Benchmark structure S1

As described in Sec. 2.1, benchmark structure S1 is the typical structure used to emphasize stress concentration effects. It withstands only tensile load, mainly in the horizontal direction.

### 6.1.1 Optimisation problem P1/P1c

A summary of the results of optimisation problems P1/P1c for benchmark structure S1 is presented in Tab. 8. The corresponding optimal distributions of non-uniform design variables are shown in Figs. 3-6.

From the results listed in Tab. 8, the following considerations can be drawn:

- Optimal solutions have a factor of safety ranging from 3.34 to 11.34.
- All solutions have better performances than LSol, with a gain varying between 4% and 252% (from 234% to 1034% with respect to RSol). In particular, the optimal VSCL-CL (i.e. the most fairly comparable to LSol) shows a factor of safety of 3.89, about 21% higher than that of LSol.
- As expected, the greater the maximum allowable curvature of the tow the better the performance of the optimal solutions. The same effect is obtained by enlarging the design space (moving from VSCL-C1 to VSCL-C3): optimal VSCL-C2 has a 72% higher factor of safety than that of the optimal VSCL-C1, while a supplementary gain of 116% is obtained by adopting a VT solution (optimal VSCL-C3 over optimal VSCL-C2).

Table 8: Summary of the optimised solutions of problems P1 and P1c for benchmark structure S1.

| Solution  | $\lambda_F$ | $\tau$  | $\rho_{0K}$ | $\rho_1$ | $\phi_1$ |
|---|-------------|---------|-------------|----------|----------|
| RSol  | 1.00        | 1       | 0.00        | 0.00     | 0.00     |
| LSol (P1 - Khani et al. (2011))                 | 3.22        | 1       | -           | -        | 0.00     |
| C1 (P1c - $\chi_{Th} = 1/250 \text{ mm}^{-1}$ ) | 3.34        | 1       | 0.61        | 0.87     | Fig. 3a  |
| C1 (P1c - $\chi_{Th} = 1/150 \text{ mm}^{-1}$ ) | 3.71        | 1       | 0.66        | 0.85     | Fig. 3b  |
| CL (P1)   | 3.89        | 1       | Fig. 4a     | Fig. 4b  | 0.00     |
| C1 (P1)   | 4.11        | 1       | 0.78        | 0.89     | Fig. 3c  |
| C2 (P1)   | 5.24        | 1       | Fig. 5a     | Fig. 5b  | Fig. 5c  |
| C3 (P1)   | 11.34       | Fig. 6a | Fig. 6b     | Fig. 6c  | Fig. 6d  |

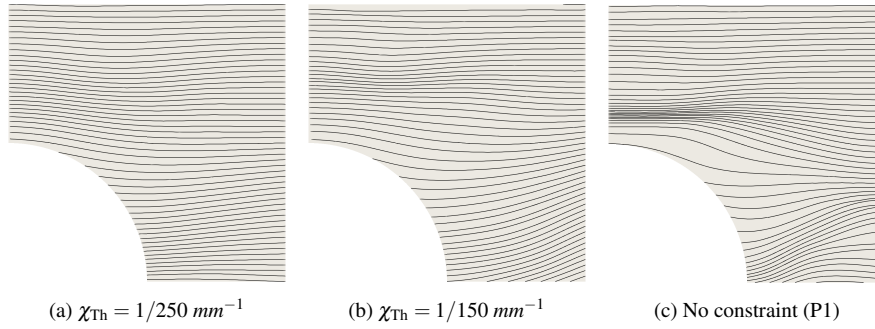


Fig. 3: Benchmark structure S1 - Optimisation problem P1c - VSCLs-C1: streamlines of the optimal distributions of the main orthotropy direction.

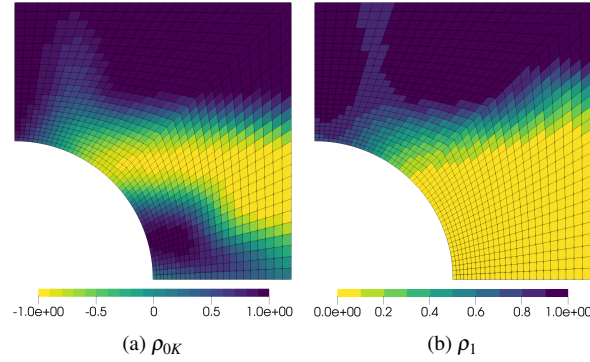


Fig. 4: Benchmark structure S1 - Optimisation problem P1 - VSCLs-CL: optimal distributions of the anisotropic moduli.

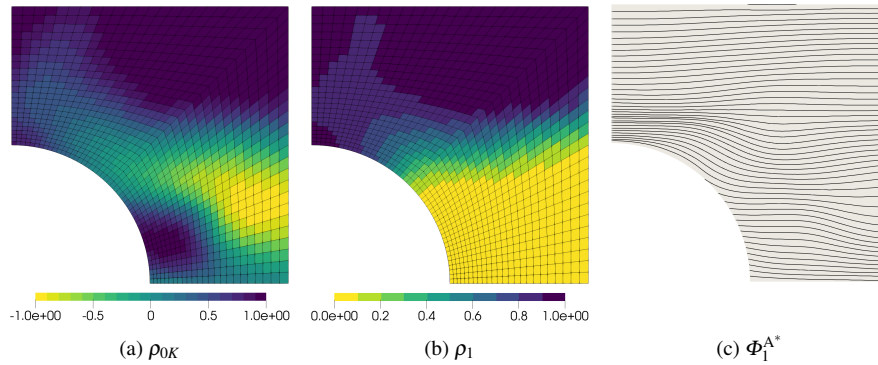


Fig. 5: Benchmark structure S1 - Optimisation problem P1 - VSCLs-C2: optimal distributions of the mechanical design variables.

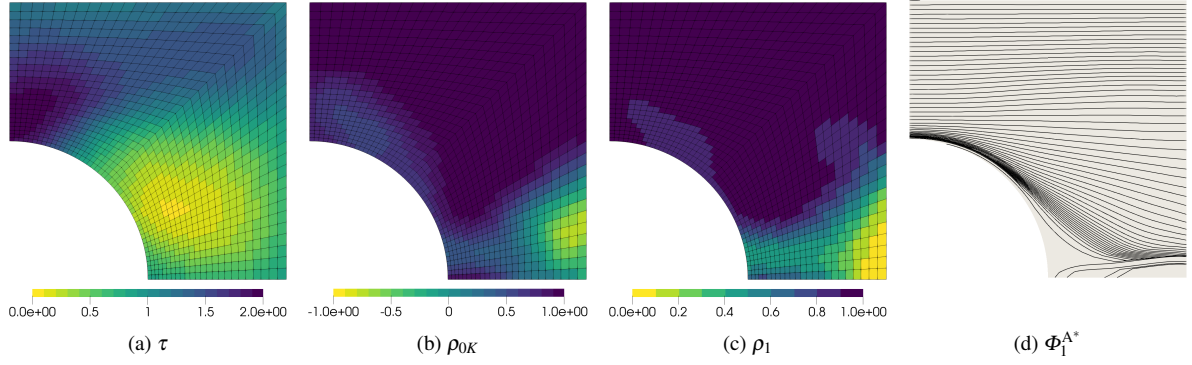


Fig. 6: Benchmark structure S1 - Optimisation problem P1 - VSCLs-C3: optimal distributions of the design variables.

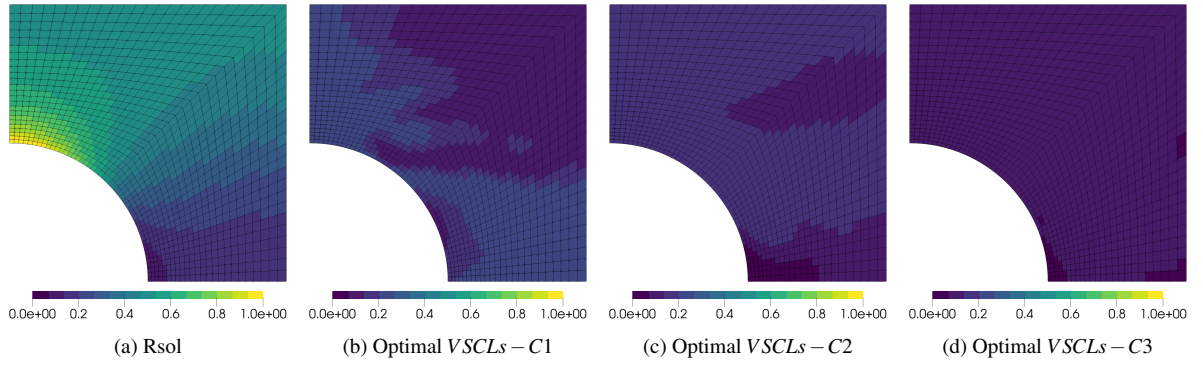


Fig. 7: Benchmark structure S1 - Optimisation problem P1: comparison of the distribution of  $1/\lambda_{F,e}$  for RSol and some optimised solutions.

Table 9: Summary of the solutions of problems P2 and P2c for benchmark structure S1.

| Design case  | $M/M_{\text{RSol}}$ | $\tau$   | $\rho_{0K}$ | $\rho_1$ | $\phi_1$ |
|--|---------------------|----------|-------------|----------|----------|
| RSol   | 1.00                | 1        | 0.00        | 0.00     | 0.00     |
| C1 (P2c - $\chi_{\text{Th}} = 1/250 \text{ mm}^{-1}$ ) | 0.30                | 0.30     | 0.63        | 0.87     | Fig. 8a  |
| C1 (P2c - $\chi_{\text{Th}} = 1/150 \text{ mm}^{-1}$ ) | 0.27                | 0.27     | 0.66        | 0.85     | Fig. 8b  |
| C1 (P2)  | 0.24                | 0.24     | 0.78        | 0.88     | Fig. 8c  |
| C2 (P2)  | 0.19                | 0.19     | Fig. 9a     | Fig. 9b  | Fig. 9c  |
| C3 (P2)  | 0.08                | Fig. 10a | Fig. 10b    | Fig. 10c | Fig. 10d |

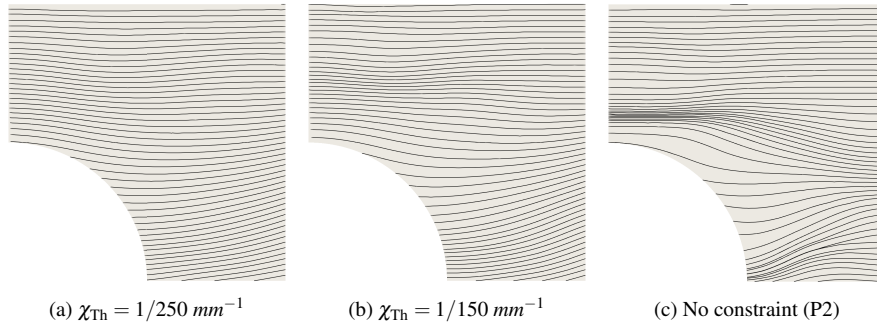


Fig. 8: Benchmark structure S1 - Optimisation problem P2c - VSCLs-C1: streamlines of the optimal distributions of the main orthotropy direction.

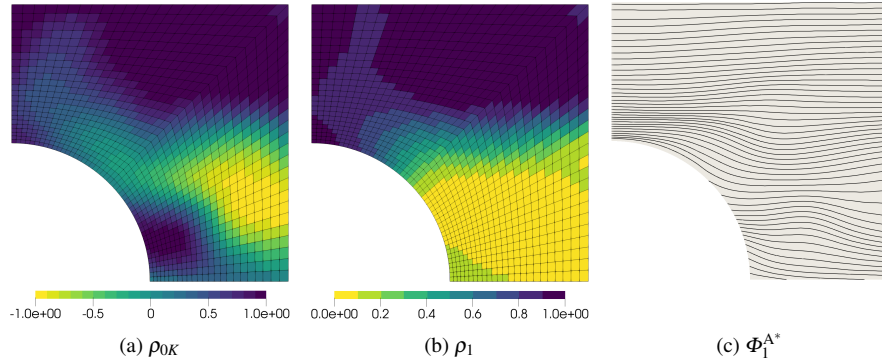


Fig. 9: Benchmark structure S1 - Optimisation problem P2 - VSCLs-C2: optimal distributions of the mechanical design variables.

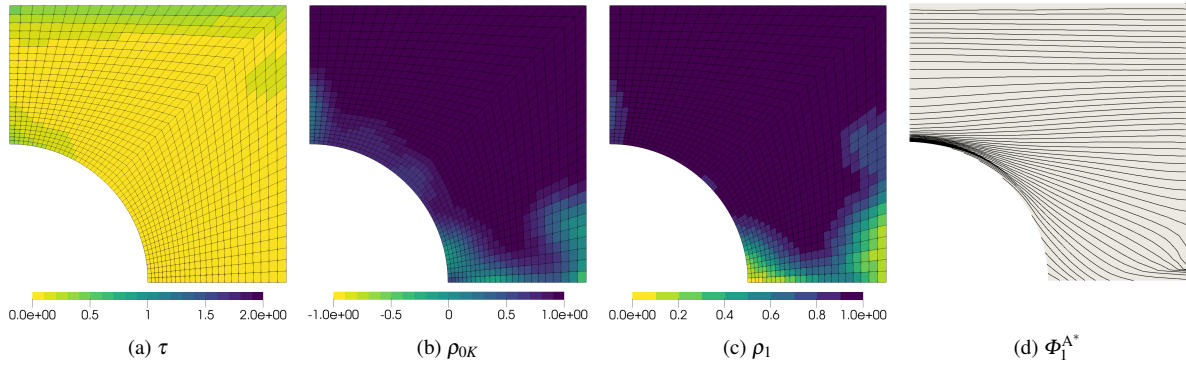


Fig. 10: Benchmark structure S1 - Optimisation problem P2 - VSCLs-C3: optimal distributions of the design variables.

The effect of the variation of  $\chi_{Th}$  can be seen in Tab. 8 and Fig. 3. The use of an increasing value of  $\chi_{Th}$  leads to:

- Solutions sharing the same type of orthotropy (the optimal values of  $\rho_{0K}$  are all positive).
- Solutions with a mechanical behaviour that is increasingly directional (because of the increase of optimal values of  $\rho_{0K}$  and stability of the optimal values of  $\rho_1$ ).
- Increasingly curved streamlines of the distributions of the main orthotropy direction.

The optimal distributions of the design variables for VSCLs-CL and VSCLs-C2 are shown in Figs. 4 and 5, respectively. The corresponding distribution of dimensionless PPs share some characteristics:

- In most of the upper half of the plate,  $\rho_{0K}$  and  $\rho_1$  assume a unit value. This corresponds to the behaviour of a mono-layer of fibres locally oriented as the main orthotropic direction.
- In the lower half of the plate, the mechanical behaviour of the optimal solution gradually evolve towards a square symmetry (because  $\rho_1$  is null) with a local change of the type of orthotropy ( $\rho_{0K}$  assumes both positive and negatives values).

Concerning the optimal VSCL-C2, the main orthotropy direction is mainly horizontal, except in the middle zone near the hole, where it follows the hole border (Fig. 5c).

Fig. 6 shows the optimal distributions of the design variables for VSCL-C3. The following remarks can be inferred:

- The optimisation takes full advantage of the possibility of having a non-uniform thickness. The upper half of the optimal plate is thicker than RSol ( $\tau \geq 1$ ), with the thickest region being at the apex of the hole (the most critical point for RSol, as clearly visible in Fig. 7a). The lower half is thinner than RSol ( $\tau \leq 1$ ). The thickness assumes values in the whole range  $[0, 2t_{RSol}]$  with an average value equal to  $t_{RSol}$ .
- Most of the plate surface (i.e. the region where  $\rho_{0K} = \rho_1 = 1$ ) behaves like a mono-layer of fibres locally parallel to the main orthotropic direction.
- In the lower half of the plate, a local change of the type of orthotropy occurs.
- The main orthotropy direction is mainly horizontal in the upper part of the plate, while it evolve to strictly follow the hole border in the lower part.

Regarding the whole set of results presented in this section, a common remark is that in all optimal solutions the upper half of the VSCL has higher stiffness in the horizontal direction than the lower half region. This is obtained either by only changing the local orientation of the main orthotropy direction (i.e. when dealing with VSCLs-C1), by locally tailoring the orthotropy shape (VSCLs-CL), or both (VSCLs-C2 and VSCLs-C3). Since, for this benchmark structure, the primary load direction is horizontal, this corresponds in a load transfer from the lower part of the VSCL to the upper one, which makes the stress concentration due to the hole presence vanish. This can be easily observed in Fig. 7 wherein the distribution of  $1/\lambda_{F,e}$  for RSol is compared to the distributions for the optimal VSCLs belonging to sub-classes C1, C2 and C3: it is clear how the stress concentration is avoided and a much more uniform, hence efficient, exploitation of the VSCL surface is obtained.

### 6.1.2 Optimisation problem P2/P2c

A summary of the results for optimisation problems P2/P2c on benchmark structure S1 is presented in Tab. 9. The results are completed by Figs. 8-10 that show the corresponding optimal distributions of non-uniform design variables.

The main remarks concerning the results presented in Tab. 9 are the following ones:

- All optimal solutions show considerable mass savings with values ranging from  $-70\%$  to  $-92\%$  with respect to RSol, while guaranteeing the same failure load.
- The trend already observed for solutions of problems P1/P1c appears: the performance of the optimal solutions increases by considering a less restrictive tow curvature constraint and by extending the design space. In particular, a weight saving of  $21\%$  is obtained by comparing the optimal VSCL-C2 to the optimal VSCL-C1, while an additional gain of  $58\%$  is obtained by adopting a VT solution (optimal VSCL-C3 over optimal VSCL-C2).

By comparing the results in Tabs. 8 and 9 (together with the related figures), one can easily notice that optimal VSCLs-C1 and VSCLs-C2 for problems P2/P2c are practically identical in terms of PPs fields to those of the corresponding dual problems P1/P1c. Of course, due to the different problem formulation, the thickness of corresponding solutions differs. This behaviour is expected because, when only membrane deformations are involved, the dependency of the LFI upon the thickness is separable from that upon the PPs, as it can be inferred from Eqs. (13-15). Considering VSCLs-C3, fewer similarities can be found: in this case, the local thickness variation generates a complete change of the stress distribution (not only of its overall intensity), making the two dependencies non-separable.

Due to these strong similarities, the remarks provided for the optimised solutions of problems P1/P1c can be repeated *verbatim* for the solutions of problem P2/P2c.

## 6.2 Benchmark structure S2

As described in Sec. 2.1, benchmark structure S2 withstands pressure and bi-axial tensile load. Due to the symmetric nature of the structure geometry and of external loads, all the obtained results concerning benchmark structure S2 show a double symmetry (with respect to the axes  $x = a$  and  $y = a$ ): for the sake of clarity, only the results of the region  $x, y \in [a, 2a]$  are presented.

### 6.2.1 Optimisation problem P1/P1c

The results of optimisation problems P1/P1c for benchmark structure S2 are presented in Tab. 10. The corresponding optimal distributions of non-uniform design variables are shown in Figs. 11-13.

The following remarks can be inferred from the analysis of the results listed in Tab. 10:

- Significant improvements in the load carrying capacity of the structure are obtained with an increase in the factor of safety with respect to RSol ranging from  $48\%$  to  $428\%$ .
- The trend observed on benchmark structure S1 holds also for benchmark structure S2 with an increase in the performance of the optimal solutions when considering a less restrictive tow curvature constraint and by moving from VSCLs-C1 to VSCLs-C3. In detail, optimal VSCL-C3 has a factor of safety  $138\%$  higher than that of the optimal VSCL-C2, in turn  $25\%$  higher than that of the best optimal VSCL-C1.

If the results presented in this section are compared to the corresponding ones presented in Sec. 6.1.1 (i.e. the solutions of problems P1/P1c on benchmark structure S1), it can be noticed that the factor of safety of the former are about half of those of the latter. At the same time, one can notice that optimal distributions of  $\rho_1$  are characterised by lower values, resulting in a general trend of the local elastic behaviour of the optimal VSCLs for benchmark structure S2 towards square orthotropy (where  $\rho_{0K} \neq 0$ ) or isotropy (where  $\rho_{0K}$  is almost 0). Both facts are consequence of the lower directionality of the loads acting on S2 in comparison to those acting on S1.

Looking at the optimal distributions of the dimensionless PPs for VSCLs-C2 (Fig. 12), it can be remarked that:

- $\rho_{0K}$  assumes values in the whole range  $[-1, 1]$  resulting in a continuous change of orthotropy type from the left and lower zones to the diagonal one.
- In large zones of the plate  $\rho_1 = 0$ : the local elastic behaviour is characterised by a square symmetry or isotropy.



Table 10: Summary of the solutions of problems P1 and P1c for benchmark structure S2.

| Solution  | $\lambda_F$ | $\tau$   | $\rho_{0K}$ | $\rho_1$ | $\phi_1$ |
|---|-------------|----------|-------------|----------|----------|
| RSol  | 1.00        | 1        | 0.00        | 0.00     | 0.00     |
| C1 (P1c - $\chi_{Th} = 1/250 \text{ mm}^{-1}$ ) | 1.48        | 1        | 0.55        | 0.24     | Fig. 11a |
| C1 (P1c - $\chi_{Th} = 1/150 \text{ mm}^{-1}$ ) | 1.60        | 1        | 0.70        | 0.23     | Fig. 11b |
| C1 (P1)   | 1.77        | 1        | 0.68        | 0.26     | Fig. 11c |
| C2 (P1)   | 2.22        | 1        | Fig. 12a    | Fig. 12b | Fig. 12c |
| C3 (P1)   | 5.28        | Fig. 13a | Fig. 13b    | Fig. 13c | Fig. 13d |

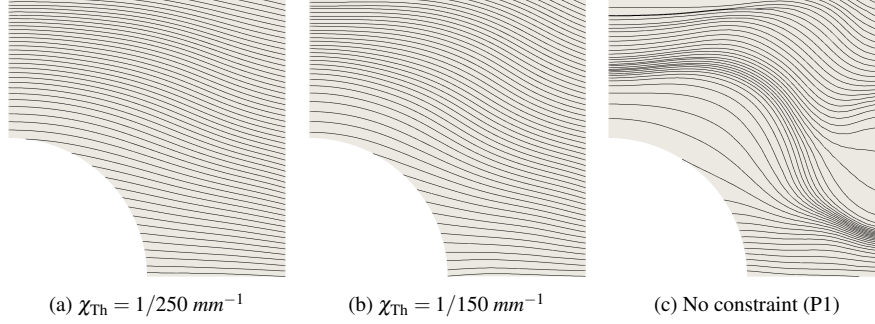


Fig. 11: Benchmark structure S2 - Optimisation problem P1c - VSCLs-C1: streamlines of the optimal distributions of the main orthotropy direction.

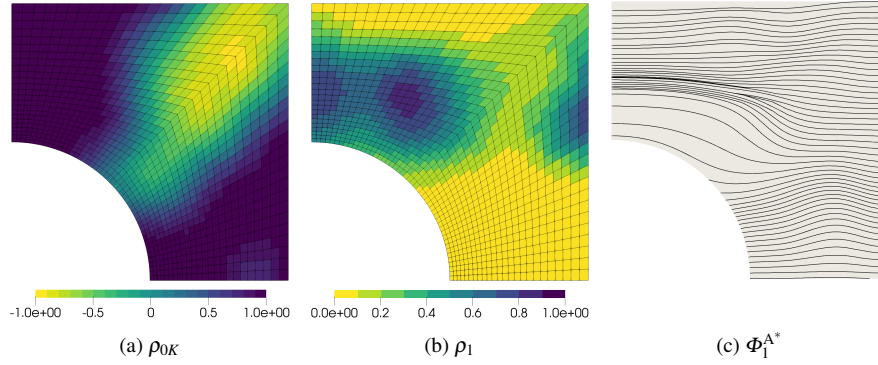


Fig. 12: Benchmark structure S2 - Optimisation problem P1 - VSCLs-C2: optimal distributions of the mechanical design variable.

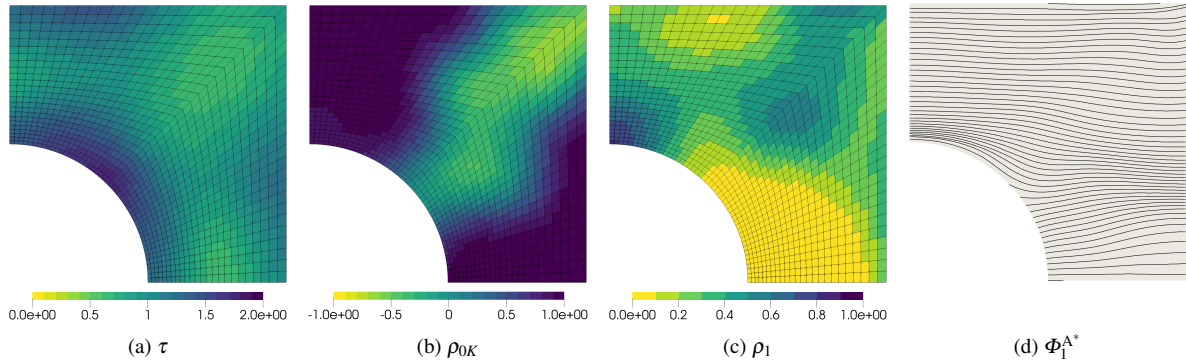


Fig. 13: Benchmark structure S2 - Optimisation problem P1 - VSCLs-C3: optimal distributions of the design variables.



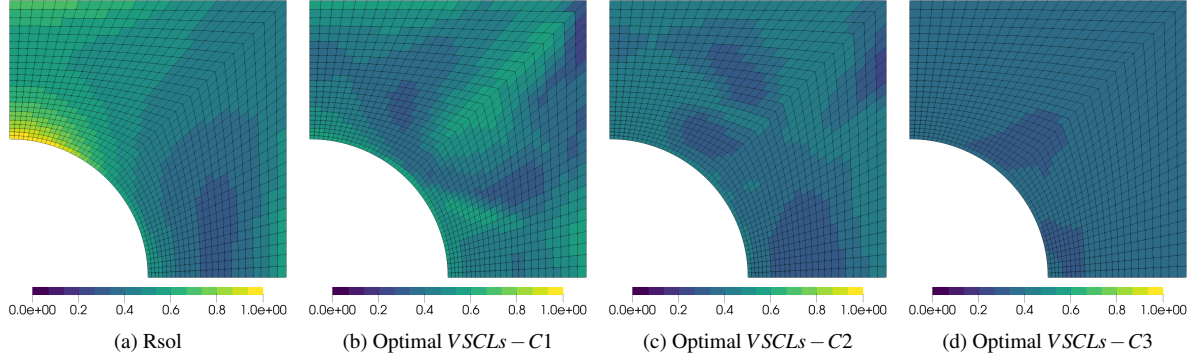


Fig. 14: Benchmark structure S2 - Optimisation problem P1: comparison of the distribution of  $1/\lambda_{F,e}$  for RSol and the optimised solutions.

Table 11: Summary of the solutions of problems P2 and P2c for benchmark structure S2.

| Design case  | $M/M_{\text{RSol}}$ | $\tau$   | $\rho_{0K}$ | $\rho_1$ | $\phi_1$ |
|--|---------------------|----------|-------------|----------|----------|
| RSol   | 1.00                | 1        | 0.00        | 0.00     | 0.00     |
| C1 (P2c - $\chi_{\text{Th}} = 1/250 \text{ mm}^{-1}$ ) | 0.76                | 0.76     | 0.65        | 0.21     | Fig. 15a |
| C1 (P2c - $\chi_{\text{Th}} = 1/150 \text{ mm}^{-1}$ ) | 0.72                | 0.72     | 0.79        | 0.185    | Fig. 15b |
| C1 (P2)  | 0.68                | 0.68     | 0.84        | 0.20     | Fig. 15c |
| C2 (P2)  | 0.58                | 0.58     | Fig. 16a    | Fig. 16b | Fig. 16c |
| C3 (P2)  | 0.43                | Fig. 17a | Fig. 17b    | Fig. 17c | Fig. 17d |

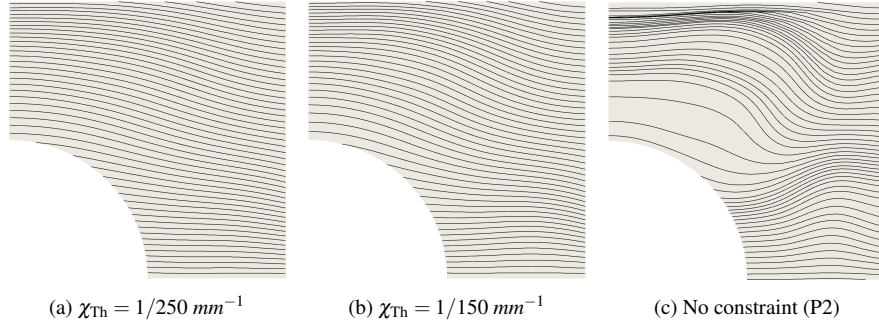


Fig. 15: Benchmark structure S2 - Optimisation problem P2c - VSCLs-C1: streamlines of the optimal distributions of the main orthotropy direction.

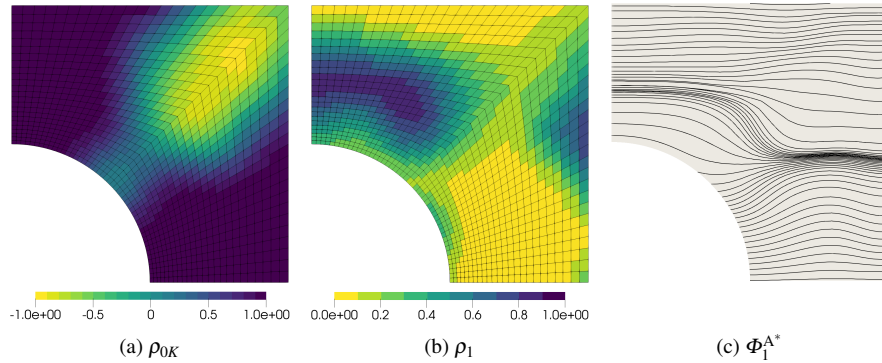


Fig. 16: Benchmark structure S2 - Optimisation problem P2 - VSCLs-C2: optimal distributions of the mechanical design variables.

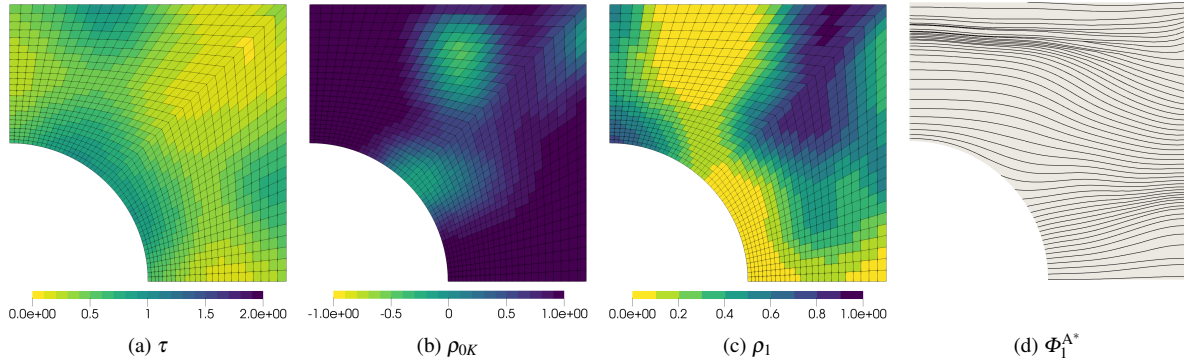


Fig. 17: Benchmark structure S2 - Optimisation problem P2 - VSCLs-C3: optimal distributions of the design variables.

Similar considerations can be done for the results obtained for sub-class VSCL-C3 (Fig. 13). Looking at the optimal thickness distribution in Fig. 13a, one can notice that the thickness variation is more limited on S2 than in the corresponding optimised solution for benchmark structure S1 (Fig. 6a) and that the whole hole edge region is here thicker than the average thickness of the plate, which is equal to  $t_{\text{RSol}}$ .

Finally, also for benchmark structure S2, a much more uniform distribution of  $1/\lambda_{F,e}$  can be obtained through optimisation in comparison to the one for RSol, as illustrated in Fig. 14.

### 6.2.2 Optimisation problem P2/P2c

A summary of the results for optimisation problems P2/P2c on benchmark structure S2 is provided in Tab. 11. Such table is completed by Figs. 15-17 that show the corresponding optimal distributions of non-uniform design variables.

Looking at the results of Tab. 11, it can be inferred that:

- All optimal solutions show significant mass savings with values from  $-24\%$  to  $-57\%$  with respect to RSol, while guaranteeing the same failure load.
- Better optimal solutions can be obtained by considering a less restrictive tow curvature constraint and by moving between considered VSCLs sub-classes: in the passage from VSCL-C1 to VSCL-C2 and then to VSCL-C3, relative weight savings of 15% and 26%, respectively, are registered.

Results of optimisation problems P2/P2c and P1/P1c on benchmark structure S2 show some similarities, therefore most of the comments provided in Sec. 6.2.1 apply to the results of this section too. Nevertheless, unlike what seen on the results obtained for benchmark structure S1, here the similarities are less pronounced. This happens because the contribution to the evaluation of the LFI related to bending deformations depends upon the thickness of the

laminate differently from the contributions related to membrane and transverse shear deformations, making impossible to separate the dependency of the LFI upon the thickness to that upon the PPs.

## 7 Conclusions

A general theoretical and numerical framework for the deterministic optimisation of variable-stiffness composite laminates involving requirements on mass, strength, and maximum tow curvature has been presented in this work. The optimisation is performed in the context of the first-level problem of the multi-scale two-level optimisation strategy for variable-stiffness composite laminates, hence at the laminate macroscopic scale. It makes use of two main ingredients: **a)** the polar method for the description of the local macroscopic elastic and strength properties of the laminates in the framework of the first-order shear deformation theory; **b)** B-spline entities for representing the distribution of the design variables.

The presented framework allows for either the global (uniform over the structure) or local (point-wise variable) tailoring of various properties of variable-stiffness composite laminates: the orthotropy type and shape, the direction of the main orthotropy axis, the thickness of the laminate. Depending on the design variables definition, various sub-classes of variable-stiffness composite laminates are identified. Optimal solutions are searched within each of these variable-stiffness composite laminates sub-classes. Among them, the most *basic* one, i.e. variable-stiffness composite laminates for which only the direction of the main orthotropy axis varies point-wise, corresponds to laminates for which suitable stacks of fibres-paths can already be retrieved in the framework of the second-level problem of the multi-scale two-level optimisation strategy. Conversely, for the other sub-classes, the numerical tools and/or the manufacturing technologies are not mature enough yet. These sub-classes are used to show the theo-

retical full potential of variable-stiffness composite laminates.

Both the failure load maximisation problem (with a constraint on the variable-stiffness composite laminate mass) and the mass minimisation one (with a constraint of the variable-stiffness composite laminate strength) are solved for two benchmark structures: the first benchmark structure is used to highlight stress concentration under in-plane load, while the second one, which also withstands out-of-plane loads, has been considered to emphasise bending and shear effects. The strength is evaluated in terms of the failure load of the structure, which is computed by applying a laminate-level failure criterion based on tensor invariants. The analytical expression of the failure load and its sensitivity to the design variables is derived and implemented in this work, taking full advantage of the properties of the B-spline entities. The effect of a constraint on the maximum tow curvature is also evaluated. To this purpose, an improved conservative formulation of the tow curvature constraint (and its gradient) in the space of polar parameters is also presented. Finally, thanks to the introduction of a shrewd change of variable, the point-wise feasibility requirement (on the existence of a suitable stack) is intrinsically satisfied without introducing explicit constraint functions in the problem formulation.

As far as numerical results are concerned, considerable improvements with respect to both reference and optimised solutions taken from the literature have been obtained through the proposed strategy. When optimising for strength, depending on the considered variable-stiffness composite laminates sub-class, the failure load can be increased between 234% and 1034%, for benchmark structure S1, and between 48% and 428%, for benchmark structure S2, with respect to the failure load of isotropic solutions. While, when optimising for lightness, the obtained mass reduction is in the range 70-92% or 24-75%, for benchmark structures S1 and S2, respectively.

Strength-driven results obtained for benchmark structure S1 have also been compared to an optimised solution taken from literature, obtained through the use of lamination parameters for the representation of macroscopic elastic properties of the variable-stiffness composite laminate: the proposed approach was able to provide solutions with an increase in the failure load between 4% and 252%, with the most comparable solution (in terms of explored design space) showing an improvement of 21%.

For one of the considered variable-stiffness composite laminates sub-classes, both the material elastic properties and the thickness are locally optimised. The optimised variable-stiffness composite laminates belonging to this sub-class represent theoretical best solutions to the respective problems. The additional possibility to also optimise the thickness distribution makes possible to obtain increases of 116-138% of the failure load or a weight saving

of 26-58%, over the corresponding best uniform-thickness solutions.

These results unequivocally show the effectiveness of the proposed optimisation strategy and the great potential of considered variable-stiffness composite laminates sub-classes motivating further research activities on this topic. Ongoing and future activities include: the application of the developed tools to the optimisation of real-life complex structures including multiple requirements; the development of the numerical tools associated to the second-level problem of the multi-scale two-level optimisation strategy to be able to retrieve stacks of fibres-paths for all presented variable-stiffness composite laminates sub-classes; the formulation of new criteria to predict the presence of manufacturing-related defects, like tows gaps and/or overlaps, in the final structure and to account for their effect on the performances since the early design phases.

### A On the choice of the threshold value of the laminate failure index

In Eq. (12), the LFI is defined as the integral average over the laminate thickness of the ply-level failure index (PFI) defined in Eq. (10).

If a laminate is subjected to a given loading condition, with a given load factor  $\lambda$ , such that the maximum value (over the surface) of the LFI is  $F = 1$ , two situations may occur:

- The most probable situation wherein some of the layers of the laminate have a PFI greater than one, while the others have a PFI lower than one.
- The unlikely situation wherein the PFI is uniform over the thickness and assumes a unit value.

In the first scenario, the failure of the structure has already been overcome, i.e. failure occurred at a load factor lower than the considered one. For such a reason, using a threshold value  $F_{Th} = 1$  represents a non-conservative choice.

On the other end of the spectrum, if the maximum LFI is  $F = 1/N_{ply}$ , where  $N_{ply}$  is the number of plies composing the laminate, it may mean that:

- Likely, the PFI assumes values both greater and lower than  $1/N_{ply}$ , but always lower than one.
- In the limit and unrealistic case, the PFI is equal to one in only one of the layers, while it is null in all the others.

Clearly, using a threshold value  $F_{Th} = 1/N_{ply}$  results in an over-conservative constraint. An intermediate value has to be used.

In this appendix, the effect of the use of different threshold values for the application of the LFI introduced in Sec. 3.2 on the optimised solution is assessed. Three possible values are considered: the two extreme values,  $F_{Th} = 1$  and  $F_{Th} = 1/N_{ply}$ , and an intermediate one,  $F_{Th} = 1/2$ , i.e. the value used to obtain the main results of this work. The effect of this choice is shown by solving optimisation problem P1 on benchmark structure S1 for VSCLs-C2. Of course, the value of the reference load is adapted to the chosen value of  $F_{Th}$  (see Sec. 2.1). The laminate is considered composed of 16 plies, as in the work by Khani et al. (2011). The results are summarised in Tab. A.1, which is completed by Fig. A.1.

From the analysis of the results presented in Tab. A.1, it can be observed that by decreasing the value of  $F_{Th}$ , even if the absolute value of the failure load ( $\bar{F}_{x,F}$ ) decreases, the possible relative gain on the failure load, represented by the load factor  $\lambda_F$ , increases. This means that, if the use of a more conservative (i.e. lower) value of  $F_{Th}$  reveals

Table A.1: Summary of the VSCLs-C2 solutions of problem P1 on benchmark structure S1 for different values of  $F_{Th}$ .

| Solution        | $\bar{F}_x$ [N] | $\bar{F}_{x,F}$ [N] | $\lambda_F$ | $\tau$ | $\rho_{0K}$ | $\rho_1$  | $\phi_1$  |
|-----------------|-----------------|---------------------|-------------|--------|-------------|-----------|-----------|
| LSol            | -               | -                   | 3.22        | 1      | -           | -         | -         |
| $F_{Th} = 1$    | 122000          | 597556              | 4.90        | 1      | Fig. A.1a   | Fig. A.1b | Fig. A.1c |
| $F_{Th} = 1/2$  | 79000           | 413960              | 5.24        | 1      | Fig. A.1d   | Fig. A.1e | Fig. A.1f |
| $F_{Th} = 1/16$ | 17200           | 147404              | 8.57        | 1      | Fig. A.1g   | Fig. A.1h | Fig. A.1i |

necessary, a higher  $\lambda_F$  of the optimised solutions will be obtained. Finally, it is noteworthy that, whichever the choice of the value  $F_{Th}$  used, the found load factor is greater than that obtained by Khani et al. (2011)<sup>2</sup>.

A study about the choice of  $F_{Th}$  is part of the current research activities of the group.

## B Setting the p-Norm for a given maximum relative difference

Consider an indexed set of positive values ( $q_e \geq 0$  with  $e \in \{1, 2, \dots, N_e\}$ ) whose maximum is  $q_{\max} := \max_e q_e$ . In agreement with Eq. (27),

$$pn(q_e) := \left( \sum_e q_e^p \right)^{1/p} = q_{\max} \left( \sum_e \eta_e^p \right)^{1/p}, \quad \text{with } \eta_e := q_e / q_{\max}. \quad (\text{B.1})$$

Since  $0 \leq \eta_e \leq 1$  and  $\max_e \eta_e = 1$ ,

$$1 \leq \left( \sum_e \eta_e^p \right)^{1/p} \leq N_e^{1/p} \quad (\text{B.2})$$

and, consequently,

$$q_{\max} \leq pn(q_e) \leq q_{\max} N_e^{1/p}. \quad (\text{B.3})$$

If a maximum relative difference  $d_{\max}$  is prescribed between the value of the p-Norm and the value  $q_{\max}$ , one can write

$$q_{\max} N_e^{1/p} \leq q_{\max} (1 + d_{\max}), \quad (\text{B.4})$$

which is satisfied if

$$p \geq \frac{\log N_e}{\log(1 + d_{\max})}. \quad (\text{B.5})$$

If  $p$  is required to be an integer, then it suffices to set

$$p_{\min} = \left\lceil \frac{\log N_e}{\log(1 + d_{\max})} \right\rceil. \quad (\text{B.6})$$

## C Failure response function gradient

According to Eqs. (38) and (30),

$$\frac{\partial f_F}{\partial \xi^{(i_1, i_2)}} = \frac{\partial \left( pn(\lambda_{F,e}^{-1}) \right)}{\partial \xi^{(i_1, i_2)}} = -(f_F + 1)^{1-p} \sum_e \left[ \lambda_{F,e}^{-(p+1)} \frac{\partial \lambda_{F,e}}{\partial \xi^{(i_1, i_2)}} \right]. \quad (\text{C.1})$$

<sup>2</sup> Unfortunately, no data are provided about the value of neither the reference load, nor the failure load of their optimised solutions.

The factor of safety of the  $e$ -th element reads

$$\lambda_{F,e} = \frac{\lambda_{FN,e}}{\lambda_{FD,e}} = \frac{-L_e + \sqrt{\Delta_e}}{2Q_e}, \quad \text{with } \Delta_e := L_e^2 + 4Q_e F_{Th}. \quad (\text{C.2})$$

The derivative of  $\lambda_{F,e}$  with respect to the design variable  $\xi^{(i_1, i_2)}$  is

$$\frac{\partial \lambda_{F,e}}{\partial \xi^{(i_1, i_2)}} = \frac{1}{\lambda_{FD,e}} \left( \frac{\partial \lambda_{FN,e}}{\partial \xi^{(i_1, i_2)}} - \lambda_{F,e} \frac{\partial \lambda_{FD,e}}{\partial \xi^{(i_1, i_2)}} \right), \quad (\text{C.3})$$

where the derivatives of the quantities  $\lambda_{FN,e}$  and  $\lambda_{FD,e}$  read:

$$\begin{aligned} \frac{\partial \lambda_{FN,e}}{\partial \xi^{(i_1, i_2)}} &= -\frac{\partial L_e}{\partial \xi^{(i_1, i_2)}} + \frac{L_e}{\sqrt{\Delta_e}} \frac{\partial L_e}{\partial \xi^{(i_1, i_2)}} + 2F_{Th} \frac{\partial Q_e}{\partial \xi^{(i_1, i_2)}}, \\ \frac{\partial \lambda_{FD,e}}{\partial \xi^{(i_1, i_2)}} &= 2 \frac{\partial Q_e}{\partial \xi^{(i_1, i_2)}}. \end{aligned} \quad (\text{C.4})$$

By injecting Eq. (C.4) in Eq. (C.3), one obtains

$$\frac{\partial \lambda_{F,e}}{\partial \xi^{(i_1, i_2)}} = c_{2,e} \frac{\partial Q_e}{\partial \xi^{(i_1, i_2)}} + c_{1,e} \frac{\partial L_e}{\partial \xi^{(i_1, i_2)}}, \quad (\text{C.5})$$

where

$$c_{2,e} = \frac{F_{Th} - \lambda_{F,e} \sqrt{\Delta_e}}{Q_e \sqrt{\Delta_e}}, \quad c_{1,e} = -\frac{\lambda_{F,e}}{\sqrt{\Delta_e}}. \quad (\text{C.6})$$

The derivatives of the terms  $Q_e$  and  $L_e$  can be inferred from Eqs. (34) and (35):

$$\begin{aligned} \frac{\partial Q_e}{\partial \xi^{(i_1, i_2)}} &= \mathbf{e}_{\text{Ref},e}^T \frac{\partial}{\partial \xi^{(i_1, i_2)}} \left( \frac{\mathbf{G}_{\text{lam},e}}{t_e} \right) \mathbf{e}_{\text{Ref},e} \\ &\quad + 2 \mathbf{e}_{\text{Ref},e}^T \frac{\mathbf{G}_{\text{lam},e}^T}{t_e} \mathfrak{B}_e \mathfrak{L}_e \frac{\partial \mathbf{u}_{\text{Ref}}}{\partial \xi^{(i_1, i_2)}}, \end{aligned} \quad (\text{C.7})$$

$$\frac{\partial L_e}{\partial \xi^{(i_1, i_2)}} = \mathbf{e}_{\text{Ref},e}^T \frac{\partial}{\partial \xi^{(i_1, i_2)}} \left( \frac{\mathbf{g}_{\text{lam},e}}{t_e} \right) + \frac{\mathbf{g}_{\text{lam},e}^T}{t_e} \mathfrak{B}_e \mathfrak{L}_e \frac{\partial \mathbf{u}_{\text{Ref}}}{\partial \xi^{(i_1, i_2)}},$$

By injecting Eq. (C.7) in Eq. (C.5), one obtains

$$\begin{aligned} \frac{\partial \lambda_{F,e}}{\partial \xi^{(i_1, i_2)}} &= \mathbf{e}_{\text{Ref},e}^T \left( c_{2,e} \frac{\partial (\mathbf{G}_{\text{lam},e}/t_e)}{\partial \xi^{(i_1, i_2)}} \mathbf{e}_{\text{Ref},e} + c_{1,e} \frac{\partial (\mathbf{g}_{\text{lam},e}/t_e)}{\partial \xi^{(i_1, i_2)}} \right) \\ &\quad + \mathbf{\Psi}_e^T \frac{\partial \mathbf{u}_{\text{Ref}}}{\partial \xi^{(i_1, i_2)}}, \end{aligned} \quad (\text{C.8})$$

where  $\mathbf{\Psi}_e$  is defined as

$$\mathbf{\Psi}_e := \mathfrak{L}_e^T \mathfrak{B}_e^T \left( 2c_{2,e} \frac{\mathbf{G}_{\text{lam},e}}{t_e} \mathbf{e}_{\text{Ref},e} + c_{1,e} \frac{\mathbf{g}_{\text{lam},e}}{t_e} \right). \quad (\text{C.9})$$

By injecting Eq. (C.8) in Eq. (C.1) and by taking into account for the B-spline blending functions local support property, one obtains

$$\begin{aligned} \frac{\partial f_F}{\partial \xi^{(i_1, i_2)}} &= -(f_F + 1)^{1-p} \left\{ \sum_{e \in \mathcal{S}_{i_1 i_2}} \left[ \lambda_{F,e}^{-(p+1)} \frac{\partial \xi_e}{\partial \xi^{(i_1, i_2)}} \right. \right. \\ &\quad \cdot \left. \mathbf{e}_{\text{Ref},e}^T \left( c_{2,e} \frac{\partial (\mathbf{G}_{\text{lam},e}/t_e)}{\partial \xi_e} \mathbf{e}_{\text{Ref},e} + c_{1,e} \frac{\partial (\mathbf{g}_{\text{lam},e}/t_e)}{\partial \xi_e} \right) \right. \\ &\quad \left. \left. + \mathbf{\Psi}_e^T \frac{\partial \mathbf{u}_{\text{Ref}}}{\partial \xi^{(i_1, i_2)}} \right] \right\}, \end{aligned}$$

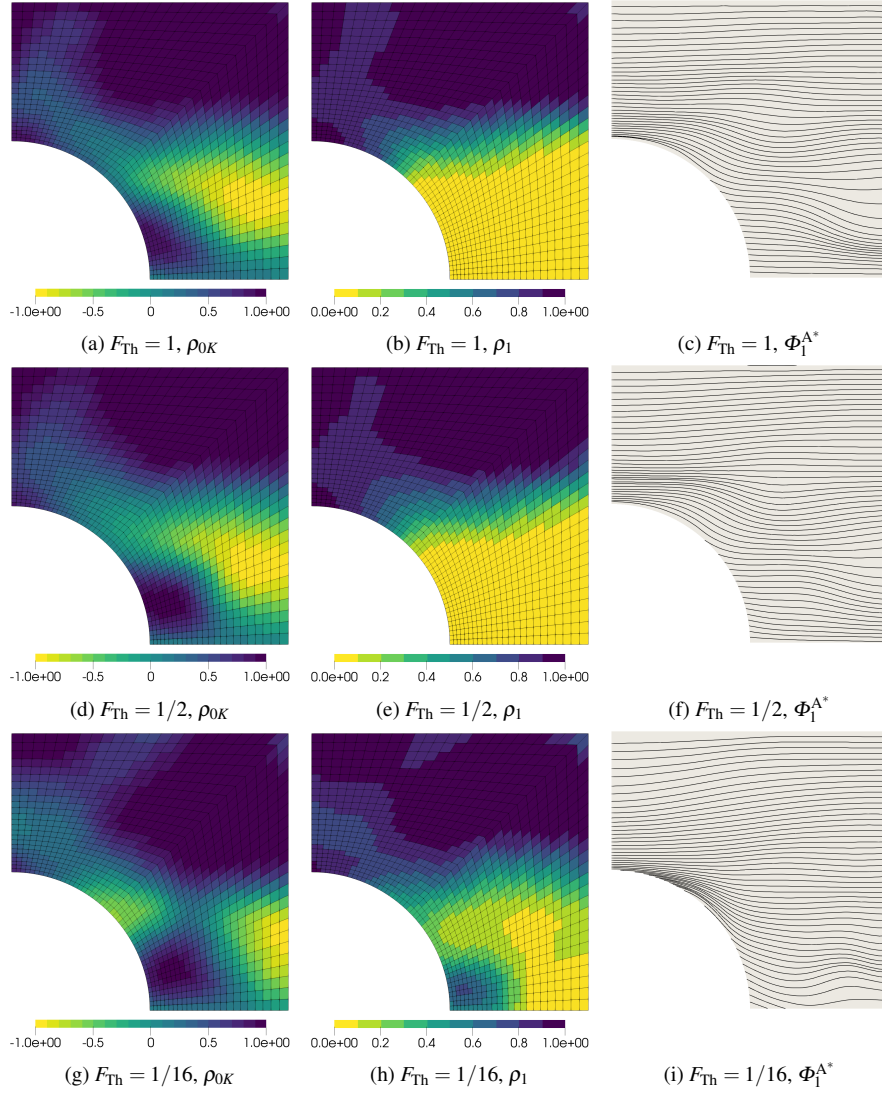


Fig. A.1: Benchmark structure S1 - Optimisation problem P1 - VSCLs-C2: optimal distributions of the mechanical design variables obtained with different values of  $F_{Th}$ .

where

$$\boldsymbol{\psi} := \sum_e \left[ \lambda_{F,e}^{-(p+1)} \boldsymbol{\psi}_e \right].$$

Consider the upper part of Eq. (26), with  $\lambda = 1$ :

$$\mathbf{K}_{FF}^* \mathbf{u}_{Ref,F}^* + \mathbf{K}_{FD}^* \mathbf{u}_{Ref,D}^* = \mathbf{f}_{Ref,F}^*.$$

Inasmuch as external forces and known DOFs do not depend upon the design variables of the problem at hand, i.e.

$$\frac{\partial \mathbf{f}_{Ref,F}^*}{\partial \xi^{(i_1, i_2)}} = \mathbf{0} \quad \text{and} \quad \frac{\partial \mathbf{u}_{Ref,D}^*}{\partial \xi^{(i_1, i_2)}} = \mathbf{0}, \quad (C.13)$$

the derivative of Eq. (C.12) reads

$$\mathbf{K}_{FF}^* \frac{\partial \mathbf{u}_{Ref,F}^*}{\partial \xi^{(i_1, i_2)}} + \frac{\partial \mathbf{K}_{FF}^*}{\partial \xi^{(i_1, i_2)}} \mathbf{u}_{Ref,F}^* + \frac{\partial \mathbf{K}_{FD}^*}{\partial \xi^{(i_1, i_2)}} \mathbf{u}_{Ref,D}^* = \mathbf{0}. \quad (C.14)$$

(C.10) Consider now the arbitrary auxiliary vector  $\boldsymbol{\mu}$ , which can be re-

ordered such that  $\boldsymbol{\mu}^{*T} := \{ \boldsymbol{\mu}_F^{*T}, \boldsymbol{\mu}_D^{*T} \}$ . If the components of such vector corresponding to the known DOFs of Eq. (26) are set null, i.e.  $\boldsymbol{\mu}_D^* = \mathbf{0}$ , the following relation holds:

$$\begin{aligned} \boldsymbol{\psi}^T \frac{\partial \mathbf{u}_{Ref}^*}{\partial \xi^{(i_1, i_2)}} &= \left\{ \begin{matrix} \boldsymbol{\psi}_F^* \\ \boldsymbol{\psi}_D^* \end{matrix} \right\}^T \frac{\partial}{\partial \xi^{(i_1, i_2)}} \left\{ \begin{matrix} \mathbf{u}_{Ref,F}^* \\ \mathbf{u}_{Ref,D}^* \end{matrix} \right\} \\ &= \boldsymbol{\psi}_F^{*T} \frac{\partial \mathbf{u}_{Ref,F}^*}{\partial \xi^{(i_1, i_2)}} + \underbrace{\boldsymbol{\psi}_D^{*T} \frac{\partial \mathbf{u}_{Ref,D}^*}{\partial \xi^{(i_1, i_2)}}}_{=0} \\ &\quad + \underbrace{\boldsymbol{\mu}_F^{*T} \left( \mathbf{K}_{FF}^* \frac{\partial \mathbf{u}_{Ref,F}^*}{\partial \xi^{(i_1, i_2)}} + \frac{\partial \mathbf{K}_{FF}^*}{\partial \xi^{(i_1, i_2)}} \mathbf{u}_{Ref,F}^* + \frac{\partial \mathbf{K}_{FD}^*}{\partial \xi^{(i_1, i_2)}} \mathbf{u}_{Ref,D}^* \right)}_{=0} \\ &\quad + \underbrace{\boldsymbol{\mu}_D^{*T}}_{=0} \left( \frac{\partial \mathbf{K}_{DF}^*}{\partial \xi^{(i_1, i_2)}} \mathbf{u}_{Ref,F}^* + \frac{\partial \mathbf{K}_{DD}^*}{\partial \xi^{(i_1, i_2)}} \mathbf{u}_{Ref,D}^* \right), \end{aligned} \quad (C.11)$$

(C.15)

where the last null term is added for the sole purpose of obtaining a more compact expression. Eq. (C.15) simplifies to

$$\Psi^T \frac{\partial \mathbf{u}_{\text{Ref}}}{\partial \xi^{(i_1, i_2)}} = \left( \Psi_F^T + \mu_F^T \mathbf{K}_{\text{FF}}^* \right) \frac{\partial \mathbf{u}_{\text{Ref}, F}^*}{\partial \xi^{(i_1, i_2)}} + \mu^T \frac{\partial \mathbf{K}}{\partial \xi^{(i_1, i_2)}} \mathbf{u}_{\text{Ref}}. \quad (\text{C.16})$$

Consider the term  $\frac{\partial \mathbf{K}}{\partial \xi^{(i_1, i_2)}} \mathbf{u}_{\text{Ref}}$  in Eq. (C.16). The stiffness matrix of the structure is defined as

$$\mathbf{K} := \sum_e \mathfrak{L}_e^T \mathbf{K}_e \mathfrak{L}_e. \quad (\text{C.17})$$

$\mathbf{K}_e$  is the stiffness matrix of the element and, for a shell element, it is defined as:

$$\mathbf{K}_e := \int_{A_e} \mathfrak{B}_e^T \mathbf{K}_{\text{lam}, e} \mathfrak{B}_e dS, \quad (\text{C.18})$$

where,  $A_e$  is the area of  $e$ -th element. By taking into account for Eqs. (C.17) and (C.18) and for the local support property, the term  $\frac{\partial \mathbf{K}}{\partial \xi^{(i_1, i_2)}} \mathbf{u}_{\text{Ref}}$  in Eq. (C.16) can be expressed as:

$$\begin{aligned} \tilde{\Psi}_{i_1 i_2} &:= \frac{\partial \mathbf{K}}{\partial \xi^{(i_1, i_2)}} \mathbf{u}_{\text{Ref}} \\ &= \sum_{e \in S_{i_1 i_2}} \left[ \frac{\partial \xi_e}{\partial \xi^{(i_1, i_2)}} \int_{A_e} \mathfrak{L}_e^T \mathfrak{B}_e^T \frac{\partial \mathbf{K}_{\text{lam}, e}}{\partial \xi_e} \mathfrak{B}_e \mathfrak{L}_e dS \right] \mathbf{u}_{\text{Ref}}. \end{aligned} \quad (\text{C.19})$$

The arbitrary vector  $\mu_F^*$  can be chosen in such a way that the term multiplying  $\frac{\partial \mathbf{u}_{\text{Ref}, F}^*}{\partial \xi^{(i_1, i_2)}}$  vanishes, i.e.

$$\mathbf{K}_{\text{FF}}^* \mu_F^* = -\Psi_F^*. \quad (\text{C.20})$$

By using Eq. (C.19) and the expression of  $\mu_F^*$  obtained by solving the auxiliary system of Eq. (C.20), Eq. (C.16) simplifies to

$$\Psi^T \frac{\partial \mathbf{u}_{\text{Ref}}}{\partial \xi^{(i_1, i_2)}} = \mu^T \tilde{\Psi}_{i_1 i_2}. \quad (\text{C.21})$$

Therefore, the final expression of the generic component of the gradient of  $f_F$  is

$$\frac{\partial f_F}{\partial \xi^{(i_1, i_2)}} = -(f_F + 1)^{1-p} \{ l_{i_1 i_2} + \mu^T \tilde{\Psi}_{i_1 i_2} \}, \quad (\text{C.22})$$

with

$$\begin{aligned} l_{i_1 i_2} &:= \sum_{e \in S_{i_1 i_2}} \left[ \lambda_{F, e}^{-(p+1)} \frac{\partial \xi_e}{\partial \xi^{(i_1, i_2)}} \right. \\ &\quad \cdot \left. \mathfrak{E}_{\text{Ref}, e}^T \left( c_{2, e} \frac{\partial (\mathbf{G}_{\text{lam}, e} / t_e)}{\partial \xi_e} \mathfrak{E}_{\text{Ref}, e} + c_{1, e} \frac{\partial (\mathbf{g}_{\text{lam}, e} / t_e)}{\partial \xi_e} \right) \right]. \end{aligned} \quad (\text{C.23})$$

**Remark C.1** The analytic expression of the derivatives  $\frac{\partial \mathbf{K}_{\text{lam}, e}}{\partial \xi_e}$ ,  $\frac{\partial}{\partial \xi_e} \left( \frac{\mathbf{g}_{\text{lam}, e}}{t_e} \right)$  and  $\frac{\partial}{\partial \xi_e} \left( \frac{\mathbf{G}_{\text{lam}, e}}{t_e} \right)$  appearing in the above formulae is provided in Appendix D.

**Remark C.2** The solution of the auxiliary system of Eq. (C.20), needed to compute the gradient of  $f_F$ , can be obtained through a FE analysis wherein all DOFs corresponding to the known DOFs of Eq. (26) are set null (i.e.  $\mu_D^* = \mathbf{0}$ ) and whose generalised external nodal forces  $\Psi$  are computed using Eq. (C.11). Of course, the components of  $\Psi$  corresponding to the known DOFs of Eq. (26), i.e.  $\Psi_D$ , are discarded by the FE solver because applied on constrained DOFs.

## D Analytical expression of the laminate stiffness and strength matrices and vector and their gradient

**Remark D.1** The hypotheses of point-wise fully orthotropy and quasi-homogeneity of the considered VSCLs (corresponding to the conditions of Eq. (7)) hold in the following.

All quantities in this section are referred to a generic element  $e$  of the structure model, but the index  $e$  is omitted for the sake of readability.

Using Eq. (6), Eq. (5) can be rewritten as

$$\mathbf{K}_{\text{lam}} = \begin{bmatrix} t \mathbf{A}^* & \mathbf{0} & \mathbf{0} \\ \frac{t^3}{12} \mathbf{A}^* & \mathbf{0} & \mathbf{0} \\ \text{sym} & t \mathbf{H}^* & \end{bmatrix}. \quad (\text{D.1})$$

Matrices  $\mathbf{A}^*$  and  $\mathbf{H}^*$  can be computed as a function of their PPs, thanks to Eqs. (2) and (1). The PPs of matrix  $\mathbf{A}^*$  can be obtained by means of Eq. (17) as

$$\begin{aligned} T_0^{A^*} &\equiv T_0^{Q_{\text{in}}}, \quad T_1^{A^*} \equiv T_1^{Q_{\text{in}}}, \quad R_0^{A^*} = R_0^{Q_{\text{in}}} |\rho_{0K}|, \quad R_1^{A^*} = R_1^{Q_{\text{in}}} \rho_1, \\ \Phi_0^{A^*} &= \Phi_1^{A^*} + \frac{\pi}{4} K^{A^*}, \quad \Phi_1^{A^*} = \frac{\pi}{2} \phi_1, \end{aligned} \quad (\text{D.2})$$

where

$$K^{A^*} = \begin{cases} 0 & \text{if } \rho_{0K} \geq 0, \\ 1 & \text{if } \rho_{0K} < 0, \end{cases} \quad (\text{D.3})$$

and can be related to the problem design variables through Eq. (20). The PPs of matrix  $\mathbf{H}^*$  depend upon those of  $\mathbf{A}^*$  and of the constitutive tow as follows (Montemurro, 2015b,a):

$$T^{H^*} = T^{Q_{\text{in}}}, \quad R^{H^*} = \frac{R^{Q_{\text{out}}}}{R_1^{Q_{\text{in}}}} R_1^{A^*}, \quad \Phi^{H^*} = \Phi^{Q_{\text{out}}} + \Phi_1^{Q_{\text{in}}} - \Phi_1^{A^*}. \quad (\text{D.4})$$

Regarding the strength properties of the laminate, by employing Eq. (14), Eq. (13) and the main results obtained by Catapano and Montemurro (2019), one can write:

$$\frac{\mathbf{G}_{\text{lam}}}{t} = \begin{bmatrix} \mathbf{G}_A^* & \mathbf{0} & \mathbf{0} \\ \frac{t^2}{12} \mathbf{G}_A^* & \mathbf{0} & \mathbf{0} \\ \text{sym} & \mathbf{G}_H^* & \end{bmatrix}, \quad \frac{\mathbf{g}_{\text{lam}}}{t} = \begin{Bmatrix} \mathbf{g}_A^* \\ \mathbf{0} \\ \mathbf{0} \end{Bmatrix}. \quad (\text{D.5})$$

Of course, also matrices  $\mathbf{G}_A^*$  and  $\mathbf{G}_H^*$  and vector  $\mathbf{g}_A^*$  can be computed as a function of their PPs. Such PPs depend on those of matrix  $\mathbf{A}^*$  and of the constitutive tow as follows (Catapano and Montemurro, 2019):

$$\begin{aligned} T_0^{G_A^*} &\equiv T_0^{G_{\text{in}}}, \quad T_1^{G_A^*} \equiv T_1^{G_{\text{in}}}, \\ R_0^{G_A^*} &= \frac{R_0^{G_{\text{in}}}}{R_0^{Q_{\text{in}}}} R_0^{A^*}, \quad R_1^{G_A^*} = \frac{R_1^{G_{\text{in}}}}{R_1^{Q_{\text{in}}}} R_1^{A^*}, \\ \Phi_0^{G_A^*} &= \Phi_0^{G_{\text{in}}} - \Phi_0^{Q_{\text{in}}} + \Phi_0^{A^*}, \\ \Phi_1^{G_A^*} &= \Phi_1^{G_{\text{in}}} - \Phi_1^{Q_{\text{in}}} + \Phi_1^{A^*}, \end{aligned} \quad (\text{D.6})$$

$$T^{G_H^*} \equiv T^{G_{\text{out}}}, \quad R^{G_H^*} = \frac{R^{G_{\text{out}}}}{R_1^{Q_{\text{in}}}} R_1^{A^*}, \quad \Phi^{G_H^*} = \Phi^{G_{\text{out}}} + \Phi_1^{Q_{\text{in}}} - \Phi_1^{A^*}, \quad (\text{D.7})$$

$$T^{g_A^*} \equiv T^{g_{\text{in}}}, \quad R^{g_A^*} = \frac{R^{g_{\text{in}}}}{R_1^{Q_{\text{in}}}} R_1^{A^*}, \quad \Phi^{g_A^*} = \Phi^{g_{\text{in}}} - \Phi_1^{Q_{\text{in}}} + \Phi_1^{A^*}. \quad (\text{D.8})$$

The derivatives of  $\mathbf{K}_{\text{lam}}$ ,  $\mathbf{G}_{\text{lam}}/t$  and  $\mathbf{g}_{\text{lam}}/t$  with respect to the value of the generic dimensionless variable  $\xi$  are:

$$\frac{\partial \mathbf{K}_{\text{lam}}}{\partial \xi} = \begin{cases} \begin{bmatrix} t \frac{\partial \mathbf{A}^*}{\partial \xi} & \mathbf{0} & \mathbf{0} \\ \frac{t^3}{12} \frac{\partial \mathbf{A}^*}{\partial \xi} & \mathbf{0} & \mathbf{0} \\ \text{sym} & t \frac{\partial \mathbf{H}^*}{\partial \xi} & \end{bmatrix} & \text{if } \xi = \rho_{0K}, \rho_1, \phi_1, \\ t_{\text{RSol}} \begin{bmatrix} \mathbf{A}^* & \mathbf{0} & \mathbf{0} \\ \frac{t^2}{4} \mathbf{A}^* & \mathbf{0} & \mathbf{0} \\ \text{sym} & \mathbf{H}^* & \end{bmatrix} & \text{if } \xi = \tau, \end{cases} \quad (\text{D.9})$$

$$\frac{\partial}{\partial \xi} \left( \frac{\mathbf{G}_{\text{lam}}}{t} \right) = \begin{cases} \begin{bmatrix} \frac{\partial \mathbf{G}_{\text{A}}^*}{\partial \xi} & \mathbf{0} & \mathbf{0} \\ \frac{t^2}{12} \frac{\partial \mathbf{G}_{\text{A}}^*}{\partial \xi} & \mathbf{0} & \mathbf{0} \\ \text{sym} & \frac{\partial \mathbf{G}_{\text{H}}^*}{\partial \xi} & \end{bmatrix} & \text{if } \xi = \rho_{0K}, \rho_1, \phi_1, \\ t_{\text{RSol}} \begin{bmatrix} \mathbf{0} & \mathbf{0} & \mathbf{0} \\ \frac{t}{6} \mathbf{G}_{\text{A}}^* & \mathbf{0} & \mathbf{0} \\ \text{sym} & \mathbf{0} & \end{bmatrix} & \text{if } \xi = \tau, \end{cases} \quad (\text{D.10})$$

$$\frac{\partial}{\partial \xi} \left( \frac{\mathbf{g}_{\text{lam}}}{t} \right) = \begin{cases} \begin{bmatrix} \frac{\partial \mathbf{g}_{\text{A}}^*}{\partial \xi} \\ \mathbf{0} \\ \mathbf{0} \end{bmatrix} & \text{if } \xi = \rho_{0K}, \rho_1, \phi_1, \\ \begin{bmatrix} \mathbf{0} \end{bmatrix} & \text{if } \xi = \tau. \end{cases} \quad (\text{D.11})$$

The derivatives of  $\mathbf{A}^*$  and  $\mathbf{G}_{\text{A}}^*$  are of type:

$$\frac{\partial \mathbf{X}}{\partial \rho_{0K}} = a_X \begin{bmatrix} c_4^X & -c_4^X & s_4^X \\ \text{sym} & -c_4^X & \end{bmatrix}, \quad (\text{D.12})$$

$$\frac{\partial \mathbf{X}}{\partial \phi_1} = b_X \begin{bmatrix} 4c_2^X & 0 & +2s_2^X \\ -4c_2^X & +2s_2^X & \\ \text{sym} & 0 & \end{bmatrix}, \quad (\text{D.13})$$

$$\begin{aligned} \frac{\partial \mathbf{X}}{\partial \rho_1} = & 2\pi\rho_{0K}a_X \begin{bmatrix} -s_4^X & +s_4^X & +c_4^X \\ & -s_4^X & -c_4^X \\ \text{sym} & & +s_4^X \end{bmatrix} \\ & + 2\pi\rho_1b_X \begin{bmatrix} -2s_2^X & 0 & +c_2^X \\ & +2s_2^X & +c_2^X \\ \text{sym} & & 0 \end{bmatrix}, \end{aligned} \quad (\text{D.14})$$

where

$$c_4^X/s_4^X = \cos/\sin(4\beta_X), \quad c_2^X/s_2^X = \cos/\sin(2\beta_X) \quad (\text{D.15})$$

and  $\mathbf{X}$ ,  $a_X$ ,  $b_X$  and  $\beta_X$  assume the values provided in Tab. D.1.

The derivatives of  $\mathbf{H}^*$  and  $\mathbf{G}_{\text{H}}^*$  are of type:

$$\frac{\partial \mathbf{Y}}{\partial \rho_{0K}} = [\mathbf{0}], \quad (\text{D.16})$$

$$\frac{\partial \mathbf{Y}}{\partial \rho_1} = b_Y \begin{bmatrix} c_2^Y & s_2^Y \\ s_2^Y & -c_2^Y \end{bmatrix}, \quad (\text{D.17})$$

Table D.1: Possible sets of  $\mathbf{X}$ ,  $a_X$ ,  $b_X$  and  $\beta_X$ .

| $\mathbf{X}$              | $a_X$              | $b_X$              | $\beta_X$   |
|---------------------------|--------------------|--------------------|---|
| $\mathbf{A}^*$            | $R_0^{\text{Qin}}$ | $R_1^{\text{Qin}}$ | $(\pi/2)\phi_1$   |
| $\mathbf{G}_{\text{A}}^*$ | $R_0^{\text{Gin}}$ | $R_1^{\text{Gin}}$ | $\Phi_0^{\text{Gin}} - \Phi_0^{\text{Qin}} + (\pi/2)\phi_1$ |

$$\frac{\partial \mathbf{X}}{\partial \phi_1} = \pi\rho_1b_Y \begin{bmatrix} s_2^Y & -c_2^Y \\ -c_2^Y & -s_2^Y \end{bmatrix}, \quad (\text{D.18})$$

where

$$c_2^Y/s_2^Y = \cos/\sin(2\beta_Y) \quad (\text{D.19})$$

and  $\mathbf{Y}$ ,  $b_Y$  and  $\beta_Y$  assume the values provided in Tab. D.2.

Table D.2: Possible sets of  $\mathbf{Y}$ ,  $b_Y$  and  $\beta_Y$ .

| $\mathbf{Y}$              | $b_Y$             | $\beta_Y$  |
|---------------------------|-------------------|--|
| $\mathbf{H}^*$            | $R^{\text{Qout}}$ | $\Phi_1^{\text{Qout}} + \Phi_1^{\text{Qin}} - (\pi/2)\phi_1$ |
| $\mathbf{G}_{\text{H}}^*$ | $R^{\text{Gout}}$ | $\Phi^{\text{Gout}} + \Phi_1^{\text{Qin}} - (\pi/2)\phi_1$   |

Finally, the derivatives of  $\mathbf{g}_{\text{A}}^*$  are:

$$\frac{\partial \mathbf{g}_{\text{A}}^*}{\partial \rho_{0K}} = \{\mathbf{0}\}, \quad (\text{D.20})$$

$$\frac{\partial \mathbf{g}_{\text{A}}^*}{\partial \rho_1} = R^{\text{Gin}} \{c_2^g \quad -c_2^g \quad s_2^g\}^T, \quad (\text{D.21})$$

$$\frac{\partial \mathbf{g}_{\text{A}}^*}{\partial \phi_1} = \pi R^{\text{Gin}} \rho_1 \{-s_2^g \quad s_2^g \quad c_2^g\}^T, \quad (\text{D.22})$$

where

$$c_2^g/s_2^g = \cos/\sin\left(2\left(\Phi^{\text{Gin}} - \Phi_1^{\text{Qin}} + (\pi/2)\phi_1\right)\right). \quad (\text{D.23})$$

**Remark D.2** According to Eq. (20), the partial derivatives of a generic function  $f(\rho_{0K}, \rho_1)$  with respect to the design variables  $\alpha_0$  and  $\alpha_1$  read:

$$\begin{aligned} \frac{\partial f}{\partial \alpha_0} &= \frac{\partial f}{\partial \rho_{0K}} (2\rho_1^2 - 2), \\ \frac{\partial f}{\partial \alpha_1} &= \frac{\partial f}{\partial \rho_{0K}} \left( 2\frac{\rho_{0K}-1}{\rho_1^2-1} \rho_1 \right) + \frac{\partial f}{\partial \rho_1}. \end{aligned} \quad (\text{D.24})$$

## References

- Albazzan MA, Harik R, Tatting BF, Gürdal Z (2019) Efficient design optimization of nonconventional laminated composites using lamination parameters: A state of the art. *Composite Structures* 209:362–374, DOI 10.1016/j.compstruct.2018.10.095
- Alhajahmad A, Abdalla MM, Gürdal Z (2008) Optimal Design of a Pressurized Fuselage Panel with a Cutout Using Tow-Placed Steered Fibers. In: *Proceedings of the International Conference on Engineering Optimization 2008*, Rio de Janeiro, Brazil



- Audoux Y, Montemurro M, Pailhès J (2020) A Metamodel Based on Non-Uniform Rational Basis Spline Hyper-Surfaces for Optimisation of Composite Structures. *Composite Structures* 247:(in press), DOI 10.1016/j.compstruct.2020.112439
- Catapano A, Montemurro M (2019) On the correlation between stiffness and strength properties of anisotropic laminates. *Mechanics of Advanced Materials and Structures* 26(8):651–660, DOI 10.1080/15376494.2017.1410906
- Catapano A, Montemurro M (2020) Strength optimisation of variable angle-tow composites through a laminate-level failure criterion. *Journal of Optimization Theory and Applications* (in press), DOI 10.1007/s10957-020-01750-6
- Catapano A, Desmorat B, Vannucci P (2015) Stiffness and Strength Optimization of the Anisotropy Distribution for Laminated Structures. *Journal of Optimization Theory and Applications* 167(1):118–146, DOI 10.1007/s10957-014-0693-5
- Catapano A, Montemurro M, Balcou JA, Panettieri E (2019) Rapid Prototyping of Variable Angle-Tow Composites. *Aerotecnica Missili & Spazio* 98(4):257–271, DOI 10.1007/s42496-019-00019-0
- Daniel IM, Ishai O (1994) Engineering mechanics of composite materials. Oxford university press New York
- Fiordilino GA, Izzi MI, Montemurro M (2020) A general isogeometric polar approach for the optimisation of variable stiffness composites: Application to eigenvalue buckling problems. *Mechanics of Materials* (in press), DOI 10.1016/j.mechmat.2020.103574
- Garulli T, Catapano A, Montemurro M, Jumel J, Fanteria D (2018) Quasi-trivial stacking sequences for the design of thick laminates. *Composite Structures* 200:614–623, DOI 10.1016/j.compstruct.2018.05.120
- Ghiasi H, Fayazbakhsh D, Pasini D, Lessard L (2010) Optimum stacking sequence design of composite materials Part II: Variable stiffness design. *Composite Structures* 93:1–13, DOI 10.1016/j.compstruct.2010.06.001
- Gurdal Z, Olmedo R (1993) In-plane response of laminates with spatially varying fiber orientations - Variable stiffness concept. *AIAA Journal* 31(4):751–758, DOI 10.2514/3.11613
- Huang J, Haftka RT (2005) Optimization of fiber orientations near a hole for increased load-carrying capacity of composite laminates. *Structural and Multidisciplinary Optimization* 30(5):335–341, DOI 10.1007/s00158-005-0519-z
- Hyer MW, Charette RF (1991) Use of curvilinear fiber format in composite structure design. *AIAA Journal* 29(6):1011–1015, DOI 10.2514/3.10697
- Hyman BI, Deturk A, Diaz R, DiGiovanni G (1969) Exploratory tests on fiber-reinforced plates with circular holes under tension. *AIAA Journal* 7(9):1820–1821, DOI 10.2514/3.5408
- IJsselmuiden ST, Abdalla MM, Gurdal Z (2008) Implementation of Strength-Based Failure Criteria in the Lamination Parameter Design Space. *AIAA Journal* 46(7):1826–1834, DOI 10.2514/1.35565
- Izzi MI, Montemurro M, Catapano A, Pailhès J (2020) A multi-scale two-level optimisation strategy integrating a global/local modelling approach for composite structures. *Composite Structures* 237:(in press), DOI 10.1016/j.compstruct.2020.111908
- Jones RM (1975) Mechanics of composite materials. McGraw-Hill
- Khani A, IJsselmuiden ST, Abdalla MM, Gurdal Z (2011) Design of variable stiffness panels for maximum strength using lamination parameters. *Composites Part B: Engineering* 42(3):546–552, DOI 10.1016/j.compositesb.2010.11.005
- Kim BC, Weaver PM, Potter K (2014) Manufacturing characteristics of the continuous tow shearing method for manufacturing of variable angle tow composites. *Composites: Part A* 61:141–151, DOI 10.1016/j.compositesa.2014.02.019
- Kraft D (1988) A software package for sequential quadratic programming. Tech. Rep. DFVLR-FB 88-28, DLR German Aerospace Center – Institute for Flight Mechanics, Koln, Germany
- Miki M, Sugiyamat Y (1993) Optimum Design of Laminated Composite Plates Using Lamination Parameters. *AIAA Journal* 31(5):921–922, DOI 10.2514/3.49033
- Montemurro M (2015a) Corrigendum to “An extension of the polar method to the first-order shear deformation theory of laminates” [*compos. struct.* 127 (2015) 328–339]. *Composite Structures* 131:1143–1144, DOI 10.1016/j.compstruct.2015.06.002
- Montemurro M (2015b) An extension of the polar method to the first-order shear deformation theory of laminates. *Composite Structures* 127:328–339, DOI 10.1016/j.compstruct.2015.03.025
- Montemurro M (2015c) The polar analysis of the third-order shear deformation theory of laminates. *Composite Structures* 131:775–789, DOI 10.1016/j.compstruct.2015.06.016
- Montemurro M, Catapano A (2016) Variational analysis and aerospace engineering: mathematical challenges for the aerospace of the future, Springer Optimization and Its Applications, vol 116, 1st edn, Springer International Publishing, chap A new paradigm for the optimum design of variable angle tow laminates, pp 375–400, DOI 10.1007/978-3-319-45680-5
- Montemurro M, Catapano A (2017) On the effective integration of manufacturability constraints within the multi-scale methodology for designing variable angle-tow laminates. *Composite Structures* 161:145–159, DOI 10.1016/j.compstruct.2016.11.018
- Montemurro M, Catapano A (2019) A general B-Spline surfaces theoretical framework for optimisation of variable angle-tow laminates. *Composite Structures* 209:561–578, DOI 10.1016/j.compstruct.2018.10.094
- Montemurro M, Catapano A, Doroszewski D (2016) A multi-scale approach for the simultaneous shape and material optimisation of sandwich panels with cellular core. *Composites Part B: Engineering* 91:458–472, DOI 10.1016/j.compositesb.2016.01.030
- Montemurro M, Izzi MI, El-Yagoubi J, Fanteria D (2019) Least-weight composite plates with unconventional stacking sequences: Design, analysis and experiments. *Journal of Composite Materials* 53(16):2209–2227, DOI 10.1177/0021998318824783
- Nagelsmith M, Guerrits W (2013) Influence of steering radius on the mechanical properties of fiber placed composite laminates. In: ICCS17-17th International Conference on Composite Structures
- Nagendra S, Kodiyalam S, Davis J, Parthasarathy V (1995) Optimization of tow fiber paths for composite design. In: 36th Structures, Structural Dynamics and Materials Conference, American Institute of Aeronautics and Astronautics, DOI 10.2514/6.1995-1275
- Picchi Scardaoni M, Montemurro M (2020) A general global-local modelling framework for the deterministic optimisation of composite structures. *Structural and Multidisciplinary Optimization* (in press), DOI 10.1007/s00158-020-02586-4
- Picchi Scardaoni M, Montemurro M (2021) Convex or non-convex? On the nature of the feasible domain of laminates. *European Journal of Mechanics - A/Solids* 85:(in press), DOI 10.1016/j.euromechsol.2020.104112
- Piegl L, Tiller W (1997) The NURBS Book. Springer-Verlag
- Reddy JN (2003) Mechanics of composite laminated plates and shells: theory and analysis. Boca Raton, FL: CRC Press
- Tian Y, Pu S, Shi T, Xia Q (2021) A parametric divergence-free vector field method for the optimization of composite structures with curvilinear fibers. *Computer Methods in Applied Mechanics and Engineering* 373:(in press), DOI 10.1016/j.cma.2020.113574
- Tosh MW, Kelly DW (2000) On the design, manufacture and testing of trajectorial fibre steering for carbon fibre composite laminates. *Composites: Part A* 31:1047–1060, DOI 10.1016/S1359-835X(00)00063-4
- Tsai SW, Wu EM (1971) A General Theory of Strength for Anisotropic Materials. *Journal of Composite Materials* 5(1):58–80, DOI 10.1177/002199837100500106
- Vannucci P (2005) Plane Anisotropy by the Polar Method. *Meccanica* 40(4-6):437–454, DOI 10.1007/s11012-005-2132-z

- Vannucci P (2013) A Note on the Elastic and Geometric Bounds for Composite Laminates. *Journal of Elasticity* 112(2):199–215, DOI 10.1007/s10659-012-9406-1
- Vannucci P, Verchery G (2001) A special class of uncoupled and quasi-homogeneous laminates. *Composites Science and Technology* 61(10):1465–1473, DOI 10.1016/S0266-3538(01)00039-2
- Verchery G (1982) Les Invariants des Tenseurs d'Ordre 4 du Type de l'Élasticité. In: Boehler JP (ed) *Mechanical Behavior of Anisotropic Solids / Comportement Mécanique des Solides Anisotropes*, Springer Netherlands, Dordrecht, pp 93–104, DOI 10.1007/978-94-009-6827-1\_7
- Virtanen P, Gommers R, Oliphant TE, Haberland M, Reddy T, Cournapeau D, Burovski E, Peterson P, Weckesser W, Bright J, van der Walt SJ, Brett M, Wilson J, Millman KJ, Mayorov N, Nelson ARJ, Jones E, Kern R, Larson E, Carey CJ, Polat I, Feng Y, Moore EW, VanderPlas J, Laxalde D, Perktold J, Cimrman R, Henriksen I, Quintero EA, Harris CR, Archibald AM, Ribeiro AH, Pedregosa F, van Mulbregt P, SciPy 10 Contributors (2020) SciPy 1.0: Fundamental Algorithms for Scientific Computing in Python. *Nature Methods* 17:261–272, DOI 10.1038/s41592-019-0686-2



---

## Conclusions and prospects

The work carried out in this Ph.D. thesis aims to allow a better exploitation of composite materials in high-performances thin-walled structures, through the development of multi-scale procedures and numerical tools for their effective and efficient design. The thesis work has been carried out at the ENSAM of Bordeaux-Talence, under the supervision of M. Montemurro, J. Pailhès and A. Catapano. It moves in the context of the European research project PARSIFAL, which has involved six partners from four countries in a multidisciplinary feasibility study on the introduction of an innovative aircraft architecture, i.e. the *PrandtlPlane*, in the market. ENSAM was the leader of the work package 5 of PARSIFAL, which focused on the structural design and analysis of the PrandtlPlane.

### 8.1 General conclusions

The work related to this thesis has intervened in all aspects of the ENSAM contribution to PARSIFAL. The objectives of the project have constituted both a motivation and an application for the various thesis activities. For this reason, thin-walled composite structures typical of the aeronautical field have been targeted in this thesis. Without loss of generality, the focus has been put on the fuselage structure. Two classes of composite materials have been considered: the constant-stiffness composites and variable-stiffness composites.

A constant-stiffness composite structure allows a per-laminate tailoring of the geometrical and the material properties. Designing a large-scale thin-walled composite structure implicates dealing with three working scales: the global macroscopic scale of the structure, the local macroscopic scale of the component, and the mesoscopic one (i.e. that of the constitutive ply). Such multi-scale nature of the design problem and the fact that a huge number of design variables is involved into the design process make the associated optimisation problem rather difficult and costly (under a computational point of view) to be solved. The bibliographic review activity presented in Chapter 2 has allowed to identify three main common limitations in currently-available design procedures: a) the limited accuracy of the methods employed for the assessment of the structure response at the various scales; b) the poor management of the scale transition; c) the non-optimal definition of the design variables involved at each scale, which are limited in various ways.

The task of defining an improved design procedure for large-scale thin-walled constant-stiffness composite structures has been tackled in two phases, corresponding to the first two phases of the thesis work described in Chapter 1.

In the first phase, corresponding to the work presented in Chapter 3, a simplified scenario has been considered: the preliminary structural design of a metallic structure, which can be seen as a sub-case of the most general one made of anisotropic materials. By doing so, there is no need to distinguish between the macroscopic and mesoscopic scales and all aspects related to the lay-up design are disregarded. Only geometrical design variables are then involved in the design process and the focus can be put on the handling of the global and local scales. This first phase has investigated the possibility to optimise this type of structures by accurately evaluating all involved mechanical responses by means of finite element analyses, without enforcing any restriction in the design variables definition, while still managing the computational cost of the process. A meaningful engineering problem has been selected as study case: the least-weight design of an aluminium fuselage barrel belonging to the aft part of a wide-body aircraft, whose geometry and basic loads are taken from the literature. Requirements on the structure stiffness, static strength, fatigue strength, and on the buckling load (no-buckling design approach), evaluated under suited loading conditions, have been considered in the design process, as well as requirements on the manufacturability of the solution. For solving such design problem, a multi-scale design procedure, i.e. the GL-MSOS, has been proposed.

When adopting the GL-MSOS, the evaluation of the mechanical responses of the structure is performed by means of *on-line* finite element analyses, employing a global-local sub-modelling approach. For each candidate solution, global-scale and local-scale finite element models are generated and solved by means of fully-parametric scripts. The models are characterised by a different level of modelling refinement, avoiding, in this way, the use of computationally expensive refined global models for the assessment of localised phenomena. Local-scale analyses are carried out by considering boundary conditions extracted, without simplifications, from the results of the global-scale analysis, thus ensuring complete coherence in the scale transition. The computational effort is kept low by automatically generating the local finite element models only for a limited set of zones of interest, identified during the global-scale analysis by means of opportune criteria. The full set of design variables is considered in the formulation of the optimisation problem, without introducing simplifying hypotheses and the solution search is carried out employing the genetic algorithm ERASMUS.

The obtained solution has been compared to an optimised one taken from the literature. This latter was obtained by solving an similar design problem by means of an iterative design procedure in which common-use simplifying rules for the definition of the design variables and analytical methods for the responses evaluations are employed. The solution obtained with the GL-MSOS and the literature one have a very similar mass (within 1.2% different), however, the former outperforms the latter. Indeed, in the literature work, no manufacturing constraints were considered, and the less restrictive post-buckling design approach was adopted. This result has been considered as a sort of numerical proof of the effectiveness of the proposed design procedure.

In the second phase, the possibility to generalise the GL-MSOS to the design of large-scale thin-walled constant-stiffness composite structures has been investigated.

The additional layer of complexity represented by the possibility of optimising the material properties of the structure, as well as the geometrical ones, has been faced by adopting a multi-level design approach, the MS2LOS. In the usual work-flow of the MS2LOS, the problem is solved at two levels, wherein two subsequent optimisation problems are faced. At the first level the structural optimisation is performed. Here, each laminate composing the structure is modelled as an equivalent single-layer plate and its macroscopic mechanical

properties, represented in terms of Polar Parameters, are optimised (together with all geometrical properties) without making any simplifying hypothesis on the nature of the underlying stacking sequence. The second-level optimisation problem is devoted to the retrieval of the laminates stacking sequences corresponding to the sets of optimum Polar Parameters found at the first level. This implies that, in order to avoid inconsistency between the two levels or the need of *repair* activities, all the requirements involved in the design problem, including those typical of the lower scales (notably, requirements concerning failure and manufacturability), have to be formulated as equivalent constraints at the macroscopic scale.

The advantages of the GL-MSOS and those of the MS2LOS have been therefore combined, obtaining the GL-MS2LOS. The integration interests the first level of the MS2LOS, where the assessment of the structural responses, at both the global and local scales, is performed by means of analyses on specific finite element models, whose coherency is ensured through the implementation of the global-local sub-modelling approach. The second level of the MS2LOS remains unaltered with respect to previous works.

The GL-MS2LOS has been presented in Chapter 5, where it has been employed for the least-weight design of a constant-stiffness composite fuselage barrel. The considered structure is identical, in terms of main geometrical properties and considered loads, to the one presented in Chapter 3, but its main structural components (except floor beams and struts) are considered made of constant-stiffness composite laminates. Also the formulation of the considered design problem is equivalent to the one faced in Chapter 3: requirements on the structural stiffness and static strength, and on the absence of buckling in the considered loading conditions have been taken into account in the design process of the composite structure, as well as requirements on the manufacturability of the solution. The strength requirement has been assessed at the macroscopic scale by means of a laminate-level failure criterion formulated in the space of Polar Parameters and feasibility conditions on the existence of suitable stacking sequences are included in the first-level problem formulation among the manufacturing constraints. Here also, the genetic algorithm ERASMUS has been employed as solution tool. The optimal composite fuselage obtained using the GL-MS2LOS has been compared to the optimal aluminium one obtained in Chapter 3. The composite solution shows a 40% weight saving over the metallic one and meets the full set of design constraints. Considering that some structural components have not been included in the design process, this result shows the big potential of the proposed design procedure.

Inasmuch as the MS2LOS constitutes a main ingredient of the GL-MS2LOS, two activities of experimental validation of its effectiveness have been planned in this thesis. The first of these activities has been presented in Chapter 4. In this work, the MS2LOS has been applied to the least-weight design of a moderately-thick constant-stiffness composite layered plate subject to requirements on its in-plane overall stiffness, its first buckling load, and its manufacturability. Numerical and experimental activities have proceeded in parallel. The formers have followed the two-level work-flow typical of the MS2LOS: first, the structural design of the plate has been carried out in terms of its macroscopical material and geometrical properties, than the lay-up design has been performed. The genetic algorithm ERASMUS has been employed to perform the solution search at both levels. At the first level, it has been interfaced with finite element analyses for the evaluation of the first buckling load of the plate. At the second level, it has been interfaced with an analytical model for computing, in the First-order Shear Deformation Theory framework, the macroscopical properties of candidate stacking sequences. The solution of the second-

level problem has been searched in the space of Quasi-Trivial stacking sequences, a family of stacks which allows to obtain exact membrane-bending uncoupling and homogeneity of the laminate, without enforcing simplifying rules on the nature of its stack (e.g. symmetry and balancing). A plate having the same geometry of the optimised one, subjected to the same boundary conditions, and whose stacking sequence has been built by using the classical rules taken from literature has been considered as reference solution and employed for defining the design requirements. Experimental buckling tests have been performed both on the reference plate, to confirm the accuracy of the finite element model employed during the optimisation process, and on the optimised one. Numerical and experimental results show an excellent agreement: the optimised plate is about 10% lighter than the reference one with similar or superior mechanical performances. These results constitute a first experimental validation of the effectiveness of both the MS2LOS and the very general stacking sequences resulting from its application.

A second experimental activity was also planned in the PARSIFAL activities. This activity, carried out in collaboration with University of Pisa, follows the same numerical-experimental work-flow presented in Chapter 4, but focuses on full-scale stiffened panels. Due to multiple delays in the manufacturing of the panels, this activity, not reported in this thesis, has not been completed and will be finalised during the next months.

The GL-MSOS and the GL-MS2LOS, presented and numerically validated in Chapters 3 and 5 respectively, have seen application in the preliminary structural design of the PrandtlPlane aircraft proposed in the PARSIFAL project. This structural design activity, whose highlights have been presented in Chapter 6, has targeted the main structural components of the fuselage and the lifting system of the aircraft, in both a metallic variant and a constant-stiffness composite one. A modular approach has been adopted for the modelling of the aircraft structure, and the related activities have been shared among three members of the PARSIFAL team at ENSAM. Due to the peculiarities of the PrandtlPlane architecture, two adaptations of the aforementioned design procedures have been devised in order to lower the computational cost for their application on such structure. From a procedural perspective, a multi-step alternated-domain approach has been adopted: the solution search has been carried out iteratively, optimising alternately the design variables belonging to the central fuselage barrel and those of the lifting system. From a modelling point of view, in the global finite element model of the whole aircraft structure, the regions not directly involved in the optimisation have been *condensed* in super elements obtained by means of the sub-structuring technique. Results, which have been obtained both in terms of macroscopic inertial properties distributions and in terms of detailed structural information for both variants of the aircraft structure, have met expectations and contributed to the correct progress of the PARSIFAL project.

In the third phase of the thesis work, the focus has been put on variable-stiffness composite laminates, a class of composite materials characterised by a point-wise variation of the macroscopic mechanical properties over the laminate surface. Variable-stiffness composite laminates offer superior tailoring possibilities than constant-stiffness composite ones, notably for structural components presenting high stress gradients, e.g. the panel surrounding a fuselage window. Various formats of variable-stiffness composite laminates are possible, whose production has been made possible by recent developments in manufacturing processes. In this thesis the focus has been put on variable angle tow laminates obtained by means of the Automated Fibre Placement process. The broad adoption of this type of laminates in the industry is still limited, on the one hand, by the newness and immaturity of the manufacturing processes, which still present some specific limitations,



and, on the other hand, by the lack of a general and established procedure for their optimal design. This phase of the thesis work aims at overcoming some of the limitations related to the procedural aspects through the development of specific theoretical and numerical design tools.

A suited design procedure for variable-stiffness composite structures should efficiently deal with design variables that assume the form of continuous and sufficiently smooth distributions across the laminate surface, and also integrate constraints related to the employed manufacturing process. Due to the nature of the related optimisation problem, the adoption of a multi-level design approach coupled with the use of a deterministic algorithm as solution tool appears advantageous. However, in order to guarantee an efficient exploitation of the deterministic algorithm, the analytical expression of the gradient of all the response functions involved in the optimisation process must be derived.

In Chapter 7, the problem of the deterministic optimisation of structural variable-stiffness composite components considering requirements on mass, strength, and maximum tow curvature has been faced. The optimisation has been performed in the context of the first-level problem of the MS2LOS, taking advantage of two main ingredients: the polar method for the representation of the local macroscopic mechanical properties of the laminates in the FSDT framework, and B-spline entities for describing the distribution of the design variables. The theoretical framework of the MS2LOS has been enriched through the formulation of the aforementioned requirements, and the design problem has been generalised to the case of variable-stiffness composite laminates with non-uniform thickness. Two benchmark structures have been considered: the first one highlights stress concentrations under in-plane load, while the second one emphasises bending and shear effects. Both the failure load maximisation problem (with a constraint on the mass) and the mass minimisation one (with a constraint on laminate strength) have been solved for both structures. The structure failure load has been defined using a laminate-level failure criterion based on tensor invariants. The effect of a constraint on the maximum tow curvature has also been evaluated and an improved conservative formulation has been proposed for this process-related manufacturability requirement. Taking advantage of the properties of the B-spline entities, the analytical expression of the response functions related to all aforementioned requirements, as well as their gradients, have been derived. Clearly, the point-wise feasibility requirement on the existence of suitable stacks has been considered too: it is intrinsically satisfied in the proposed formulation of the optimisation problem, without the need of introducing explicit constraints. From a numerical perspective, the numerical platform DOMES (Deterministic Optimisation of Macroscopic laminatEs via Splines) has been created. Developed in the Python environment, it constitutes, essentially, an interface between a deterministic optimisation algorithm and a finite element software, and it establishes a data structure for the definition of the design variables and a modular implementation of the various requirements.

Various properties of the variable-stiffness composite laminates have been tailored either uniformly or locally over the laminates surface: the orthotropy type and shape, the direction of the main orthotropy axis, the thickness. Depending on the design variables definition, various sub-classes of variable-stiffness composite laminates, including both manufacturable solutions and theoretical ones, have been identified. Multiple design cases, corresponding to various possible combinations of considered structure, problem formulation and sub-class of the variable-stiffness composite laminates, have been considered. The results have been compared, in terms of their performances, to quasi-homogeneous isotropic solutions. When optimising for strength, the failure load can be increased between

48% and 1034%, while, when optimising for lightness, the obtained mass reduction is in the range 24-92%. Theoretical variable-thickness variable-stiffness composite laminates outperform their uniform-thickness counterparts, showing an additional increase of 116-138% of the failure load or an additional weight saving of 26-58%. Finally, strength-optimised solutions have also been compared to an optimised variable-stiffness composite solution taken from the literature, obtained by means of the representation based on Lamination Parameters: the proposed approach was able to provide solutions with an increase in the failure load between 4% and 252%; the most comparable solution (in terms of explored design space) shows an improvement of 21%.

Considerable results have also been obtained facing the buckling load maximisation problem of variable-stiffness composite laminates. Such activity, not reported in this thesis, has been carried out in collaboration with Ph.D. student G. A. Fiordilino and recently published (Fiordilino, Izzi, and Montemurro, 2021). Two benchmark problems have been considered, and obtained results have been compared to both quasi-homogeneous isotropic solutions and to optimised variable-stiffness composite solutions taken from the literature: an increase of the buckling load up to 230% and up to 16% has been found, respectively. The above results unequivocally show the great potential of variable-stiffness composite laminates and the effectiveness of the proposed optimisation strategy.

## 8.2 Prospects

The application of the GL-MS2LOS to simplified, although representative, design cases, allowed to obtain encouraging results, proving that it is a viable and effective alternative to other common-use design procedures for large-scale thin-walled constant-stiffness composite structures. However, there is still room for improvement and/or future development. The adoption of a *post-buckling* design approach, instead of the *no-buckling* approach employed in this thesis, is supposed to allow obtaining lighter optimal configurations. The efficient integration of requirements on the post-buckling behaviour of the structure in the presented procedure constitutes a challenging task. In fact, because of its non-linear nature, the assessment of the post-buckling behaviour of structures is usually carried out through path-following analyses which reveal too computationally expensive to be integrated into an optimisation process. A valid alternative is the adoption of asymptotic methods (e.g. the Koiter's method or the Asymptotic-Numerical Method) which provide, at a reasonable computational cost, a good approximation of the initial post-buckling response.

In order to be able to face more complete industrial-level design cases, the problem formulation should be enriched. Additional requirements should be integrated, e.g. specific design criteria for the sizing of frames, floor beams and struts, and additional loading conditions should be considered for the evaluation of the aircraft responses. Moreover, from a modelling perspective, the presence of principal openings, like fuselage doors and windows, should also be taken into account in this design phase, in order to maximise compatibility with the following one.

The use of a genetic algorithm as optimisation tool, thanks to its good exploration capability, surely helps in avoiding get trapped in local minima when solving non-convex problems, but it may converge to sub-optimal solutions as a consequence of loss of population diversity. Further improvements could be obtained by letting the meta-heuristic optimisation phase be followed by an additional deterministic optimisation one. Ideally, this latter phase should be supported by the derivation of the analytical expression of

the gradient of all response functions involved in the optimisation process. Notably, the gradient of local-scale requirements must properly take into account the scale transition (through the gradient of the boundary displacements of the local finite element models) and the possibility that the position of the zones of interest could vary during the optimisation process. This latter need could be satisfied in different ways: a) by aggregating into the gradient the responses of all possible local models; b) by properly defining the design zones (i.e. portions of the structure where the components share the same properties); c) by means of a combination of both approaches. Activities on this topic have already been started in this research group and need further development.

The activities carried out in the third phase of the thesis work allowed to confirm the great potential of variable-stiffness composite laminates. The integration of variable-stiffness composite structural components in large-scale thin-walled composite structures seems, thus, desirable. However, further development of the theoretical and numerical tools associated to both levels of the MS2LOS for variable-stiffness composite laminates is still needed.

At the first level of the MS2LOS, it is important to formulate new criteria for the prediction of the presence of defects related to the manufacturing of variable-stiffness composite laminates, like tows gaps and/or overlaps, in the final structure and to account for their effect on the structural responses since the early design phases. The implementation of both new requirements and previously formulated ones (e.g. those concerning the compliance and the buckling load) should take advantage of the data structure established in the DOMES numerical platform. Moreover, this platform could be integrated into the suite of numerical optimisation tools developed by the research group at the I2M laboratory.

At the second level of the MS2LOS, the efforts should be put on the development of tools allowing to retrieve fibres-paths for all possible sub-classes of variable-stiffness composite laminates.

The execution of coupled numerical-experimental design activities on both simple and more complex variable-stiffness composite structural components should be the natural following step.

To conclude, the long-term prospect of the work presented in this thesis is the definition of the procedural aspects linked to the adoption of the GL-MS2LOS for the efficient and effective design of large-scale thin-walled variable-stiffness composite structures.

---

*Cave et aude*

Charles Darwin's family motto



---

# Dissemination activity

## Research articles published in international journals

- **M. I. Izzi**, M. Montemurro, A. Catapano, D. Fanteria, and J. Pailhès. Multi-scale optimisation of thin-walled structures by considering a global/local modelling approach. *Proceedings of the Institution of Mechanical Engineers, Part G: Journal of Aerospace Engineering*, 235(2): 171–188, 2020. [www.doi.org/10.1177/0954410020939338](https://www.doi.org/10.1177/0954410020939338)
- M. Montemurro, **M. I. Izzi**, J. El-Yagoubi, and D. Fanteria. Least-weight composite plates with unconventional stacking sequences: Design, analysis and experiments. *Journal of Composite Materials*, 53(16): 2209–2227, 2019. [www.doi.org/10.1177/0021998318824783](https://www.doi.org/10.1177/0021998318824783)
- **M. I. Izzi**, M. Montemurro, A. Catapano, and J. Pailhès. A multi-scale two-level optimisation strategy integrating a global/local modelling approach for composite structures. *Composite Structures*, 237 (in press), 2020. [www.doi.org/10.1016/j.compstruct.2020.111908](https://www.doi.org/10.1016/j.compstruct.2020.111908)
- G. A. Fiordilino, **M. I. Izzi**, and M. Montemurro. A general isogeometric polar approach for the optimisation of variable stiffness composites: Application to eigenvalue buckling problems. *Mechanics of Materials*, 153 (in press), 2021. [www.doi.org/10.1016/j.mechmat.2020.103574](https://www.doi.org/10.1016/j.mechmat.2020.103574)
- **M. I. Izzi**, A. Catapano, and M. Montemurro. Strength and mass optimisation of variable-stiffness composites in the polar parameters space. *Structural and Multidisciplinary Optimisation*, (in press), 2021. [www.doi.org/10.1007/s00158-021-02963-7](https://www.doi.org/10.1007/s00158-021-02963-7)

## Presentations in international conferences

- **M. I. Izzi**, M. Montemurro, D. Fanteria, and J. El-Yagoubi. Instrumented buckling test on laminated composite plates. *7th International Symposium on Air/Craft Materials (ACMA2018)*, Compiègne, France, April 2018.
- M. Montemurro, **M. I. Izzi**, J. El-Yagoubi, and D. Fanteria. Multi-scale optimisation of thin-walled structures by considering a global/local modelling approach.

*6th European Conference on Computational Mechanics (ECCM 6) and 7th European Conference on Computational Fluid Dynamics (ECFD 7)*, Glasgow, United Kingdom, June 2018.

- M. Montemurro, **M. I. Izzì**, J. El-Yagoubi, and D. Fanteria. An experimental validation of the effectiveness of quasi-trivial solutions for composite laminates. *First International Conference on Mechanics of Advanced Materials and Structures (ICMAMS 2018)*, Turin, Italy, June 2018.
- **M. I. Izzì**, E. Panettieri, A. Catapano, M. Montemurro, and J. Pailhès. Multi-scale optimization of a composite fuselage by considering a global/local modelling approach. *21st International Conference on Composite Structures (ICCS 21)*, Bologna, Italy, Sept. 2018.
- M. Picchi Scardaoni and **M. I. Izzì**, E. Panettieri, and M. Montemurro. PrandtlP-plane aircraft least-weight design: a multi-scale optimisation strategy. *Italian Association of Aeronautics and Astronautics (AIDAA) XXV International Congress*, Rome, Italy, Sept. 2019.
- **M. I. Izzì**, M. Montemurro, A. Catapano, and J. Pailhès. Multi-scale two-level optimisation of a composite fuselage barrel integrating a global-local finite element modelling approach. *7th ECCOMAS Thematic Conference on the Mechanical Response of Composites (COMPOSITES 2019)*, Girona, Spain, Sept. 2019.
- **M. I. Izzì**, M. Montemurro, A. Catapano, and J. Pailhès. Accounting for strength and manufacturing requirements in the multi-scale optimisation of variable angle tow laminates. *14th World Congress in Computational Mechanics (WCCM 14) and ECCOMAS Congress 2020*, Virtual Congress, Jan. 2021.
- **M. I. Izzì**, A. Catapano, and M. Montemurro. Failure load maximisation of variable-stiffness composites with mass and manufacturability constraints. *14th World Congress of Structural and Multidisciplinary Optimization (WCSMO 14)*, Virtual Congress, June 2021.

## Presentations in national conferences

- **M. I. Izzì**, M. Montemurro, A. Catapano, and J. Pailhès. Integration of a global-local finite element modelling approach in the multi-scale two-level optimisation strategy: application to the optimisation of a composite fuselage barrel. *21ème Journées Nationales sur les Composites (JNC 21) de l'Association pour les Matériaux Composites (AMAC)*, Bordeaux, France, July 2019.
- **M. I. Izzì**, E. Panettieri, M. Picchi Scardaoni, and M. Montemurro. Design of an aircraft composite wing-box: integrating a global/local modelling approach into the multi-scale optimization method. *21èmes Journées Nationales sur les Composites (JNC 21) de l'Association pour les Matériaux Composites (AMAC)*, Bordeaux, France, July 2019.
- **M. I. Izzì**, A. Catapano, and M. Montemurro. Failure load maximisation of variable-stiffness composites with mass and manufacturability constraints. *22èmes Journées Nationales sur les Composites (JNC 22) de l'Association pour les Matériaux Composites (AMAC)*, Virtual Congress, June 2021.

---

# Thesis overview in French

## Préambule

### Le contexte de la thèse : le projet PARSIFAL

Au cours des dernières décennies, le trafic aérien de passagers a connu une augmentation remarquable. Les données historiques montrent que le nombre de kilomètres-passagers payants annuels<sup>1</sup> a connu une croissance logarithmique presque constante, avec une augmentation annuelle moyenne de 4,3%, soit un doublement tous les quinze ans. La récente épidémie de COVID-19 a sûrement eu un fort impact sur le marché du transport aérien, mais ce marché a montré une forte résilience aux chocs économiques externes dans le passé et, selon les récentes prévisions, la tendance mondiale ne devrait pas être considérablement affectée sur le long terme. Le marché du transport aérien doit faire face à cette augmentation constante de la demande dans un contexte difficile. En fait, la plupart des infrastructures aéroportuaires actuelles sont déjà encombrées avec une possibilité d'expansion très limitée voire inexistante, notamment en Europe. De plus, la réglementation sur l'impact environnemental des aéronefs (tant en termes de bruit que d'émissions) devient de plus en plus restrictive. La configuration de l'avion classique *tube and wing* a connu de grandes améliorations au cours des dernières décennies, mais a atteint maintenant son potentiel maximal avec de petites marges laissées pour l'amélioration de ses performances. Ce scénario pousse au développement de configurations d'avions innovantes et disruptives.

PARSIFAL (Prandtlplane ARchitecture for the Sustainable Improvement of Future AirpLane) est un projet de recherche<sup>2</sup> financé par l'Union européenne dans le cadre du programme Research and Innovation Horizon 2020, lancé en mai 2017 qui s'est conclu en Juillet 2020. Il visait à proposer une solution aux défis auxquels l'industrie aéronautique est confrontée. Huit partenaires, originaires de quatre pays européens, ont collaboré au projet PARSIFAL : Université de Pise (UNIFI), le coordinateur du projet, d'Italie, le centre français de recherche aérospatiale ONERA à Paris et l'école d'ingénieurs Arts et Métiers Sciences et Technologies de Bordeaux-Talence (ENSAM) en France, l'Université de Technologie de Delft (TUD) aux Pays-Bas, le Centre aérospatial allemand (DLR) et l'entreprise SkyBox Engineering en Italie. De plus, un comité consultatif composé de consultants indépendants de l'industrie aéronautique et de représentants d'avionneurs (Leonardo, Airbus),

---

<sup>1</sup>Généralement appelé RPKs (revenue passenger kilometres) : il s'agit du nombre cumulé de kilomètres parcourus par les passagers pour le transport desquels un transporteur aérien reçoit une rémunération commerciale.

<sup>2</sup>[www.parsifalproject.eu](http://www.parsifalproject.eu)

de sociétés de gestion d'aéroports (aéroports de Milan et de Toscane) et de compagnies aériennes (KLM) a soutenu les activités de recherche en représentant les intérêts du marché.

La solution proposée dans PARSIFAL est la configuration PrandtlPlane, représentée dans une représentation artistique de la Fig. 1.1. Cette configuration, introduite pour la première fois par Prandtl en 1924, est caractérisée par un système de portance en forme de rectangle en vue de face. Une telle configuration minimise la traînée induite parmi tous les systèmes de sustentation possibles ayant la même portée et la même quantité de portance. Pour un gros avion, la traînée induite constitue de 40 à 45% de la traînée totale en croisière et environ 80% au décollage. En employant la configuration PrandtlPlane, une réduction de cette composante d'environ 20-30% peut être obtenue pour des applications type. L'augmentation conséquente de l'efficacité aérodynamique (le rapport entre la portance et la traînée) peut être utilisée pour réduire la consommation de carburant (pour un scénario de mission et charge utile donné) ou pour augmenter la capacité de charge utile (pour une consommation de carburant et mission donnée). Dans les deux cas, cela se traduit par une réduction de l'impact environnemental et du coût par passager.

L'objectif principal du projet PARSIFAL était de démontrer la faisabilité de l'introduction de la configuration PrandtlPlane sur le marché, et l'intérêt de le faire. Cette étude de faisabilité a été menée par les différents partenaires évaluant différents aspects : économique, aérodynamique, architectural, structurel, environnemental, propulsif, mécanique de vol, etc. Une analyse de marché préliminaire menée dans les premières phases du projet, a permis d'identifier le meilleur segment de marché à cibler dans le projet : il est décrit à travers un ensemble de performances cibles appelé *top-level aircraft requirements*, qui sont présentés dans le Tab. 1.1. Ces performances identifient un aéronef qui opère sur les mêmes routes courtes à moyennes distances (moins de 4000 km) des familles d'avions Airbus A320 et Boeing 737 (B737), ayant le même encombrement, mais capable de transporter environ 50% de passagers en plus (une capacité typique des gros avions comme l'A330 et le B767). D'autres caractéristiques principales de la proposition de PARSIFAL sont présentées dans le Tab. 1.2, dans lequel le PrandtlPlane est également comparé à un avion concurrent conventionnel, et des représentations visuelles sont fournies dans les Figures 1.4 et 1.5.

Outre la réduction de la traînée induite, la configuration PrandtlPlane apporte d'autres avantages et opportunités intéressants : une sécurité accrue grâce à un comportement de décrochage régulier et une phase post-décrochage caractérisée par une réduction seulement partielle de la maniabilité et de la contrôlabilité ; un amortissement du tangage supérieur à celui d'une configuration classique, ce qui se traduit par plus de confort et de sécurité ; la possibilité d'adopter des schémas de manœuvre innovants comme le *direct lift control*<sup>3</sup> et le *pure couple control*<sup>4</sup> grâce à la possibilité de loger les gouvernes sur les ailes avant et arrière ; la capacité de concevoir une structure plus légère en tirant parti de l'architecture particulière ; la possibilité d'évaluer l'emploi de différentes solutions de propulsion innovantes. D'un autre côté, la nouveauté de la configuration proposée rend les données statistiques classiques et les solutions établies connues non *a priori* dignes de confiance, ou pas du tout applicables. Cela a constitué un défi majeur dans le projet PARSIFAL, mais aussi a été stimulant pour le développement de nouvelles connaissances et méthodes de conception. Cela est particulièrement vrai pour la conception structurelle de l'aéronef, car, contrairement à ce qui se passe avec une configuration conventionnelle, le fuselage et les voilures sont surcontraints.

---

<sup>3</sup>La possibilité de modifier la quantité de portance sans affecter le moment de tangage.

<sup>4</sup>La capacité de générer un moment de tangage pur sans altérer la portance.



Le projet a été organisé en huit work packages différents, organiquement répartis entre les partenaires, avec de multiples interactions (voir Fig. 1.6). L'ENSAM Bordeaux a été le responsable du work package 5, intitulé *Structural Analysis of the PrandtlPlane*, qui a été réalisé en collaboration avec UNIPi et DLR.

Les activités du work package 5 avaient quatre objectifs principaux :

1. Développer des procédures d'optimisation innovantes à utiliser pour la conception préliminaire de structures aéronautiques, métalliques ou composites. Ces procédures d'optimisation devraient pouvoir :
  - 1.1 Surmonter les limitations des procédures d'optimisation courantes pour les structures à parois minces (composites) de grande taille et gérer correctement la nature hyperstatique de l'architecture PrandtlPlane.
  - 1.2 Intégrer efficacement tous les critères de conception pertinents dans cette phase de conception (notamment, ceux liés à la fabricabilité de solutions composites innovantes constituées de stratifiés à rigidité variable et de stratifiés à rigidité constante de type *blended*), afin de maximiser la conformité des solutions obtenues avec les phases de conception suivantes.
2. Valider les procédures d'optimisation développées :
  - 2.1 Numériquement, grâce à la solution de problèmes de référence tirés de la littérature.
  - 2.2 Expérimentalement, via des tests sur des structures composites simples et sur des panneaux raidis en matériau composite.
3. Effectuer une conception structurelle préliminaire du PrandtlPlane, à la fois pour une variante métallique et pour une composite, en utilisant les procédures d'optimisation développées en ciblant, en particulier :
  - 3.1 Les principaux composants structuraux du fuselage.
  - 3.2 Les principaux composants structuraux générant la portance.
4. Vérifier la conformité du PrandtlPlane métallique optimal par rapport aux phénomènes d'aéroélasticité.

Toutes les activités connexes ont été menées à l'ENSAM, à l'exception de celles liées à l'Objectif 4, qui ont été réalisées par UNIPi et l'Université Carlos III de Madrid, dans le rôle de sous-traitant de UNIPi. Concernant les activités liées à l'Objectif 3, les zones de connexion entre le fuselage et le système générant la portance ont été modélisées uniquement à travers des modèles aux éléments finis à basse fidélité à l'ENSAM, tandis qu'une activité de type *design of experiments*, basée sur une modélisation plus détaillée, a été réalisée par J.-N. Walthers au DLR.

## Les objectifs de la thèse

Le travail lié à cette thèse est intervenu dans toutes contributions de l'ENSAM au projet PARSIFAL. Les objectifs du projet ont constitué à la fois une motivation et une application pour les différentes activités de la thèse. Pour cette raison, les structures stratifiées composites à parois minces typiques du domaine aéronautique ont été ciblées dans cette thèse et, sans perte de généralité, l'accent a été mis sur la structure du fuselage.

Les structures composites à parois minces de grande taille présentent une nature multi-échelle, dû, d'une part, à leurs caractéristiques géométriques, et, d'autre part, à la nature inhérente des matériaux composites. L'architecture *semi-monocoque* constitue le choix standard pour les structures du fuselage et de l'aile. Cette architecture de structure (dont un exemple est illustré à la Fig. 1.7) est modulaire, composée de sous-structures (les *panneaux raidis*), qui sont à leur tour constituées de plaques minces. Pour leurs propriétés géométriques, les structures de ce type présentent deux échelles caractéristiques auxquelles se produisent différents phénomènes, ceux qui correspondent à autant de critères impliqués à prendre en compte dans le processus de conception. Les critères de conception liés à la masse de la structure, à sa rigidité, aux phénomènes aéroélastiques, sont formulées à l'échelle *globale* de la structure, c'est-à-dire l'échelle de l'aéronef entier. À l'échelle *locale*, c'est-à-dire l'échelle des panneaux raidis et des plaques dont sont composées les structures d'aile et de fuselage, d'autres phénomènes se produisent, notamment ceux liés au flambement de la structure. Du point de vue des matériaux, les stratifiés composites présentent un comportement multi-échelle qui conduit à l'identification de trois échelles caractéristiques : l'échelle *microscopique*, régie par les propriétés des phases constitutives (fibres et matrice), et par leur interaction ; l'échelle *mésoscopique* des plis, considérés comme des couches anisotropes homogènes équivalentes ; l'échelle *macroscopique* du stratifié, où une plaque monocouche anisotrope homogène équivalente est considérée.

Lorsqu'une structure composite à parois minces de grande taille est considérée, une description macroscopique du stratifié est suffisante pour évaluer les phénomènes à l'échelle globale et à l'échelle locale décrits ci-dessus. Cependant, le phénomène de rupture des matériaux composites est généralement évalué à l'échelle mésoscopique et la définition des séquences d'empilement des stratifiés est une étape clé du processus de conception de ces structures. Concernant l'échelle microscopique, même si certains phénomènes pertinents se produisent également à cette échelle, elle n'a pas fait l'objet d'étude dans cette thèse et, par conséquent, elle a été ignorée. Par conséquent, trois échelles de travail sont considérées dans cette thèse : l'échelle macroscopique globale de la structure, l'échelle macroscopique locale du composant et l'échelle mésoscopique (c'est-à-dire celle du pli constitutif).

Les travaux réalisés dans cette thèse visent à permettre une meilleure exploitation des matériaux composites dans les structures à parois minces à hautes performances, à travers le développement de procédures multi-échelle et d'outils numériques pour leur conception structurelle efficace.

Deux classes de matériaux composites ont été considérées : les composites à rigidité constante (constant-stiffness composite (CSC)) et les composites à rigidité variable (variable-stiffness composite (VSC)).

Toutes les méthodologies et tous les outils développés ont été validés, soit numériquement, en les appliquant à des structures de référence tirées de la littérature, soit à travers des activités expérimentales. La plupart d'entre elles ont également été appliquées à la conception préliminaire de la structure de l'aéronef proposé dans PARSIFAL ; cela a nécessité de actions spécifiques pour tenir compte de la configuration PrandtlPlane ayant une structure interne surcontrainte.

## État de l'art

La revue bibliographique présentée dans le Chapitre 2 a permis d'évaluer l'état de l'art des procédures de conception pour les structures CSC et VSC à parois minces de grande taille.

Le format standard actuel des matériaux composites utilisés lorsque des performances structurelles élevées sont requises est le stratifié CSC, c'est-à-dire une plaque stratifiée constituée de plis contenant de longues fibres droites continues (non-tissées). La conception correcte des structures CSC nécessite l'optimisation des propriétés géométriques et matérielles de chaque stratifié qui les compose. Le problème de conception associé peut être formulé comme un problème de programmation non linéaire contraint (constrained non-linear programming problem (CNLPP)) qui implique des réponses physiques de la structure et la mise en place de variables de conception à toutes les échelles de travail. La solution d'un tel problème multi-échelle dans le domaine des orientations des plis des stratifiés composant la structure, s'il est formulé de la manière la plus générale, apparaît non viable en raison du grand nombre de variables de conception impliquées et du coût élevé. Par conséquent, les concepteurs interviennent généralement sur de multiples aspects du processus de conception en essayant de trouver le meilleur compromis entre la généralité de la formulation du problème et le coût de calcul nécessaire à sa solution.

Concernant l'évaluation des réponses structurelles, de nos jours, l'utilisation des analyses aux éléments finis pour l'évaluation des phénomènes à l'échelle globale est assez courante ; à l'inverse, des méthodes approximées analytiques ou semi-empiriques sont encore largement employées à l'échelle locale. Ces méthodes reposent sur des hypothèses limitatives rendant leur applicabilité pas toujours justifiable. Certains auteurs ont proposé l'utilisation de *surrogate models* basés sur des analyses aux éléments finis pour décrire les réponses à l'échelle locale. Mais certaines approximations sur la géométrie des modèles de panneaux raidis, les conditions aux limites considérées, ou les deux sont alors obligatoirement introduites.

D'un point de vue procédural, le transfert d'informations entre les échelles globale et locale est souvent mal géré, et la redistribution des contraintes se produisant à l'échelle globale en raison des changements des variables de conception à l'échelle locale est négligée. Cela conduit à un manque de précision dans les évaluations des réponses structurelles qui, d'une part, a un effet néfaste sur la recherche de solution dans la phase de conception préliminaire et, d'autre part, introduit des incohérences avec la phase de conception détaillée. Les approches de modélisation global-local (GL) permettent de surmonter certaines des limitations citées ci-dessus. Lors de l'adoption de telles approches, les réponses structurelles aux l'échelles globale et locale sont évaluées avec précision et efficacité au moyen d'analyses aux éléments finis, et un transfert d'information cohérent entre les échelles est garanti.

En ce qui concerne la définition des variables de conception du problème, des règles de simplification non nécessaire et des règles métier sont généralement appliquées. Celles-ci interviennent sur la nature des séquences d'empilement des stratifiés et limitent les orientations possibles des plis dans un ensemble prédéfini limité. Ceci est généralement fait pour réduire le nombre de variables de conception et pour imposer de manière incorrecte certaines propriétés élastiques souhaitées du stratifié. Cependant l'espace de conception est extrêmement réduit et, par conséquent, les possibilités de trouver le véritable optimum global du problème sont réduites. L'adoption d'une approche de conception de type *multi-niveau* permet de simplifier le problème d'optimisation à la fois par une relaxation de sa non-convexité et par une forte réduction du nombre de variables de conception, théoriquement sans réduire l'espace de conception. L'adoption d'une telle approche permet de formuler et de résoudre le problème d'optimisation structurelle en termes de propriétés macroscopiques des stratifiés, en reportant la conception des séquences d'empilement à un deuxième niveau du processus de conception. Cependant, l'approche multi-niveau la plus

couramment employée, c'est-à-dire celle basée sur l'utilisation des *Lamination Parameters* pour la représentation du comportement macroscopique du stratifié, montre quelques limitations. Notamment, une utilisation systématique des règles de simplification susmentionnées est effectuée lors de l'adoption d'une telle représentation. Cela annule certains des avantages attendus d'une approche multi-niveau, mais introduit également un effet collatéral : l'espace de conception des *Lamination Parameters* résultant ne permet pas une optimisation facile de la direction d'orthotropie principale du stratifié.

Bien que moins employée, la représentation basée sur les Paramètre Polaires montre des avantages intrinsèques liés à sa formulation basée sur des invariants tensoriels. De plus, contrairement à celle basée sur les *Lamination Parameters*, cette représentation est bien adaptée pour la description du comportement mécanique macroscopique de stratifiés moyennement épais et épais. Le cadre de la *Multi-Scale Two-Level optimisation strategy* (MS2LOS), une stratégie de conception à plusieurs niveaux introduite par Montemurro et al. (2012a,b) et basée sur l'utilisation des Paramètre Polaires, a été adopté dans ce travail.

Les procédés de fabrication modernes permettent la production de stratifiés dans lesquels une optimisation ponctuelle des propriétés mécaniques est possible, les stratifiés composites à rigidité variable. Les stratifiés VSC offrent des possibilités d'optimisation supérieures à celles des stratifiés CSC, notamment pour les composants structuraux présentant des gradients de contraintes élevés, par exemple le panneau entourant une fenêtre de fuselage. Différents formats de stratifiés VSC sont possibles et, dans cette thèse, l'accent a été mis sur les stratifiés à direction des fibres variable (variable angle tow) obtenus au moyen du procédé de dépose automatisée de fibres (Automated Fibre Placement). L'adoption généralisée de ce type de stratifiés dans l'industrie est encore limitée, d'une part, par la nouveauté et l'immaturité des processus de fabrication et, d'autre part, par l'absence d'une procédure générale et établie pour leur conception optimale. La conception ponctuelle des stratifiés VSC est conceptuellement similaire à celle des stratifiés CSC, donc toutes les remarques ci-dessus valent également pour ces premiers. Cependant, certaines difficultés spécifiques surviennent, qui sont liées à la variation spatiale des variables de conception à travers la surface des stratifiés VSC, et à la nécessité de prendre en compte des critères de fabricabilité plus contraignants.

## Le travail de thèse

Dans la première partie du travail de thèse, les structures CSC à parois minces de grande taille ont été ciblées. La tâche consistant à définir une procédure de conception améliorée pour ces structures a été abordée en deux phases.

Dans la première phase, correspondant aux travaux présentés dans le Chapitre 3, un scénario simplifié a été envisagé : la conception structurelle préliminaire d'une structure métallique, qui peut être vue comme un sous-cas de celui plus général d'une structure en matériaux anisotropes. Ce faisant, il n'est pas nécessaire de faire la distinction entre les échelles macroscopique et mésoscopique et tous les aspects liés à la conception des séquences d'empilement sont ignorés. Seules les variables de conception géométriques sont alors utilisées dans le processus de conception et l'accent peut être mis sur la gestion des échelles globale et locale. Cette première phase a étudié la possibilité d'optimiser ce type de structures en évaluant avec précision toutes les réponses mécaniques impliquées au moyen d'analyses aux éléments finis, sans imposer aucune restriction dans la définition des variables de conception, tout en gérant le coût de calcul du processus. Un problème

d'ingénierie significatif a été retenu comme cas d'étude : la conception en minimisant le poids d'un tronçon de fuselage en aluminium appartenant à la partie arrière d'un avion *wide-body*, dont la géométrie et les charges de base sont tirées de la littérature. Les critères de conception relatifs à la rigidité de la structure, à la tenue statique, à la tenue en fatigue et à la charge de flambage (approche de conception sans flambage), évaluées dans des conditions de chargement adaptées, ont été pris en compte dans le processus de conception, ainsi que les critères relatifs à la fabricabilité de la solution. Pour résoudre ce problème de conception, une procédure de conception multi-échelle, c'est-à-dire la stratégie GL-MSOS (global-local multi-scale optimisation strategy), a été proposée.

Lors de l'adoption de la stratégie GL-MSOS, l'évaluation des réponses mécaniques de la structure est effectuée au moyen d'analyses *on-line* aux éléments finis, employant l'approche de type global-local de *sub-modelling*. Pour chaque solution candidate, des modèles aux éléments finis à l'échelle globale et à l'échelle locale sont générés et résolus au moyen de scripts entièrement paramétriques. Les modèles sont caractérisés par un niveau différent de raffinement de la modélisation, évitant ainsi l'utilisation de modèles globaux raffinés coûteux en calcul pour l'évaluation de phénomènes localisés. Les analyses à l'échelle locale sont effectuées en considérant les conditions aux limites extraites, sans simplifications, des résultats de l'analyse à l'échelle globale, assurant ainsi une cohérence complète dans la transition d'échelle. L'effort de calcul est faible en générant automatiquement les modèles aux éléments finis locaux uniquement pour un ensemble limité de *zones d'intérêt*, identifiés lors de l'analyse à l'échelle globale au moyen de critères appropriés. L'ensemble complet des variables de conception est pris en compte dans la formulation du problème d'optimisation sans introduire d'hypothèses simplificatrices et la recherche de la solution est effectuée en utilisant l'algorithme génétique ERASMUS.

La solution obtenue a été comparée à une solution optimisée tirée de la littérature. Ce dernier a été obtenu en résolvant un problème de conception similaire au moyen d'une procédure de conception itérative dans laquelle sont utilisées des règles de simplification communes pour la définition des variables de conception et des méthodes analytiques pour les évaluations des réponses. La solution obtenue avec la stratégie GL-MSOS et celle tirée de la littérature ont une masse très similaire (avec une différence inférieure à 1,2%), cependant, la première surclasse la seconde en performances. En effet, dans le travail de référence, aucune contrainte de fabrication n'a été prise en compte, et la moins restrictive approche de conception *post-flambage* a été adoptée. Ce résultat a été considéré comme une preuve numérique de l'efficacité de la procédure de conception proposée.

Dans la seconde phase, la possibilité de généraliser la stratégie GL-MSOS à la conception de structures CSC à parois minces de grande taille a été étudiée.

La couche supplémentaire de complexité représentée par la possibilité d'optimiser les propriétés matérielles de la structure, ainsi que les propriétés géométriques, a été confrontée en adoptant une approche de conception à multi-niveau, la stratégie MS2LOS. Dans le flux de travail habituel de la stratégie MS2LOS, le problème est résolu à deux niveaux, dans lesquels deux problèmes sont confrontés. Au premier niveau, l'optimisation structurelle est effectuée. Chaque stratifié composant la structure est modélisé comme une plaque monocouche équivalente et ses propriétés mécaniques macroscopiques, représentées en termes de Paramètres Polaires, sont optimisées (avec toutes les propriétés géométriques) sans faire d'hypothèses simplificatrices sur la nature de la séquence d'empilement sous-jacente. Le problème d'optimisation de second niveau est consacré à la récupération des séquences d'empilement des stratifiés correspondant aux ensembles de Paramètres Polaires optimaux trouvés au premier niveau. Cela implique que, pour éviter les incohérences entre les deux

niveaux ou le besoin d'activités de *réparation*, tous les critères impliqués dans le problème de conception, y compris ceux typiques des échelles inférieures (notamment ceux concernant la rupture et la fabricabilité des composants structuraux), doivent être formulés comme des contraintes équivalentes à l'échelle macroscopique.

Les avantages de la GL-MSOS et ceux de la MS2LOS ont donc été combinés, obtenant la stratégie GL-MS2LOS. L'intégration intéresse le premier niveau de la stratégie MS2LOS, où l'évaluation des réponses structurelles, aux échelles globale et locale, est réalisée au moyen d'analyses sur des modèles aux éléments finis spécifiques, dont la cohérence est assurée par l'utilisation l'approche de type globale-locale de *sub-modelling*. Le deuxième niveau de la stratégie MS2LOS reste inchangé par rapport aux travaux précédents.

La stratégie GL-MS2LOS a été présentée dans le Chapitre 5, où elle a été utilisée pour la conception minimisant le poids d'un tronçon de fuselage CSC. La structure considérée est identique, en termes de propriétés géométriques principales et de charges considérées, à celle présentée dans le Chapitre 3, mais ses principaux composants structuraux (à l'exception des poutres et éléments structurels de plancher) sont considérés comme constitués de stratifiés CSC. De plus, la formulation du problème de conception considéré est équivalente à celle rencontrée dans le Chapitre 3 : les critères de conception concernant la rigidité structurelle et la résistance statique, ainsi que l'absence de flambage dans les conditions de chargement considérées ont été prises en compte dans le processus de conception de la structure composite. Également ont été pris en compte les critères sur la fabricabilité de la solution. La tenue de la structure a été évaluée à l'échelle macroscopique au moyen d'un critère de rupture formulé dans l'espace des Paramètre Polaires et les conditions de faisabilité sur l'existence de séquences d'empilement appropriées sont incluses dans la formulation du problème de premier niveau parmi les contraintes de fabrication. Ici aussi, l'algorithme génétique ERASMUS a été utilisé comme outil de solution. Le fuselage composite optimal obtenu en utilisant la stratégie GL-MS2LOS a été comparé à celui en aluminium optimal obtenu dans le Chapitre 3. La solution composite montre une diminution de poids de 40% par rapport à la solution métallique et respecte l'ensemble des contraintes de conception. Étant donné que certains des composants structuraux modélisés n'ont pas été inclus dans le processus d'optimisation, ce résultat montre le grand potentiel de la procédure de conception proposée.

Dans la mesure où la MS2LOS constitue un élément principal de la stratégie GL-MS2LOS, deux activités de validation expérimentale de son efficacité ont été prévues dans cette thèse.

La première de ces activités a été présentée dans le Chapitre 4. Dans ce travail, la stratégie MS2LOS a été appliquée à la conception en minimisant le poids d'une plaque CSC modérément épaisse soumise à des contraintes sur sa rigidité globale dans le plan, sur sa première charge de flambage, et sur sa fabricabilité. Les activités numériques et expérimentales se sont déroulées en parallèle. Les premières ont suivi le flux de travail à deux niveaux typique de la stratégie MS2LOS : premièrement, la conception structurelle de la plaque a été réalisée en termes de propriétés mécaniques macroscopique et de propriétés géométriques, puis la conception de la séquence d'empilement a été effectuée. L'algorithme génétique ERASMUS a été utilisé pour effectuer la recherche de solution aux deux niveaux. Au premier niveau, il a été interfacé avec des analyses aux éléments finis pour l'évaluation de la première charge de flambage de la plaque. Au deuxième niveau, il a été interfacé avec un modèle analytique pour calculer les propriétés macroscopiques des séquences d'empilement candidates. La solution du problème de second niveau a été recherchée dans l'espace des séquences d'empilement *Quasi Triviales*, une famille d'empilements qui permet d'obte-

nir un découplage flexion-membrane et une homogénéité exacts du stratifié, sans imposer de règles simplificatrices sur son empilement (par exemple symétrie et équilibrage). Une plaque ayant la même géométrie que celle optimisée, soumise aux mêmes conditions aux limites, et dont la séquence d'empilement a été construite en utilisant les règles classiques tirées de la littérature a été considérée comme solution de référence et utilisée pour définir les critères de conception. Des tests expérimentaux de flambage ont été réalisés, à la fois sur la plaque de référence, pour confirmer la précision du modèle aux éléments finis utilisé lors du processus d'optimisation, et sur celle optimisée. Les résultats numériques et expérimentaux montrent une excellente concordance : la plaque optimisée est environ 10% plus légère que la plaque de référence avec des performances mécaniques similaires ou supérieures. Ces résultats constituent une première validation expérimentale de l'efficacité à la fois de la stratégie MS2LOS et des séquences d'empilement très générales résultantes de son application.

Une deuxième activité expérimentale était également prévue dans les activités de PARSIFAL. Cette activité, réalisée en collaboration avec UNIP, suit la même procédure de travail numérique-expérimental présentée dans le Chapitre 4, mais se concentre sur les panneaux raidis à l'échelle 1. En raison de multiples retards dans la fabrication des panneaux, cette activité, non rapportée dans cette thèse, n'est pas terminée et sera finalisée au cours des prochains mois.

Les stratégies GL-MSOS et GL-MS2LOS, présentées et validées numériquement dans les Chapitres 3 et 5 respectivement, ont vu une application dans la conception structurelle préliminaire de l'avion PrandtlPlane proposé dans le projet PARSIFAL. Cette activité de conception structurelle, dont les faits marquants ont été présentés dans le Chapitre 6, a ciblé les principaux composants structuraux du fuselage et du système de voilure de l'avion, à la fois dans une variante métallique et une CSC. Une approche modulaire a été adoptée pour la modélisation de la structure de l'avion, et les activités associées ont été partagées entre trois membres de l'équipe PARSIFAL à l'ENSAM. En raison des particularités de l'architecture PrandtlPlane, deux adaptations des procédures de conception ont été réalisées afin de réduire le temps de calcul nécessaire pour leur application sur une telle structure. D'un point de vue procédural, une approche multi-étape a été adoptée : la recherche de solution a été réalisée de manière itérative, en optimisant alternativement les variables de conception appartenant au tronçon central du fuselage et celles du système de voilure. Du point de vue de la modélisation, dans le modèle global aux éléments finis de l'ensemble de la structure de l'avion, les régions non directement impliquées dans l'optimisation ont été *condensées* dans des *super éléments* obtenus au moyen de la technique de *sub-structuring*. Les résultats, obtenus à la fois en termes de distributions macroscopiques des propriétés inertielles et en termes d'informations structurelles détaillées pour les deux variantes de la structure de l'avion, ont répondu aux attentes et ont contribué au bon déroulement du projet PARSIFAL.

Dans une troisième phase du travail de thèse, l'accent a été mis sur les stratifiés VSC dans le but de surmonter certaines limites des procédures courantes pour leur conception optimale grâce au développement d'outils de conception théoriques et numériques spécifiques.

Une procédure de conception adaptée pour les structures VSC devrait traiter efficacement les variables de conception qui prennent la forme de distributions continues et suffisamment lisses sur la surface du stratifié, et intégrer également les contraintes liées au processus de fabrication utilisé. En raison de la nature du problème d'optimisation associé, l'adoption d'une approche de conception multi-niveau couplée à l'utilisation d'un algorithme

déterministe comme outil de solution semble avantageuse. Cependant, afin de garantir une exploitation efficace de ce type d'algorithmes, l'expression analytique du gradient de toutes les fonctions de réponse impliquées dans le processus d'optimisation doit être définie.

Dans le Chapitre 7, le problème de l'optimisation déterministe des composants structuraux VSC selon des critères de conception liés à la masse, à la résistance et à la courbure maximale des fibres a été abordé. L'optimisation a été réalisée dans le cadre du problème de premier niveau de la stratégie MS2LOS, en tirant parti de deux éléments principaux : la méthode polaire pour la représentation des propriétés mécaniques macroscopiques locales des stratifiés et des entités B-spline pour décrire la distribution des variables de conception. Le cadre théorique de la stratégie MS2LOS a été enrichi par la formulation des critères présentés ci-dessus, et le problème de conception a été généralisé au cas des stratifiés VSC d'épaisseur non uniforme.

Deux structures de référence ont été considérées : la première met en évidence les concentrations de contraintes sous charge dans le plan, tandis que la seconde met l'accent sur les effets de flexion et de cisaillement. Le problème de la maximisation de la charge de rupture (avec une contrainte sur la masse) et celui de la minimisation de la masse (avec une contrainte sur la résistance du stratifié) ont été résolus pour les deux structures. La charge de rupture de la structure a été définie en utilisant un critère de rupture au niveau du stratifié basé sur des invariants tensoriels. L'effet d'une contrainte sur la courbure maximale des fibres a également été évalué et une formulation macroscopique de cette contrainte liée au procédé de fabrication a été proposée. En tirant parti des propriétés des entités B-spline, l'expression analytique des fonctions de réponse liées à tous les critères, ainsi que leurs gradients, ont été dérivées. Évidemment, le critère ponctuel sur l'existence de séquences d'empilement correspondantes a également été considérée : grâce à un changement de variables adroit, il est intrinsèquement satisfait dans la formulation proposée pour le problème d'optimisation, sans qu'il soit nécessaire d'introduire des contraintes équivalentes explicites. D'un point de vue numérique, la plate-forme numérique DOMES (Deterministic Optimisation of Macroscopic laminatEs via Splines) a été créée. Développée dans l'environnement Python, elle constitue une interface entre un algorithme d'optimisation déterministe et un logiciel aux éléments finis, et établit une structure de données pour la définition des variables de conception et une implémentation modulaire des différents critères de conception.

Différentes propriétés des stratifiés VSC ont été optimisées soit uniformément, soit localement sur la surface des stratifiés : le type et la forme de l'orthotropie, la direction de l'axe principal d'orthotropie et l'épaisseur. En fonction de la définition des variables de conception, diverses sous-classes de stratifiés VSC, comprenant à la fois des solutions fabricables et des solutions seulement théoriques, ont été identifiées. Plusieurs cas de conception, correspondant à diverses combinaisons possibles de structure considérée, de formulation du problème d'optimisation et de sous-classe des stratifiés VSC, ont été considérés. Les résultats ont été comparés, en termes de performances, à des solutions isotropes quasi homogènes. Lors de l'optimisation de la résistance, la charge de rupture peut être augmentée entre 48% et 1034%, tandis que, lors de l'optimisation de la masse, la diminution du poids obtenue est comprise entre 24% et 92%. Les stratifiés VSC à épaisseur non uniforme surpassent en performances leurs homologues à épaisseur uniforme, montrant une augmentation supplémentaire de 116-138% de la charge de rupture ou une diminution de poids supplémentaire de 26-58%. Enfin, des solutions optimisées en résistance ont également été comparées à une solution VSC optimisée tirée de la littérature, obtenue au moyen



de la représentation basée sur les *Lamination Parameters* : l'approche proposée dans cette thèse a donné des solutions avec une augmentation de la charge de rupture entre 4% et 252% ; la solution la plus comparable (en termes d'espace de conception exploré) montre une amélioration de 21%.

Des résultats intéressants ont également été obtenus lors du problème de maximisation de la charge de flambage des stratifiés VSC. Cette activité, non rapportée dans cette thèse, a été réalisée en collaboration avec le doctorant G. A. Fiordilino et récemment publié (Fiordilino, Izzi, and Montemurro, 2021). Deux problèmes de référence ont été considérés et les résultats obtenus ont été comparés à la fois à des solutions isotropes quasi homogènes et à des solutions VSC optimisées tirées de la littérature : une augmentation de la charge de flambage jusqu'à 230% et jusqu'à 16% a été respectivement trouvée.

Les résultats ci-dessus montrent sans équivoque le grand potentiel des stratifiés VSC et l'efficacité de la stratégie d'optimisation proposée.

## Perspectives

L'application de la stratégie GL-MS2LOS à des cas de conception simplifiés, bien que représentatifs, a permis d'obtenir des résultats encourageants, prouvant qu'il s'agit d'une alternative viable et efficace à d'autres procédures de conception d'usage courant pour les structures CSC à parois minces de grande taille. Cependant, il reste encore de la place pour des améliorations et/ou des développements futurs.

L'adoption d'une approche de conception de type *post-flambage*, au lieu de l'approche *sans flambage* employée dans cette thèse, est censée permettre d'obtenir des configurations optimales plus légères. L'intégration efficace de critères de conception sur le comportement post-flambage de la structure dans la procédure présentée constitue une tâche difficile. En effet, du fait de son caractère non linéaire, l'évaluation du comportement post-flambage des structures est généralement réalisée à travers des analyses de suivi de trajectoire (en utilisant par exemple la méthode *arc-length*) qui révèlent un coût de calcul trop élevé pour être intégré dans un processus d'optimisation. Une alternative valable est l'adoption de méthodes asymptotiques (par exemple la méthode de Koiter ou la Méthode Asymptotique-Numérique) qui fournissent, à un coût de calcul raisonnable, une bonne approximation de la réponse initiale après flambement.

Afin de pouvoir faire face à des cas de conception plus complets de niveau industriel, la formulation du problème doit être enrichie. Des critères de conception supplémentaires devraient être intégrés, par exemple des critères de conception spécifiques pour le dimensionnement des cadres, des éléments structurels de plancher, et des conditions de chargement supplémentaires devraient être prises en compte pour l'évaluation des réponses de l'aéronef. Par ailleurs, du point de vue de la modélisation, la présence des ouvertures principales, comme portes et fenêtres dans le fuselage, doit également être prise en compte dans cette phase de conception, afin de maximiser la compatibilité avec la phase suivante. L'utilisation d'un algorithme génétique comme outil d'optimisation, grâce à sa bonne capacité d'exploration, aide sûrement à éviter d'être piégé dans les minima locaux lors de la résolution de problèmes non convexes, mais il peut converger vers des solutions sous-optimales en raison de la perte de diversité de la population. Des améliorations supplémentaires pourraient être obtenues en faisant suivre à la phase d'optimisation méta-heuristique une phase d'optimisation déterministe. Idéalement, cette dernière phase devrait être supportée par la dérivation de l'expression analytique du gradient de toutes les fonctions de réponse impliquées dans le processus d'optimisation. Notamment, le gradient des réponses

à l'échelle locale doit bien prendre en compte la transition d'échelle (à travers le gradient des déplacements à la frontière des modèles locaux aux éléments finis) et la possibilité que la position de la zone d'intérêt puisse varier lors du procès d'optimisation. Ce dernier besoin pourrait être satisfait de différentes manières : a) en agrégeant dans le gradient les réponses de tous les modèles locaux possibles ; b) en définissant correctement les zones de conception (c'est-à-dire les parties de la structure où les composants partagent les mêmes propriétés) c) au moyen d'une combinaison des deux approches. Des activités sur ce sujet ont déjà été lancées dans ce groupe de recherche et nécessitent de développements supplémentaires.

Les activités menées dans la troisième phase du travail de thèse ont permis de confirmer le grand potentiel des stratifiés VSC. L'intégration de composants structuraux VSC dans des structures composites à parois minces de grande taille semble donc souhaitable. Cependant, un développement plus poussé des outils théoriques et numériques associés aux deux niveaux de la stratégie MS2LOS pour les stratifiés VSC est nécessaire.

Au premier niveau de la stratégie MS2LOS, il est important de formuler de nouveaux critères pour la prédiction de la présence de défauts liés à la fabrication des stratifiés VSC, comme les écarts et/ou les chevauchements entre bandes de fibres adjacentes dans la structure finale. Il est important également de pouvoir prendre en compte leur effet sur les réponses structurelles depuis les premières phases de conception. La mise en œuvre à la fois des nouveaux critères et des critères précédemment formulés (par exemple ceux concernant la compliance et la charge de flambement) devrait tirer parti de la structure de données établie dans la plate-forme numérique DOMES. De plus, cette plateforme pourrait être intégrée à la suite d'outils d'optimisation numérique développée par le groupe de recherche du laboratoire I2M.

Au deuxième niveau de la stratégie MS2LOS, les efforts devraient être mis sur le développement d'outils permettant de récupérer des trajectoires des fibres pour toutes les sous-classes possibles de stratifiés VSC.

L'exécution d'activités couplées numériques-expérimentales sur des composants structuraux VSC simples et complexes devrait être l'étape suivante naturelle.

Pour conclure, la perspective à long terme du travail présenté dans cette thèse est la définition des aspects procéduraux liés à l'adoption de la stratégie GL-MS2LOS pour la conception efficace de structures VSC à parois minces de grande taille.

---

## Bibliography

- S. Adali, V. E. Verijenko, and M. Walker. Optimal laminate configurations with symmetric lay-ups for maximum postbuckling stiffness. *Composites Engineering*, 4(11):1119–1127, 1994. URL [www.doi.org/10.1016/0961-9526\(95\)91286-P](http://www.doi.org/10.1016/0961-9526(95)91286-P).
- S. Adali, A. Richter, V. E. Verijenko, and E. B. Summers. Optimal design of hybrid laminates with discrete ply angles for maximum buckling load and minimum cost. *Composite Structures*, 32(1-4):409–415, 1995. URL [www.doi.org/10.1016/0263-8223\(95\)00067-4](http://www.doi.org/10.1016/0263-8223(95)00067-4).
- S. Adali, M. Walker, and V. E. Verijenko. Multiobjective optimization of laminated plates for maximum prebuckling, buckling and postbuckling strength using continuous and discrete ply angles. *Composite Structures*, 35(1):117–130, 1996. URL [www.doi.org/10.1016/0263-8223\(96\)00030-X](http://www.doi.org/10.1016/0263-8223(96)00030-X).
- S. Adali, F. Lene, G. Duvaut, and V. Chiaruttini. Optimization of laminated composites subject to uncertain buckling loads. *Composite Structures*, 62(3-4):261–269, 2003. URL [www.doi.org/10.1016/j.compstruct.2003.09.024](http://www.doi.org/10.1016/j.compstruct.2003.09.024).
- Airbus s.a.s. Global Market Forecast 2018-2037, 2019. URL [www.gmf.airbus.com](http://www.gmf.airbus.com).
- M. Akterskaia, E. Jansen, S. Hühne, and R. Rolfes. Efficient progressive failure analysis of multi-stringer stiffened composite panels through a two-way loose coupling global-local approach. *Composite Structures*, 183:137–145, 2018. URL [www.doi.org/10.1016/j.compstruct.2017.02.011](http://www.doi.org/10.1016/j.compstruct.2017.02.011).
- M. A. Albazzan, R. Harik, B. F. Tatting, and Z. Gürdal. Efficient design optimization of nonconventional laminated composites using lamination parameters: A state of the art. *Composite Structures*, 209:362–374, 2019. URL [www.doi.org/10.1016/j.compstruct.2018.10.095](http://www.doi.org/10.1016/j.compstruct.2018.10.095).
- A. Alhajahmad, M. M. Abdalla, and Z. Gürdal. Optimal Design of a Pressurized Fuselage Panel with a Cutout Using Tow-Placed Steered Fibers. In *Proceedings of the International Conference on Engineering Optimization 2008*, Rio de Janeiro, Brazil, 2008.
- B. K. Anderson and T. T. Takahashi. Conceptual Fuselage Design with Direct CAD Modeling. In *17th AIAA Aviation Technology, Integration, and Operations Conference*, Denver, Colorado, 2017. American Institute of Aeronautics and Astronautics. URL [www.doi.org/10.2514/6.2017-3940](http://www.doi.org/10.2514/6.2017-3940).

- Y. Audoux, M. Montemurro, and J. Pailhès. A Metamodel Based on Non-Uniform Rational Basis Spline Hyper-Surfaces for Optimisation of Composite Structures. *Composite Structures*, 247:112439, 2020. URL [www.doi.org/10.1016/j.compstruct.2020.112439](http://www.doi.org/10.1016/j.compstruct.2020.112439).
- F. Aymerich and M. Serra. Optimization of laminate stacking sequence for maximum buckling load using the ant colony optimization (ACO) metaheuristic. *Composites Part A: Applied Science and Manufacturing*, 39(2):262–272, 2008. URL [www.doi.org/10.1016/j.compositesa.2007.10.011](http://www.doi.org/10.1016/j.compositesa.2007.10.011).
- C. Bisagni and R. Vescovini. A fast procedure for the design of composite stiffened panels. *The Aeronautical Journal*, 119(1212):185–201, 2015. URL [www.doi.org/10.1017/S0001924000010332](http://www.doi.org/10.1017/S0001924000010332).
- A. W. Blom, M. M. Abdalla, and Z. Gürdal. Optimization of course locations in fiber-placed panels for general fiber angle distributions. *Composites Science and Technology*, 70(4):564–570, 2010. URL [www.doi.org/10.1016/j.compscitech.2009.12.003](http://www.doi.org/10.1016/j.compscitech.2009.12.003).
- M. Bloomfield, J. Herencia, and P. Weaver. Optimisation of Anisotropic Composite Plates Incorporating Non-Conventional Ply Orientations. In *49th AIAA/ASME/ASCE/AHS/ASC Structures, Structural Dynamics, and Materials Conference, 16th AIAA/ASME/AHS Adaptive Structures Conference, 10th AIAA Non-Deterministic Approaches Conference, 9th AIAA Gossamer Spacecraft Forum, 4th AIAA Multidisciplinary Design Optimization Specialists Conference*, Schaumburg, IL, Apr. 2008. American Institute of Aeronautics and Astronautics. URL [www.doi.org/10.2514/6.2008-1918](http://www.doi.org/10.2514/6.2008-1918).
- L. Boni. *Methodologies for the optimum design of fuselage structures of transport aircraft*. PhD Thesis, University of Pisa, Pisa, Italy, 2004.
- L. Boni and D. Fanteria. Development of analytical methods for fuselage design: validation by means of finite element analyses. *Proceedings of the Institution of Mechanical Engineers, Part G: Journal of Aerospace Engineering*, 218(5):315–327, 2004. URL [www.doi.org/10.1243/0954410042467022](http://www.doi.org/10.1243/0954410042467022).
- K. R. Bramsiepe, V. Handojo, Y. M. Meddaikar, M. Schulze, and T. Klimmek. Loads and Structural Optimization Process for Composite Long Range Transport Aircraft Configuration. In *2018 Multidisciplinary Analysis and Optimization Conference*, Atlanta, Georgia, 2018. American Institute of Aeronautics and Astronautics. URL [www.doi.org/10.2514/6.2018-3572](http://www.doi.org/10.2514/6.2018-3572).
- E. F. Bruhn. *Analysis and design of flight vehicle structures*. Tri-State Offset Co., 1973.
- A. Catapano and M. Montemurro. A multi-scale approach for the optimum design of sandwich plates with honeycomb core. Part I: homogenisation of core properties. *Composite Structures*, 118:664–676, 2014a. URL [www.doi.org/10.1016/j.compstruct.2014.07.057](http://www.doi.org/10.1016/j.compstruct.2014.07.057).
- A. Catapano and M. Montemurro. A multi-scale approach for the optimum design of sandwich plates with honeycomb core. Part II: the optimisation strategy. *Composite Structures*, 118:677–690, 2014b. URL [www.doi.org/10.1016/j.compstruct.2014.07.058](http://www.doi.org/10.1016/j.compstruct.2014.07.058).

- A. Catapano and M. Montemurro. On the correlation between stiffness and strength properties of anisotropic laminates. *Mechanics of Advanced Materials and Structures*, 26(8):651–660, 2019. URL [www.doi.org/10.1080/15376494.2017.1410906](http://www.doi.org/10.1080/15376494.2017.1410906).
- A. Catapano and M. Montemurro. Strength Optimisation of Variable Angle-Tow Composites Through a Laminate-Level Failure Criterion. *Journal of Optimization Theory and Applications*, 187(3):683–706, 2020. URL [www.doi.org/10.1007/s10957-020-01750-6](http://www.doi.org/10.1007/s10957-020-01750-6).
- A. Catapano, B. Desmorat, and P. Vannucci. Invariant formulation of phenomenological failure criteria for orthotropic sheets and optimisation of their strength. *Mathematical Methods in the Applied Sciences*, 35(15):1842–1858, 2012. URL [www.doi.org/10.1002/mma.2530](http://www.doi.org/10.1002/mma.2530).
- A. Catapano, B. Desmorat, and P. Vannucci. Stiffness and Strength Optimization of the Anisotropy Distribution for Laminated Structures. *Journal of Optimization Theory and Applications*, 167(1):118–146, 2015. URL [www.doi.org/10.1007/s10957-014-0693-5](http://www.doi.org/10.1007/s10957-014-0693-5).
- CeRAS. Short range reference aircraft. Technical Report CSR01, CeRAS Central Reference Aircraft data System. URL <http://ceras.ilr.rwth-aachen.de/trac/wiki/CeRAS/AircraftDesigns/CSR01>.
- N. G. Cormier, B. S. Smallwood, G. B. Sinclair, and G. Meda. Aggressive submodelling of stress concentrations. *International Journal for Numerical Methods in Engineering*, 46(6):889–909, 1999. URL [www.doi.org/10.1002/\(SICI\)1097-0207\(19991030\)46:6<889::AID-NME699>3.0.CO;2-F](http://www.doi.org/10.1002/(SICI)1097-0207(19991030)46:6<889::AID-NME699>3.0.CO;2-F).
- P. Cresta, O. Allix, C. Rey, and S. Guinard. Nonlinear localization strategies for domain decomposition methods: Application to post-buckling analyses. *Computer Methods in Applied Mechanics and Engineering*, 196(8):1436–1446, 2007. URL [www.doi.org/10.1016/j.cma.2006.03.013](http://www.doi.org/10.1016/j.cma.2006.03.013).
- K. Croft, L. Lessard, D. Pasini, M. Hojjati, J. Chen, and A. Yousefpour. Experimental study of the effect of automated fiber placement induced defects on performance of composite laminates. *Composites Part A: Applied Science and Manufacturing*, 42(5):484–491, 2011. URL [www.doi.org/10.1016/j.compositesa.2011.01.007](http://www.doi.org/10.1016/j.compositesa.2011.01.007).
- C. G. Diaconu, M. Sato, and H. Sekine. Feasible Region in General Design Space of Lamination Parameters for Laminated Composites. *AIAA Journal*, 40(3):559–565, 2002a. URL [www.doi.org/10.2514/2.1683](http://www.doi.org/10.2514/2.1683).
- C. G. Diaconu, M. Sato, and H. Sekine. Layup optimization of symmetrically laminated thick plates for fundamental frequencies using lamination parameters. *Structural and Multidisciplinary Optimization*, 24(4):302–311, 2002b. URL [www.doi.org/10.1007/s00158-002-0241-z](http://www.doi.org/10.1007/s00158-002-0241-z).
- D. O. Evans. Fiber Placement. In D. B. Miracle and S. L. Donaldson, editors, *Composites*, volume 21 of *ASM Handbook*, pages 477–479. ASM International, 2001. URL [www.doi.org/10.31399/asm.hb.v21.a0003410](http://www.doi.org/10.31399/asm.hb.v21.a0003410).
- G. A. Fiordilino, M. I. Izzi, and M. Montemurro. A general isogeometric polar approach for the optimisation of variable stiffness composites: Application to eigenvalue buckling

- problems. *Mechanics of Materials*, 153:(in press), 2021. URL [www.doi.org/10.1016/j.mechmat.2020.103574](http://www.doi.org/10.1016/j.mechmat.2020.103574).
- M. Fischer, D. Kennedy, and C. A. Featherston. Multilevel framework for optimization of lightweight structures. *Proceedings of the Institution of Mechanical Engineers, Part G: Journal of Aerospace Engineering*, 226(4):380–394, 2012. URL [www.doi.org/10.1177/0954410011411637](http://www.doi.org/10.1177/0954410011411637).
- A. Frediani and G. Montanari. Best wing system: an exact solution of the prandtl’s problem. In *Variational Analysis and Aerospace Engineering*, pages 183–211, New York, NY, 2009. Springer New York. URL [www.doi.org/10.1007/978-0-387-95857-6\\_11](http://www.doi.org/10.1007/978-0-387-95857-6_11).
- T. Garulli, A. Catapano, M. Montemurro, J. Jumel, and D. Fanteria. Quasi-trivial stacking sequences for the design of thick laminates. *Composite Structures*, 200:614–623, 2018. URL [www.doi.org/10.1016/j.compstruct.2018.05.120](http://www.doi.org/10.1016/j.compstruct.2018.05.120).
- L. Gendre, O. Allix, P. Gosselet, and F. Comte. Non-intrusive and exact global/local techniques for structural problems with local plasticity. *Computational Mechanics*, 44(2):233–245, 2009. URL [www.doi.org/10.1007/s00466-009-0372-9](http://www.doi.org/10.1007/s00466-009-0372-9).
- G. Gerard. The Crippling Strength of Compression Elements. *Journal of the Aerospace Sciences*, 25(1):37–52, 1958. URL [www.doi.org/10.2514/8.7482](http://www.doi.org/10.2514/8.7482).
- H. Ghiasi, D. Pasini, and L. Lessard. Optimum stacking sequence design of composite materials Part I: Constant stiffness design. *Composite Structures*, 90(1):1–11, 2009. URL [www.doi.org/10.1016/j.compstruct.2009.01.006](http://www.doi.org/10.1016/j.compstruct.2009.01.006).
- H. Ghiasi, K. Fayazbakhsh, D. Pasini, and L. Lessard. Optimum stacking sequence design of composite materials Part II: Variable stiffness design. *Composite Structures*, 93(1):1–13, 2010. URL [www.doi.org/10.1016/j.compstruct.2010.06.001](http://www.doi.org/10.1016/j.compstruct.2010.06.001).
- S. Grihon, L. Krog, and D. Bassir. Numerical Optimization applied to structure sizing at AIRBUS: A multi-step process. *International Journal for Simulation and Multidisciplinary Design Optimization*, 3(4):432–442, 2009a. URL [www.doi.org/10.1051/ijsmdo/2009020](http://www.doi.org/10.1051/ijsmdo/2009020).
- S. Grihon, M. Samuelides, A. Merval, A. Remouchamps, M. Bruyneel, B. Colson, and K. Hertel. Fuselage Structure Optimisation. In *Advances in Collaborative Civil Aeronautical Multidisciplinary Design Optimization*, AIAA Progress in Astronautics and Aeronautics. American Institute of Aeronautics and Astronautics, 2009b. URL [www.doi.org/10.2514/4.867279](http://www.doi.org/10.2514/4.867279).
- P. A. Guidault, O. Allix, L. Champaney, and J. P. Navarro. A two-scale approach with homogenization for the computation of cracked structures. *Computers & Structures*, 85(17-18):1360–1371, 2007. URL [www.doi.org/10.1016/j.compstruc.2006.08.085](http://www.doi.org/10.1016/j.compstruc.2006.08.085).
- Z. Gurdal and R. Olmedo. In-plane response of laminates with spatially varying fiber orientations - Variable stiffness concept. *AIAA Journal*, 31(4):751–758, 1993. URL [www.doi.org/10.2514/3.11613](http://www.doi.org/10.2514/3.11613).
- R. T. Haftka and J. L. Walsh. Stacking-sequence optimization for buckling of laminated plates by integer programming. *AIAA Journal*, 30(3):814–819, 1992. URL [www.doi.org/10.2514/3.10989](http://www.doi.org/10.2514/3.10989).

- J. E. Herencia, P. M. Weaver, and M. I. Friswell. Initial sizing optimisation of anisotropic composite panels with T-shaped stiffeners. *Thin-Walled Structures*, 46(4):399–412, 2008. URL [www.doi.org/10.1016/j.tws.2007.09.003](http://www.doi.org/10.1016/j.tws.2007.09.003).
- I. Hirai, B. P. Wang, and W. D. Pilkey. An efficient zooming method for finite element analysis. *International Journal for Numerical Methods in Engineering*, 20(9):1671–1683, 1984. URL [www.doi.org/10.1002/nme.1620200910](http://www.doi.org/10.1002/nme.1620200910).
- I. Hirai, Y. Uchiyama, Y. Mizuta, and W. D. Pilkey. An exact zooming method. *Finite Elements in Analysis and Design*, 1(1):61–69, 1985. URL [www.doi.org/10.1016/0168-874X\(85\)90008-3](http://www.doi.org/10.1016/0168-874X(85)90008-3).
- J. Huang and R. T. Haftka. Optimization of fiber orientations near a hole for increased load-carrying capacity of composite laminates. *Structural and Multidisciplinary Optimization*, 30(5):335–341, 2005. URL [www.doi.org/10.1007/s00158-005-0519-z](http://www.doi.org/10.1007/s00158-005-0519-z).
- O. F. Hughes, B. Ghosh, and Y. Chen. Improved prediction of simultaneous local and overall buckling of stiffened panels. *Thin-Walled Structures*, 42(6):827–856, 2004. URL [www.doi.org/10.1016/j.tws.2004.01.003](http://www.doi.org/10.1016/j.tws.2004.01.003).
- M. W. Hyer and R. F. Charette. Use of curvilinear fiber format in composite structure design. 29(6):1011–1015, 1991. URL [www.doi.org/10.2514/3.10697](http://www.doi.org/10.2514/3.10697).
- M. W. Hyer and H. H. Lee. The use of curvilinear fiber format to improve buckling resistance of composite plates with central circular holes. *Composite Structures*, 18(3):239–261, 1991. URL [www.doi.org/10.1016/0263-8223\(91\)90035-W](http://www.doi.org/10.1016/0263-8223(91)90035-W).
- B. I. Hyman, A. Deturk, R. Diaz, and G. DiGiovanni. Exploratory tests on fiber-reinforced plates with circular holes under tension. *AIAA Journal*, 7(9):1820–1821, 1969. URL [www.doi.org/10.2514/3.5408](http://www.doi.org/10.2514/3.5408).
- S. T. IJsselmuiden, M. M. Abdalla, and Z. Gürdal. Implementation of Strength-Based Failure Criteria in the Lamination Parameter Design Space. *AIAA Journal*, 46(7):1826–1834, 2008. URL [www.doi.org/10.2514/1.35565](http://www.doi.org/10.2514/1.35565).
- S. T. IJsselmuiden, M. M. Abdalla, and Z. Gurdal. Optimization of Variable-Stiffness Panels for Maximum Buckling Load Using Lamination Parameters. *AIAA Journal*, 48(1):134–143, 2010. URL [www.doi.org/10.2514/1.42490](http://www.doi.org/10.2514/1.42490).
- F.-X. Irisarri, D. H. Bassir, N. Carrere, and J.-F. Maire. Multiobjective stacking sequence optimization for laminated composite structures. *Composites Science and Technology*, 69(7-8):983–990, 2009. URL [www.doi.org/10.1016/j.compscitech.2009.01.011](http://www.doi.org/10.1016/j.compscitech.2009.01.011).
- F.-X. Irisarri, F. Laurin, F.-H. Leroy, and J.-F. Maire. Computational strategy for multiobjective optimization of composite stiffened panels. *Composite Structures*, 93(3):1158–1167, 2011. URL [www.doi.org/10.1016/j.compstruct.2010.10.005](http://www.doi.org/10.1016/j.compstruct.2010.10.005).
- M. I. Izzi, M. Montemurro, A. Catapano, and J. Pailhès. A multi-scale two-level optimisation strategy integrating a global/local modelling approach for composite structures. *Composite Structures*, 237:(in press), 2020. URL [www.doi.org/10.1016/j.compstruct.2020.111908](http://www.doi.org/10.1016/j.compstruct.2020.111908).

- M. I. Izzi, A. Catapano, and M. Montemurro. Strength and mass optimisation of variable-stiffness composites in the polar parameters space. *Structural and Multidisciplinary Optimisation*, (in press), 2021a. URL [www.doi.org/10.1007/s00158-021-02963-7](http://www.doi.org/10.1007/s00158-021-02963-7).
- M. I. Izzi, M. Montemurro, A. Catapano, D. Fanteria, and J. Pailhès. Multi-scale optimisation of thin-walled structures by considering a global/local modelling approach. *Proceedings of the Institution of Mechanical Engineers, Part G: Journal of Aerospace Engineering*, 235(2):171–188, 2021b. URL [www.doi.org/10.1177/0954410020939338](http://www.doi.org/10.1177/0954410020939338).
- C. C. Jara-Almonte and C. E. Knight. The specified boundary stiffness/force SBSF method for finite element subregion analysis. *International Journal for Numerical Methods in Engineering*, 26(7):1567–1578, 1988. URL [www.doi.org/10.1002/nme.1620260708](http://www.doi.org/10.1002/nme.1620260708).
- A. Jibawy, C. Julien, B. Desmorat, A. Vincenti, and F. Léné. Hierarchical structural optimization of laminated plates using polar representation. *International Journal of Solids and Structures*, 48(18):2576–2584, 2011. URL [www.doi.org/10.1016/j.ijsolstr.2011.05.015](http://www.doi.org/10.1016/j.ijsolstr.2011.05.015).
- R. M. Jones. *Mechanics of composite materials*. McGraw-Hill, 1975.
- A. Khani, S. T. IJsselmuiden, M. M. Abdalla, and Z. Gürdal. Design of variable stiffness panels for maximum strength using lamination parameters. *Composites Part B: Engineering*, 42(3):546–552, 2011. URL [www.doi.org/10.1016/j.compositesb.2010.11.005](http://www.doi.org/10.1016/j.compositesb.2010.11.005).
- B. C. Kim, K. Hazra, P. Weaver, and K. Potter. Limitations of fibre placement techniques for variable angle tow composites and their process-induced defects. In *Proceedings of the 18th International Conference on Composite Materials (ICMM18)*, pages 21–26, Jeju, Korea, 2011.
- B. C. Kim, K. Potter, and P. M. Weaver. Continuous tow shearing for manufacturing variable angle tow composites. *Composites Part A: Applied Science and Manufacturing*, 43(8):1347–1356, 2012. URL [www.doi.org/10.1016/j.compositesa.2012.02.024](http://www.doi.org/10.1016/j.compositesa.2012.02.024).
- B. C. Kim, P. M. Weaver, and K. Potter. Manufacturing characteristics of the continuous tow shearing method for manufacturing of variable angle tow composites. *Composites Part A: Applied Science and Manufacturing*, 61:141–151, 2014. URL [www.doi.org/10.1016/j.compositesa.2014.02.019](http://www.doi.org/10.1016/j.compositesa.2014.02.019).
- P. Kuhn, J. P. Peterson, and L. R. Levin. Summary of diagonal tension. Technical Note TN-2661, NACA, 1952.
- M. Lan, D. Cartié, P. Davies, and C. Baley. Influence of embedded gap and overlap fiber placement defects on the microstructure and shear and compression properties of carbon–epoxy laminates. *Composites Part A: Applied Science and Manufacturing*, 82:198–207, 2016. URL [www.doi.org/10.1016/j.compositesa.2015.12.007](http://www.doi.org/10.1016/j.compositesa.2015.12.007).
- R. Le Riche and R. T. Haftka. Optimization of laminate stacking sequence for buckling load maximization by genetic algorithm. *AIAA Journal*, 31(5):951–956, 1993. URL [www.doi.org/10.2514/3.11710](http://www.doi.org/10.2514/3.11710).



- R. Le Riche and R. T. Haftka. Improved genetic algorithm for minimum thickness composite laminate design. *Composites Engineering*, 5(2):143–161, 1995. URL [www.doi.org/10.1016/0961-9526\(95\)90710-S](http://www.doi.org/10.1016/0961-9526(95)90710-S).
- B. Liu, R. T. Haftka, and P. Trompette. Maximization of buckling loads of composite panels using flexural lamination parameters. *Structural and Multidisciplinary Optimization*, 26(1-2):28–36, 2004. URL [www.doi.org/10.1007/s00158-003-0314-7](http://www.doi.org/10.1007/s00158-003-0314-7).
- S. Liu, Y. Hou, X. Sun, and Y. Zhang. A two-step optimization scheme for maximum stiffness design of laminated plates based on lamination parameters. *Composite Structures*, 94(12):3529–3537, 2012. URL [www.doi.org/10.1016/j.compstruct.2012.06.014](http://www.doi.org/10.1016/j.compstruct.2012.06.014).
- C. S. Lopes, Z. Gürdal, and P. P. Camanho. Variable-stiffness composite panels: Buckling and first-ply failure improvements over straight-fibre laminates. *Computers & Structures*, 86(9):897–907, 2008. URL [www.doi.org/10.1016/j.compstruc.2007.04.016](http://www.doi.org/10.1016/j.compstruc.2007.04.016).
- J. Loughlan. The buckling performance of composite stiffened panel structures subjected to combined in-plane compression and shear loading. *Composite Structures*, 29(2):197–212, 1994. URL [www.doi.org/10.1016/0263-8223\(94\)90100-7](http://www.doi.org/10.1016/0263-8223(94)90100-7).
- K. M. Mao and C. T. Sun. A refined global-local finite element analysis method. *International Journal for Numerical Methods in Engineering*, 32(1):29–43, 1991. URL [www.doi.org/10.1002/nme.1620320103](http://www.doi.org/10.1002/nme.1620320103).
- A. Marouene, R. Boukhili, J. Chen, and A. Yousefpour. Buckling behavior of variable-stiffness composite laminates manufactured by the tow-drop method. *Composite Structures*, 139:243–253, 2016. URL [www.doi.org/10.1016/j.compstruct.2015.12.025](http://www.doi.org/10.1016/j.compstruct.2015.12.025).
- M. Miki and Y. Sugiyamat. Optimum Design of Laminated Composite Plates Using Lamination Parameters. *AIAA Journal*, 31(5):921–922, 1993. URL [www.doi.org/10.2514/3.49033](http://www.doi.org/10.2514/3.49033).
- M. Montemurro. *Optimal design of advanced engineering modular systems through a new genetic approach*. PhD Thesis, UPMC, Paris VI, France, 2012. URL [www.tel.archives-ouvertes.fr/tel-00955533](http://www.tel.archives-ouvertes.fr/tel-00955533).
- M. Montemurro. An extension of the polar method to the First-order Shear Deformation Theory of laminates. *Composite Structures*, 127:328–339, 2015a. URL [www.doi.org/10.1016/j.compstruct.2015.03.025](http://www.doi.org/10.1016/j.compstruct.2015.03.025).
- M. Montemurro. Corrigendum to “an extension of the polar method to the First-order Shear Deformation Theory of laminates” [compos. struct. 127 (2015) 328-339]. *Composite Structures*, 131:1143–1144, 2015b. URL [www.doi.org/10.1016/j.compstruct.2015.06.002](http://www.doi.org/10.1016/j.compstruct.2015.06.002).
- M. Montemurro. The polar analysis of the Third-order Shear Deformation Theory of laminates. *Composite Structures*, 131:775–789, 2015c. URL [www.doi.org/10.1016/j.compstruct.2015.06.016](http://www.doi.org/10.1016/j.compstruct.2015.06.016).
- M. Montemurro. *A contribution to the development of design strategies for the optimisation of lightweight structures*. HDR Thesis, Université de Bordeaux, Bordeaux, France, 2018. URL <http://hdl.handle.net/10985/15155>.

- M. Montemurro and A. Catapano. A New Paradigm for the Optimum Design of Variable Angle Tow Laminates. In A. Frediani, B. Mohammadi, O. Pironneau, and V. Cipolla, editors, *Variational Analysis and Aerospace Engineering*, volume 116 of *Springer Optimization and Its Applications*, pages 375–400. Springer International Publishing, Cham, 2016. URL [www.doi.org/10.1007/978-3-319-45680-5\\_14](http://www.doi.org/10.1007/978-3-319-45680-5_14).
- M. Montemurro and A. Catapano. On the effective integration of manufacturability constraints within the multi-scale methodology for designing variable angle-tow laminates. *Composite Structures*, 161:145–159, 2017. URL [www.doi.org/10.1016/j.compstruct.2016.11.018](http://www.doi.org/10.1016/j.compstruct.2016.11.018).
- M. Montemurro and A. Catapano. A general B-Spline surfaces theoretical framework for optimisation of variable angle-tow laminates. *Composite Structures*, 209:561–578, 2019. URL [www.doi.org/10.1016/j.compstruct.2018.10.094](http://www.doi.org/10.1016/j.compstruct.2018.10.094).
- M. Montemurro, A. Vincenti, and P. Vannucci. A Two-Level Procedure for the Global Optimum Design of Composite Modular Structures—Application to the Design of an Aircraft Wing: Part 1: Theoretical Formulation. *Journal of Optimization Theory and Applications*, 155(1):1–23, 2012a. URL [www.doi.org/10.1007/s10957-012-0067-9](http://www.doi.org/10.1007/s10957-012-0067-9).
- M. Montemurro, A. Vincenti, and P. Vannucci. A Two-Level Procedure for the Global Optimum Design of Composite Modular Structures—Application to the Design of an Aircraft Wing: Part 2: Numerical Aspects and Examples. *Journal of Optimization Theory and Applications*, 155(1):24–53, Oct. 2012b. URL [www.doi.org/10.1007/s10957-012-0070-1](http://www.doi.org/10.1007/s10957-012-0070-1).
- M. Montemurro, A. Vincenti, and P. Vannucci. Design of the elastic properties of laminates with a minimum number of plies. *Mechanics of Composite Materials*, 48(4):369–390, 2012c. URL [www.doi.org/10.1007/s11029-012-9284-4](http://www.doi.org/10.1007/s11029-012-9284-4).
- M. Montemurro, A. Catapano, and D. Doroszewski. A multi-scale approach for the simultaneous shape and material optimisation of sandwich panels with cellular core. *Composites Part B: Engineering*, 91:458–472, 2016. URL [www.doi.org/10.1016/j.compositesb.2016.01.030](http://www.doi.org/10.1016/j.compositesb.2016.01.030).
- M. Montemurro, A. Pagani, G. A. Fiordilino, J. Pailhès, and E. Carrera. A general multi-scale two-level optimisation strategy for designing composite stiffened panels. *Composite Structures*, 201:968–979, 2018. URL [www.doi.org/10.1016/j.compstruct.2018.06.119](http://www.doi.org/10.1016/j.compstruct.2018.06.119).
- M. Montemurro, M. I. Izzi, J. El-Yagoubi, and D. Fanteria. Least-weight composite plates with unconventional stacking sequences: Design, analysis and experiments. *Journal of Composite Materials*, 53(16):2209–2227, 2019. URL [www.doi.org/10.1177/0021998318824783](http://www.doi.org/10.1177/0021998318824783).
- S. Nagendra, S. Kodiyalam, J. Davis, and V. Parthasarathy. Optimization of tow fiber paths for composite design. In *Proceeding of the 36th Structures, Structural Dynamics and Materials Conference*, volume AIAA 95-1275, New Orleans, LA, USA, 1995. American Institute of Aeronautics and Astronautics. URL [www.doi.org/10.2514/6.1995-1275](http://www.doi.org/10.2514/6.1995-1275).

- S. Nagendra, D. Jestin, Z. Gürdal, R. T. Haftka, and L. T. Watson. Improved genetic algorithm for the design of stiffened composite panels. *Computers & Structures*, 58(3): 543–555, 1996. URL [www.doi.org/10.1016/0045-7949\(95\)00160-I](http://www.doi.org/10.1016/0045-7949(95)00160-I).
- M. A. Nik, K. Fayazbakhsh, D. Pasini, and L. Lessard. Optimization of variable stiffness composites with embedded defects induced by Automated Fiber Placement. *Composite Structures*, 107:160–166, 2014. URL [www.doi.org/10.1016/j.compstruct.2013.07.059](http://www.doi.org/10.1016/j.compstruct.2013.07.059).
- M. C. Y. Niu. *Airframe structural design: practical design information and data on aircraft structures*. Connilit Pr, 1988.
- A. Nuti, F. Bertini, V. Cipolla, and G. Di Rito. Design of a Fuselage-Mounted Main Landing Gear of a Medium-Size Civil Transport Aircraft. *Aerotecnica Missili & Spazio*, 97(2):85–95, 2018. URL [www.doi.org/10.1007/BF03405803](http://www.doi.org/10.1007/BF03405803).
- PARSIFAL Project Consortium. Report on socio-economic scenarios and expectations. Project deliverable D1.1, PARSIFAL Project, 2017a. URL [www.parsifalproject.eu](http://www.parsifalproject.eu).
- PARSIFAL Project Consortium. Requirements for the adoption of the prandtlplane as a mean of transport. Project deliverable D2.1, PARSIFAL Project, 2017b. URL [www.parsifalproject.eu](http://www.parsifalproject.eu).
- PARSIFAL Project Consortium. Preliminary design of the reference prandtlplane. Project deliverable D3.2, PARSIFAL Project, 2018. URL [www.parsifalproject.eu](http://www.parsifalproject.eu).
- PARSIFAL Project Consortium. Report on operational and economic assessment. Project deliverable D1.2, PARSIFAL Project, 2020a. URL [www.parsifalproject.eu](http://www.parsifalproject.eu).
- PARSIFAL Project Consortium. Structural analysis of the baseline prandtlplane. Project deliverable D5.1 (confidential), PARSIFAL Project, 2020b. URL [www.parsifalproject.eu](http://www.parsifalproject.eu).
- PARSIFAL Project Consortium. Optimized solutions for prandtlplane fuselage and lifting system made of composite materials. Project deliverable D5.3 (confidential), PARSIFAL Project, 2020c. URL [www.parsifalproject.eu](http://www.parsifalproject.eu).
- B. Pearce. Covid-19: June data and revised air travel outlook, 2020a. URL [www.iata.org/en/iata-repository/publications/economic-reports/june-data-and-revised-air-travel-outlook](http://www.iata.org/en/iata-repository/publications/economic-reports/june-data-and-revised-air-travel-outlook).
- B. Pearce. Covid-19: Downgrade for global air travel outlook, 2020b. URL [www.iata.org/en/iata-repository/publications/economic-reports/downgrade-for-global-air-travel-outlook](http://www.iata.org/en/iata-repository/publications/economic-reports/downgrade-for-global-air-travel-outlook).
- D. M. J. Peeters, S. Hesse, and M. M. Abdalla. Stacking sequence optimisation of variable stiffness laminates with manufacturing constraints. *Composite Structures*, 125:596–604, 2015. URL [www.doi.org/10.1016/j.compstruct.2015.02.044](http://www.doi.org/10.1016/j.compstruct.2015.02.044).
- M. Petrolo, editor. *Advances in Predictive Models and Methodologies for Numerically Efficient Linear and Nonlinear Analysis of Composites*. PoliTO Springer Series. Springer International Publishing, 2019. URL [www.doi.org/10.1007/978-3-030-11969-0](http://www.doi.org/10.1007/978-3-030-11969-0).

- M. Picchi Scardaoni and M. Montemurro. Convex or non-convex? On the nature of the feasible domain of laminates. *European Journal of Mechanics - A/Solids*, 85:(in press), 2021. URL [www.doi.org/10.1016/j.euromechsol.2020.104112](http://www.doi.org/10.1016/j.euromechsol.2020.104112).
- M. Picchi Scardaoni, M. Montemurro, and E. Panettieri. PrandtlPlane wing-box least-weight design: A multi-scale optimisation approach. *Aerospace Science and Technology*, 106:(in press), 2020a. URL [www.doi.org/10.1016/j.ast.2020.106156](http://www.doi.org/10.1016/j.ast.2020.106156).
- M. Picchi Scardaoni, M. Montemurro, E. Panettieri, and A. Catapano. New blending constraints and a stack-recovery strategy for the multi-scale design of composite laminates. *Structural and Multidisciplinary Optimization*, page (in press), 2020b. URL [www.doi.org/10.1007/s00158-020-02725-x](http://www.doi.org/10.1007/s00158-020-02725-x).
- L. Prandtl. Induced drag of multiplanes. Technical Note NACA-TN-182, National Advisory Committee for Aeronautics, 1924. URL <https://ntrs.nasa.gov/citations/19930080964>.
- K. Risse, K. Schäfer, F. Schültke, and E. Stumpf. Central Reference Aircraft data System (CeRAS) for research community. *CEAS Aeronautical Journal*, 7(1):121–133, Mar. 2016. ISSN 1869-5582, 1869-5590. doi: 10.1007/s13272-015-0177-9. URL <http://link.springer.com/10.1007/s13272-015-0177-9>.
- R. M. Rivello. *Theory and analysis of flight structures*. McGraw-Hill College, 1969.
- J. W. Rustenburg, D. A. Skinn, and D. O. Tipps. Statistical Loads Data for the Airbus A-320 Aircraft in Commercial Operations. Technical report DOT/FAA/AR-02/35, U.S. Department of Transportation Federal Aviation Administration, Office of Aviation Research, Washington, D.C. 20591, 2002. URL [www.tc.faa.gov/its/worldpac/techrpt/ar02-35.pdf](http://www.tc.faa.gov/its/worldpac/techrpt/ar02-35.pdf).
- S. Setoodeh, M. M. Abdalla, and Z. Gürdal. Design of variable-stiffness laminates using lamination parameters. *Composites Part B: Engineering*, 37(4-5):301–309, 2006. URL [www.doi.org/10.1016/j.compositesb.2005.12.001](http://www.doi.org/10.1016/j.compositesb.2005.12.001).
- J. Sobieszczanski and D. Loendorf. A Mixed Optimization Method for Automated Design of Fuselage Structures. *Journal of Aircraft*, 9(12):805–811, 1972. URL [www.doi.org/10.2514/3.59080](http://www.doi.org/10.2514/3.59080).
- D. G. Stamatelos, G. N. Labeas, and K. I. Tserpes. Analytical calculation of local buckling and post-buckling behavior of isotropic and orthotropic stiffened panels. *Thin-Walled Structures*, 49(3):422–430, 2011. URL [www.doi.org/10.1016/j.tws.2010.11.008](http://www.doi.org/10.1016/j.tws.2010.11.008).
- C. T. Sun and K. M. Mao. A global-local finite element method suitable for parallel computations. *Computers & Structures*, 29(2):309–315, 1988. URL [www.doi.org/10.1016/0045-7949\(88\)90264-7](http://www.doi.org/10.1016/0045-7949(88)90264-7).
- B. F. Tatting and Z. Gürdal. Analysis and design of tow-steered variable stiffness composite laminates. In *American Helicopter Society Hampton Roads Chapter, Structure Specialists’ Meeting, Williamsburg, VA*, 2001.
- B. F. Tatting and Z. Gürdal. Design and Manufacture of Elastically Tailored Tow Placed Plates. Contractor Report CR-2002-211919, NASA Langley Research Center, Hampton, Virginia, 2002. URL [www.ntrs.nasa.gov/api/citations/20020073162/](http://www.ntrs.nasa.gov/api/citations/20020073162/).

- A. Todoroki and R. T. Haftka. Stacking sequence optimization by a genetic algorithm with a new recessive gene like repair strategy. *Composites Part B: Engineering*, 29(3): 277–285, 1998. URL [www.doi.org/10.1016/S1359-8368\(97\)00030-9](http://www.doi.org/10.1016/S1359-8368(97)00030-9).
- E. Torenbeek. Development and Application of a Comprehensive, Design-sensitive Weight Prediction Method for Wing Structures of Transport Category Aircraft. Report LR-693, Delft University of Technology, Faculty of Aerospace Engineering, 1992. URL <http://resolver.tudelft.nl/uuid:b45a61fe-317a-4201-82f0-dfae51ceb687>.
- M. W. Tosh and D. W. Kelly. On the design, manufacture and testing of trajectorial fibre steering for carbon fibre composite laminates. *Composites Part A: Applied Science and Manufacturing*, 31(10):1047–1060, 2000. URL [www.doi.org/10.1016/S1359-835X\(00\)00063-4](http://www.doi.org/10.1016/S1359-835X(00)00063-4).
- S. W. Tsai and E. M. Wu. A General Theory of Strength for Anisotropic Materials. *Journal of Composite Materials*, 5(1):58–80, 1971. URL [www.doi.org/10.1177/002199837100500106](http://www.doi.org/10.1177/002199837100500106).
- U.S. Department of Defense. Metallic materials and elements for aerospace vehicle structures. Technical Report MIL-HDBK-5J, United States of America, 2003.
- U.S. Department of Defense. Laminate stacking sequence effects. In *Composite Materials Handbook MIL-HDBK-17-3F*, volume 3, pages 5.68–5.71. United States of America, 2002.
- W. J. Vankan, R. Maas, and S. Grihon. Efficient optimisation of large aircraft fuselage structures. *The Aeronautical Journal*, 118(1199):31–52, 2014a. URL [www.doi.org/10.1017/S0001924000008915](http://www.doi.org/10.1017/S0001924000008915).
- W. J. Vankan, B. A. T. Noordman, and K. Kueres. High and low fidelity finite element modelling in aircraft composite fuselage structural analysis and optimisation. Technical report NLR-TP-2013-197, National Aerospace Laboratory NLR, 2014b.
- P. Vannucci. Plane Anisotropy by the Polar Method. *Meccanica*, 40(4-6):437–454, 2005. URL [www.doi.org/10.1007/s11012-005-2132-z](http://www.doi.org/10.1007/s11012-005-2132-z).
- P. Vannucci. On Special Orthotropy of Paper. *Journal of Elasticity*, 99(1):75–83, 2010. URL [www.doi.org/10.1007/s10659-009-9232-2](http://www.doi.org/10.1007/s10659-009-9232-2).
- P. Vannucci. A Note on the Elastic and Geometric Bounds for Composite Laminates. *Journal of Elasticity*, 112(2):199–215, 2013. URL [www.doi.org/10.1007/s10659-012-9406-1](http://www.doi.org/10.1007/s10659-012-9406-1).
- P. Vannucci and G. Verchery. A special class of uncoupled and quasi-homogeneous laminates. *Composites Science and Technology*, 61(10):1465–1473, 2001. URL [www.doi.org/10.1016/S0266-3538\(01\)00039-2](http://www.doi.org/10.1016/S0266-3538(01)00039-2).
- S. Venkataraman and R. T. Haftka. Structural optimization complexity: what has moore’s law done for us? *Structural and Multidisciplinary Optimization*, 28(6):375–387, 2004. URL [www.doi.org/10.1007/s00158-004-0415-y](http://www.doi.org/10.1007/s00158-004-0415-y).

- G. Verchery. Les Invariants des Tenseurs d'Ordre 4 du Type de l'Élasticité. In J.-P. Boehler, editor, *Mechanical Behavior of Anisotropic Solids / Comportment Mécanique des Solides Anisotropes*, pages 93–104. Springer Netherlands, Dordrecht, 1982. URL [www.doi.org/10.1007/978-94-009-6827-1\\_7](http://www.doi.org/10.1007/978-94-009-6827-1_7).
- J. D. Whitcomb. Iterative global/local finite element analysis. *Computers & Structures*, 40(4):1027–1031, 1991. URL [www.doi.org/10.1016/0045-7949\(91\)90334-I](http://www.doi.org/10.1016/0045-7949(91)90334-I).
- J. E. Wignot, H. Combs, and A. F. Ensrud. Analysis of circular shell-supported frames. Technical Note TN-929, NACA, 1944. URL [www.nttrs.nasa.gov/api/citations/19930090564](http://www.nttrs.nasa.gov/api/citations/19930090564).
- D. Williams. *An introduction to the theory of aircraft structures*. Arnold, 1960.
- K. Wu, B. Tatting, B. Smith, R. Stevens, G. Occhipinti, J. Swift, D. Achary, and R. Thornburgh. Design and Manufacturing of Tow-Steered Composite Shells Using Fiber Placement. In *50th AIAA/ASME/ASCE/AHS/ASC Structures, Structural Dynamics, and Materials Conference*, Palm Springs, California, 2009. American Institute of Aeronautics and Astronautics. URL [www.doi.org/10.2514/6.2009-2700](http://www.doi.org/10.2514/6.2009-2700).
- K. C. Wu, B. K. Stanford, G. A. Hrinda, Z. Wang, R. A. Martin, and H. A. Kim. Structural Assessment of Advanced Tow-Steered Shells. In *54th AIAA/ASME/ASCE/AHS/ASC Structures, Structural Dynamics, and Materials Conference*, Boston, Massachusetts, 2013. American Institute of Aeronautics and Astronautics. URL [www.doi.org/10.2514/6.2013-1769](http://www.doi.org/10.2514/6.2013-1769).
- Z. Wu, P. M. Weaver, G. Raju, and B. Chul Kim. Buckling analysis and optimisation of variable angle tow composite plates. *Thin-Walled Structures*, 60:163–172, 2012. URL [www.doi.org/10.1016/j.tws.2012.07.008](http://www.doi.org/10.1016/j.tws.2012.07.008).
- Z. Wu, G. Raju, and P. M. Weaver. Framework for the Buckling Optimization of Variable-Angle Tow Composite Plates. *AIAA Journal*, 53(12):3788–3804, 2015. URL [www.doi.org/10.2514/1.J054029](http://www.doi.org/10.2514/1.J054029).











**Michele Iacopo IZZI**



# **Multi-scale optimisation of thin-walled composite structures integrating a global-local modelling strategy**

## **Résumé**

Cette thèse porte sur le développement de procédures d'optimisation multi-échelle pour la conception de structures composites à parois minces. Deux types de structures composites sont analysées : les structures composites de grande taille à rigidité constante, typiques du domaine aéronautique, et les composants structuraux composites à rigidité variable, caractérisés par une variation ponctuelle des propriétés mécaniques macroscopiques du stratifié. Concernant les premières, leur conception préliminaire implique des phénomènes intervenants à différentes échelles de la structure et un grand nombre de variables de conception. Pour concevoir ce type de structures, la procédure d'optimisation GL-MS2LOS (de l'anglais *global-local multi-scale two-level optimisation strategy*) a été développée : cette procédure combine la précision dans l'évaluation des réponses physiques et la gestion de bonne qualité de la transition d'échelle d'une approche *Global-Local*, à la définition efficace des variables de conception de la stratégie MS2LOS. Concernant les composites à rigidité variable, pour favoriser leur conception optimale, d'une part, la stratégie MS2LOS a été enrichie par la formulation de critères de conception liés à la masse, à la résistance, au flambage et à la fabricabilité de la structure, et, d'autre part, des outils numériques spécifiques ont été développés. Le travail de thèse est complété par l'application de la procédure GL-MS2LOS à la conception structurelle de l'aéronef PrandtlPlane présenté dans le projet H2020 PARSIFAL, et également par des activités de validation expérimentale sur des composants structuraux optimisés.

Optimisation multi-échelle • Approche de modélisation global-local • Composites à rigidité variable • Méthode Polaire • Méthode aux éléments finis • B-spline

## **Résumé en anglais**

This thesis deals with the problem of the optimal design of lightweight thin-walled composite structures through the development of multi-scale procedures and numerical tools for their effective and efficient design. Two types of structures are considered: large-scale constant-stiffness composite structures, typical of the aeronautical field, and variable-stiffness composite structural components, characterised by a point wise variation of the macroscopic mechanical properties over the laminate surface. Concerning the formers, their preliminary design involves requirements related to responses at different scales of the structure and a huge number of design variables. To perform this operation the Global-Local Multi-Scale Two-Level Optimisation Strategy (GL-MS2LOS) has been developed, which combines the accuracy in responses evaluation and the proper handling of the scale transition of Global-Local approaches, with the efficient definition of the design variables of the MS2LOS. Regarding variable-stiffness composites, to foster their optimal design, on the one hand, the MS2LOS has been enhanced by the formulation of requirements on mass, strength, buckling and manufacturability, and, on the other hand, dedicated numerical tools have been developed. The application of the developed procedures to the structural design of the PrandtlPlane aircraft, presented in the H2020 project PARSIFAL, and experimental activities on optimised structural components complete the thesis work.

Multi-scale optimisation • Global-local modelling approach • Variable-stiffness composite • Polar Method • Finite element method • B-spline